https://ntrs.nasa.gov/search.jsp?R=19780005065 2020-03-22T06:48:11+00:00Z

NASA CR-152032
Available to the Public

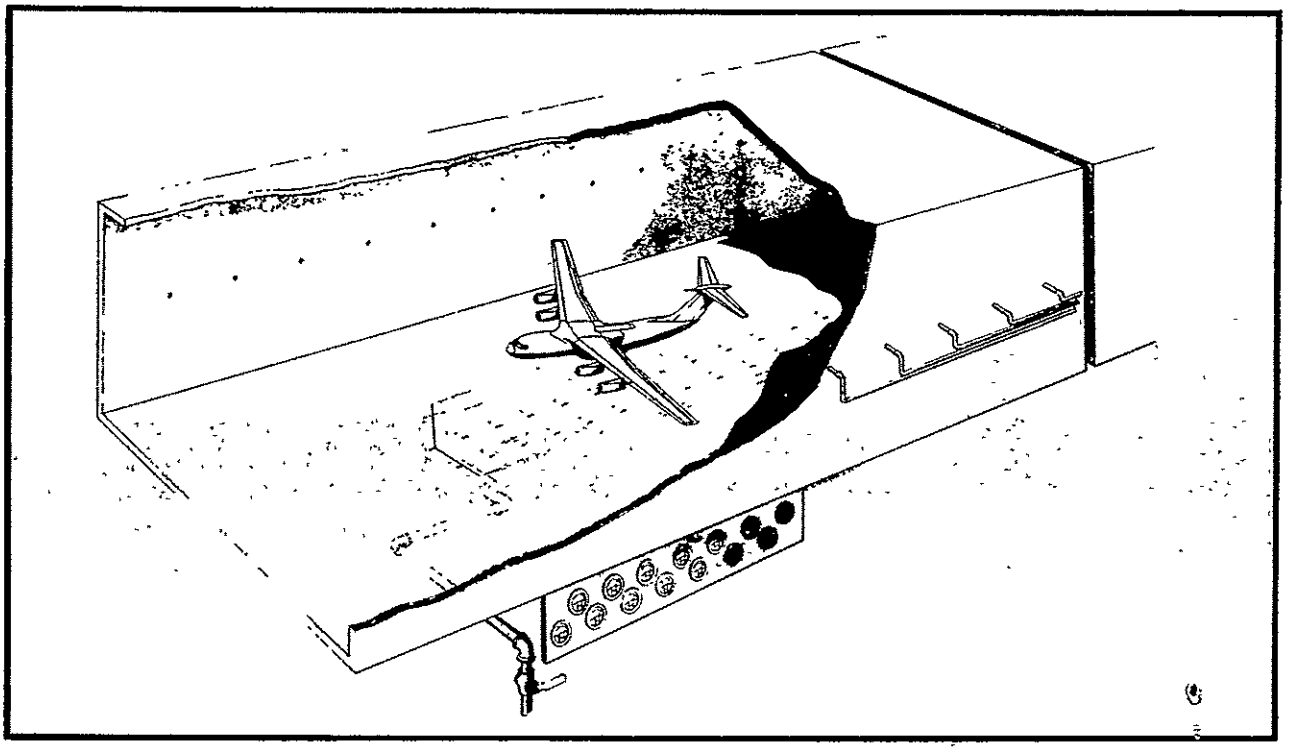

GROUND SIMULATION AND TUNNEL BLOCKAGE FOR A SWEPT, JET-FLAPPED WING TESTED TO VERY HIGH LIFT COEFFICIENTS

by J. E. Hackett and R. A. Boles

June 1977

(NASA-CR-152032) · GROUND SIMULATION AND TUNNEL BLOCKAGE FOR A SWEPT, JET-FLAPPED WING TESTED TO VERY HIGH LIFT COEFFICIENTS (Lockheed Missiles and Space Co.) 159 p HC A08/MF A01 CSCL 01A G3/02
N78-13008
Unclas
55030

LOCKHEED-GEORGIA COMPANY
Marietta, Georgia 30063
for
NATIONAL AERONAUTICS AND SPACE ADMINISTRATION
Ames Research Center

NATIONAL AERONAUTICS AND SPACE ADMINISTRATION
AMES RESEARCH CENTER
MOFFETT FIELD, CALIFORNIA 94035

REPLY TO ATTN OF: NAS 2-9349
AT:241-12-36

December 16, 1977

NASA Representative
Scientific and Technical Information Facility
P. O. Box 8757
Baltimore/Washington International Airport
Maryland 21240

Subject: Transmittal of Contractor Report: "Ground Simulation and Tunnel Blockage for a Swept, Jet-Flapped Wing Tested to Very High Lift Coefficients", dated June 1977, by J. E. Hackett and R. A. Boles of Lockheed-Georgia Company

Reference: Program Code - 505-10-41

The subject report prepared under NASA Contract NAS 2-9349 has been reviewed at Ames and is recommended for release in STAR as CR-152032.

Paul Bennett
Chief, Technical Information Division

Enclosure:
1 cy of subject report

cc:
NASA Hqrs., Code KSI (w/o enc.)

NASA CR-152032
Available to the Public

GROUND SIMULATION AND TUNNEL BLOCKAGE FOR A SWEPT, JET-FLAPPED WING TESTED TO VERY HIGH LIFT COEFFICIENTS

By

J. E. Hackett
R. A. Boles

JUNE 1977

Distribution of this report is provided in the interest of information exchange. Responsibility for the contents resides in the authors or organization that prepared it.

Prepared under Contract No. NAS2-9155 by
LOCKHEED-GEORGIA COMPANY
Marietta, Georgia

for Ames Research Center

NATIONAL AERONAUTICS AND SPACE ADMINISTRATION

ORIGINAL PAGE IS
OF POOR QUALITY

CONTENTS

PRECEDING PAGE BLANK NOT FILMED

Page

LIST OF FIGURES

ORIGINAL PAGE IS
OF POOR QUALITY

LIST OF FIGURES

LIST OF FIGURES

ORIGINAL PAGE IS
OF POOR QUALITY

LIST OF FIGURES

LIST OF FIGURES

LIST OF SYMBOLS

A_{noz}	blown flap slot area
AR	aspect ratio
b	base model wing span
BLC	boundary layer control
B	tunnel span
c	nominal wing chord
C_D	drag coefficient, based on S
$\tilde{C}_D$	blown flap slot discharge coefficient
C_L	lift coefficient, based on S
C_{L_Γ}	circulation lift coefficient (lift minus vertical component of thrust)
C_ℓ	lift coefficient, based on c
C_{ℓ_h}	lift coefficient, based on h
C_m	pitching moment coefficient, based on S, about wing 1/4 c
C_p	static pressure coefficient $(p - p_o)/q$
C_I	tunnel working section area
C_μ	momentum coefficient, based on S
FRL	fuselage reference line
GP	ground plane
H	total pressure in model
h	model height above ground plane
KBF	knee-blown flap
LE	leading edge
M	Mach number
p	local static pressure

p_o	static pressure at model station
p_∞	static pressure at infinity
Q	source strength
q	dynamic pressure
q_{uc}	uncorrected dynamic pressure
RPM	revolutions per minute
S	wing area
U_∞	free-stream velocity
u	local induced longitudinal velocity
X	distance measured axially downstream from model wing 1/4 chord
Y	distance measured laterally from tunnel centerline
Y_ℓ	lower surface wing ordinate
Y_u	upper surface wing ordinate
y	distance above flap perpendicular flap upper surface
Z	distance measured vertically from tunnel floor
z	distance above wing reference plane
α	angle of attack
γ	ratio of specific heats
ΔC_{p_2}	model induced change in the mean of the upstream and downstream working section mean static pressure
ΔP	static pressure rise through the tunnel contraction section: $(H_c - p_c)$
δ	incidence correction factor
ε_s	solid blockage coefficient
ε_w	wake blockage coefficient
η	spanwise station 2y/b
ρ	air density
ω	angular velocity

SUMMARY

Ground effects experiments and large/small-tunnel interference studies were carried out on a model with a 20-inch (50.8 cm) 25-degree swept wing. The wing is slatted, has a 60-degree knee-blown flap and can be fitted with unflapped tips. A tail-rake of pitch-yaw probes can be fitted to the fuselage. Certain check tests were also made with a very similar straight-wing model tested previously.

Three-component internal balance measurements, made with a fixed ground equipped with blowing boundary layer control, were compared with datum, moving ground results. BLC requirements were determined using dial-type pressure gauges connected to ground skin friction sensors. Datum and BLC-ground results were indistinguishable up to C_L=10 at h/c=2 and up to 6 at h/c=1. At larger C_L's, BLC thickened the ground layer more significantly and pitch-down resulted on the swept wing at high angles of attack. Since this was caused by the wing tip entering the ground layer, reduced BLC span is recommended to relieve the problem.

Matched sets of center-tunnel high-lift tests were made on the swept model in the NASA/AAMRDL 7' x 10' Wind Tunnel and in the Lockheed 30" x 43" Low-Speed Wind Tunnel. Wake blockage corrections, derived from working section wall static pressures, were applied in real time to provide "corrected q" in the working section of the small tunnel. The moving ground was run routinely in that tunnel. Tests extended to extremely high C_μ's (up to 10) and three-dimensional circulation lift limits were noted. Detailed rotating vorticity meter measurements in the two tunnels showed that the reduced vortex wake penetration into the smaller tunnel was consistent with the flow correction applied during constraint corrections to angle of attack. Good comparisons were obtained between large-tunnel and corrected small-tunnel force and moment results. Anomalies in previous tests which showed "drag flip back" when the wing flow separated in the small tunnel did not recur in the present tests for either wing. This is attributed, in part, to the fact that the small tunnel test section length was increased just prior to the present tests.

Wall-pressure signatures at mid-tunnel height were measured routinely. Examples quoted demonstrate a number of model and tunnel aerodynamic effects including the occurrence of separation aft of the model. This distorted the tunnel flow and slight overcorrection for blockage resulted at very high lift. Under the most extreme conditions, but beyond C_L's of practical interest, tunnel flow breakdown occurred despite the use of the moving ground.

A copy of this document is retained in the Lockheed-Georgia Company Engineering Report files. The identifying number is LG77ER0131.

ORIGINAL PAGE IS
OF POOR QUALITY

ACKNOWLEDGEMENTS

The authors wish to offer their thanks and appreciation to the following people for their help in this program:

Gil Moorehouse and the operating staff of the AAMRDL 7' x 10' tunnel for their assistance in these tests.

Doug Lilley for data acquisition and data processing help during and after the tests at Lockheed-Georgia.

Claude V. Pierce for help in conducting the ground effects tests in the 30" x 43" tunnel.

Barbara Reagan for seemingly tireless efforts in typing and other clerical assistance.

1. INTRODUCTION

1.1 Background

The present work is part of a continuing series of NASA-sponsored studies concerning problems of low-speed wind tunnel testing, with particular emphasis on V/STOL. The earliest studies (refs. 1 to 3) dealt with powered-lift testing with the specific objective of avoiding the use of a moving-belt to simulate the motion of the ground below the aircraft during takeoff or landing. Using small-scale tests with a moving ground to establish datum results, references 2 and 3 showed that the objective can be met by the use of tangential blowing, at the tunnel floor surface, from a position somewhat forward of the model. Extensive model surface-pressure measurements confirmed that proper flow structures were set up with such ground blowing. However, no direct measurements were made of forces or moments.

For the next test series (ref. 4), a three-component sting balance was installed and a tail was added to the knee-blown-flap, straight-winged model used previously. A worst-case was created by low-mounting the tail to see whether there were serious adverse effects as it approached the ground layer at high angles of attack. Other new configurations were created by adding unflapped tips and removing tip or main-wing slats in various combinations. Lift, drag, and pitching moment measurements confirmed the promise of the earlier tests and validated most of the features of a ground blowing design study (ref. 5) for the 40' x 80' wind tunnel at NASA-Ames.

In reference 3, Hackett and Boles disclosed the results of some Lockheed-Georgia in-house studies involving a new method for wind tunnel blockage estimation. The same, knee-blown-flap model was used as for the studies above, and wing pressure distributions were again measured. The blockage estimation method, which relies upon static pressure measurements at the upstream and downstream ends of the test section, was applied to integrated pressure results during data analysis. Comparisons with "free-air" measurements, made in the Lockheed-Georgia $16\frac{1}{4} \times 23\frac{1}{4}$ ft. low speed wind tunnel, were most encouraging. In order to provide powered-model force and moment data for correlating the new blockage estimation method, the reference 4 force and moment measurements were extended to include center tunnel cases. The NASA/AAMRDL 7' x 10' tunnel was used as the free-air datum facility. In these later tests, blockage correction was implemented on-line in the small tunnel using working section pressures to to drive a simple analog circuit which displayed corrected 'q' at the tunnel console. With the exception of certain problems with separated-flow cases (which are resolved in the present report), the tests of reference 4 confirmed that the new blockage estimations worked and extended the correlation to other configurations (see above) at lift coefficients up to twenty.

As will be seen in Section 1.3, the knee-blown flap models are remarkably clean, aerodynamically, even at extreme lift. In-house work at Lockheed-Georgia revealed that the success of the above blockage studies rested heavily on this fact, since the estimation method failed to account for solid blockage or for the bubble-type of blockage encountered in heavily separated flows. To

ORIGINAL PAGE IS
OF POOR QUALITY

rectify this omission, Hackett and Wilsden (ref. 6) devised an extension of the method which uses pressures along the whole test section length at mid-tunnel height, between the end-values used previously. Solid/bubble blockage estimation turns out to be considerably more complex than solely for wakes, because an inverse, three-dimensional problem must be solved, using the whole wall pressure signature as input. Nonetheless, tests with flap plates normal to the stream (ref. 6) have demonstrated that good results are possible. Conventional, model-volume solid-blockage corrections are made in the present report, but no corrections are made of the Hackett/Wilsden type.

1.2 The Sensitive Wind Tunnel

Both of the schemes just discussed involve the use of sensors which provide feedback to tunnel controls. Because of this use of feedback, we may characterize a facility which uses it as a "sensitive wind tunnel." Figure 1.1 is a sketch which shows, approximately to scale, all of the features recommended in references 3 to 6, together with small changes indicated by the current work.

The "sensitive wind tunnel" should not be confused with the adaptive or "smart" tunnel which attempts to change the tunnel boundary to match a free-air stream-surface. It is intended that the schemes epitomized in Figure 1.1 shall be readily retrofittable to the very large number of existing fixed-wall low speed tunnels, if so desired. The feedback in the presently proposed schemes is used in a way which parallels conventional correction techniques (in the case of blockage) or which uses BLC to prevent conventional corrections from being invalidated by unwanted separations from tunnel surfaces.

Though the ground-blowing and blockage-feedback aspects of the sensitive wind tunnel were developed separately, each complements the other. For example, the ground blowing slot, installed for near-ground testing, should also be used during center-tunnel testing if the skin friction sensors (figure 1.1) so indicate. Details of these sensors, and their arrangement, are given in Figure 7.3. Conversely, if ground BLC is inadequate, or if some other surface separates elsewhere in the test section, there will be an indication of this from the wall static orifices. Examples of both kinds may be found among the test results in this report.

Though Figure 1.1 includes the most important features of a sensitive wind tunnel, others could be added. In particular, a line of pressure orifices, like that on the side wall, should be installed along the top of the tunnel for floor-mounted, half-model testing. This same row, in conjunction with the floor statics could also be used to determine angle of attack correction due to lift. The analytical methods required for this closely parallel those for blockage (ref. 6) but employ theoretical line vortices rather than line sources and sinks. Taken to the extreme, runs could be made at corrected angle of attack and true-q simultaneously, thus eliminating post-test tunnel corrections.

1.3 The Present Tests

As previously (refs. 2 and 4), the aim has been to provide the most stringent tests possible for the blockage and ground-blowing schemes, but now using a swept wing. The new wing has a lift capability which takes it well into the range where no further circulation lift can be generated by an increase in blowing, either in free air or in ground effect (see Section 7). Power would be applied in direct-lift (e.g. round jet) form well before this point in practical V/STOL designs.

Figure 1.2 shows tuft photographs of the new swept wing taken in the Ames 7' x 10' tunnel at very high blowing rates and angles of attack. The flows are evidently power-dominated, as indicated by the fact that tufts lie normal to the blowing-slot, rather than parallel to the mainstream, in the left-hand photos. The photographs also demonstrate the high degree of leading-edge protection provided by the slat: only beyond 30-degrees do significant upper-surface separations appear.

The lift and drag data added to Figure 1.2 show that the model can test the two major "sensitive tunnel" concepts under much more stringent conditions than are usually encountered.

Further details of the model and its calibration are given in Section 2, while tunnel and rig data may be found in Section 3. Sections 4, 5, and 6 all deal with wind tunnel interference studies. In Section 4, certain anomalies and omissions in previous tests with the straight wing (ref. 4) are resolved. Tests on the new, swept wing are described in Section 5. Concurrently with the straight and the swept-wing tests, wind tunnel wall pressure signatures were measured and retained for later analysis. Documentation in the present report (Section 6) will be restricted to examples which illustrate particular phenomena of interest.

The development of the on-line, ground-skin-friction sensing and feedback (Section 7) is regarded as a breakthrough in ground-blowing technology. The 'production' ground effects tests (Section 8) testify to its effectiveness. Section 9 summarizes the conclusions from both the blockage and the ground blowing studies and presents recommendations.

ORIGINAL PAGE IS
OF POOR QUALITY

2. WIND TUNNEL MODELS AND THEIR CALIBRATION

2.1 Straight- and Swept-Wing Models

Two models were used in the present work; a straight winged, knee-blown flap model tested previously (refs. 2 and 4) and a new, 25-degree swept-wing variant of the same basic design. For the new model, the flap angle was reduced from 76 degrees (upper surface), used for the straight wing, to a streamwise angle of 60 degrees. This produced decelerating forces more representative of practical approach configurations.

Figure 2.1 shows the straight-winged model, with tips removed, supported by its air supply pipe. The tailplane was not used for the present tests, but was replaced by a pitch/yaw rake (figure 2.2) in certain instances. Both this and the vortex meter will be described in Section 3. Figure 2.3 shows the assembled swept-wing model at one chord altitude during a ground-effect test.

General dimensional details, which are largely the same for both models, are given in Figure 2.4. Both wings have a span of 76.2 cm (30") with tips fitted and a tip chord of 12.78 cm (5.03"), giving a reference area of 973.8 sq. cm (1.048 sq. ft). However, tips-off reference dimensions are used throughout this report, as previously (refs. 2 and 4). These are: span, 50.8 cm (20"); chord, 10.16 cm (4"); and area 516.1 sq. cm (0.556 sq. ft). Full dimensional details are given in Table I.

Figure 2.5 gives sectional details for the straight and the swept flapped sections and for the tip section, which is the same for both wings. Except for the flap region, the airfoil section is derived from a supercritical design, thickened on the lower surface to approximately 16% total thickness. It is modified to accommodate an internal air duct and a fixed, highly deflected flap with knee blowing. The slot upper member is supported by posts at intervals along the span, giving a mean gap of .0415 cm (.0163 in.), which increases when pressurized. More of these posts were used for the swept wing because of it's aluminum, rather than steel, construction. The tip section was designed as a compromise fairing which fitted to the main wing with minimal spanwise discontinuities. Slats can be fitted separately to basic wing and to the tip extensions.

The rather deep fuselage fairing accommodates a strain gauged sting balance with a bellows-type air bridge mounted above it (see figure 2.6). Though this introduces fairly high axial loads, these oppose the chordwise component of drag and can be calibrated accurately. Internal total tubes and static orifices were used for measurement and control of slot blowing rates. C_μ values up to 6.0 were employed at a tunnel 'q' of 5 psf (239.4 N/sq.m), requiring a pressure ratio of approximately 3.2 in the plenum. Higher C_μ's were obtained at reduced tunnel speed.

The model sting was attached to an incidence quadrant mounted beneath the wind tunnel floor. Incidence was measured using an accelerometer attached to this quadrant. For ground effects testing, the quadrant, sting, and model were raised and lowered as a unit by means of a permanently installed hydraulically powered lift table. Generally similar arrangements were used in the 7' x 10' NASA/AAMRDL tunnel (see figure 2.7). At that tunnel, the model was run upright, as shown, rather than inverted as for the reference 4 tests.

2.2 Slot Momentum and Thrust Calibrations

Considerable care was necessary in these calibrations because the model slot opened somewhat under pressure and because the air bridge bellows area was not sufficiently large that dynamic tares (momentum flux) could be neglected. For the straight wing, this yielded the equation

$$\frac{A_{noz}}{S} = 0.0336 + 0.00061 \left(\frac{H}{p_o}\right) \tag{2.1}$$

where S is the without-tips reference area. The swept wing equation was similar. These blowing-slot area equations were used in conjunction with the conventional expression for momentum coefficient, namely

$$C_\mu = \gamma \tilde{C}_D M^2 \left(\frac{p_o}{q}\right) \left(\frac{A_{noz}}{S}\right) \tag{2.2}$$

where $\tilde{C}_D$ is a slot discharge coefficient, taken as 0.98 and Mach number is derived from

$$M^2 = \left(\frac{2}{\gamma-1}\right) \left\{\left(\frac{H}{p_o}\right)^{\frac{\gamma-1}{\gamma}} - 1\right\} \tag{2.3}$$

Since the varying slot area affects the axial force tare on the air bridge and because of the impact on drag measurements, a special dynamic tare calibration rig was made which replaced the model wing with a spanwise plenum with long carefully aligned holes drilled at each end. Directing the air spanwise at right angles to the balance axis and in opposite directions permitted full mass flows to be passed through the air bridge without any lift, drag, or pitching moment due to jet reaction. Bellows tares could then be directly measured by the balance at various exit areas depending upon the number of holes left open. The tares were found to be of order 5% over the exit area range of interest.

Static thrust tests showed that thrust coefficient* was closely proportional to $(H/p_\infty - 1)$ and was somewhat less than the calculated isentropic value, as is usually the case. For the straight wing, turning improved quite rapidly up to a thrust coefficient of two and asymptoted to about 68 degrees thereafter.

Further details of calibration procedures and results may be found in reference 4.

Defined as (Measured Thrust Resultant)/qS.

ORIGINAL PAGE IS
OF POOR QUALITY

3. TEST FACILITIES AND INSTRUMENTATION

3.1 The Lockheed-Georgia 30" x 43" Low Speed Wind Tunnel

The tunnel is located in the Lockheed-Georgia Company Research Laboratory. The test section nominal dimensions give a height-to-width ratio of 0.7 and a cross-sectional area of 0.832 square meters. The tunnel, shown in figures 3.1 and 3.2, utilizes a constant-speed motor running at 1200 rpm and rated at 400 horsepower. A six-foot (1.82 m) diameter fan is manually controlled via an eddy current variable speed unit.

Figure 3.1 shows the tunnel in its original configuration, as used for the tests of references 2 and 4. Prior to the present tests, a new seven-foot long (213.4 cm) test section was built — about double the original length. This permitted tunnel-wall static orifices to be installed, for blockage estimation purposes, in accordance with the recommendations of reference 6. The new test section and wall statics may be seen in figure 3.2, with dimensional details in figure 3.3.

The model was sting mounted via an internal three-component strain gauge balance. The sting is attached to a motor-driven quadrant for attitude control. Two ganged 48-port type D-3 scanivalves were used to measure model internal and supply pressures, Preston tube readings, boundary layer rake pressures, tunnel wall static pressures, and the 35 pressures of the rake of seven five-holed probes. A 50 psi transducer was used for the internal and supply pressures and a 2.5 psi transducer for all others. The low pressure readings were not all taken on every run because of space limitations on the scanivalve. Instead, the quick disconnect feature of the scanivalve pressure tube adaptor was used to switch the low pressure transducer to the appropriate group of pressure orifices for each series of runs.

The tunnel speed was maintained manually utilizing a display of corrected dynamic pressure, which is described further in Section 3.4. The mass flow through the model was initially measured with an orifice in the auxiliary air supply line. This permitted estimation of the discharge coefficient at the blown flaps at which time the orifice was removed and all subsequent measurements made on the basis of model plenum pressure. The resulting momentum coefficient, and the internal balance pressure tares associated with it, were then obtained in the manner outlined in Section 2.

The data acquisition process was fully automatic and utilized a Lockheed Electronics MAC-16 digital computer. The acquisition and reduction of the data is further described in reference 4.

3.2 The NASA/AAMRDL 7 x 10-Foot Wind Tunnel

The NASA/AAMRDL 7 x 10-foot wind tunnel is located in the NASA-Ames Research Center complex at Moffett Field, California. This tunnel is a single-return type with the settling chamber vented to atmosphere. The contraction ratio of 14 and the test section design result in a very small difference between contraction pressure drop and measured dynamic pressure at the model location for the speed range employed in the subject test. The balance, air bridge, and air supply pipe used in the small-tunnel test were retained for the test in the AAMRDL tunnel. The air supply pipe was fastened to an articulated sting as shown in Figure 2.7. The sting drive mechanism provides infinitely variable pitch and yaw capability within an approximately 40-degree cone. High-pressure air for the knee-blown flap was piped through the sting to the model air supply pipe.

The model plenum pressure was controlled from the control room by exercising direct control over the dome pressure of a large pressure regulator located in the air supply line.

The rotating vorticity meter which is evident in Figure 2.7, was mounted on a remotely controlled traverse mechanism which can position it virtually anywhere in the test section, barring mechanical interference with the model or support system.

Model internal pressures, bellows-pressures, and air supply pressures were measured using two scanivalves with ±50 psi transducers. Additionally, the specific model plenum and air line pressures used to compute model C_μ and and pressure tares, respectively, were monitored separately using individual ±50 psid Statham transducers. The flap rake pressure data were measured using two additonal scanivalves with ±2.5 psid transducers.

Test section dynamic pressure was calibrated prior to model entry using a precision pitot tube and two ±0.15 psid Statham pressure transducers supplied by Lockheed. These transducers were also used to monitor and record the tunnel contraction pressures during the test.

A twelve-channel data system was used to automatically record balance output, model internal pressures, tunnel conditions, and rake scanivalve information, and angle of attack. Vorticity meter position data were input manually. All of the data were displayed continuously in the control room

Preliminary, on-line reduced data were available throughout the test. The basic data were also recorded on IBM cards, providing a method for correcting and updating the data prior to final reduction.

3.3 Ground-Plane Configurations

Four ground-plane configurations were available in the 30" x 43" wind tunnel test section: the normal solid floor, a moving-belt ground plane (figure 3.4), and two types of tangentially-blown, boundary-layer-controlled

ORIGINAL PAGE IS
OF POOR QUALITY

floor (figures 3.5 and 3.6). Dimensional details may be found in figure 3.3. Configuration change is accomplished in about eight hours.

The moving-ground (figure 3.4) spans 76.2 cm (30 inches) of the 109.2 cm (43-inch) test section width and has an effective length of 88.7 cm (34.9 inches) between roller centers. The belt is powered by a hydraulic motor rated at approximately 20 H.P., which is adequate up to more than 30.5 m/sec (100 ft/sec). The belt speed, which is continuously variable, is monitored via the voltage output of a "Globe" DC motor, coupled to the nondriven roller and used as a tachogenerator. The belt speed was maintained at the free-stream velocity of the test section for all moving ground tests. Calibration was made using a pulse counter and a digital voltmeter.

Tracking of the belt is monitored and adjusted manually. Tension adjustments are made at one end of the nondriven roller, the other end being permanently set. Principal adjustments are found to be necessary during startup and shutdown, though some changes have to be made when model lift is increased under near-to-ground conditions. Significant increases in power are usually required in these circumstances.

The boundary layer controlled ground plane configurations are variants of the original multiple-slot device used in the tests of references 2 and 4. From previous tests, an optimum slot position/height combination was chosen for the main, continuous slot test runs. This unswept slot, shown in figure 3.5, is sized and located as indicated in figure 3.3.

The second BLC ground configuration employs multiple nozzles, spaced at regular intervals across the test section (see Figure 3.6). In order to allow the individual jets, which are inclined slightly downwards, to attach and spread they are situated some distance upstream of the continuous slot position. The nozzle area, per unit tunnel width, is approximately half that for the continuous slot and high, subsonic blowing velocities may be used. The general design is copied from a system in use in the Lockheed-Georgia 23' x 16' Low Speed Wind Tunnel, though it proved unfeasible to scale that system directly to the small tunnel size.

The BLC ground plane skin friction instrumentation used in previous tests (references 2 and 4) was again used, though some tubes had become unserviceable. Dimensional details and operational procedures are described in Section 7.

3.4 Test Section Flow Calibration and Control in the 30" x 43" Tunnel

The tunnel calibration and control procedures used in the current tests were identical to those used in reference 4, but will be repeated here in abridged form.

Differing test-section speed-control procedures were followed for ground effects and for tunnel interference studies. Since no corrections were desired in the former case and comparisons were being made in the same tunnel, a

conventional contraction pressure-drop type of calibration was employed, based upon a center-tunnel calibration using a 5/8-inch pitot static probe and a precision water manometer.

For center-tunnel testing, strong blockage effects were expected, and it was highly desirable to correct for these in real time, both to permit testing at "whole" C_μ's and thereby avoid cross-plotting during data reduction and also because comparisons were to be made with another tunnel of larger size.

The method used is an automatic version of the wake blockage correction method devised by Hackett and Boles (reference 3). A full explanation of the setup and calibration of the system may be found in reference 4. Contraction pressures were measured using two ±0.7 psid pressure transducers. One transducer was connected across the upstream and downstream contraction pressure rings to measure contraction pressure drop in the conventional manner; the other was connected to the upstream piezometer ring. The second transducer, which would normally be vented to atmosphere, was referenced to the test section static orifice located at the 0.485B station (figure 3.3). This was done for consistency with the previous tests which were run in the unmodified test section with the breather slot at this location.

A voltage divider network (ref. 4) is arranged so that the mean of the model-induced static pressure change between the contraction downstream reference pressure and the 0.485B orifice pressure is "seen" by the system as the reference static pressure, which defines 'q'. Suitable differencing with the contraction upstream static pressure then permits a blockage-corrected 'q' to be displayed for use in tunnel control, which is manual.

3.5 Procedures for Tunnel Constraint Tests

In the tunnel-constraint tests, the configurations were the same and the procedures were very similar in both large and small tunnels.

Both test sections were calibrated prior to the respective tests using a precision pitot tube and pressure transducers supplied by Lockheed. Tunnel conditions and model plenum pressure were closely monitored during the tests. On-line data reduction in the large tunnel facilitated the monitoring operation by providing immediate print-out of computed momentum coefficient. The normal procedure was to repeat points in which dynamic pressure or momentum coefficient fell outside specified tolerances. On-line data reduction was not available during the small-tunnel test. Limited print-out of the raw data was available, however; and frequent checks of model plenum pressure were made using a hand-held calculator. The automatic C_μ system employed in the small tunnel provided real time monitoring of corrected dynamic pressure. Because of the extreme lift range of tests (C_L up to 19), a moving belt ground plane moving at free-stream velocity was used during the small tunnel tests to prevent separation.

The basic procedure for the center tunnel tests was as follows:

ORIGINAL PAGE IS
OF POOR QUALITY

1. Perform force tests on various model configurations in the small tunnel using the "corrected-q" technique described in Section 3.4.

2. Repeat selected runs with the pitch/yaw rake fitted at the tailplane position.

3. Carry out rotating vorticity-meter traverses so as to determine the locations of flap and tip trailing vortex centers.

4. Duplicate 1 and 3, above, in the large tunnel, making no corrections (assuming data to be recorded under "free-air" conditions).

5. Compare fully-corrected small-tunnel data with the uncorrected large-tunnel data. The results of this comparison may be found in Sections 4 and 5.

To determine if either the model or the instrumentation or the procedures had changed, certain reference 4 tests on the straight wing model were repeated in both the 30" x 43" tunnel and in the 7' x 10' tunnel. Limited additional tests were carried out in connection with anomalous drag results obtained in the small tunnel when the main wing separated. For this purpose, a rake of total pressure tubes was fitted, parallel to the flap upper surface, at the trailing edge location. The results are discussed in Section 4.3.

The straight wing configurations tested were the no-tips condition with slat (configuration A1) and the no-tips condition with the slat removed (configuration F). The swept wing configurations tested were the no-tips condition with slat (configuration SA1) and the with-tips condition with slat (configuration SB).

3.6 Procedures for Ground Effects Tests

Ground effects tests were carried out on the swept wing without and with tips fitted, with the slats fitted at all times. As mentioned above, certain runs were repeated with a tail rake fitted which replaced the tailplane previously used. Heights-above-ground of one- and two-chords were employed, measured to the main-wing quarter-chord point at the wing root. Since the tests were intended for a "one-on-one" comparison within a single facility, they were run on a contraction pressure-drop basis rather than using on-line q-correction. Any q-changes induced by the ground BLC system were thereby debited to it in the force and moment results.

The velocity of the moving ground was controlled by manually adjusting the flow of fluid to the hydraulic motor powering the downstream pully. Speed was monitored by visual observation of the voltage output of a DC Globe motor attached to the shaft of the upstream pulley. The DC motor was previously calibrated in volts/RPM. Belt speed was then calculated using the DC motor output (RPM) and the measured diameter of the pulley.

The floor blowing rates were calibrated, set, and monitored using a 76 cm (30-inch) water manometer attached to the floor blowing plenum. With the

multiple nozzles in use, which required a greater blowing pressure, a dial-type gauge was substituted for the water manometer. The flow distribution from the floor blowing slot was surveyed using a hand-held total pressure tube. Flow distribution was determined to be constant except for small regions (approximately 0.635 cm ~ .25 inches wide) immediately downstream of the slot spacers.

After carrying out datum, moving-ground tests over a matrix of α and C_μ combinations (varying α at fixed values of C_μ), one of two procedures was followed. Procedure 'A', which was a repeat of that used in reference 4, relied upon the use of measured lift coefficients in combination with a calibration in terms of the parameter $C_L(c/h)$. Procedure 'B' has several variants (see Section 7), all of which rely on a feedback of ground skin friction indications. Tests using Procedure 'A' were regarded as a backup, since the eventual success of Procedure 'B' was not predictable at the outset.

3.7 Data Accuracy

It is difficult to evaluate the absolute accuracy of test data because of unsteady test conditions, calibration errors, and unknown flow anomalies. Throughout these tests, the effects of unsteady flow conditions were minimized by multiple sampling and averaging of data. Calibrations of the strain gage instrumentation were done with utmost care and it is felt that the calibration data are accurate to within one percent of the applied load for pressure transducers and one percent of rated load for the internal balance.

Both tunnels were calibrated immediately prior to each test with the appropriate model support mechanism in place. The same pitot-static tube and pressure transducers were used for the calibration and tests. The effects of unknown wind tunnel flow anomalies should be minimal for comparisons within a test set-up since the same anomalies apply to all runs. Where comparisons between the two tunnels are made, there may be small differences due to flow angles or turbulence. It is felt that, once all due care has been taken in data averaging and calibration technique, the best indicator of data accuracy (especially for comparisons within a task) is data repeatability. Analysis of repeat points throughout these tests show repeatability of data to be within the following limits.

C_L ~ ±0.20
C_D ~ ±0.20
C_m ~ ±0.50
C_p ~ ±0.02 (wall pressures)
C_μ ~ ±0.06

Examination of the results presented herein shows a quality of data which is generally better than what might be expected from the above repeatability figures. It is felt that the results and conclusions of this document are not compromised in any significant way by data scatter or repeatability.

ORIGINAL PAGE IS
OF POOR QUALITY

4. WIND TUNNEL INTERFERENCE STUDIES: STRAIGHT-WING MODEL

4.1 Introduction

Despite the fact that the major objectives of the present tests concern the extension of the tunnel constraint correlations to swept wings, limited further tests on the straight wing were felt to be needed. This was largely because the reference 4 tests revealed a radical and unexplained drag change, in the small tunnel, which occurred at higher C_μ's when the wing flow separated. On the drag polar, the effect was to move the high C_μ curves bodily (in some cases) from the right side (drag) to the left side (thrust) of the lift axis. This gave rise to the descriptor "drag flip back."

Section 4.2 examines first the general repeatability of the tests described in reference 4, in the light of several model-related and tunnel modifications, and then examines the 'drag flip back' phenomenon. Blown-flap total pressure rake measurements, aimed at shedding light on the 'flip-back' question, are described in Section 4.3.

The equations used to correct the small tunnel data for blockage and tunnel-induced angle-of-attack effects are presented in Section 4.4, together with an example of their application. Finally, in Section 4.5, a complete set of force/moment runs with the basic straight wing is described with and without slats fitted. These new results for the two-tunnel comparison supplement the data of reference 4.

4.2 Repeatability checks

Because of changes to the small tunnel, the first level of repeatability check must concern 7' x 10 tunnel results. Figure 4.1 shows sets of lift curves measured in 1975 (open points) and during the present, 1977, test series (filled points). Though the general trends are repeated very faithfully in the 1977 curves, there is a small incremental decrease in the lift at any particular value of C_μ. Some limited changes were made to the model and data handling in the interim (new, larger air-bridge bellows; modified balance matrix), but there is no obvious reason for this loss in performance.

At the lower C_μ's, the current tests show a later stall. In this regime, flap separation precedes main-wing separation (see Section 4.3), and it may be concluded that the flap flow is more firmly attached in the present test series. Flap surface flow observations in the present tests showed multiple turbulent wedges, in otherwise laminar flow, which had origins roughly one-third of the way around the flap radius. It is not known whether these were present in earlier tests when the (newer) model was undoubtedly aerodynamically cleaner but, if they were absent then, the flap would have been more prone to laminar separation.

Figure 4.2 shows the 1975 and 1977 (stretched working section) lift curves measured in the 30" x 43" wind tunnel. The differences between these sets of curves include not only the above effects, but also the consequences of the tunnel modification. These, slats-on, results have never exhibited the 'flip-back' phenomenon in the drag polar [see reference 4, figure 5.2(b)]. However, comparison with Figure 4.1 shows that C_μ-dependent lift changes have been introduced in the smaller tunnel. Inspection of the tunnel-wall pressure signatures (Section 6) suggests that the downstream reference pressure is probably lower in relation to that at the model position in the present tests than it was previously: as a consequence of the test section extension. This appears to have caused a small degree of over-correction for blockage. Changes in the downstream pressure characteristics, with C_μ, are such as to cause an increasing amount of over-correction at the higher C_μ's. The large-tunnel later-stall, characteristic of the current tests (see above), was repeated in the small tunnel.

Figure 4.3(a) repeats a reference 4 figure and shows the 'drag flip-back' phenomenon which occurred in 1975 with slats-off and during other tests in which there was wing leading edge separation. However, Figure 4.3(b) shows that 'flip-back' did not recur in the present tests. The reason for this has not been established conclusively. However, a number of factors suggest the reference 4 hypothesis, that flap separation caused drag flip-back, is correct. The fact that the flap flow is more firmly attached in the present tests has already been discussed. In addition, the presence of the diffuser very closely aft of the model in the 1975 tests could have raised the trailing edge pressure (in relation to the present tests) and thereby increased the likelihood of flap separation.

The occurrence of 'drag flip-back' in the previous test series may have been due, in part, to too-short a test section. A need to check blown-flaps for unrepresentative laminar separations has also been demonstrated.

4.3 Flap Rake and Stall Studies

The significance of the flap rake studies was diluted by the fact that drag 'flip-back' did not occur in the present tests. Nonetheless, comprehensive data were obtained with the flap rake over the test ranges of C_μ and angle of attack. These have proved useful in identifying flap and wing stall conditions at the 70% semispan station. Only typical profiles will be presented.

Figure 4.4(a) shows flap rake profiles measured in the 7' x 10' and 30" x 43" tunnels, at $C_\mu = 1$, for increasing angles of attack. The profiles have the usual wall-jet shape up to 20 degrees. However, at $\alpha = 25.8$ degrees the profile in the small tunnel has collapsed and negative C_p's are indicated by the upper tubes of the rake, indicating wing separation. In the large tunnel, the corresponding profile remained much the same as at lower angles and only at almost 40 degrees was the profile comparable with the small tunnel 25-degree case. This illustrates a difference between the two tunnels in the angle of attack for wing separation.

ORIGINAL PAGE IS
OF POOR QUALITY

Figure 4.4(b) shows profiles taken at the same flap C_μ, but with the wing leading edge slat removed. At the lower angles of attack, the profiles are little altered by slat removal. However, at approximately 12 degrees, a lower energy layer develops next to the flap surface in both tunnels. By 18-degrees both profiles have collapsed and are comparable with the previous 25.8 and 39.7 degree cases in the small and large tunnels, respectively.

Figure 4.5 was prepared from a large number of plots like Figures 4.4, analyzed to determine conditions for flap and wing separation. The trends are very similar to those given in Figure 4.12 of reference 4, which were based upon wool-tuft observations. Up to C_μ's in the 1 to 2 range, slat on, the flap separated first [i.e. as in Figure 4.4(b)]. Beyond this, wing separation was the first event and flap separation lagged (in α) by an increasing amount as C_μ increased. Separation invariably occurred earlier (slat-on) in the smaller tunnel. The general trends were similar with the slat removed, though the stall occurred earlier. However, in this case, it was in the large tunnel that the stall occurred first.

4.4 Wind Tunnel Correction Equations and Their Application

Hackett and Boles (ref. 3) quote the following equations which include both image constraint and blockage effects.

$$\Delta\alpha = \frac{\delta}{1 + 2\ C_\mu/\pi AR}\left(\frac{S}{C_1}\right) C_L \tag{4.1}$$

$$\Delta C_L = C_L\ \tfrac{1}{2}\Delta C_{p_2} - C_D\ \Delta\alpha \tag{4.2}$$

$$\Delta C_D = C_D\ \tfrac{1}{2}\Delta C_{p_2} + C_L\ \Delta\alpha \tag{4.3}$$

$$\Delta C_\mu = C_\mu\ \tfrac{1}{2}\Delta C_{p_2} \tag{4.4}$$

where δ is the conventional incidence correction factor commonly applied without the denominator in Equation (4.1). S/C_1 is the ratio of model reference area to tunnel cross-sectional area. The denominator term in (4.1) is suggested by Williams and Butler (ref. 7) and provides correction for tunnel-induced increases in jet-sheet curvature. Though reference 7 also suggests related corrections to C_μ, these make linear assumptions about angles which are violated in the present experiments and unreasonable corrections are obtained.

The $C_D\Delta\alpha$ term in Equation (4.2) is frequently discarded. However, both C_D and $\Delta\alpha$ can be quite large in the present experiments and their product cannot be ignored.

The quantity $(\frac{1}{2}\Delta C_{p_2})$ in Equations (4.2) to (4.4) is the deviation, due to tunnel blockage, of the dynamic pressure from its nominal (i.e. contraction-pressure-drop) value. As blockage, and thus ΔC_{p_2}, increases with C_μ or α, the

the tunnel fan speed must be reduced when the 'q-pot', true-q system is in operation (see Sections 3.4 and 3.5). 'Production' runs are carried out at constant C_μ with α varying. Figures 4.6 show that, at the lower C_μ values, the tunnel speed adjustments are quite small as α is increased. At the higher C_μ values, however, very substantial reductions in speed control setting are required during a particular run.

Since compensation for tunnel blockage is automatically provided on-line with the true-q system in operation, the ΔC_{p_2} terms in Equations (4.2) to (4.4) are eliminated, leaving

$$\Delta C_L = - C_D \Delta\alpha \tag{4.5}$$

$$\Delta C_D = + C_L \Delta\alpha \tag{4.6}$$

and

$$\Delta C_\mu = 0. \tag{4.7}$$

The ability to hold constant C_μ [Equation (4.7)] is the chief attraction of the 'true-q' system.

The diamond-shaped points in Figure 4.7 show some typical straight-wing results in the "raw" state (based on contraction-pressure drop 'q'). The triangles show the same data after correction for blockage and the circles also include corrections for tunnel-induced $\Delta\alpha$. A reduced number of points has been plotted, in order that the successive stages of correction may be identified for each data point.

The $C_\mu = 10$ case, in Figure 4.7, is extreme and it will be seen later that, although the very large blockage corrections improve the agreement with large-tunnel data (Section 4.5), profound changes have occurred in the test section, despite the use of a moving ground, which are reflected in the tunnel wall pressure signatures (see Section 6). Tests in this regime are of doubtful value. At medium C_μ's, blockage-correction reduces the lift coefficient quite significantly and causes some reduction in lift curve slope. During 'production' testing, this part of the correction is, of course, achieved via tunnel speed adjustment (see figure 4.1).

It is interesting to note that, at $C_\mu = 6$ for example, a linear lift characteristic with α is converted to a peaking curve by the correction process. Comparisons with large-tunnel data (Section 4.5) will show that this is correct.

4.5 Large/Small Tunnel Force and Moment Comparisons (Straight Wing Model)

Figures 4.8(a), (b), and (c) show respectively the lift curve, the drag polar and pitching moment characteristics for the straight wing (slat-on) at various C_μ levels up to ten. The good agreement between the corrected small-

ORIGINAL PAGE IS
OF POOR QUALITY

tunnel and the large-tunnel data is comparable to that reported in reference 4 except at $C_\mu = 10$, where the previous agreement was better. Overcorrection for blockage again occurred at the higher angles of attack at this C_μ. It has already been noted that the small tunnel conditions are so distorted at this C_μ that any degree of agreement is surprising.

The drag polars from the two tunnels agree well [Figure 4.8(b)] except at $C_\mu = 10$. However, there is a systematic pitch-down tendency in the small tunnel at intermediate C_μ values. The reason for this cannot be firmly established, however, there is a possibility that tunnel-induced changes in jet-sheet trajectory [i.e. beyond those included via Equation (4.1)] were responsible. As the sheet straightens out, at higher C_μ's, the effects at the model diminish.

Figures 4.9 show that the agreement between tunnels, with the slat removed from the basic wing, was at least as good as with it on. In Figure 4.9(a) the familiar early stall break at $C_\mu = 10$ is followed by a recovery and there is surprising agreement at high α. At lower C_μ's the two-tunnel agreement in the stall characteristic is remarkably good.

In contrast to the corresponding Reference 4 result, which displayed the "drag flip-back" phenomenon, the small- and large-tunnel drag polars agree well in Figure 4.9(b). Possible reasons for this were discussed in Section 4.1.

In Figure 4.9(c), pitching moment agreement between tunnels follows the slat-on trends at low α, but exhibits post-stall scatter with stronger fluctuations in the smaller tunnel. This is undoubtedly due to rough flow associated with the combination of wing separation and jet impingement on the tunnel floor.

5. WIND TUNNEL INTERFERENCE STUDIES: SWEPT WING MODEL

5.1 Trailing Vortex Position

The general comments made in reference 4 concerning wing aerodynamics and the relation to limit-lift in three dimensions also apply equally to the present tests and will not be repeated here. However, certain open items in the previous trailing vortex position data, notably the lack of high-C_μ small tunnel data and an unexplained lateral drift, have been resolved in the present tests, but using the swept wing.

In the interest of reducing test and analysis time, traverses were made with a rotating velocity meter (see Figures 2.2 and 2.7) rather than the previous rake of pitch/yaw probes. This also removed over-ranging problems and made the vortex centers more obvious because vorticity itself, rather than flow angle, was indicated. Figure 5.1 shows contours of vorticity-meter RPM for a relatively low C_μ case. At higher C_μ's the kidney-shaped high-RPM contour in the flap vortex developed into an annular ridge of high vorticity, with lower vorticity at the vortex core. It is not known whether this is a genuine result-indicating a burst vortex — or a consequence of instrument interference with the vortex. It is immaterial which is the case, since it is the comparison between tunnels which is important.

Figure 5.2 shows vortex center positions for various C_μ-values in both large and small wind tunnels. These have been derived from a number of plots like Figure 5.1. Because of the complexities near the core, the centers shown in Figure 5.2 were derived from the outer RPM contours. The x/c value in Figure 5.2 is greater than the corresponding reference 4 value, but both traverse planes are the same distance aft of the wing tip of the basic configuration (A in Figure 5.2). In comparing with reference 4, it must be remembered that the present results include the effects of sweep together with a lower flap angle.

As previously (ref. 4), there is less downward penetration of the flap vortex in the small tunnel, at any given C_μ. With the tips off (configuration A), this is accompanied by reduced inboard movement from the flap-end. This may be a swept-wing effect which reflects the influence of bound vortex-induced spanwise flow acting on a vortex with reduced penetration. With the tips added, the flap vortex penetration is increased and the small tunnel vortex positions at lower C_μ's are now on the same locus as the large tunnel positions, but at lessened penetration. At $C_\mu = 4$, small tunnel floor-image effects have caused some outboard drift of the flap vortex.

The tip vortex is lower and further outboard for the swept wing than for the straight wing. This is because the traverse plane is closer to the physical tip than previously, due to sweep. There are no systematic differences between the tip vortex positions measured in the large and small tunnels.

ORIGINAL PAGE IS
OF POOR QUALITY

There are some differences between the previous (straight-wing) and the present (swept-wing) results but these concern only details: the overall conclusions are the same. The vortex wake at the tail plane position is almost identical in the two tunnels. Most of the observed small-tunnel reduction in vortex penetration is accounted for when correcting for tunnel-image-induced flow rotation. What remains is unlikely to have measurable effect.

5.2 Large/Small Tunnel Force and Moment Comparisons (Swept-Wing Model)

Figure 5.3(a) shows excellent agreement between lift measurements in large and small tunnels at the lower C_μ's, including faithful reproduction of the stall. At high C_μ, high-α combinations the current correction methods again overestimate blockage (see Section 4.2) and the corrected small tunnel $C_L - \alpha$ curves drop away from those for the large tunnel. However, in the up-to-ten C_L range of greatest interest, this effect is not serious.

The drag and pitching moment results [Figure 5.3(b) and 5.3(c)] reflect the trends just discussed. The two-tunnel agreement in pitching moment is particularly impressive.

On adding tips [Figures 5.4(a), (b), and (c)] the above trends are largely repeated. The $C_\mu = 10$ break in the small- tunnel lift curve is more extreme; but as mentioned earlier, good results should not be expected here because of the extreme disturbance to the tunnel. There was evidently a bad run for $C_\mu = 2.0$, though the stall is well reproduced in the small tunnel.

It is interesting to note that, while the addition of tips increases $C_{L_{max}}$ from 2.2 to only 2.6 at $C_\mu = 0$, there is an increase from 8.1 to 10.6 at $C_\mu = 2$ and from 18.9 to 21.6 at $C_\mu = 10$. It appears, from the latter two cases, that there is a limit of about 2.5 in the lift obtainable on adding the tip. [All coefficients in this report employ the plain-wing (no tips) reference span.]

The success of the above two-tunnel comparisons rests heavily on the use of a moving ground in the small tunnel during high C_μ tests. The observed differences are, in a large part, due to its inadequate downstream length for center-tunnel testing. With improved tunnel floor flow control and slight refinement to the blockage correction procedures, most of the remaining differences could probably be eliminated.

6. WIND TUNNEL WALL PRESSURES SIGNATURES

6.1 Background

Blockage correction, in the two previous sections, was limited to the removal of wake-blockage effects via the use of side-wall pressure measurements upstream and downstream of the model. As has already been recognized (reference 3) the success of these corrections rests heavily on the fact that the present model is aerodynamically "clean," even at extreme lift, and significant bubble-type separations are generally absent.

In their AGARD paper (ref. 6), Hackett and Wilsden demonstrated the feasibility of extending the method to include solid blockage estimation. Since solid blockage is a local effect, wind tunnel wall pressures are required in the region opposite to the model position as well as the test section entry and exit. Figure 3.3 shows the distribution of pressure orifices along the test section walls.

Figure 6.1 is a schematic, taken from reference 6, which shows tunnel wall super-velocities and effective model shape with both solid/bubble and wake blockage present. An array of sources and sinks is also shown which generates the same pressure signature as the model itself and which therefore may replace the model for blockage estimation purposes. Reference 6 describes how this is achieved and also points out the need for a relatively long test section so that the wake blockage asymptote can be found with adequate accuracy.

The fact that the current swept-wing tests include large and small tunnel force and moment data, provided an opportunity to gather definitive powered-model data under extreme conditions; to be used in later analyses. This objective was attained. The data are voluminous, so only samples will be presented in this report, selected to demonstrate important effects and trends. As will be seen below, the wall pressure measurements confirmed some expected trends and also showed that certain phenomena are more important than had been suspected previously.

Unless stated otherwise, all of the results quoted were taken with the moving ground in operation.

6.2 Datum Cases

Figure 6.2 shows that, at low to moderate C_μ values, the tunnel wall pressure signatures reflect very little solid blockage, showing the monotonic decrease in pressure, along the test section, which characterizes purely wake blockage. It is the predominance of this type of characteristic, across the spectrum of model configurations and test conditions, which leads to the successful correlations between large and small tunnels, described in Sections 4 and 5.

ORIGINAL PAGE IS
OF POOR QUALITY

At $C_\mu = 4$ (figure 6.2, lower) new features emerge. Just aft of the model (arrow) a mild suction peak is seen, followed by a large peak which will be discussed in subsection 6.4. The fact that the first peak lies just aft of the model position suggests either that entrainment into the blowing jet, aft of the model, has become important or bubble-type separation has occurred from the wing. Tuft and flap-rake studies rule out the latter possibility. It is pointed out that the specific cause of any particular feature observed in the wall pressure signatures is immaterial when determining tunnel blockage.

6.3 Effects of Model Configuration

Figure 6.3 (upper) shows a case where a suction peak just aft of the model may be identified positively with wing leading edge separation, since the angle of attack was 29 degrees and the slat was absent. Comparison may also be made with the slat-on case. The increased scatter of the slat-off data is characteristic of separated flow. What is perhaps the most remarkable feature of the comparison is the wide difference in lift level and in drag level for the two curves. It is apparent that blockage is quite similar for the two cases — a fact which probably would not emerge from conventional blockage calculations.

Figure 6.3 (lower) shows the effect of adding the unflapped tip extensions to the basic model. After allowing for a shift in tunnel pressure level, it is observed that wake blockage is not changed noticeably on adding tips, but the first suction peak is raised by about 0.05. The reasons for these changes are not known.

Figure 6.4 shows comparisons between unswept and swept wing knee-blown flap models, tested at the high C_μ. In addition to the sweep effect, the fact that the flap upper surface angle was reduced to 60-degrees on the swept wing (straight wing: 76 degrees) is of major importance. The combined effect is to reduce the severity of tunnel wall and floor conditions imposed by the swept-wing model. The floor separation is later (only partially due to sweep) and the height of the second suction peak is less.

6.4 Tunnel Flow Control

In the vicinity of $x/B = 1$, working plots of tunnel wall C_p versus α for a given model C_μ's showed rapid changes in slope as the second suction peak started to emerge. Checks against a fixed ground impingement curve, derived from tuft studies (reference 4) showed strong correlation with this change in slope, despite the fact that a moving ground was employed in the present tests. The moving ground ends at $x/B = 0.39$. Up to this point, there is good pressure recovery from the first suction peak for all curves except $C_\mu = 1.0$ (figure 6.5). Just aft of the downstream end of the moving ground, there appears to be either a separation or rapid thickening of the ground layer, which causes the second suction peak.

Figure 6.6 explores the phenomenon further by comparing wall pressure signatures for a fixed ground, a moving ground and ground blowing BLC. The ground BLC setting was determined from skin friction measurements, monitored on-line. Ground blowing was increased until all skin friction indications were zero or greater. After shifting the curves to a common upstream pressure datum, it was found that moving and blown grounds both shifted the premature, fixed-ground separation downstream by about the same amount. The fixed-ground suction peak near the model was reduced successively by moving and BLC ground treatment.

Figure 6.7 shows the effect of increasing the amount of ground blowing. For these particular tests, multiple nozzle rather than continuous slot blowing BLC was employed. The $H/p = 1$ case infers a small amount of boundary layer control because air at mainstream total pressure was ejected into the boundary layer. As H/p is increased, it is evident that the separation point is pushed back. The height of the first suction peak is also reduced and, at $H/p = 1.40$ ($C_{\mu_{ground}} = 1.2$), this peak is virtually absent.

Casual consideration might suggest that, in achieving an almost-zero pressure gradient along the wind tunnel wall, the higher blowing rates in Figure 6.7 produced ideal test conditions. However, the target pressure distribution is that which exists in free air, which probably will not be flat. It is therefore possible that excessive ground BLC will, in itself, over-correct for tunnel blockage.

To minimize the risk of ground boundary layer control having the above adverse effects, ground blowing should be applied ahead of impingement at a point just upstream of separation. The amount of control applied may be determined with the help of ground skin friction meters using the techniques as for ground-effects testing described in Sections 7 and 8. Check calibrations, tunnel empty, should also be made at the model position, with the ground blowing set at a typical rate.

6.5 Discussion

A full discussion of the consequences of ground impingement and the attendant tunnel pressure changes is beyond the scope of the present work. However, an attempt will be made to place the results in perspective.

Following conventional practice, we may characterize the major tunnel flow events in terms of the parameter $C_L(c/h)$. The present tests yield the following values, which may be used for guidance

	$C_L \frac{c}{h}$	Present Test C_L	Limit For
Impingement Starts	2	7.5	Fixed Ground
Second Peak Dominant	3	11.25	Ground BLC
Catastropic Breakdown	4	15.0	All Testing

ORIGINAL PAGE IS
OF POOR QUALITY

For the present models, which have a powered span of about half the tunnel width, the above C_L-values lie at the top of or beyond the normally accepted STOL range. Tests beyond $C_L = 10$ must be considered academic in this regard but nontheless have demonstrated that blockage corrections are feasible in this regime. However, the fact that results in the "catastropic breakdown" range were corrected successfully must be considered fortuitous.

Because of symmetry, among other considerations, the Reference 6 blockage estimation methods should not be extended to treat the second peak. If circumstances dictate that testing shall be carried out well into the impingement range, some form of ground BLC is mandatory.

7. GROUND EFFECTS EXPERIMENTS: INTRODUCTION

7.1 Model/Ground Interactions

As an aircraft on approach descends into ground effect, it becomes influenced by the images in the ground plane of its trailing and bound vortex systems. At first, the influence of the trailing vortex image is dominant and this produces upwash ("ground cushion") at the aircraft. However, this positive ground effect is replaced by a negative one ("suckdown") at lower altitudes if the aircraft lift coefficient is sufficiently large. The lift loss is caused by counter-velocities induced by the bound vortex image. Figure 7.1 illustrates this degradation for the swept KBF model shown in Figure 2.3. The closeness of the bound vortex system to the ground at $h/c = 1$ is illustrated in Figure 7.2.

It has been realized for some time that the above effects are distorted in the wind tunnel if a fixed ground is used. Boundary layer separation from the ground occurs prematurely and adverse ground effects are magnified (see References 2 and 3). Though a belt-type moving ground prevents this in small tunnels, moving-ground logistical and operational problems are formidable for large tunnels.

Ground boundary layer control is an obvious alternative to a moving ground. Early studies (ref. 1) showed that tangential blowing rather than boundary layer suction provides appropriate flow conditions near to the ground surface. Only tangential blowing BLC can provide sufficient total pressure to establish the correct chordwise positions for the stagnation points beneath high-lift, powered models when tested close to the ground.

Moving and blowing BLC ground tests were carried out in 1972 on the unswept knee-blown flap model described in Section 2 (see reference 2). Sectional pressure plots comfirmed that proper flow structure (as compared with moving ground results) could be established between the model and the ground by ground-blowing BLC. The work was also extended to a round-jet VTOL model. A new fuselage containing a three-component sting balance and air bridge (see figures 2.1 and 2.6) was fitted to the unswept jet-flapped wing in 1975. Comparisons of force and moment measurements between moving and BLC grounds confirmed that ground boundary layer control gave a proper simulation at least with regard to model lift and drag (see reference 4). However, the situation regarding pitching moment was obscured somewhat by tailplane stall problems.

Against the above background, and recognizing the need to test a configuration more representative of a practical design, the following major objectives were defined for the present test series:

- Check out the application of ground blowing BLC in ground effect tests on a high-lift, swept wing design (see figures 2.2 to 2.4). In particular, determine whether swept-wing pitching moments are correctly reproduced.

ORIGINAL PAGE IS
OF POOR QUALITY

- Devise a method for relating ground-blowing requirements to local conditions at the ground, rather than to model lift and height, as previously (see Section 7.2).

- Use flow measurements at the tail position, rather than tail-on/tail-off moment comparisons, to determine any differences between blowing BLC and moving ground flow characteristics in the tailplane region (see Section 7.3).

- Check out the use of an operationally simple, higher-pressure, multiple-nozzle scheme (see Figure 3.6) as an alternate to the standard continuous slot (see Section 8.4).

7.2 Ground Blowing Requirements

In previous tests, ground blowing requirements were established on the basis of a lift parameter $C_L(c/h)$, which, in effect, nondimensionalizes lift using the area between the wing and the ground, normal to the mainstream. For a given sweep and span load shape, this parameter also defines the ground pressure distribution and thereby the pressure gradients which the boundary layer must overcome. To this extent, the method is soundly based and has proved useful for system design purposes and in application to a particular class of models. However, there is no obvious way of extending this technology to unusual configurations, other than by carrying out small-scale checks with moving and BLC ground configurations.

The above shortcomings were recognized in the previous test series. Some attempts were therefore made to use ground conditions directly by employing firstly boundary layer rake readings and, later, skin friction meter readings to determine ground BLC settings. Practical problems made these approaches appear unpromising at the time of the reference 4 tests. However, retrospective analysis of the skin friction data showed that, with better on-line pressure instrumentation, this method might be feasible.

Figure 7.4 shows an array of center-zero differential pressure meters connected to the skin friction gauges mapped in Figure 7.3. A reading to the left shows a total tube pressure below static, i.e. separated flow. The fact that dials 8 and 13 through 17 read negatively in the upper photograph shows that an extensive separation region is present with a fixed ground. Application of BLC (lower photo) "pegs" the early dials on the positive side (because of the BLC blowing) and, after "fine tuning," places the most critical gauges (i.e. 14 to 17) at or near to zero. This condition (i.e. all gauges positive or zero) is used to define the amount of ground blowing required. Other criteria, based on the same array of readings, were also tried. These will be discussed in Section 8.

In addition to monitoring the skin friction via the dial gauges, a scanivalve hook-up was also used to obtain a permanent record. Lags due to large dial-gauge internal volume made impractical the simultaneous use of both

systems. Figures 7.5 and 7.6 show the ground pressure distribution below the model centerline and transversely at three ground BLC blowing pressure ratios. Skin friction, which is now represented by the difference between full and broken curves, follows essentially the same trends as described above and high number gauges are again critical. It is noteworthy that, at the fully attached condition, ten of the seventeen static orifices experienced C_p's of 1.0 or above. This is attributable to the interaction between the ground BLC wall jet and jet air which moves forward from the impingement point: total pressures exceeding mainstream total are present.

Figure 7.7 shows ground BLC setting as a function of model angle-of-attack and model C_μ at two heights. The setting shown is the lowest that will remove all negative skin friction readings. It is evident that, as before, the below-wing gauges are critical for almost all of the $h/c = 1$ cases. At $h/c = 2$, the trends are generally similar but, at low C_μ the extra height has relieved the adverse pressure gradients considerably, as evidenced by the much-reduced blowing requirements, and impingement probably does not occur. When impingement does occur, at $C_\mu = 2$, the centerline gauges aft of the model are the critical ones (#9 and #10). However, the large distances between gauges 9, 10, and 11 evidently permits a separation bubble between them to go undetected in this case and a proper trend with α is not established. The consequences of this to model forces and tail flow will be discussed later. It must be concluded that more instrumentation is needed aft of the model.

Figure 7.8 places the present results for ground blowing requirements on the same basis as used previously, i.e. as a function of the lift parameter $C_L(c/h)$. On this basis, the $h/c = 1$ blowing requirements for the present model are noticeably larger than previously. It was pointed out in Reference 4, Figure 6.6, that the ground was separated under high α, high C_μ conditions. By definition, the present approach rectified this except when the test blowing limit was reached. The latter cases have been excluded from Figure 7.8.

A marked feature of Figure 7.8 is that the $h/c = 2$ and $h/c = 1$ results no longer collapse to a single curve. Direct control of conditions at the ground thus reveals that the lift parameter, $C_L(c/h)$ does not uniquely define blowing requirements. In fact, Figure 7.8 could equally well be plotted against C_L, which would be more realistic since the $h/c = 2$ curve would then lie below that for $h/c = 1$.

Figure 7.9 returns to the format of Figure 7.7 and presents blowing requirements for the multiple nozzle array shown in Figure 3.6. The multiple-nozzle trends are virtually identical to those for the continuous slot. The total nozzle area is about half that for the continuous slot and this is reflected by the higher blowing pressure ratios required. The fact that ground C_μ's are also much higher is attributable to (at least) two causes. Firstly, the C_μ's quoted are derived from blowing plenum pressure and nozzle area: nozzle entry, turning and internal friction losses are therefore included. To allow the layer to two-dimensionalize, the multiple nozzles also placed some distance upstream of the continuous slot. Losses in this region, which may be considerable, also contribute to the increased C_μ requirement in Figure 7.9.

With the tips added to the basic wing, the ground BLC blowing requirements changed little up to $C_\mu = 1$. Beyond this, a slight increase in ground BLC was required. As a result of detailed improvements to the system, the test limit for ground blowing was raised from 1.075 to 1.11. This compensated for the extra blowing requirement at high C_μ. The anomalies for the $h/c = 2$, $C_\mu = 2$ case, found for the plain wing, were also found with tips present.

17.3 Flow Studies at the Tailplane Position

In order to distinguish between swept-wing-related pitching moments and tailplane effects, no tail was fitted to the model in the present test series and tail-on moment-increment results were replaced by equivalent, flow angle measurements. Figure 7.10 shows typical flow angle vectors in a cross flow plane, plotted relative to the horizontal, at $h/c = 1$ for the highest and lowest C_μ values employed. Successive horizontal lines of vectors were made at increasing wing angles of attack, the pitch yaw probe being mounted on the model fuselage at the tail position. Model angle-of-attack has been subtracted from the flow vectors shown.

At 10-degrees angle of attack, $C_\mu = 0.4$, the inboard end of the rake is evidently intersected by a counter-clockwise vortex from the flap root. This vortex position apparently stays fairly constant, with angle-of-attack, since α's below 10 degrees all display tip-ward flow while at 12 degrees, the flow is inboard. At $C_\mu = 4.0$ the vortex has evidently moved down slightly and spanwise flows are generally less intense. Somewhat surprisingly, the vertical flow components do not increase much with C_μ.

Figure 7.11 shows the corresponding results at two-chords altitude. Here, the suppression of vertical velocities by the ground is much less and there is a distinct increase in downwash at $C_\mu = 4.0$. Vortex formation is once again evident, but the center now lies below the 16-degree position.

Figure 7.12 and 7.13 contain the same data as the previous figures, but show the pitch component only, now plotted relative to the fuselage datum line. Moving ground results have been added for comparative purposes. Because of the nature of the curves, such comparisons are not easy. Increments between moving and BLC ground cases were therefore obtained graphically with the aid of tracing paper, using judgement to determine the best fit between shifted curves. Figure 7.14, which results from this exercise, also includes the intermediate C_μ values.

At one-chord altitude, upflow due to ground BLC lies generally in the range of 1- to 3-degrees. However, at $C_\mu = 4.0$ an uncharacteristic trend is noticed, with upwash values up to 6-degrees at the tail position. Reference to Figure 7.7 shows, however, that there was insufficient air supply to meet the zero-skin friction criterion above 2-degrees angle of attack at this C_μ. It is reasonable to assume that, with sufficient ground blowing, tail upwash increments would be reduced to an acceptable level. A similar conclusion may be drawn for the $C_\mu = 2$ case at two-chords height. Here, ground blowing was again known to be insufficient, but on this occasion due to inadequate

ORIGINAL PAGE IS
OF POOR QUALITY

instrumentation. Otherwise, the tail environment for blown and moving grounds may be considered essentially the same at two chords altitude.

7.4 Comment

Perhaps the most questionable aspect of ground blowing BLC concerns the possibility that tailplane flow will be distorted, at low altitude, high α conditions, due to excessive ground-layer thickness. The above studies show that this effect leads only to 2 or 3 degrees upwash increment, at most, at one-chord altitude and it is negligible at two chords. For high-mounted tails, these errors would be less.

Two off-standard cases (see Figure 7.14) clearly demonstrated the need for care in monitoring ground BLC, both with regard to quantity and the placement of skin friction instrumentation. The good results described above are a direct consequence of the use of skin-friction feedback and probably would not have been possible on the previous $C_L(c/h)$ basis.

ORIGINAL PAGE IS
OF POOR QUALITY

8. GROUND EFFECTS EXPERIMENTS: FORCE AND MOMENT DATA

8.1 General Comments

In all of the near-ground experiments, the angle-of-attack range was physically reduced, compared to center-tunnel tests, and a reduced C_μ range was employed compatible with the current center-tunnel experiments and with previous experiments (refs. 2 to 4). The range used, to $C_\mu = 4$, was sufficient to ensure that ground-limited circulation lift was encountered (Figure 7.1). These factors all reduced the total loads while at the same time, buffet-induced unsteadiness reduced the accuracy of the data. The latter is liable to degrade drag accuracy, in particular, since a 0.1 degree angle-of-attack error translates to a drag coefficient error of 0.14 under typical ground testing conditions. The reduced drag range near the ground also exposes the basic balance inaccuracies: One percent of the axial force range represents approximately 0.14 in drag coefficient and the drag component of 1 percent of the normal force range equals about half this at 10-degrees angle of attack. Though airbridge tares are high, high-accuracy pressure measurements restrict errors in their estimation to about 0.02 in C_D. One percent of full balance range lift and pitching moment coefficients each convert to about 0.4 on the scales used for the basic model. It is evident from the center-tunnel experiments that achieved repeatability was probably noticeably better than the 1% full-scale values just quoted. However, this probably will no longer be true under buffet conditions in ground effect.

Two complete sets of data are presented, the first being for ground BLC via continuous slot blowing (Figures 8.1 to 8.12) followed by multiple-nozzle data (Figures 8.13 to 8.24). Each set includes lift, drag and pitching moment at one- and two-chords altitude for swept-wing configurations without and with tips.

Since the prime objective of the present tests was to compare moving and BLC ground results, neither wind tunnel constraint nor blockage corrections have been applied. The tunnel was run on the basis of contraction pressure drop calibrations, carried out at the relevant model positions, rather than using the 'q-pot' scheme as for center tunnel tests. Possible wind tunnel blockage changes between blc and moving ground configurations, found to be small, were discussed in Section 6.4.

8.2 Force and Moment Data: Continuous Slot Ground BLC

Lift. - Figures 8.1 to 8.12, which are arranged as indicated in Figure 8.0, include lift, drag and pitching moment data for the model without and with wing tips fitted. The balance results are plotted against angle of attack and grouped according to model C_μ. For each C_μ, there is a fixed ground curve (triangles), a moving ground curve (circles), and a blown ground curve with the most critical skin friction meter neutral (squares). For no-tips runs, two further curves have been added, corresponding to a ground

plenum gauge pressure increase of 20% (labelled "20% overblow") and corresponding to a lower blowing condition for which the transverse row of skin friction indicators was ignored ("Critical Centerline Meter Neutral"). Discussion of the latter two curves will be deferred to Section 8.3.

The most striking changes from the fixed ground data, using either a moving or a BLC ground at $h/c = 1.0$, appear in the lift component (see Figure 8.1). The fixed ground caused a C_L-loss of about one, which the BLC ground restored very effectively, even at $C_\mu = 4.0$, when blowing quantity was known to be inadequate. Adding wing tips (Figure 8.2) doubled the fixed-ground lift error and ground BLC again was effective in reproducing the moving belt result. However, at $C_\mu = 4.0$, the lift errors due to underblowing the ground BLC were large.

Raising model altitude to two chords (Figures 8.3 and 8.4) greatly reduced the lift errors with ground fixed, except at high C_μ and α. The ground BLC was again effective.

Drag. - The drag curves (Figures 8.5 to 8.8) at a given C_μ are generally quite closely grouped, though systematic differences in trend exist for the fixed ground. A potential hazard — that the thick ground blowing layer would strike the flap at high α and cause drag increase — evidently did not materialize to a significant degree.

Pitching Moment. - Comparison between current pitching moment measurements (Figures 8.9 to 8.12) and the previous, unswept wing tests (reference 4) shows more consistent trends and generally-improved agreement between blown- and moving ground tests in the present swept-wing tests. The improved consistency of the present results is almost certainly attributable to the introduction of ground-condition monitoring and feedback via the skin friction gauges. Though moving/blown ground agreement was generally good, there were exceptions under high C_μ, near-ground conditions which will be discussed later.

Reference to previous results (reference 4) shows that use of a fixed ground caused pitch-up for the straight wing, reflecting an increase in the size of an aft-located undersurface suction bubble due to premature ground separation (see also reference 2). The present results for the swept wing show pitch-down with the fixed ground. This could be caused by the same basic mechanism: a higher lift-loss towards the wing root, where adverse ground pressure gradients are more severe, combines with a lower lift loss towards the tip to produce pitch-down on the swept wing. Additional flow mechanisms may be present in the tips-on cases because the tips have no flaps on them.

In the discussions which follow, moving ground results will be regarded as the "correct" datum condition.

The ability of the blown-ground to remove the above adverse fixed ground effects was evidently very good under all conditions at $h/c = 2$ and up to $C_\mu = 2$ at $h/c = 1$ (see Figures 8.9 to 8.12). However, at $h/c = 1$ with $C_\mu = 2$ and above, ground blowing introduced noticeable and spurious pitch-down without or with tips. In the with-tips case the ground-blowing-induced pitch-down increased continuously with model angle of attack. This suggests that lift on

ORIGINAL PAGE IS
OF POOR QUALITY

the wing increased as it approached the ground-blowing layer. Reference to the corresponding lift results supports this thesis. On checking pitching moment and lift results for multiple-nozzle ground blowing, where the ground layer was known to be thicker (see Section 8.4), the same trends were observed, but at increased amplitude.

It is interesting to observe that when the blowing air supply became inadequate during the $C_\mu = 4$ run (see Figure 8.10b) the blown-ground-induced pitch-down decreased, with α, reversing the previous trend.

It should be noted that the present tests exaggerate the above effects slightly, because the model rotation point was situated too far forward, being situated at the root 50% chord point rather than at the MAC. At 12-degrees angle of attack, this lowered the trailing edge of the tip extension from 10 cm (2.5") to 7.9 cm (2.0") above the ground.

Comment. - Although the angle measurements at the tail position showed that the present ground-blowing methods are sensitive and reproduce the moving-ground tailplane environment quite well, the above results show that conditions at the extended tips are not well reproduced. Adverse pressure gradients at the ground are less severe here and blowing at the same level over the full model span evidently produces a degree of "overkill" at the wing tip. It may therefore be appropriate to restrict the spanwise extent of floor blowing to the heavily-lifting, powered section of the wing span. This would also permit significant savings in blowing air.

8.3 Choice of Blowing Strategy: Continuous Slot Ground BLC

During the initial experiments on ground blowing, two other strategies were explored in addition to the "most critical meter neutral" philosophy used for the tests discussed above. To keep the test schedule within reasonable bounds, these were applied only to the basic swept wing configuration (see odd-numbered Figures from 8.1 to 8.11).

For the "20% overblow" cases, the boundary layer plenum gauge pressure was raised 20% above the "most critical meter neutral" value. The basis for this lay in the realization that the present instrumentation probably failed to detect separation in some locations. Thus, if very extensive instrumentation had been present, the blowing requirement fed back would almost certainly have increased. The 20%-overblowing tests represent an attempt to determine the consequences of this. Examination of the test results (diamond-shaped points in the odd-numbered figures) showed generally poorer correlations with moving ground for the overblowing cases.

The strategy for the underblowing tests was a little different. Here, it was assumed that the chief emphasis should be on tailplane conditions and only the skin friction indications from centerline row of skin friction gauges should be considered. The test results (asterisk points) show errors of very much the same magnitude as for the "most critical meter neutral" strategy, however, the trends with angle of attack were somewhat better

reproduced in the latter case. On this basis, the decision was made to use the "most critical meter neutral" strategy as the standard.

8.4 Force and Moment Data: Multiple-Nozzle Ground BLC

At $h/c = 2$ and for low angles of attack at $h/c = 1$ the agreement between multiple nozzle data and moving ground results was just as good as for the continuous slot. However, the pitching moment and lift discrepancies discussed above are amplified for multiple nozzles at $h/c = 1$ and appear at a lower value of C_μ (see Figures 8.13 to 8.24). In addition, there is now a pitch-down increase and a lift increase, with α, for the basic configuration as well as with tips fitted.

The present results therefore indicate that relatively-crude multiple nozzles, arranged in the present configuration, are not suitable for swept wing tests at $h/c = 1$, because of lift and pitching-moment interference. At $h/c = 2$ and above, this multiple nozzle approach is perfectly adequate and could be used with confidence for center-tunnel testing.

Despite the above adverse effects for multiple nozzles at $h/c = 1$, the tests provided valuable guidance in establishing the reasons for the anomalies in the continuous slot results. This comparison also makes it clear that even the continuous slot results could be improved by thinning the layer which reaches the wing. The use of a swept slot or the introduction of a second slot, nearer to the wing might permit this. These possibilities were first noted in references 1, 2 and 5, but multiple slots were dropped subsequently because there was no clear way to define the blowing requirements. With ground skin-friction feedback, as in the present tests, this barrier is removed.

ORIGINAL PAGE IS
OF POOR QUALITY

9. CONCLUSIONS AND RECOMMENDATIONS

Tests have been carried out on a 20-inch span swept, jet-flapped wing with two major aims: to provide large/small tunnel correlation of a new wind tunnel blockage estimation method and to complete the development of a ground-blowing scheme which replaces the moving belt technique in near-ground tests. The tests reported here supplement those of reference 4, which involved an unswept wing of very similar design to that used in the present tests.

9.1 Wind Tunnel Interference Studies

Three-component balance measurements and limited flow measurements were carried out at center-tunnel in the NASA/AAMRDL 7' x 10' tunnel and in the Lockheed-Georgia 30" x 43" tunnel. These concerned mainly the swept-wing model without and with tips added, but certain check tests were made with the straight wing. Since the previous tests, the test section length of the Lockheed tunnel had been increased from four to seven feet. The new blockage techniques and angle of attack corrections for the smaller tunnel are described in Section 4.4. The following conclusions were reached:

1. Vorticity meter readings in the two tunnels showed very similar trailing vortex wake structures. After allowance for flow rotation corrections in the small tunnel, any remaining differences were too small to have significant effect on the model (see Section 5).

2. The previously-experienced 'drag flip-back' problem in the small tunnel did not recur. It appears that laminar separation of the flap flow, previously, was aggravated by the proximity of the wind tunnel diffuser. With the new longer test section, stall characteristics correlated well between large and small tunnels (see Section 4).

3. Up to C_L's of ten, there was excellent agreement between tunnels in lift, drag, and pitching moment for all configurations (see Sections 4 and 5).

4. At very high C_L's, side-wall pressure measurements showed a suction region which started just behind the aft end of the moving ground, suggesting that ground separation had occurred. It was found that this could be shifted downstream by increasing amounts of ground blowing BLC (see Section 6).

5. Because of the above suction region, blockage corrections were overestimated somewhat at very high C_L's (see Sections 4 and 5). Under the most extreme conditions (C_L about 16, plain wing; 20, with tips), the side-wall pressures showed that the small tunnel flow had broken down entirely, despite ground BLC (see Section 6). However, the 10-C_μ required to do this is well outside practical limits.

6. The high level of success of the blockage correction method rests heavily on the aerodynamic cleanness of the models used, particulary the excellent leading-edge protection provided by their slats (see Section 1.3).

Because of this, correction solely for wake blockage was adequate. In other circumstances, where there is significant model or separation bubble volume, more advanced blockage estimation methods would be required (see Section 6.1).

9.2 Ground Effects Experiments

Three-component balance measurements and tail-rake flow measurements were carried out on the swept wing with and without tips at $h/c = 1$ and 2. A moving ground was used for datum measurements and trials were made with two blown-ground geometries and several blowing-quantity strategies. Major aims were to develop improved blowing techniques and to determine if swept wing testing is adversely affected by tip-penetration of the ground blowing layer. The following conclusions were reached:

1. Ground blowing may be monitored and controlled successfully via the use of ground skin-friction instrumentation connected to sensitive, center-zero, dial-type gauges. This approach, which is regarded as a breakthrough, supplants the previous $C_L(c/h)$-method of control (see Section 7).

2. With the above scheme in operation, force and moment results at $h/c = 2$ were indistinguishable from those with a moving ground. This remained true up to $C_L = 6$ at $h/c = 1$.

3. Above $C_L = 6$ at $h/c = 1$, lift and pitching moment suggested that extra tip lift occurred which increased with angle of attack. The magnitude of the effect increased with tips added, suggesting that the span of the blowing slot, which equalled the with-tips span, was excessive.

4. The tail-rake measurements were very sensitive to ground blowing rate. However, at optimum ground-blowing rate, there were no changes from the moving ground pitch angle values at $h/c = 2$ and only 1- to 3-degrees pitch up at $h/c = 1$. Certain erroneous blowing cases showed much higher values.

5. The continuous blowing slot, used routinely, was replaced by a multiple-nozzle array for some tests (see Section 8.4). This produced a thicker layer which increased the swept-wing pitch/lift problem. In the form used, the multiple-nozzle arrangement is only suitable for tests at $h/c = 2$ and above.

9.3 Recommendations

General

1. Ground BLC must be used for both center tunnel, high-lift and ground-effects testing if $C_L(c/h)$ exceeds 2. If a moving ground is not feasible, it should be replaced by ground-blowing as detailed below.

ORIGINAL PAGE IS
OF POOR QUALITY

2. Ground skin friction monitoring should be employed to determine ground blowing rate, using a "most critical meter neutral" strategy and on-line instrumentation (see Section 7.2). Skin friction gauge details are outlined below.

3. Separation must be prevented to a point somewhat aft of the model but overblowing (as indicated by the friction sensors) must be avoided.

Tunnel Blockage

4. The present on-line, wake-blockage correction method should be augmented to include solid/bubble blockage (see Section 6 and reference 6).

5. The new tunnel blockage correction method should be tested for VTOL and propeller-powered configurations.

Ground Instrumentation Details

6. The pitch of the chordwise row of skin friction gauges at the model centerline (see Figure 7.3) should be maintained constant to a position aft of the tailplane location. (In the present tests, insufficient aft gauges caused errors at $h/c = 2$).

7. To monitor off-centerline conditions, a second chordwise row of skin friction gauges is favored, rather than the spanwise row used in the present tests. This second, chordwise row should be situated at approximately the 50% semispan location, or below a local load peak if this is present (near a simulated engine, for example).

Ground Blowing Details

8. The thickness of the blowing layer should be minimized. This favors continuous-slot blowing. Design C_μ requirements may be established with the help of Figure 7.7.

9. The chordwise run from the ground blowing slot to the wing should be minimized. The use of slot sweep equal to the wing sweep is strongly recommended.

10. The spanwise distribution of slot blowing should roughly match the wing span load distribution. In the present tests, it is believed that a reduction of the blowing slot span, to equal the model flap span, would have been beneficial.

The floor-blowing design recommended in reference 5 includes many of the above blowing-slot features, but should be amended in the following respects:

11. Extra care should be taken to minimize blowing-layer thickness: an in-floor slot design may be preferable, though the sweep feature should be retained.

12. Provision should be made to vary the spanwise extent of blowing in consonance with model geometry and span distribution of lift/power.

13. Ground-surface, skin-friction instrumentation should be added as indicated above, connected suitably for real-time, preferably analogue, read-out.

14. Ground blowing mass flow and momentum requirements and specifications should be reviewed in the light of the current results.

10. REFERENCES

1. Hackett, J. E.; and Praytor, E. B.: Ground Effect for V/STOL Aircraft Configurations and Its Simulation in the Wind Tunnel, Part I — Introduction and Theoretical Studies. NASA CR 114,495. November 1972.

2. Hackett, J. E.; Boles, R. A.; and Praytor, E. B.: Ground Effect for V/STOL Aircraft Configurations and Its Simulation in the Wind Tunnel, Part II - Experimental Studies. NASA CR 114,496, November 1972.

3. Hackett, J. E.; and Boles, R. A.: High Lift Testing in Closed Wind Tunnels AIAA Paper No. 74-641, July 1974 (also see *J. Aircraft*, Aug. 1976).

4. Hackett, J. E.; Boles, R. A.; and Lilley, D. E.: Ground Simulation and Tunnel Blockage for a Jet-Flapped, Basic STOL Model Tested to Very High Lift Coefficients. NASA CR 137,857, March 1976.

5. Hackett, J. E.; Praytor, E. B.; and Caldwell, E. O.: Ground Effect for V/STOL Aircraft Configurations and Its Simulation in the Wind Tunnel, Part III - Application to the NASA-Ames 40- by 80-foot Wind Tunnel. NASA CR 114,497, November 1972.

6. Hackett, J. E.; and Wilsden, D. J.: Determination of Low Speed Wake-Blockage Corrections via Tunnel-Wall Static Pressure Measurements." Presented to AGARD Wind Tunnel Design and Testing Techniques Conference, October 1975 in London, England. AGARD CP 174, Paper 23.

7. Williams, J.; and Butler, S. F.: Experimental Methods for Testing High Lift BLC and Circulation Control Models. In *Boundary Layer and Flow Control* by Lachman (ed), Vol. I, Pergamon Press, 1961, p. 395.

TABLE I

MODEL DIMENSIONS

Fuselage:		
length	31.55 cm	(12.42 in)
maximum width	4.46 cm	(1.76 in)
maximum height	7.76 cm	(3.06 in)
maximum cross-section	30.30 cm^2	(4.70 in^2)
equivalent diameter	6.21 cm	(2.44 in)
nose location	FS 0.00 cm	(FS 0.00 in)
fineness ratio	5.08	5.08
balance centerline location:		
water line	40.64 cm	(16.00 in)
butt line	0.00 cm	0.00 cm
reference point:		
fuselage station	0.00 cm	(0.00 in)
water line*	0.00 cm	(0.00 in)
butt line	0.00 in	(0.00 in)
Straight Wing:		
sweep	0°	0°
quarter chord MAC location:		
fuselage station	1.27 cm	(0.50 in)
water line	38.10 cm	(15.00 in)
butt line	12.70 cm	(5.00 in)
Swept Wing:		
sweep	25°	25°
quarter chord MAC location:		
fuselage station	6.64 cm	(2.71 in)
water line	38.10 cm	(15.00 in)
butt line	12.70 cm	(5.00 in)
Straight and Swept Wings:		
wing:		
area	517.00 cm^2	(0.556 ft^2)
aspect ratio (on nominal chord)	5.00	
span	50.80 cm	(20.00 in)
nominal chord (constant)	10.16 cm	(4.00 in)
quarter chord water line	38.10 cm	(15.00 in)
twist	0°	0°

**Water line 0.0 is small tunnel floor with model on tunnel centerline.*

ORIGINAL PAGE IS
OF POOR QUALITY

TABLE I - Continued

MODEL DIMENSIONS

wing and tips:		
area	968.00 cm^2	(1.042 ft^2)
aspect ratio (on nominal chord)	6.00	
span	76.20 cm	(30.00 in)
nominal chord	12.70 cm	(5.00 in)
leading edge slat:		
area (projected onto maximum chord):		
wing only	103.00 cm^2	(0.111 ft^2)
wing and tips	155.00 cm^2	(0.167 ft^2)
span:		
wing only	50.80 cm	(20.00 in)
wing and tips	76.20 cm	(30.00 in)
chord (maximum)	2.03 cm	(0.80 in)
slot width	0.127 cm	(0.050 in)
deflection	80.00	
trailing edge flap:		
area (projected onto maximum chord)	234.00 cm^2	(0.252 ft^2)
span	50.80 cm	(20.00 in)
chord (maximum)	4.60 cm	(1.81 in)
slot width	0.041 cm	(0.016 in)
deflections (wing chord to flap upper surface)		
straight wing	76.00°	76.00°
swept wing	60.00°	60.00°

ORIGINAL PAGE IS
OF POOR QUALITY

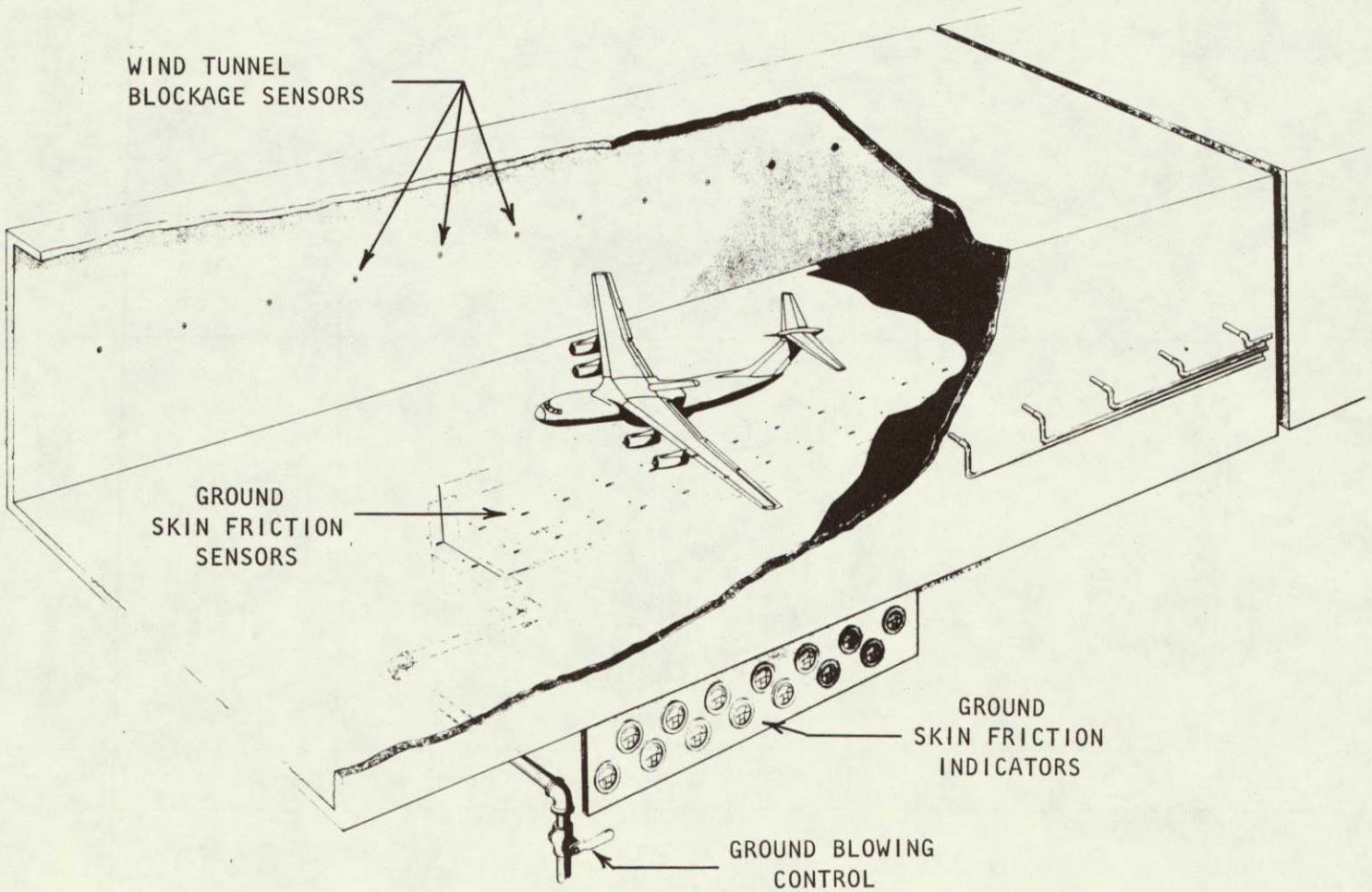

Figure 1.1 The Sensitive Wind Tunnel

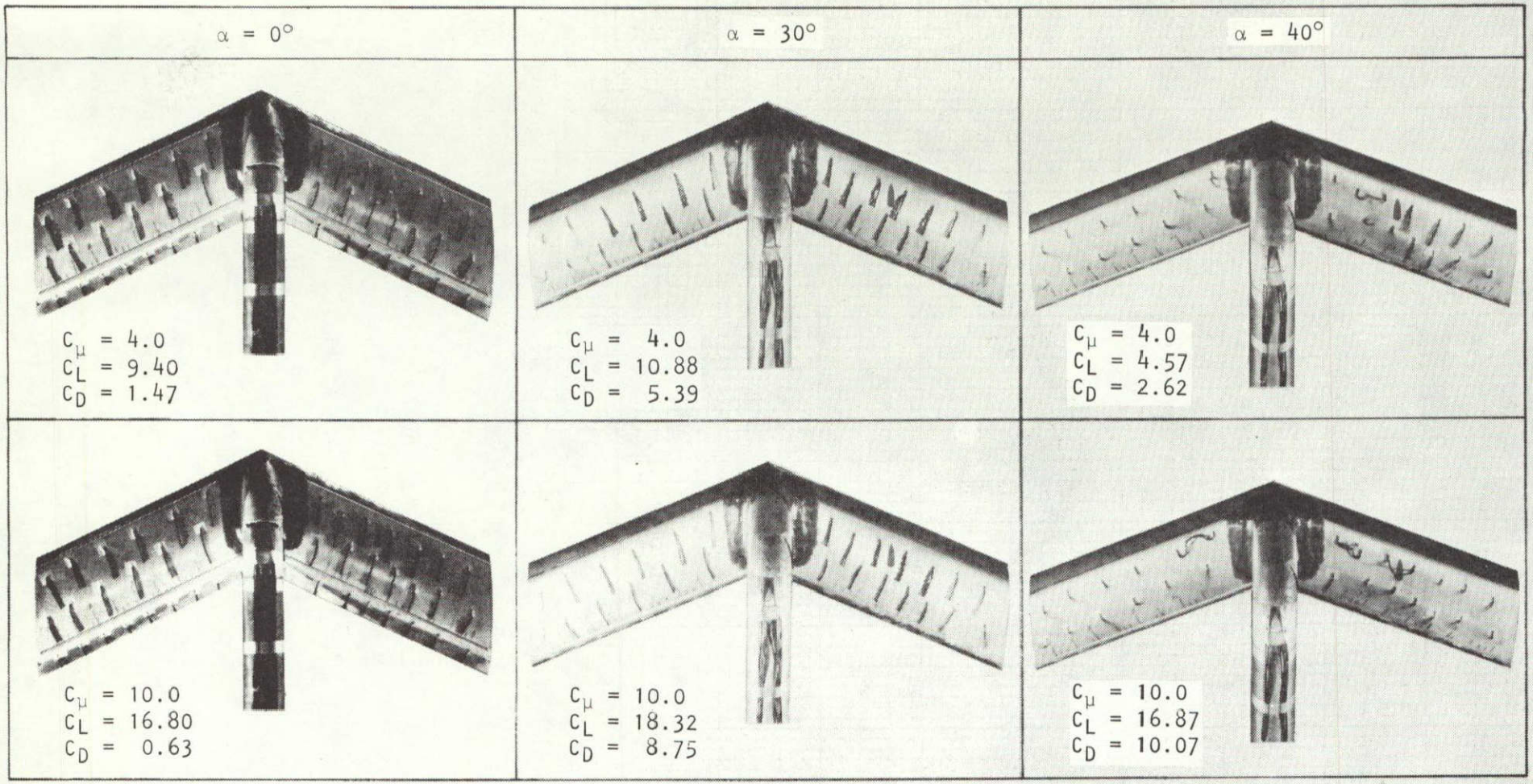

Figure 1.2 Properties of the Swept Wing, Knee-Blown Flap Model
(Tips Off Configuration)

ORIGINAL PAGE IS
OF POOR QUALITY

ORIGINAL PAGE IS
OF POOR QUALITY

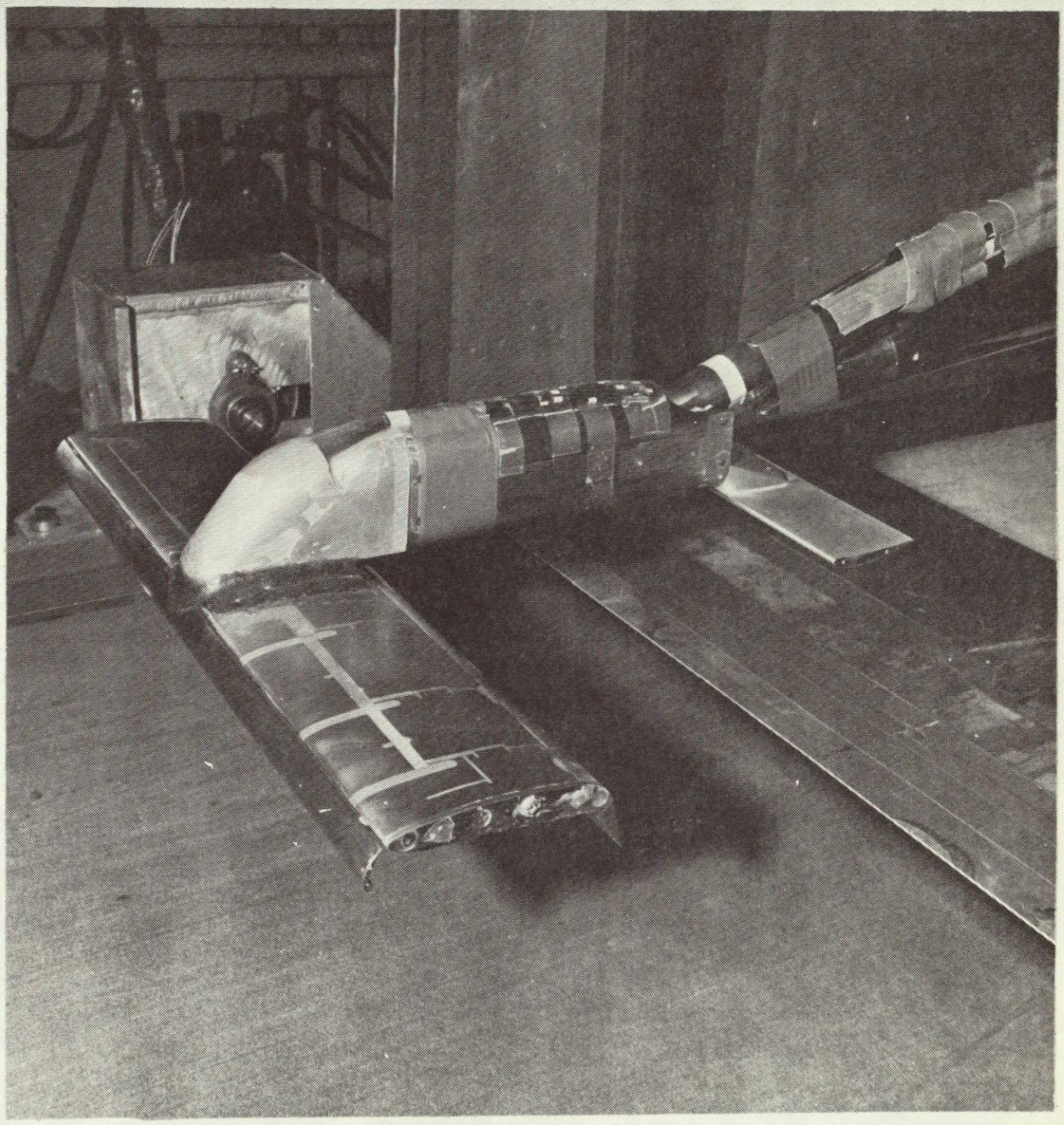

Figure 2.1 The Straight Wing KBF Model (Configuration A-2) in the Unmodified 30 x 43 Inch Wind Tunnel — Moving Ground Present

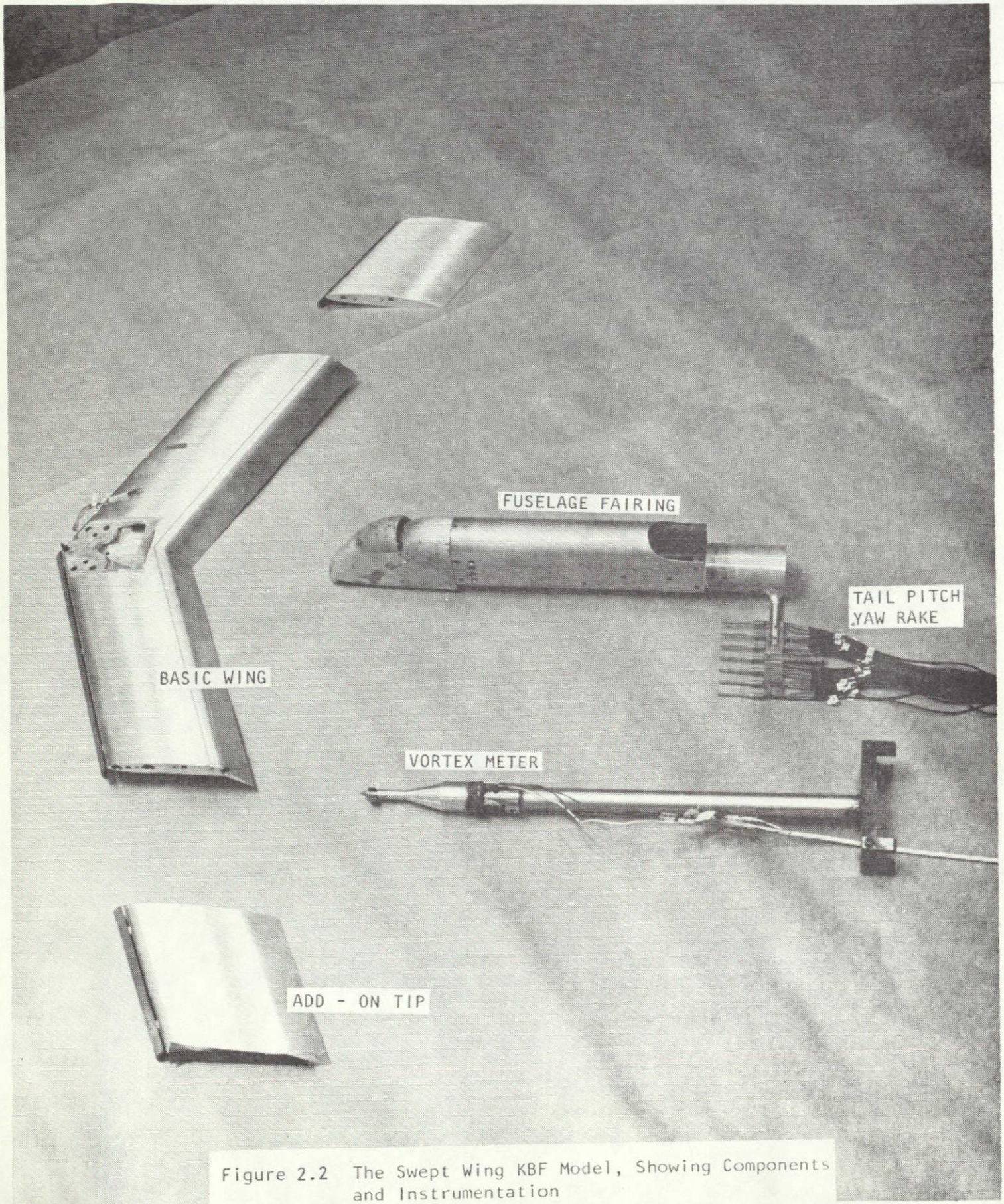

Figure 2.2 The Swept Wing KBF Model, Showing Components and Instrumentation

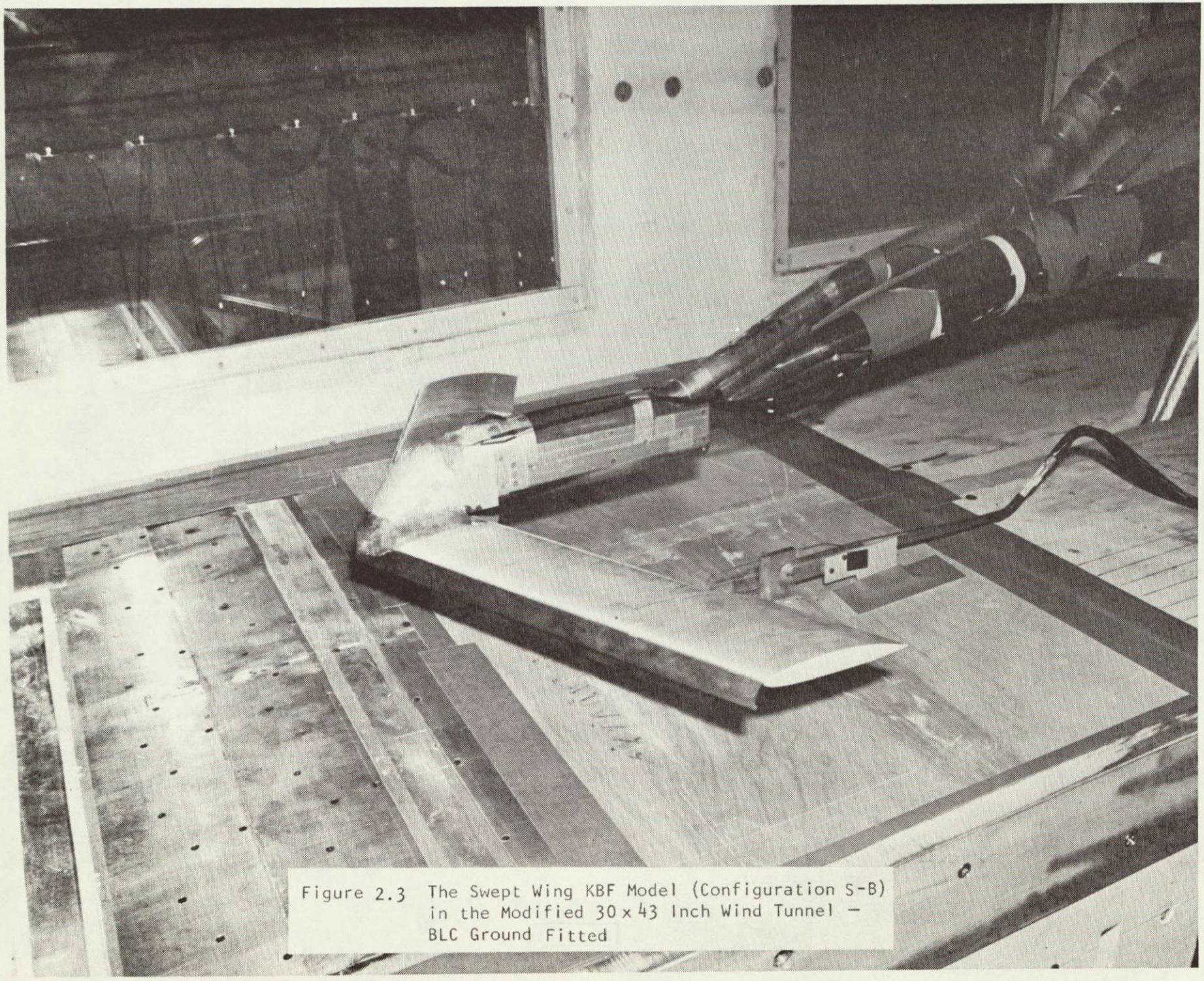

Figure 2.3 The Swept Wing KBF Model (Configuration S-B) in the Modified 30 x 43 Inch Wind Tunnel — BLC Ground Fitted

ORIGINAL PAGE IS
OF POOR QUALITY

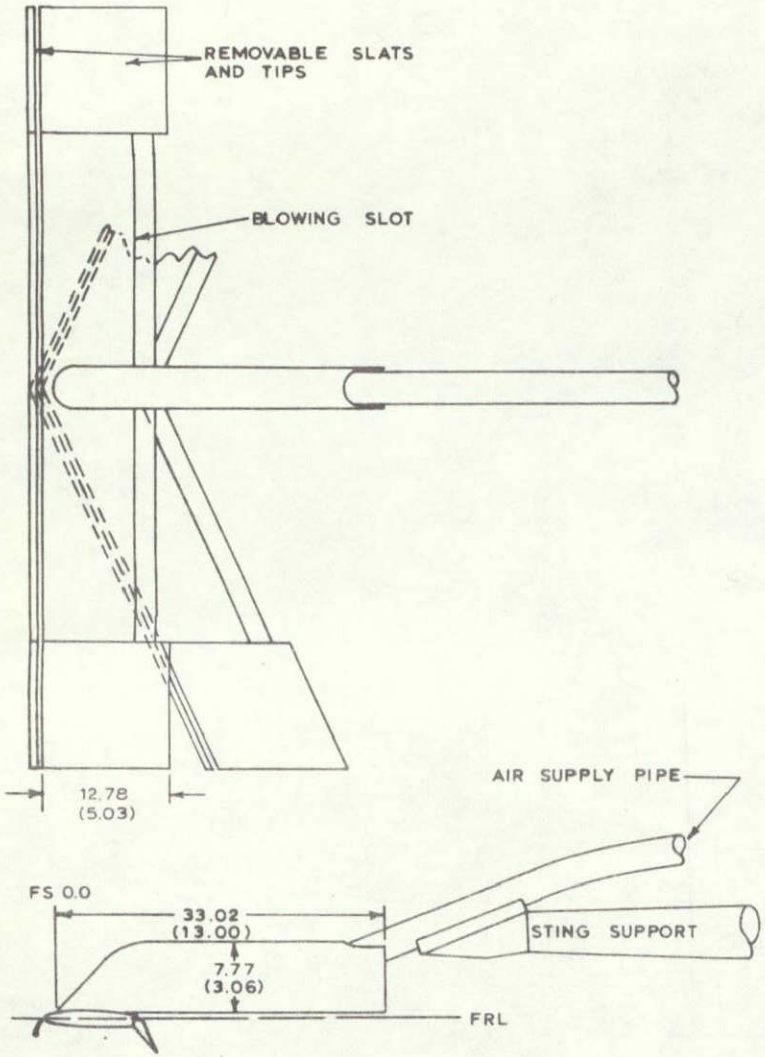

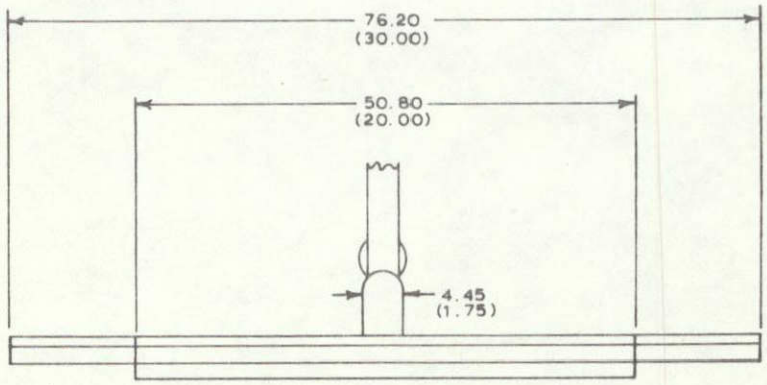

Figure 2.4 General Arrangements of Models

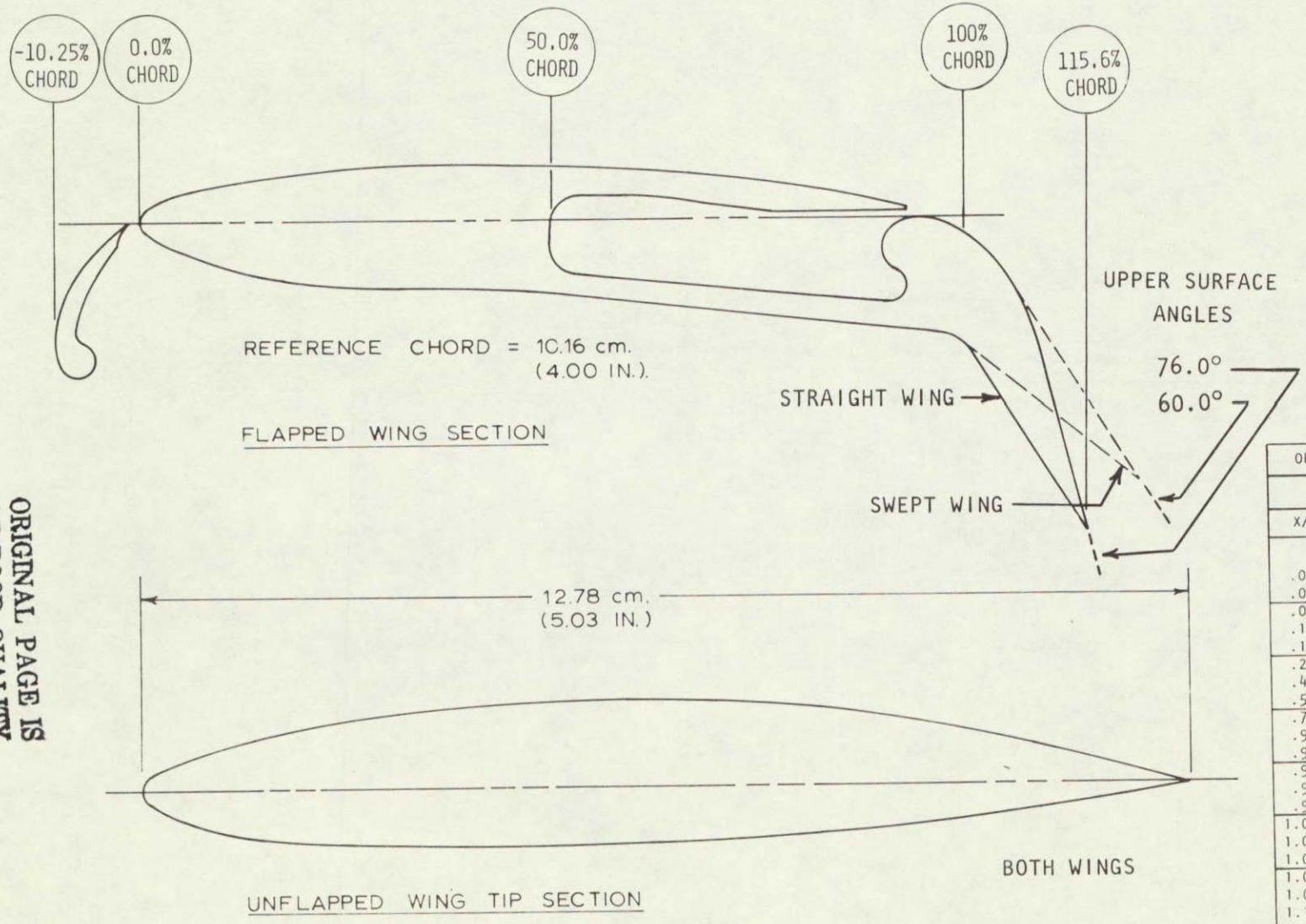

ORDINATES OF UNFLAPPED WING TIP SECTION

X/C	YU/C	YL/C
0	0	0
.010	.015	-.015
.020	.020	-.020
.049	.032	-.033
.099	.045	-.045
.148	.056	-.050
.198	.064	-.053
.247	.071	-.055
.296	.077	-.056
.395	.082	-.056
.494	.083	-.053
.593	.079	-.049
.692	.069	-.042
.791	.051	-.032
.889	.028	-.019
.988	.002	-.003
1.000	0	0

ORDINATES OF FLAPPED WING SECTION

	STRAIGHT WING		SWEPT WING	
X/C	YU/C	YL/C	YU/C	YL/C
0	0	0		
.017	.019	-.019		
.038	.028			
.067	.038	-.044		
.103	.045			
.147	.053			
.250	.062	-.076	SAME AS STRAIGHT WING	SAME AS STRAIGHT WING
.414	.069	-.081		
.585	.063	-.096		
.750	.047	-.114		
.913	.020			
.936	-.001			
.965		-.138		
.968	-.003			
.990	-.010			
1.015	-.021	-.170	-.020	-.145
1.025				-.151
1.037	-.037		-.036	
1.074	-.080		-.078	
1.082	-.096			
1.156	-.389	-.391		
1.214			-.324	-.324

Figure 2.5 Wing Section Ordinates (Chordwise Plane)

ORIGINAL PAGE IS
OF POOR QUALITY

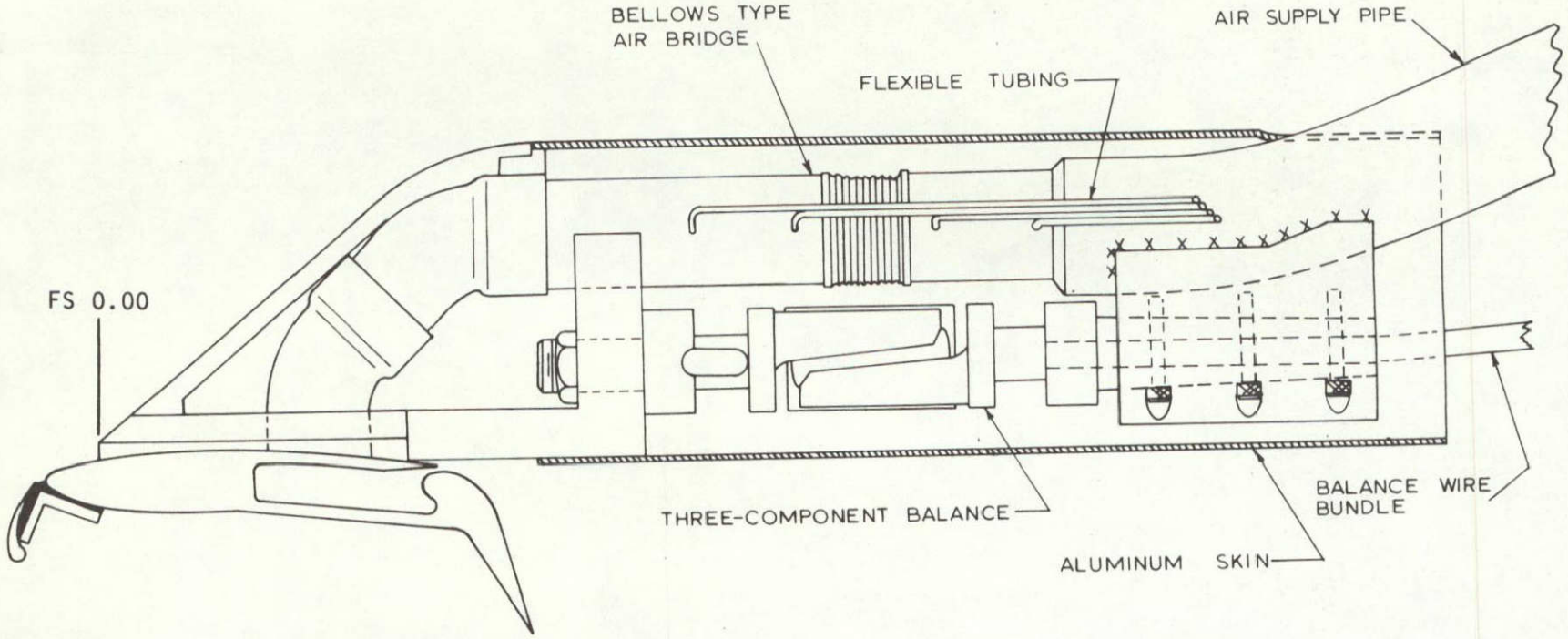

Figure 2.6 Balance and Air Bridge Details

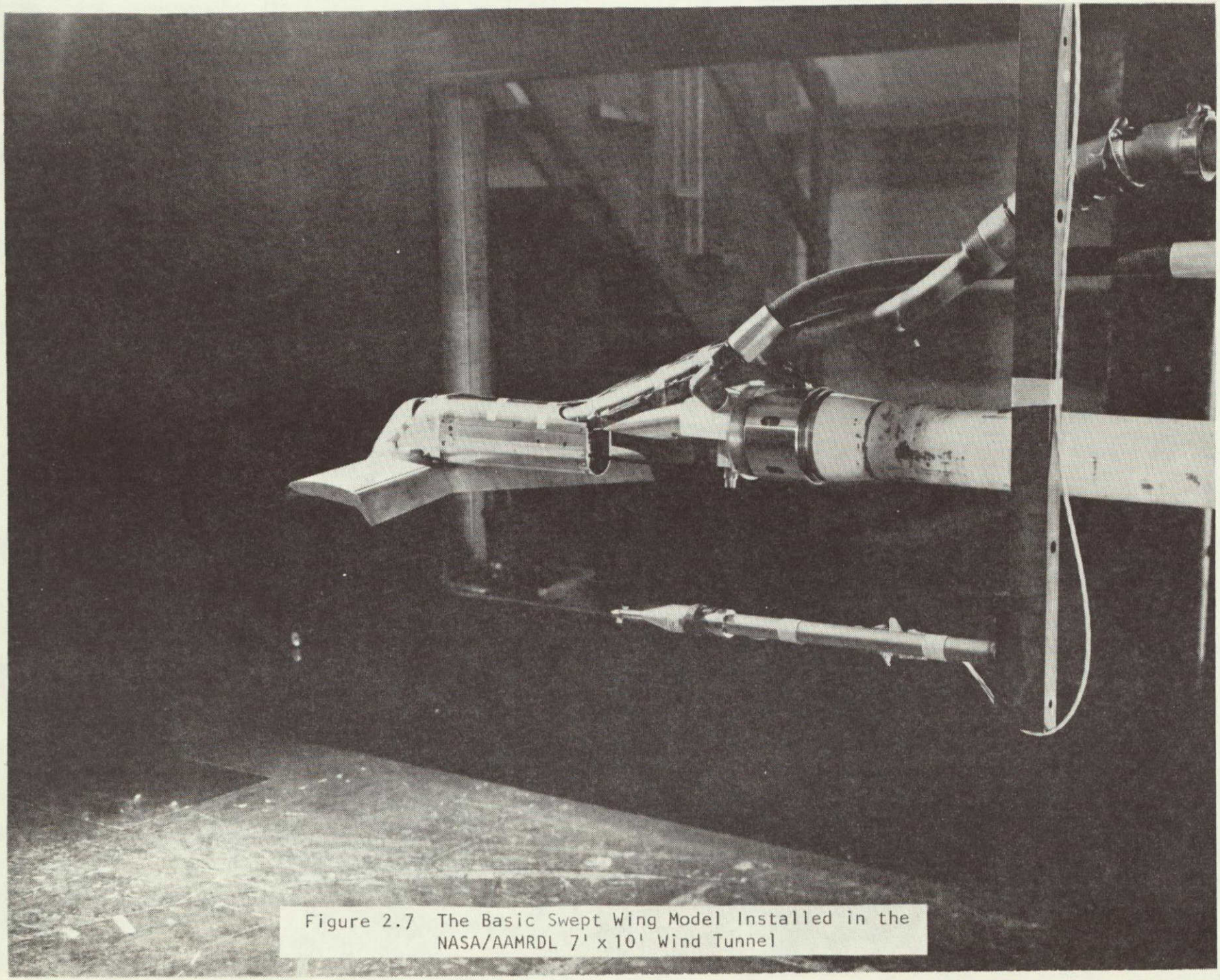

Figure 2.7 The Basic Swept Wing Model Installed in the NASA/AAMRDL 7' x 10' Wind Tunnel

ORIGINAL PAGE IS
OF POOR QUALITY

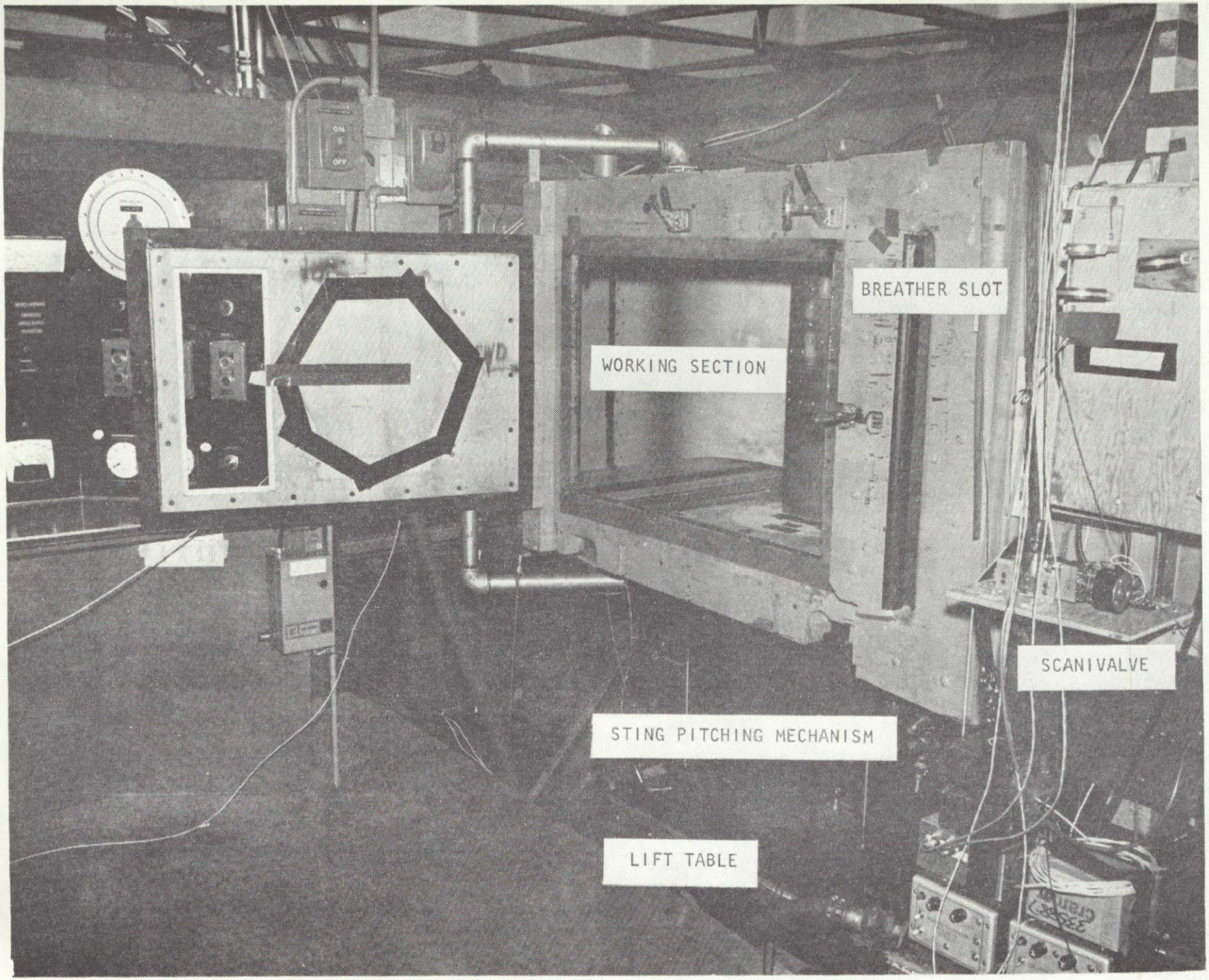

Figure 3.1 The 30 x 43 Inch Low Speed Tunnel - Original Configuration

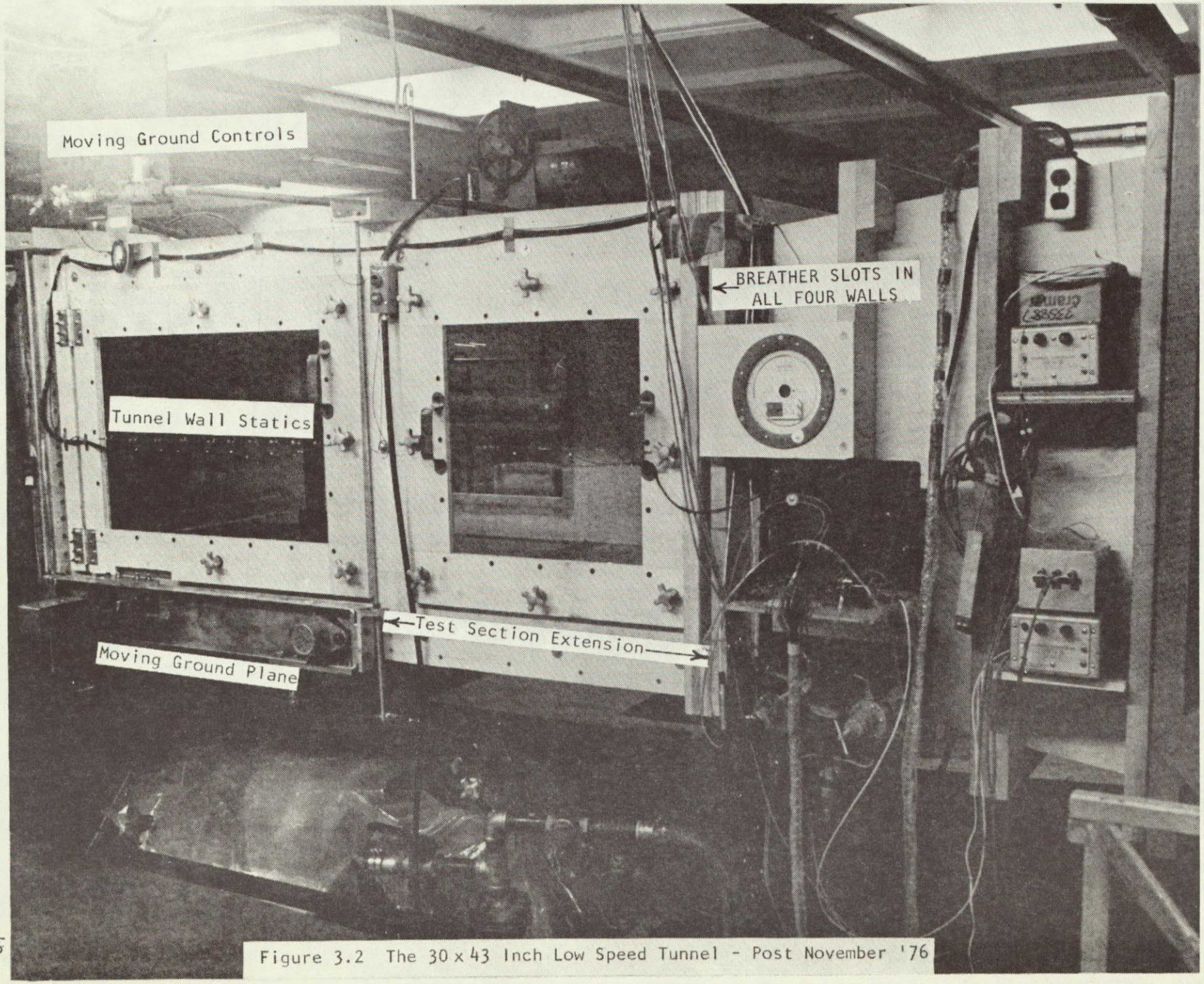

Figure 3.2 The 30 x 43 Inch Low Speed Tunnel - Post November '76

ORIGINAL PAGE IS
OF POOR QUALITY

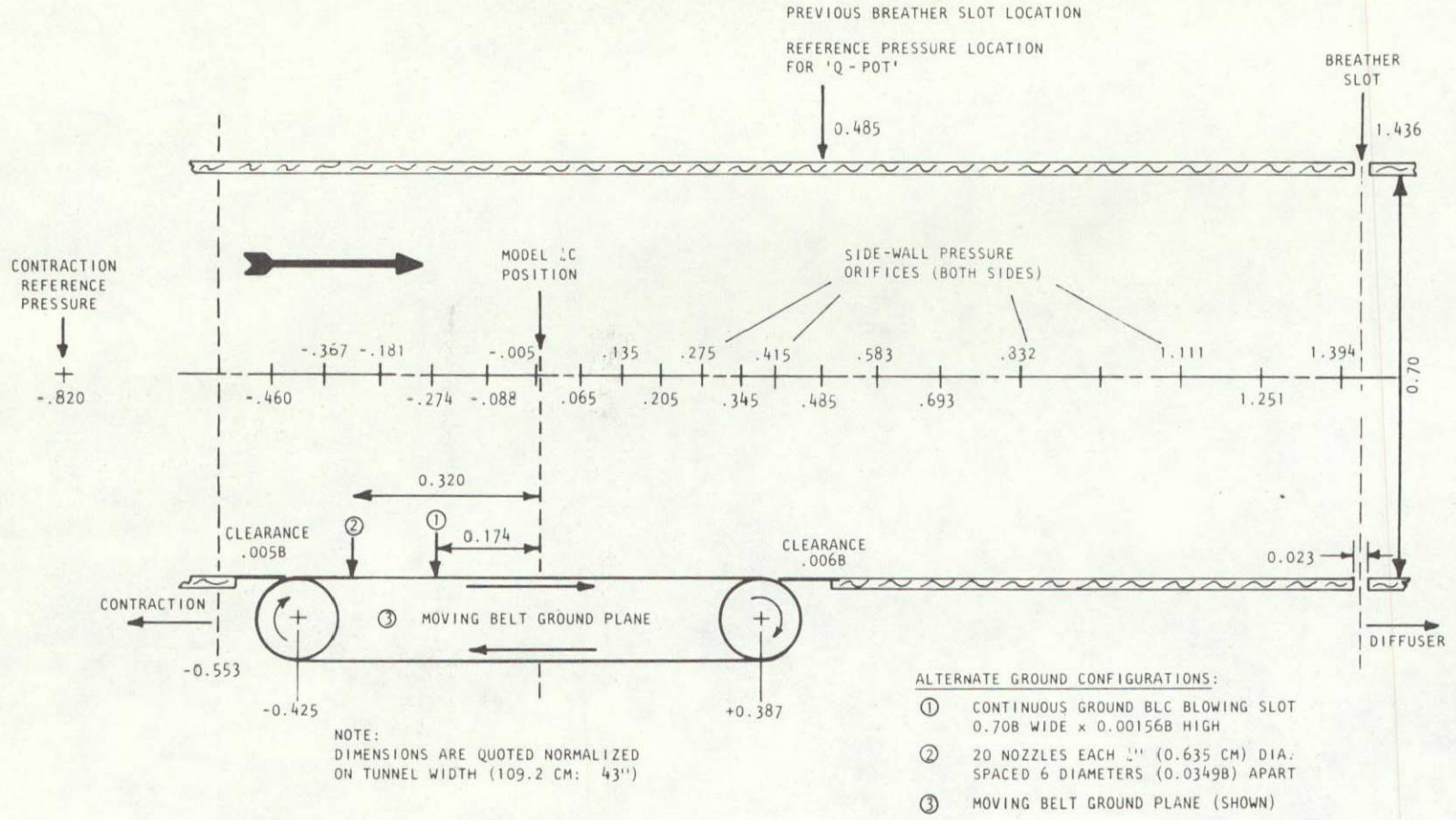

Figure 3.3 Layout of Test Section, Ground-Planes and Wall Pressure Orifices

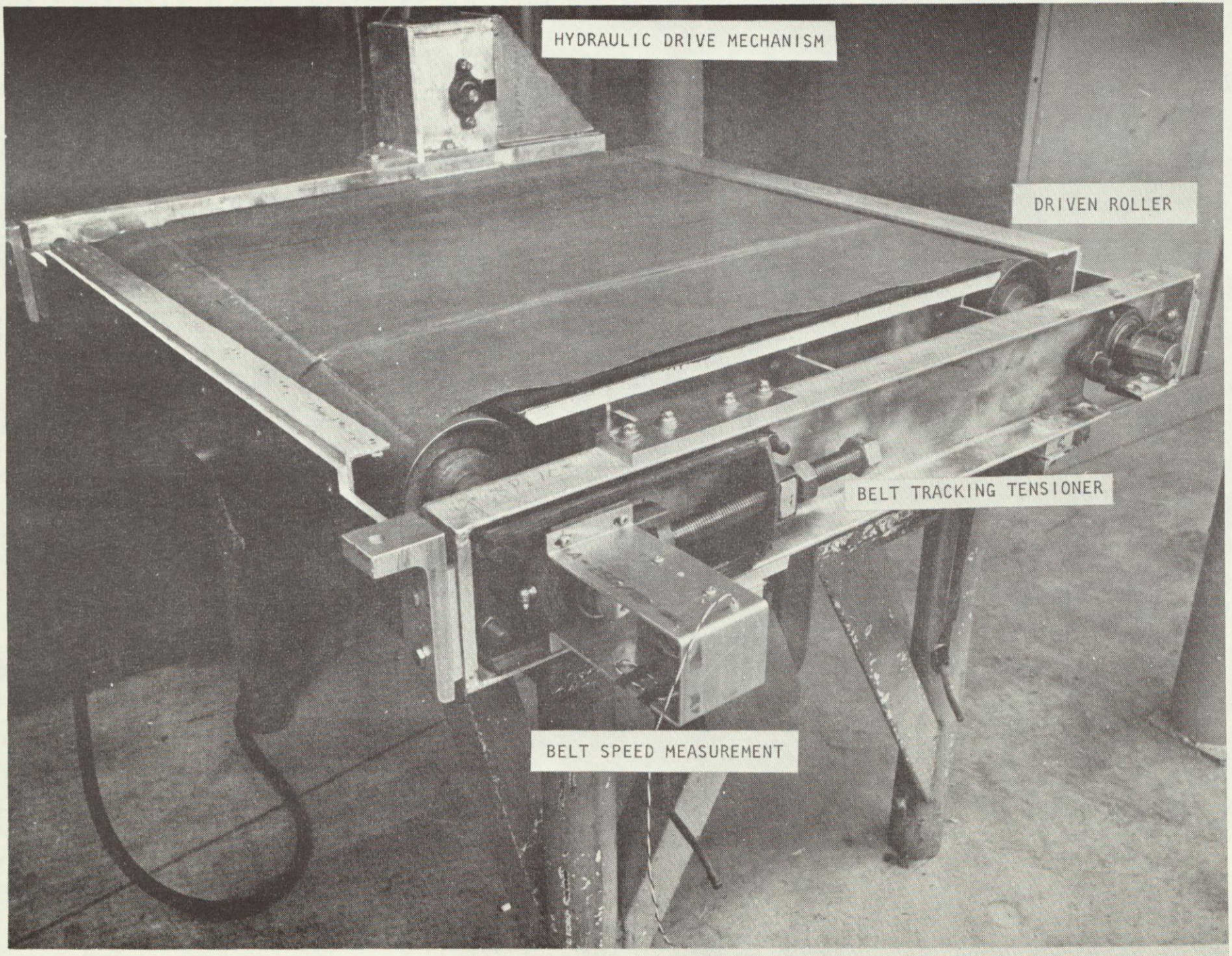

Figure 3.4 The Moving Belt Ground Plane

ORIGINAL PAGE IS
OF POOR QUALITY

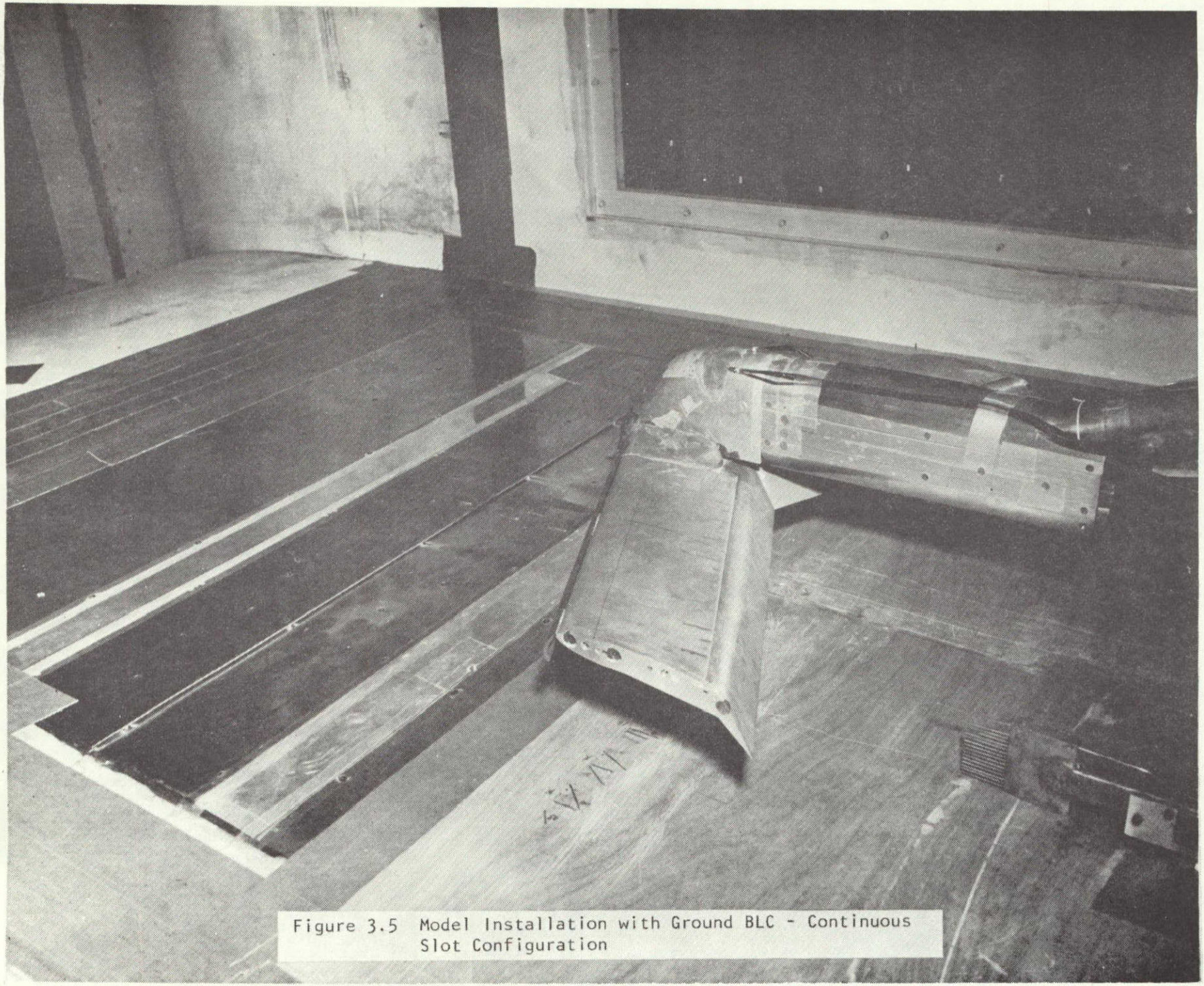

Figure 3.5 Model Installation with Ground BLC - Continuous Slot Configuration

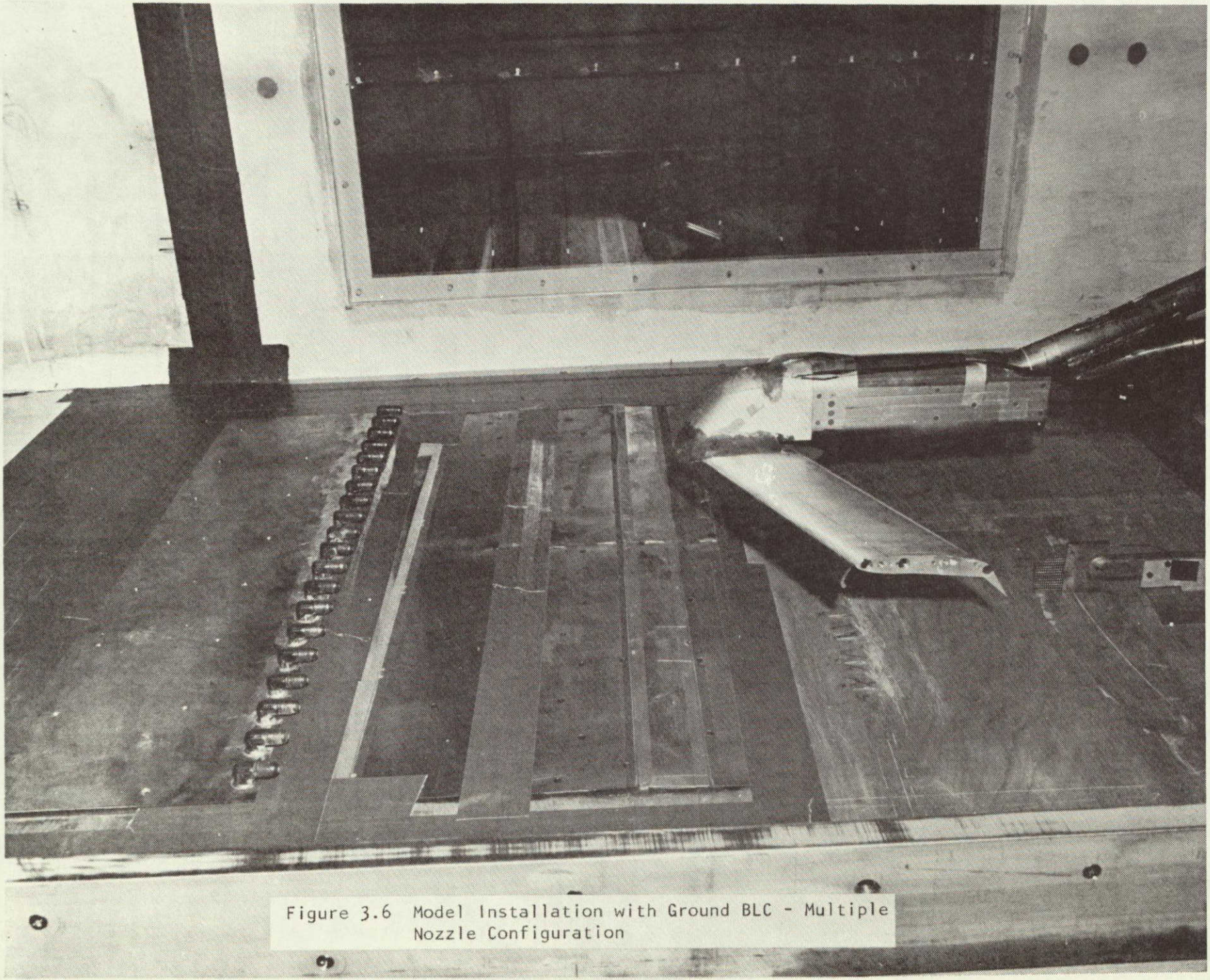

Figure 3.6 Model Installation with Ground BLC - Multiple Nozzle Configuration

ORIGINAL PAGE IS
OF POOR QUALITY

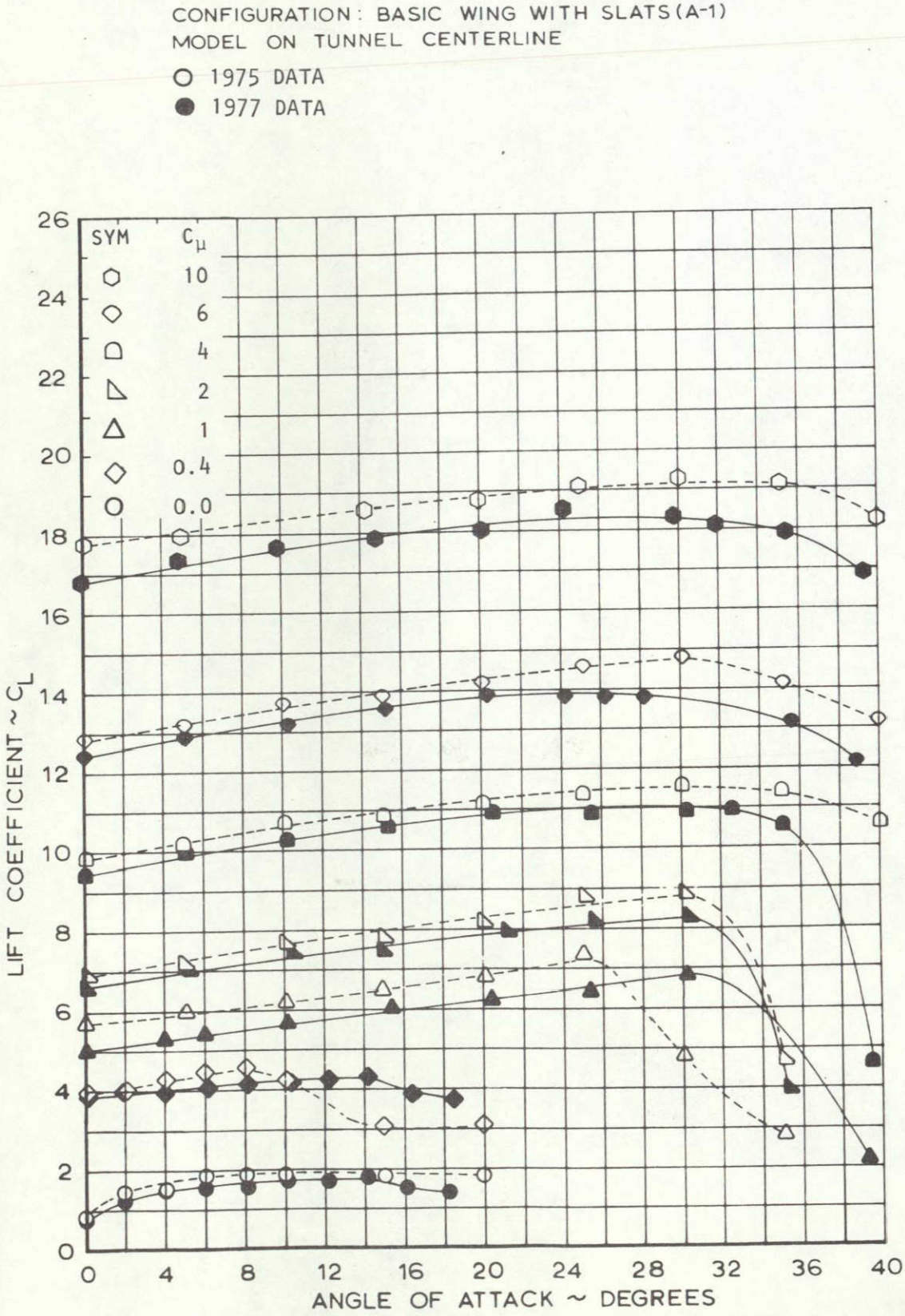

Figure 4.1 Comparison of 1975 and 1977 Test Results in the NASA/AAMRDL 7' x 10' Wind Tunnel (Basic Straight Wing)

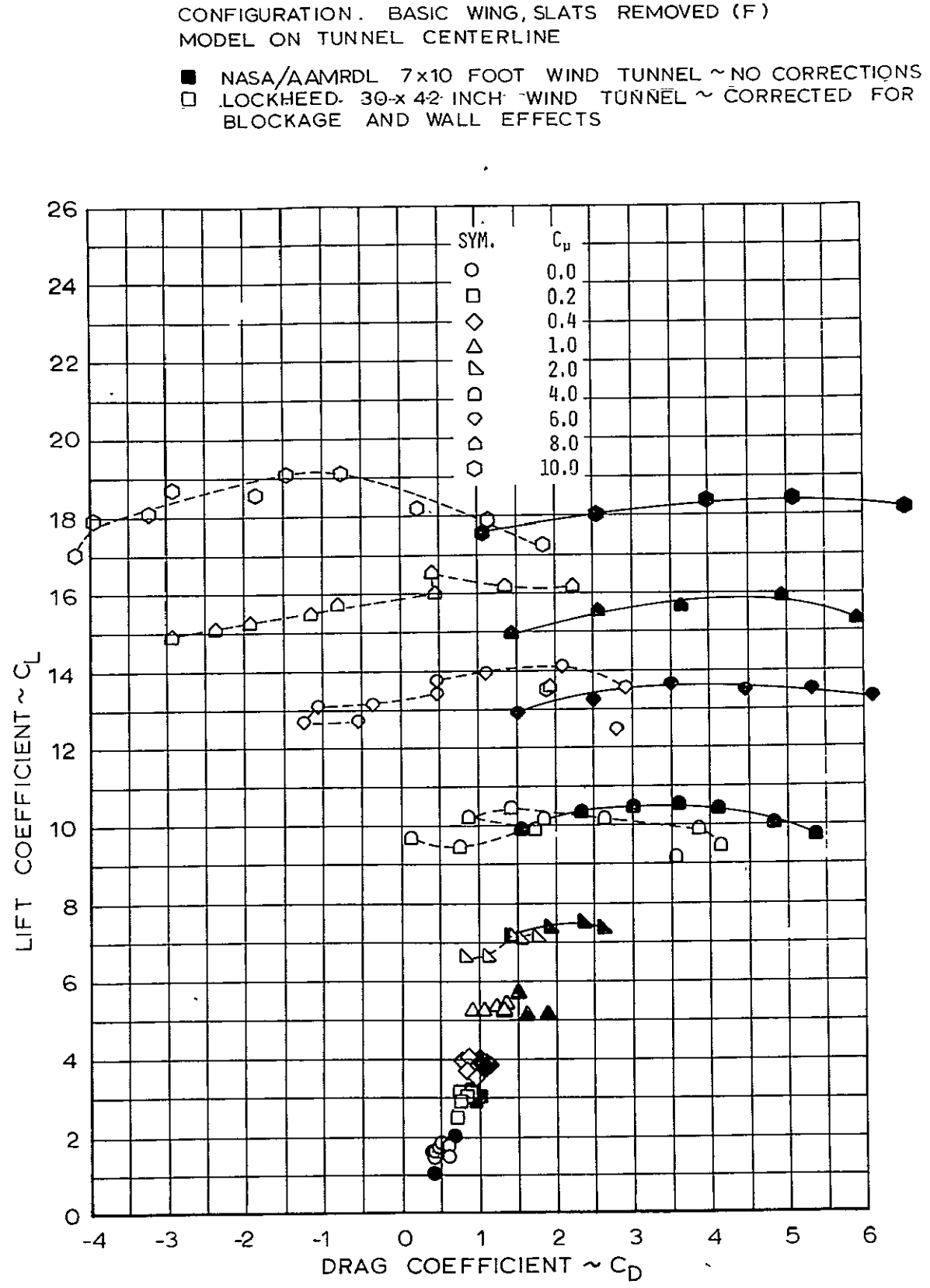

Figure 4.3(a) Drag Polar, Slats Removed, Before Small Tunnel Modification

CONFIGURATION BASIC WING, SLATS REMOVED (F)
MODEL ON TUNNEL CENTERLINE

■ NASA/AAMRDL 7x10 FOOT WIND TUNNEL ~ NO CORRECTIONS
□ LOCKHEED 30 x 42 INCH WIND TUNNEL ~ CORRECTED FOR BLOCKAGE AND WALL EFFECTS

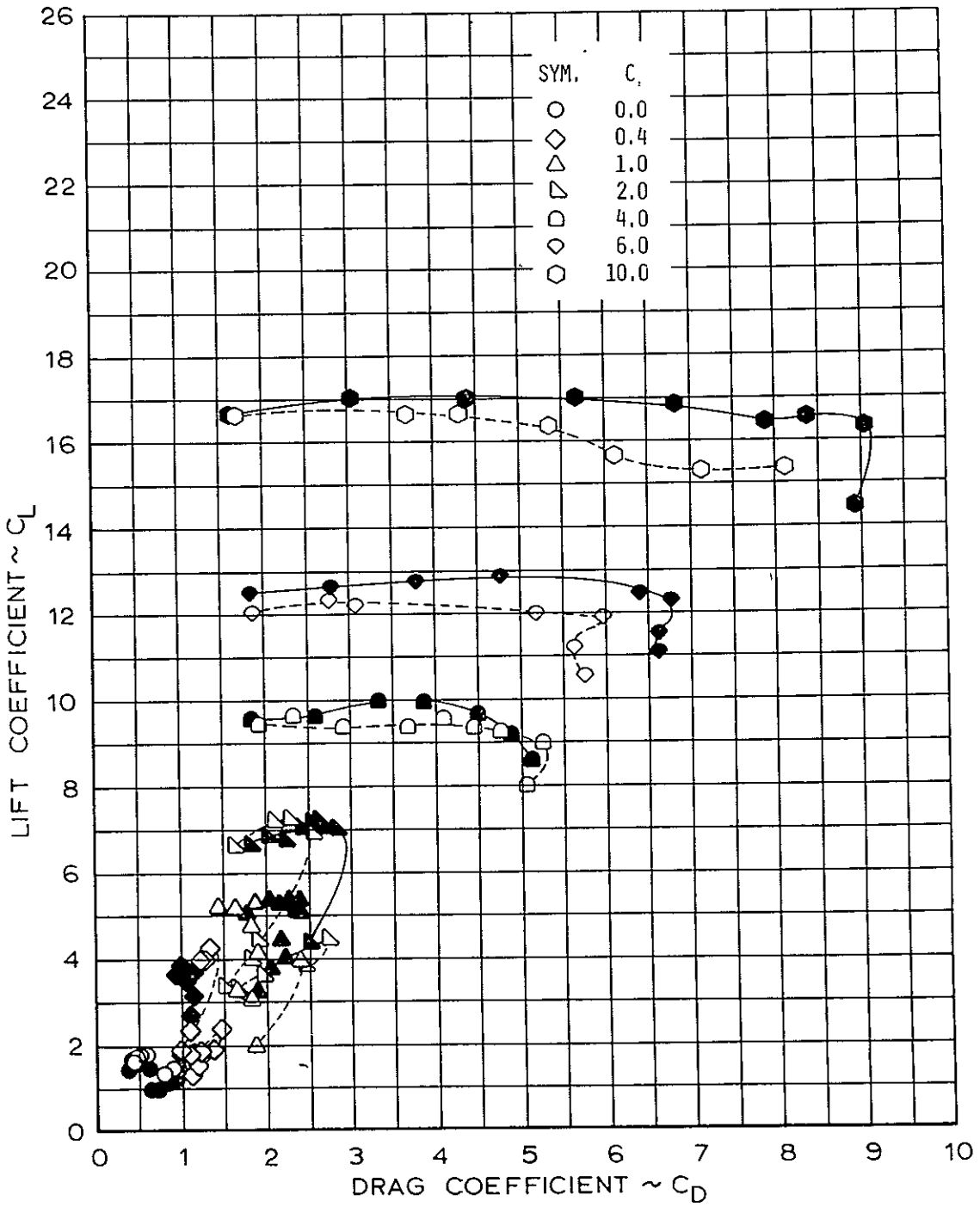

Figure 4.3(b) Drag Polar, Slats Removed, After Small Tunnel Modification

ORIGINAL PAGE IS
OF POOR QUALITY

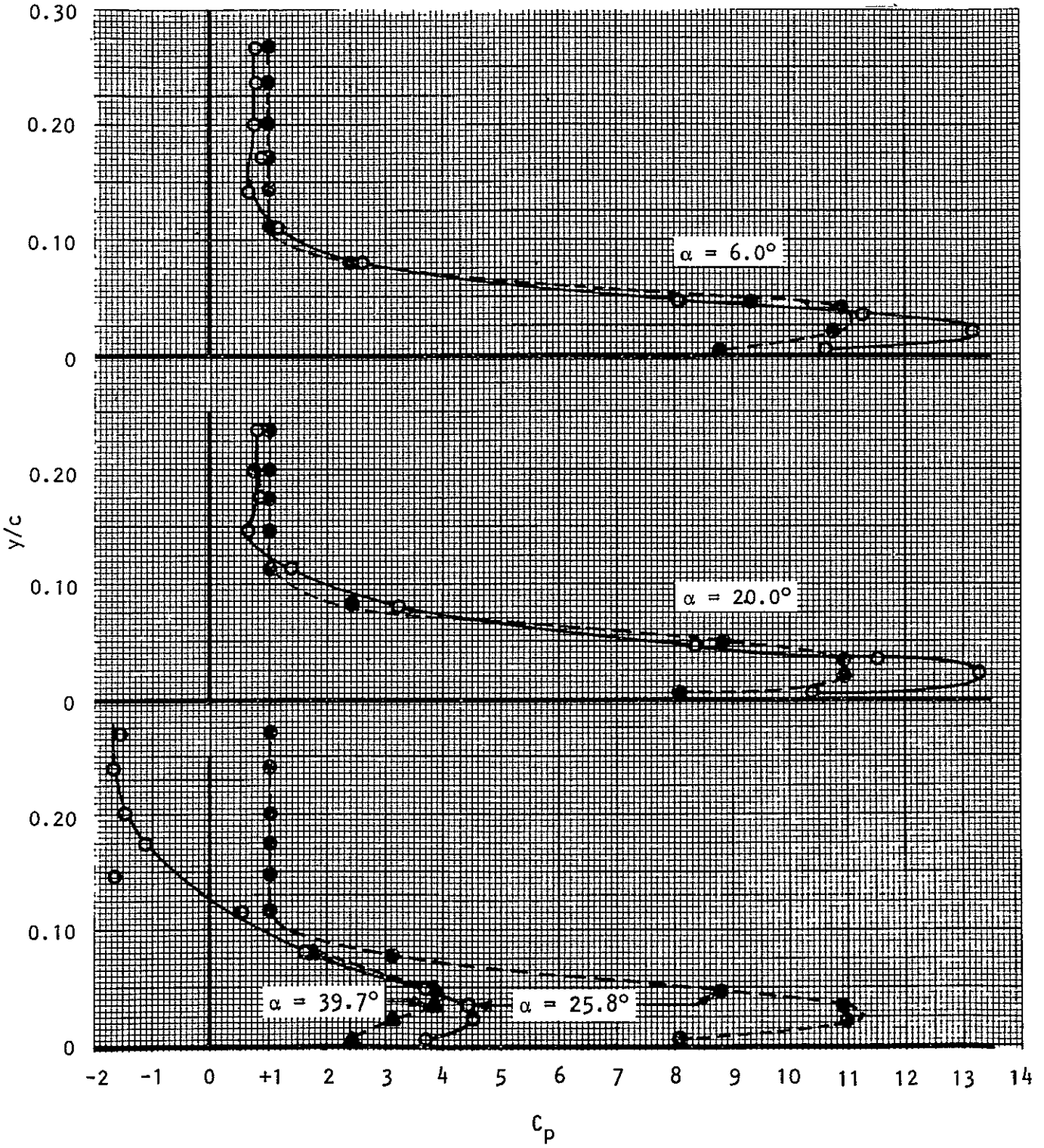

Figure 4.4(a) Flap Rake Profiles, Illustrating Wing Separation (η = 0.70, C_μ = 1.0)

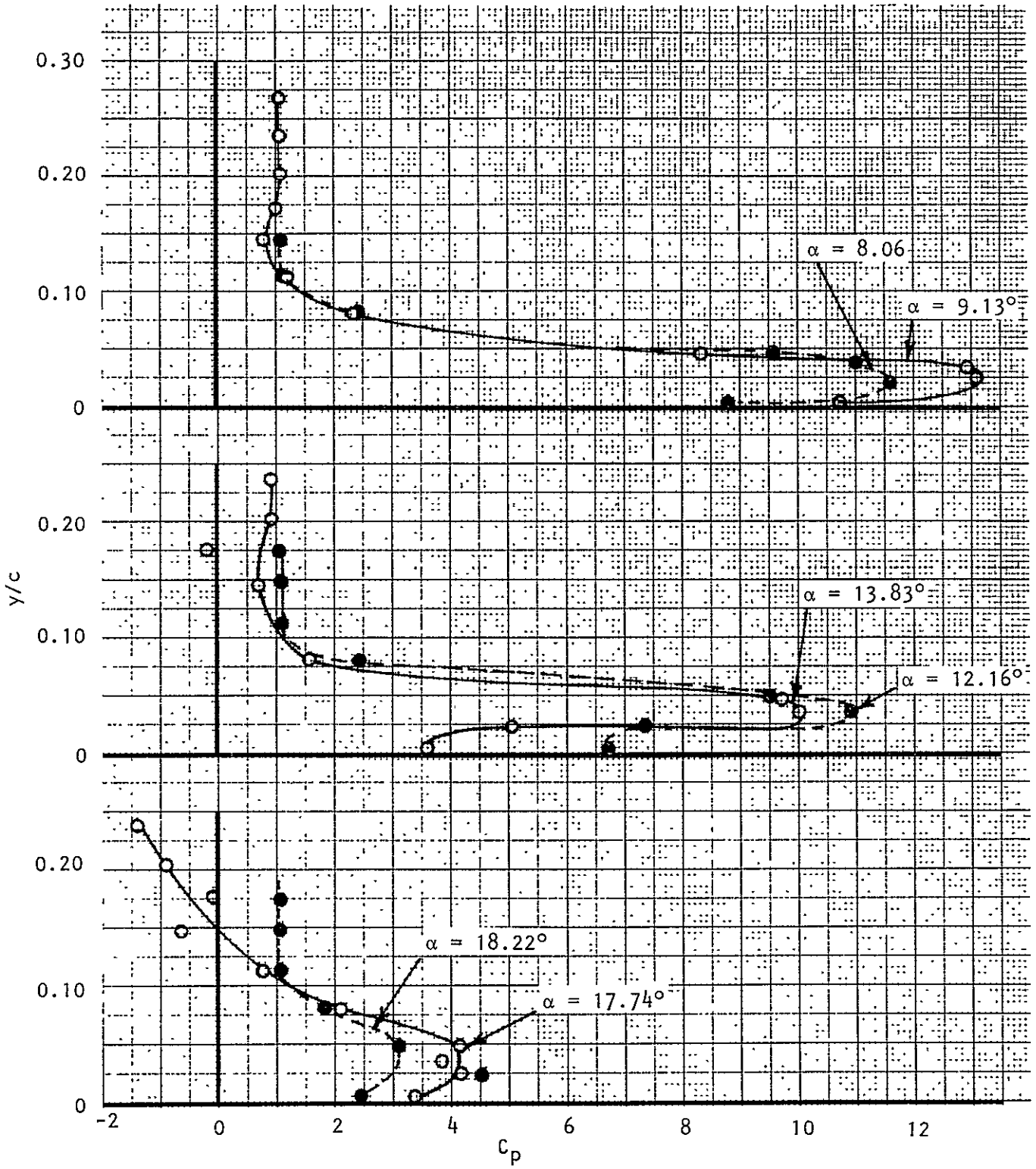

Figure 4.4(b) Flap Rake Profiles, Illustrating Flap, Then Wing Separation (η = 0.70, C_μ = 1.0)

ORIGINAL PAGE IS
OF POOR QUALITY

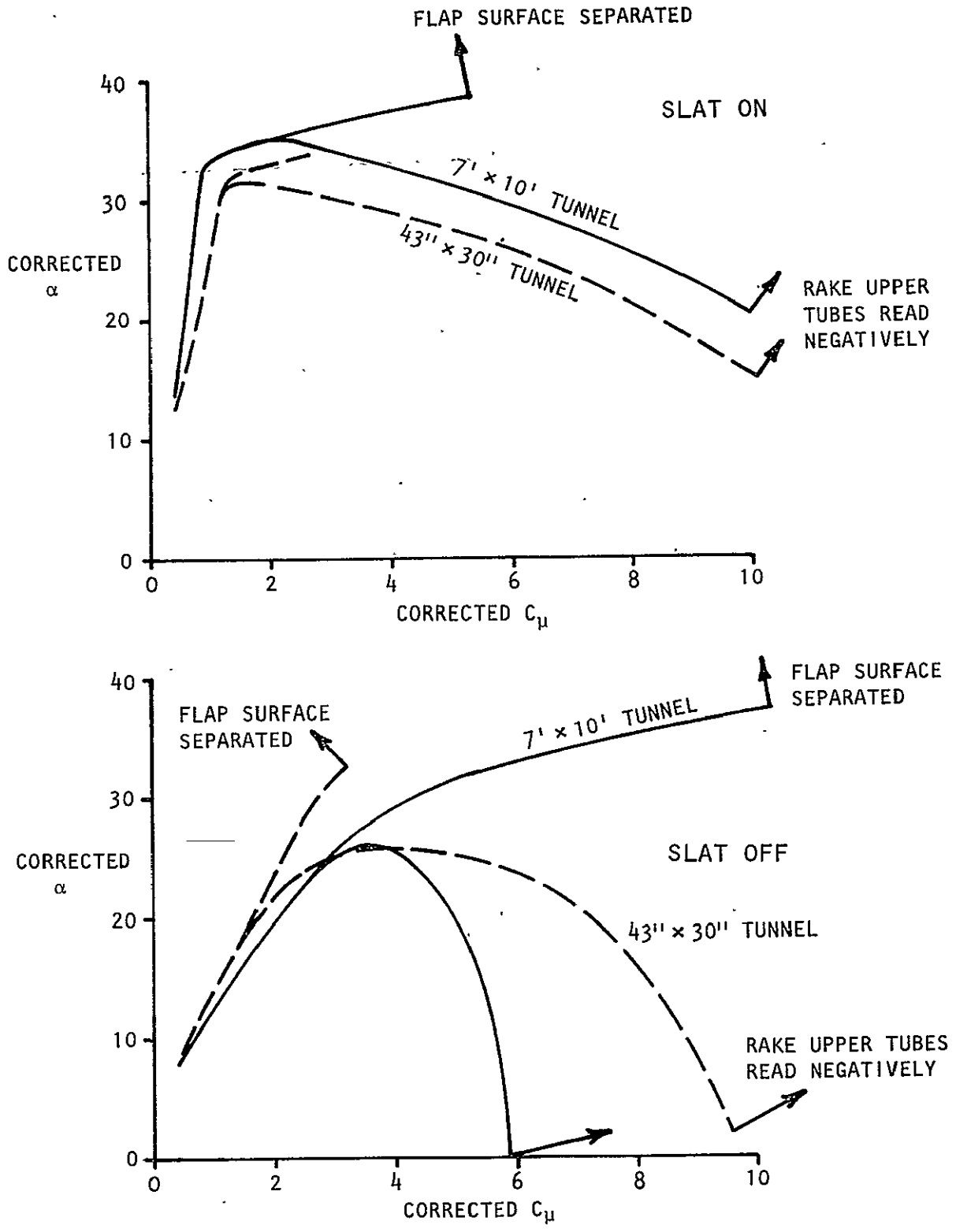

Figure 4.5 Conditions for Flap and Wing Separation in Two Tunnels
Basic Straight Wing

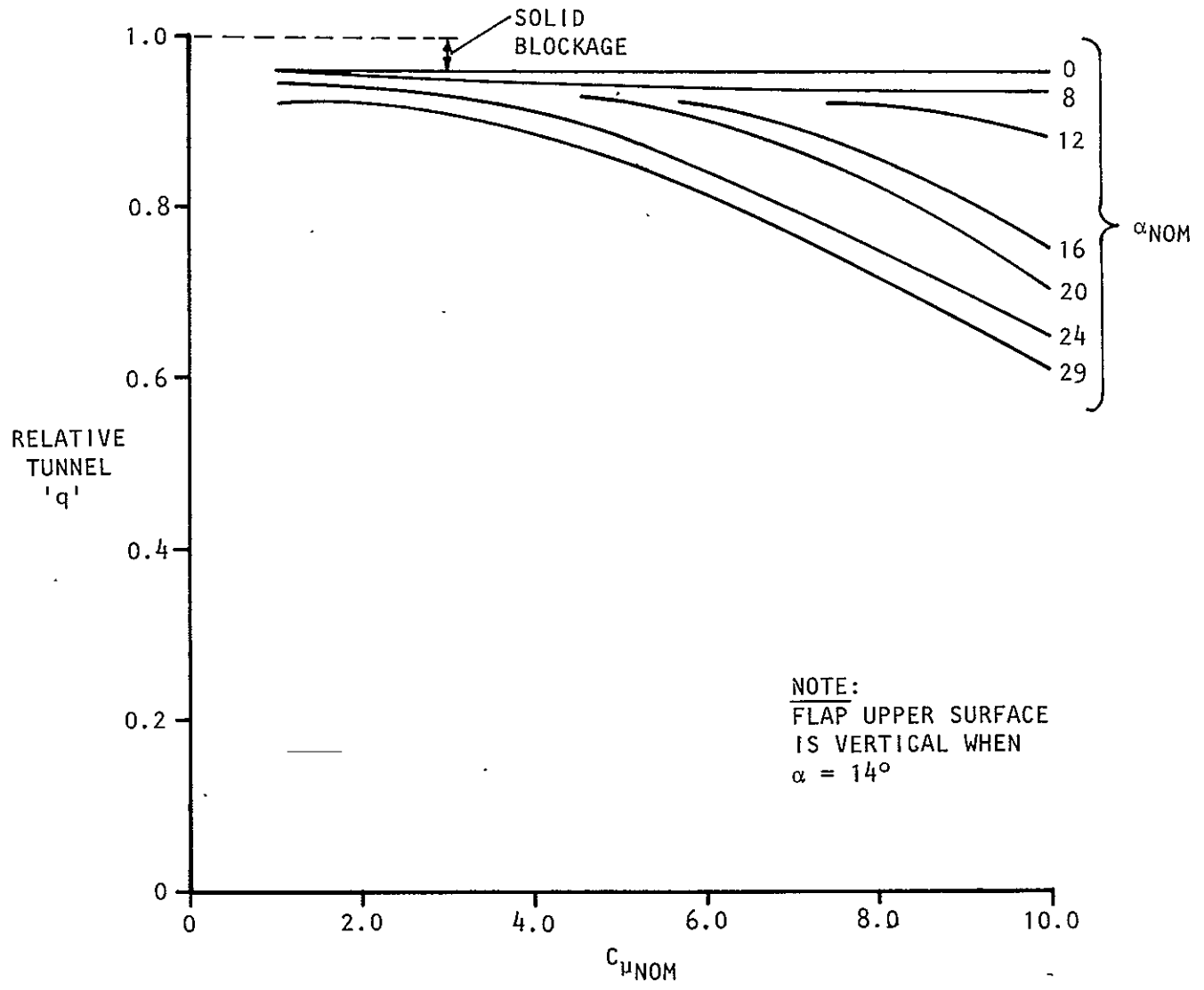

Figure 4.6 Typical Tunnel Settings for "True-q" Operation

ORIGINAL PAGE IS
OF POOR QUALITY

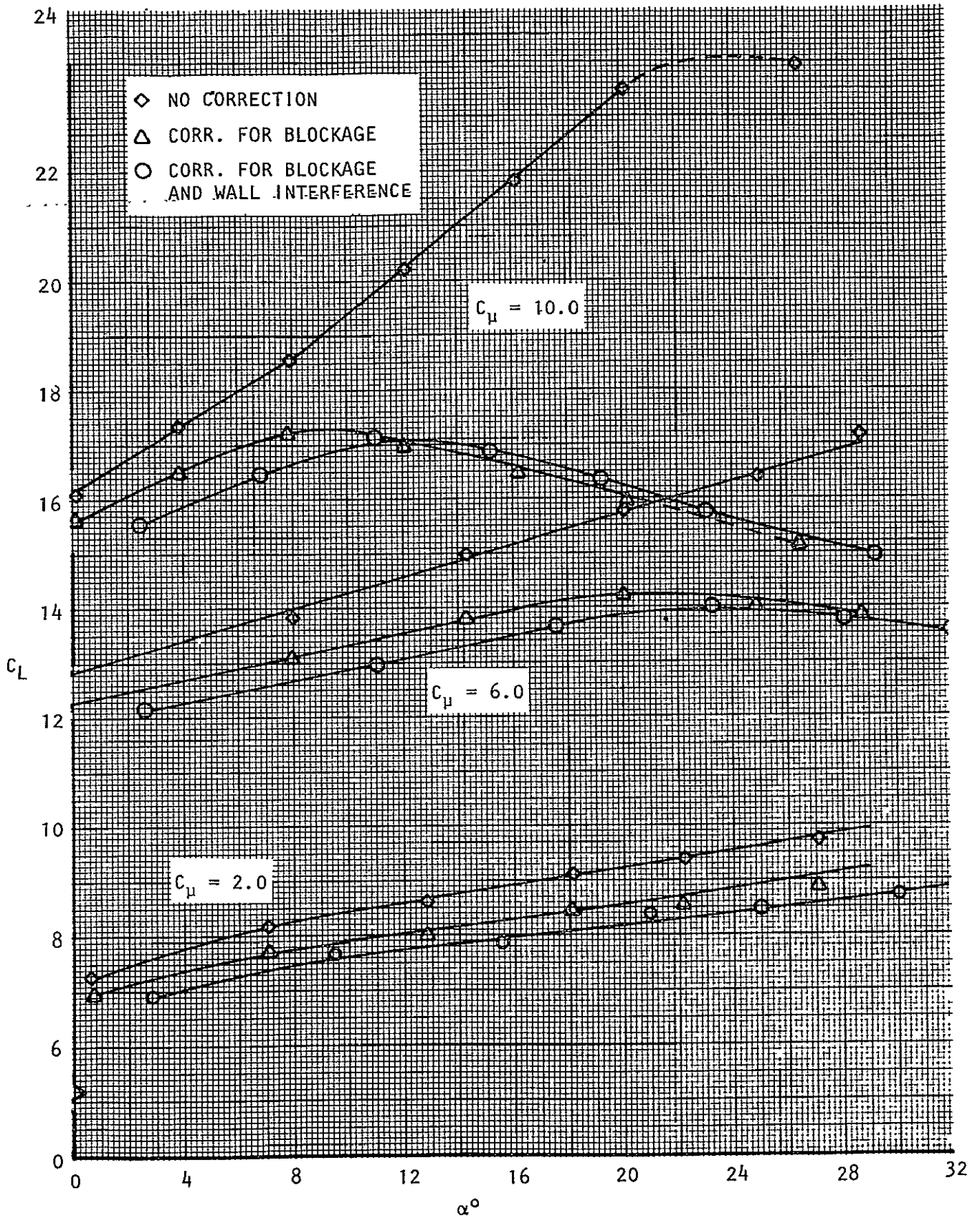

Figure 4.7 Application of Corrections to Small-Tunnel Results, Straight Wing with Slats

CONFIGURATION: STRAIGHT WING WITH SLATS (A-1)
MODEL ON TUNNEL CENTERLINE

--- NASA/AAMRDL 7 x 10 FOOT WIND TUNNEL - NO CORRECTIONS
—— LOCKHEED 30 x 43 INCH WIND TUNNEL - CORRECTED FOR BLOCKAGE AND WALL EFFECTS

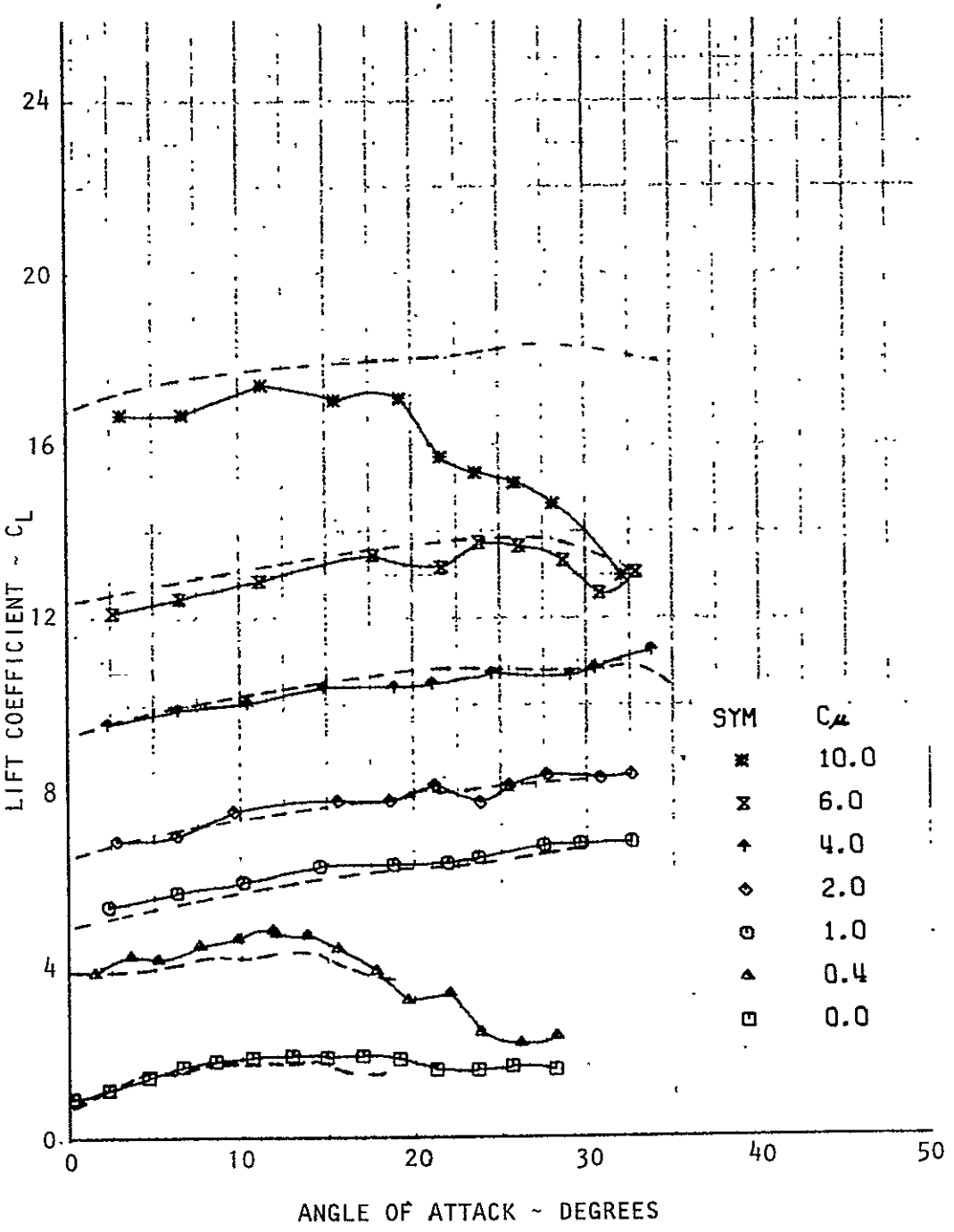

ORIGINAL PAGE IS
OF POOR QUALITY

Figure 4.8(a) Basic Lift Data, Straight Wing With Slats

CONFIGURATION: STRAIGHT WING WITH SLATS (A-1)
MODEL ON TUNNEL CENTERLINE

--- NASA/AAMRDL 7 x 10 FOOT WIND TUNNEL - NO CORRECTIONS
—— LOCKHEED 30 x 43 INCH WIND TUNNEL - CORRECTED FOR BLOCKAGE AND WALL EFFECTS

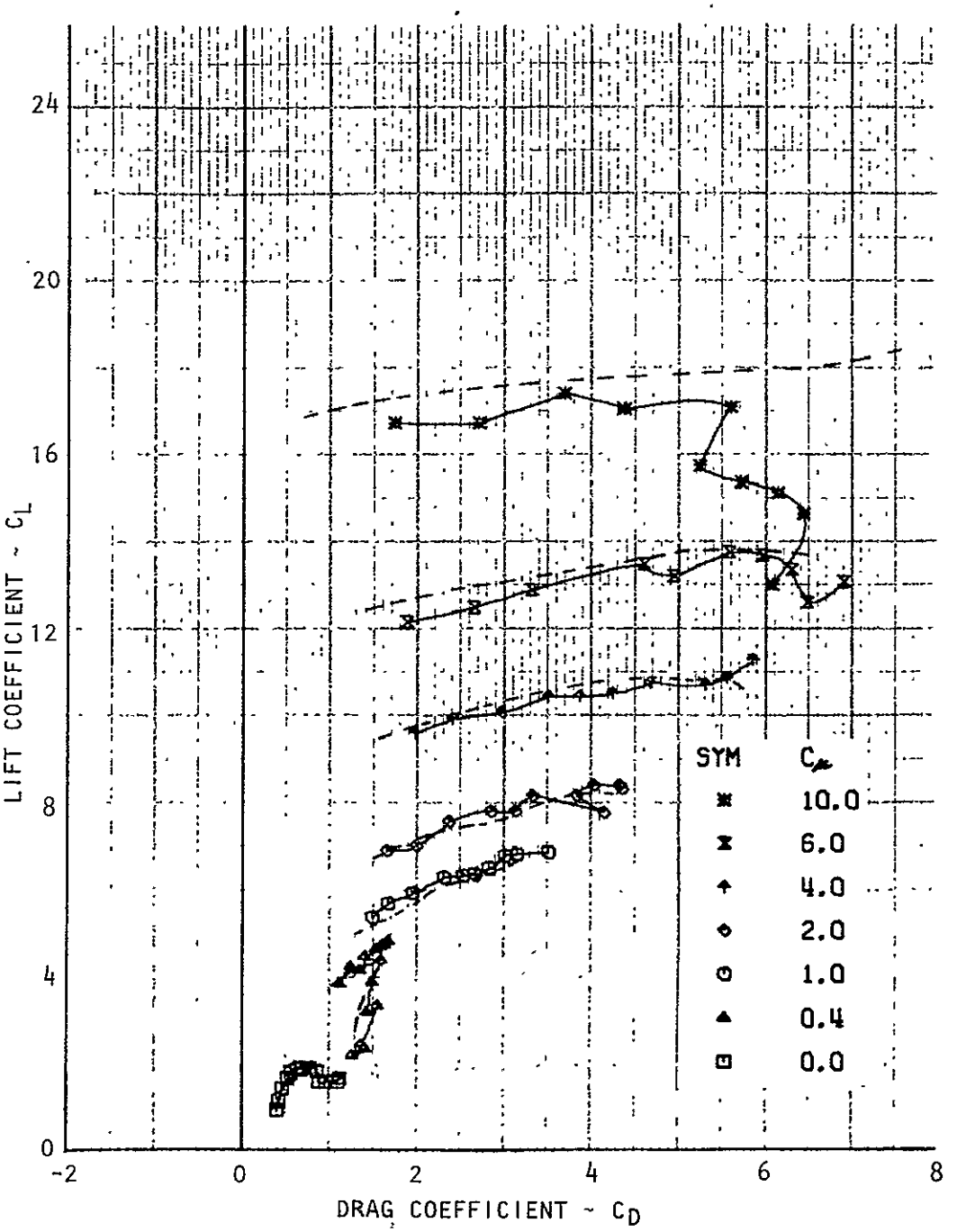

Figure 4.8(b) Basic Drag Data, Straight Wing with Slats

CONFIGURATION: STRAIGHT WING WITH SLATS (A-1)
MODEL ON TUNNEL CENTERLINE

--- NASA/AAMRDL 7 x 10 FOOT WIND TUNNEL - NO CORRECTIONS
—— LOCKHEED 30 x 43 INCH WIND TUNNEL - CORRECTED FOR BLOCKAGE AND WALL EFFECTS

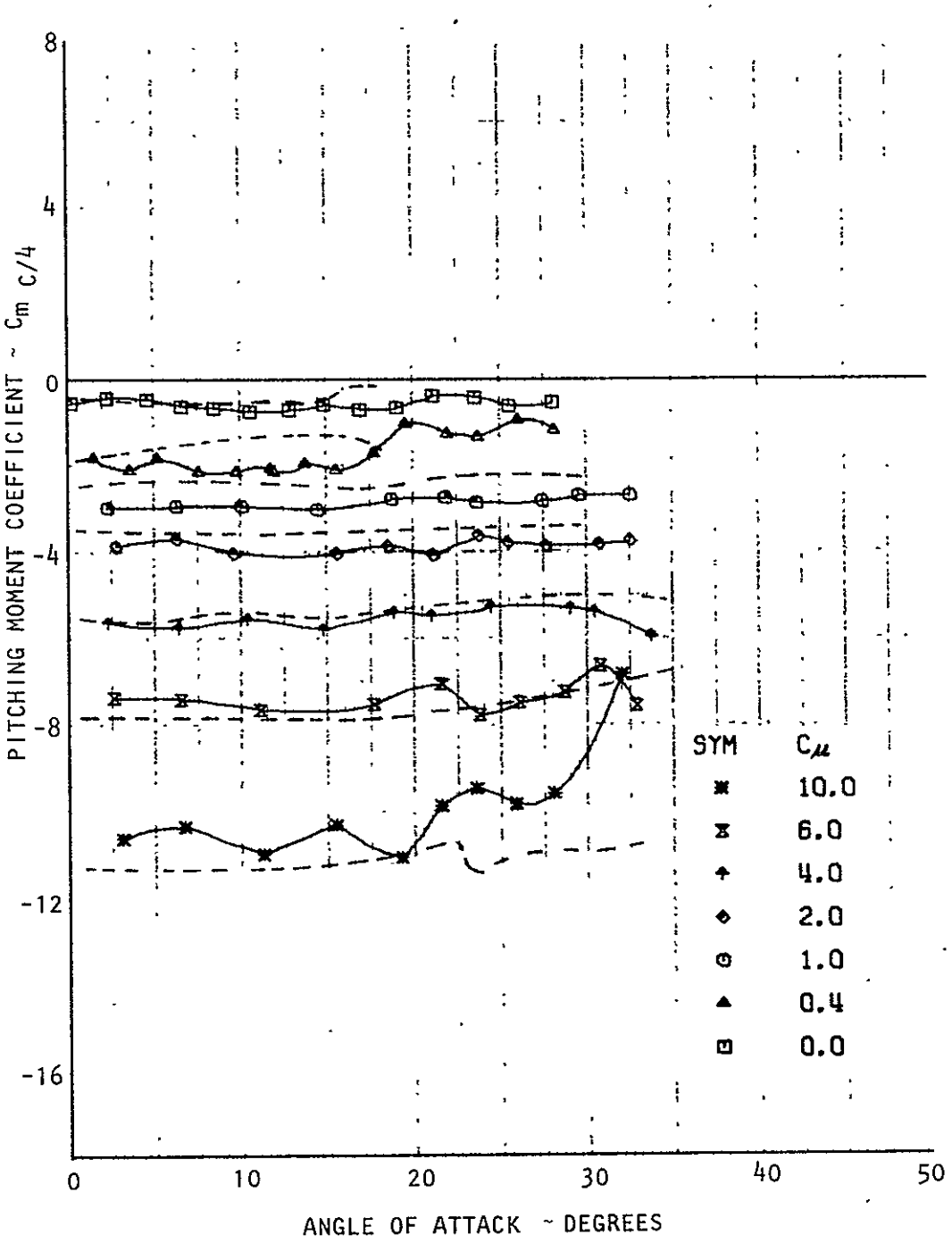

ORIGINAL PAGE IS
OF POOR QUALITY

Figure 4.8(c) Basic Pitching Moment Data, Straight Wing With Slats

CONFIGURATION: STRAIGHT WING (F)
MODEL ON TUNNEL CENTERLINE

--- NASA/AAMRDL 7 x 10 FOOT WIND TUNNEL - NO CORRECTIONS
—— LOCKHEED 30 x 43 INCH WIND TUNNEL - CORRECTED FOR BLOCKAGE AND WALL EFFECTS

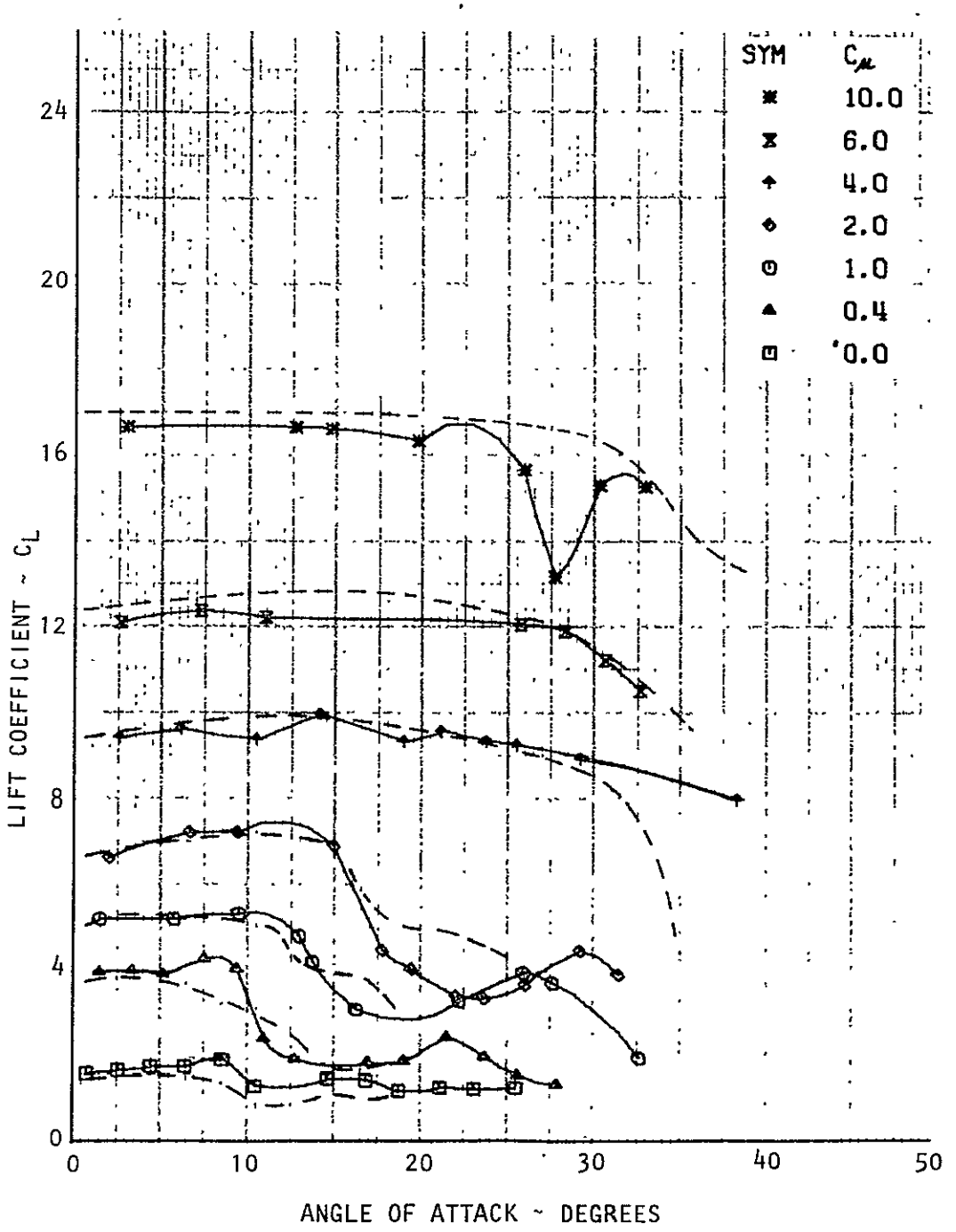

Figure 4.9(a) Basic Lift Data, Straight Wing, No Slats

CONFIGURATION: STRAIGHT WING (F)
MODEL ON TUNNEL CENTERLINE

– – – NASA/AAMRDL 7 x 10 FOOT WIND TUNNEL ~ NO CORRECTIONS
——— LOCKHEED 30 x 43 INCH WIND TUNNEL ~ CORRECTED FOR BLOCKAGE AND WALL EFFECTS

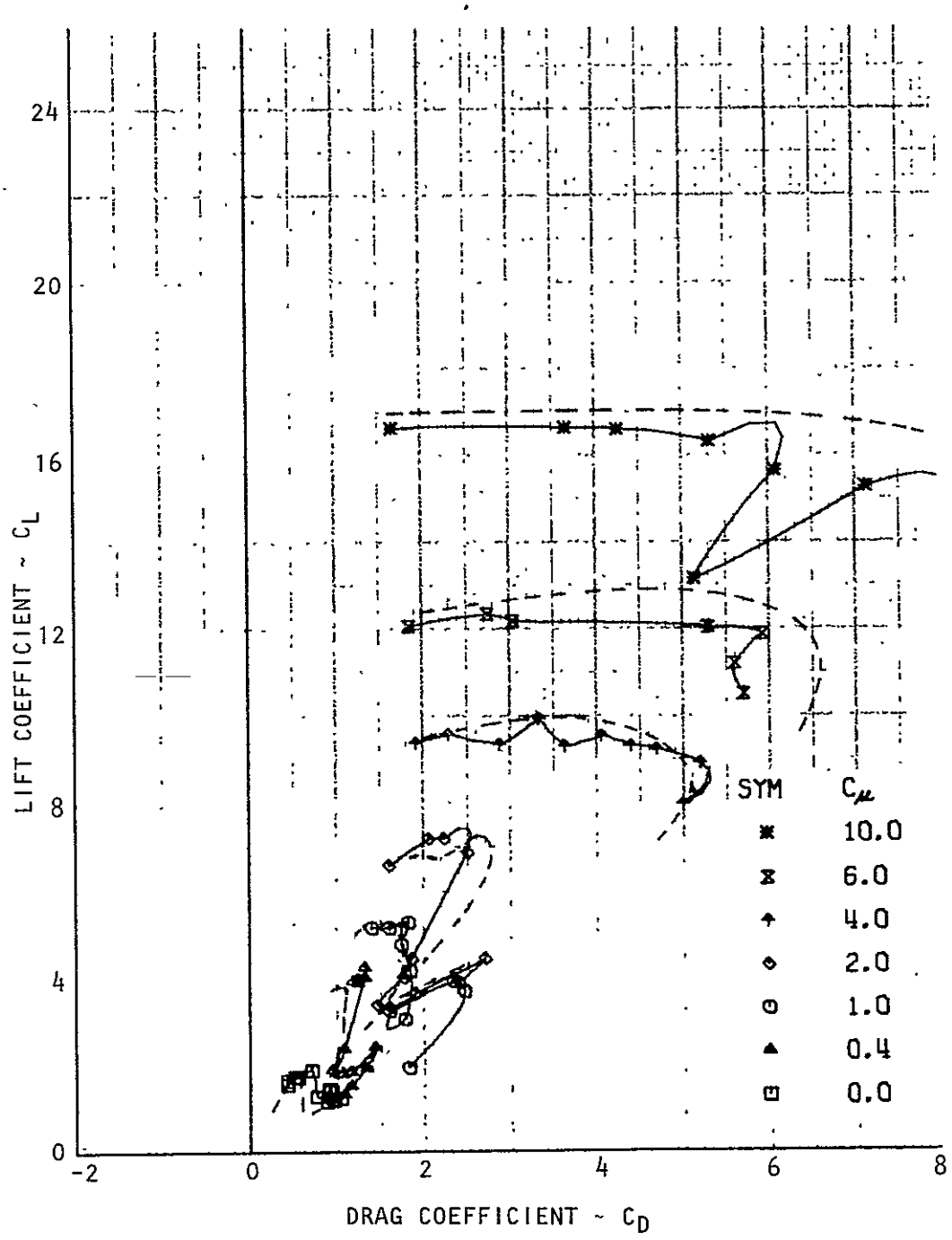

ORIGINAL PAGE IS
OF POOR QUALITY

Figure 4.9(b) Basic Drag Data, Straight Wing, No Slats

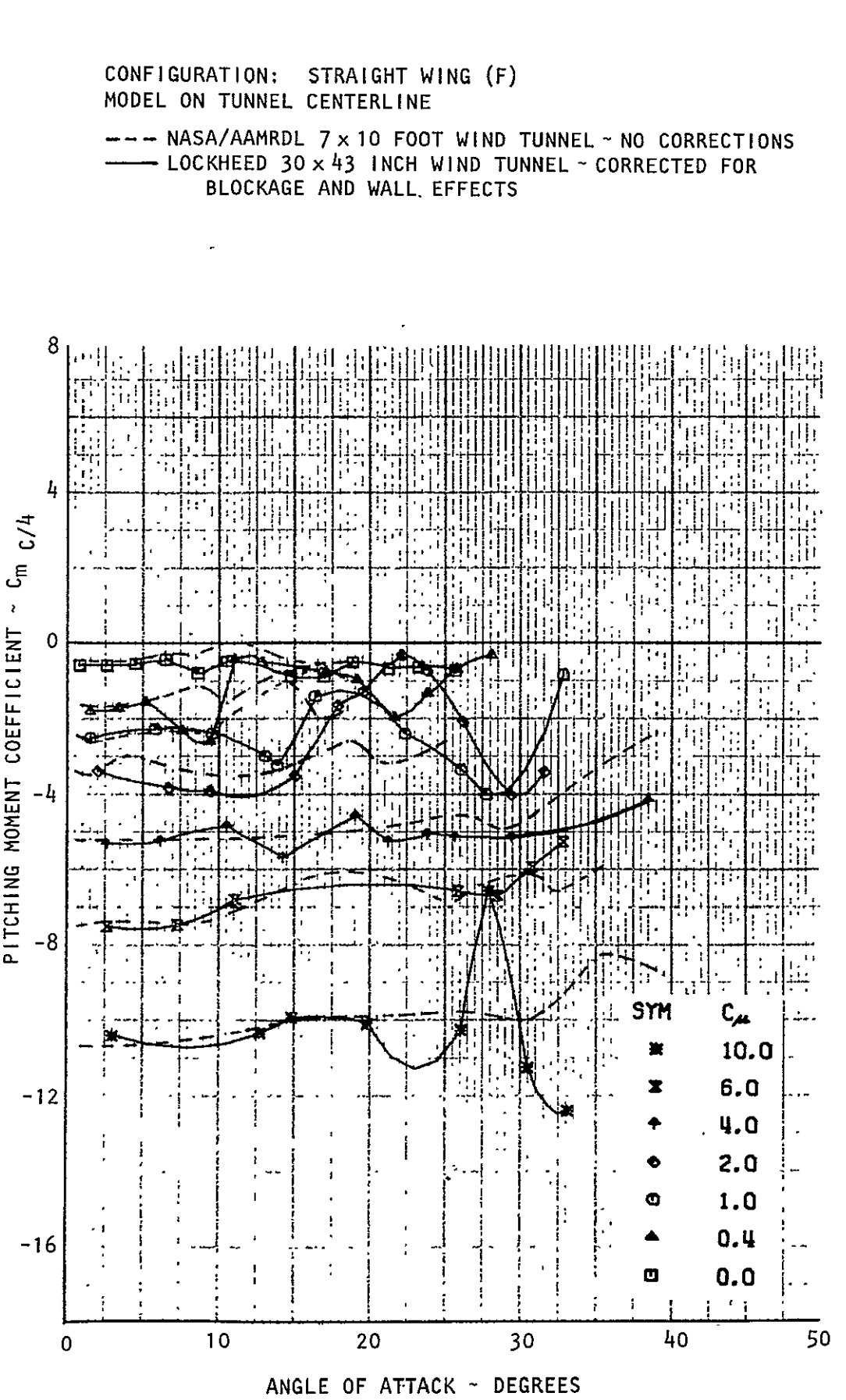

Figure 4.9(c) Basic Pitching Moment Data, Straight Wing, No Slats

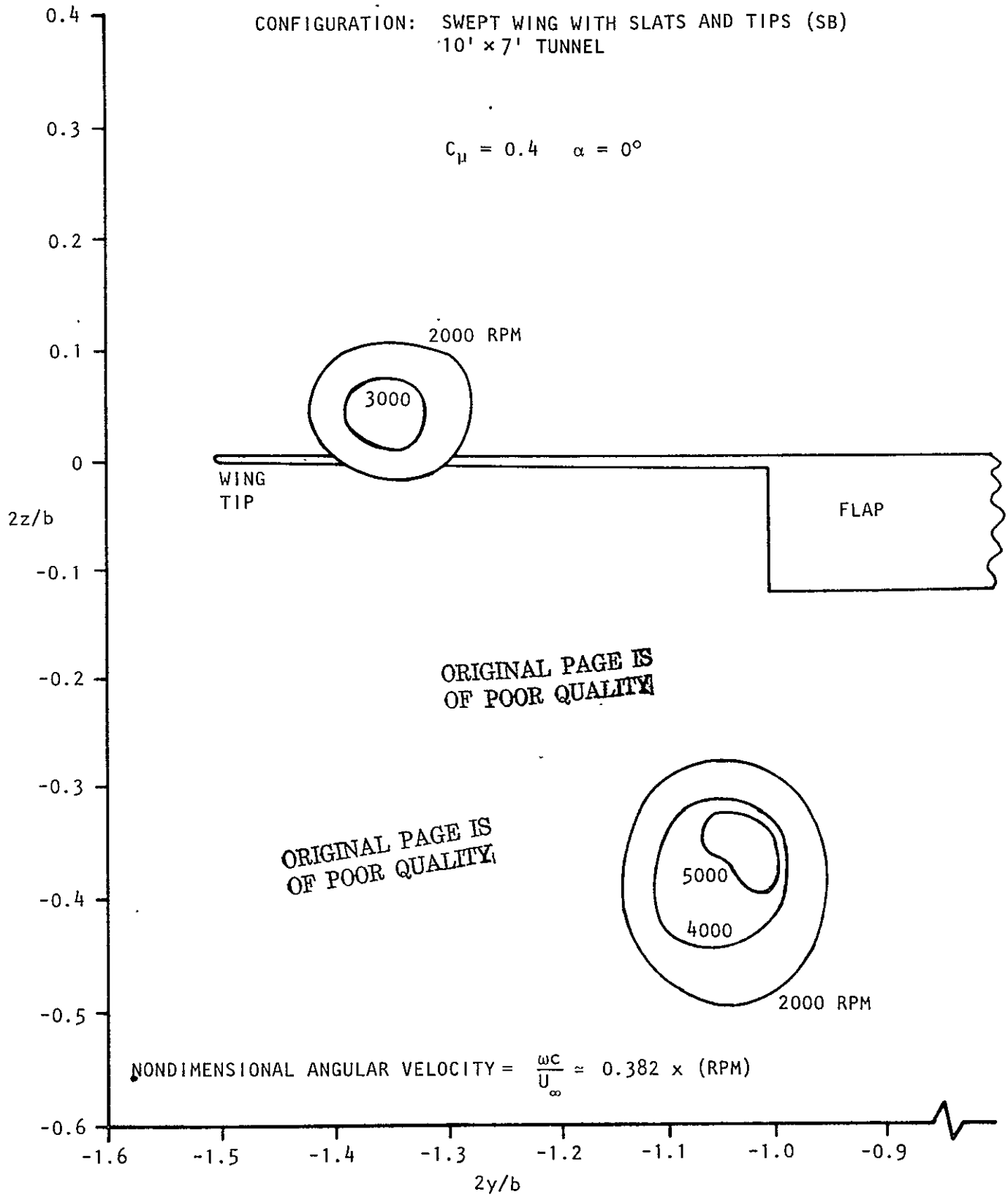

Figure 5.1 Contours of Vorticity Meter Reading at x/c = 5.13

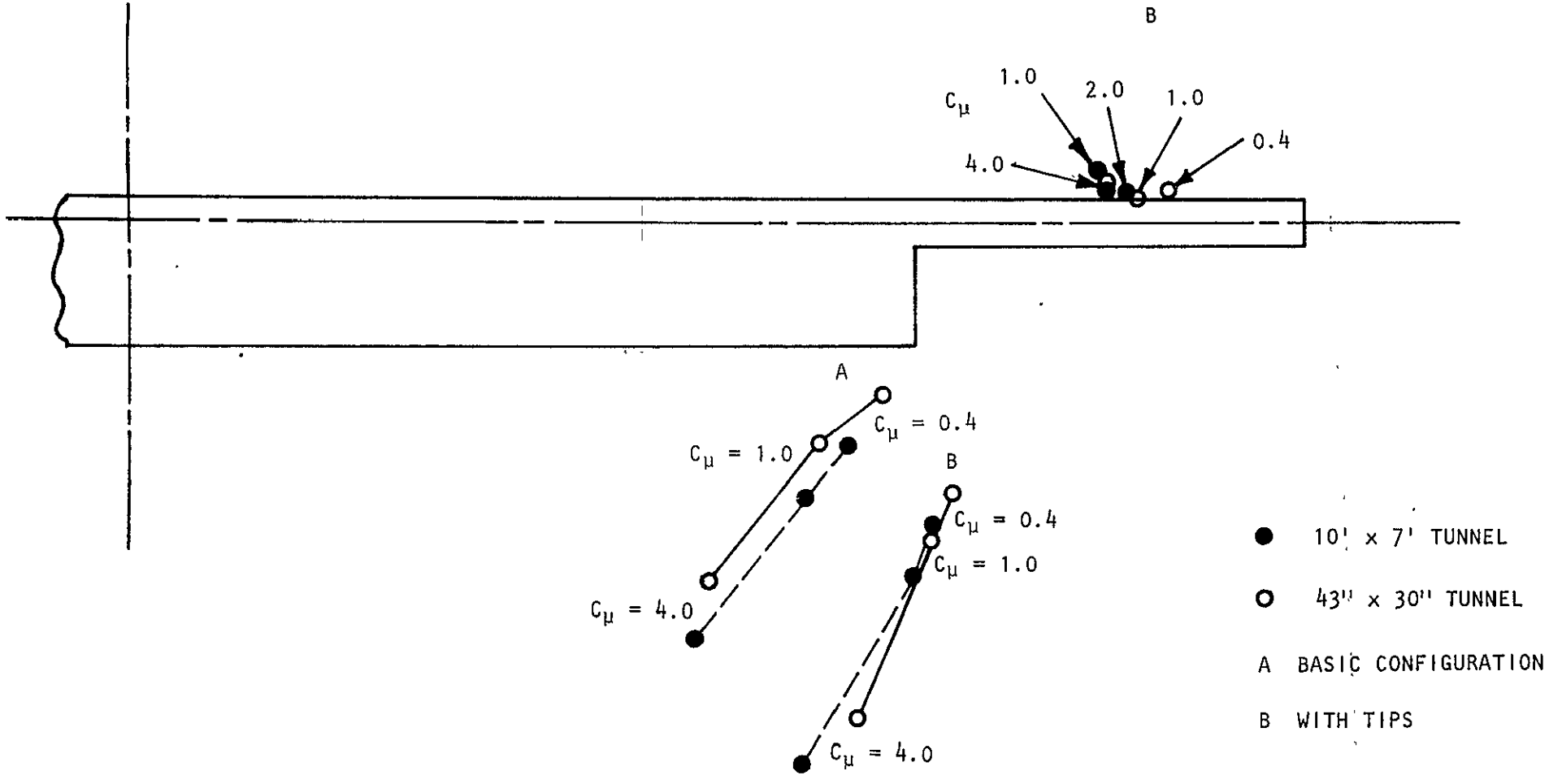

Figure 5.2 Measured Vortex Positions in Large and Small Tunnels
$x/c = 5.13$ $\alpha = 0°$

CONFIGURATION: SWEPT WING WITH SLATS (SA-1)
MODEL ON TUNNEL CENTERLINE

– – – NASA/AAMRDL 7 x 10 FOOT WIND TUNNEL -NO CORRECTIONS
——— LOCKHEED 30 x 43 INCH WIND TUNNEL - CORRECTED FOR BLOCKAGE AND WALL EFFECTS

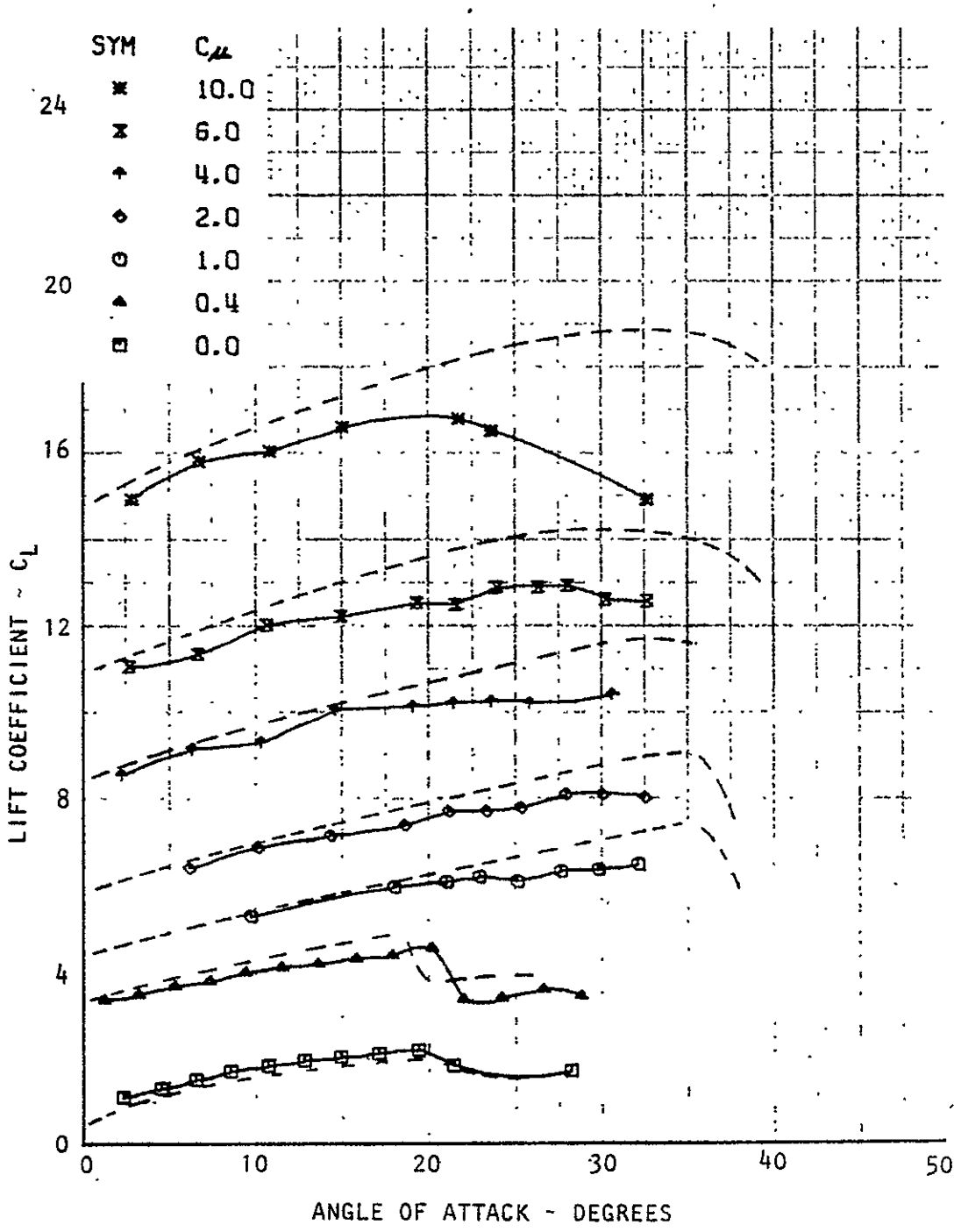

ORIGINAL PAGE IS
OF POOR QUALITY

Figure 5.3(a) Basic Lift Data, Swept Wing With Slats

CONFIGURATION: SWEPT WING WITH SLATS (SA-1)
MODEL ON TUNNEL CENTERLINE

——— NASA/AAMRDL 7 x 10 FOOT WIND TUNNEL - NO CORRECTIONS
——— LOCKHEED 30 x 43 INCH WIND TUNNEL - CORRECTED FOR BLOCKAGE AND WALL EFFECTS

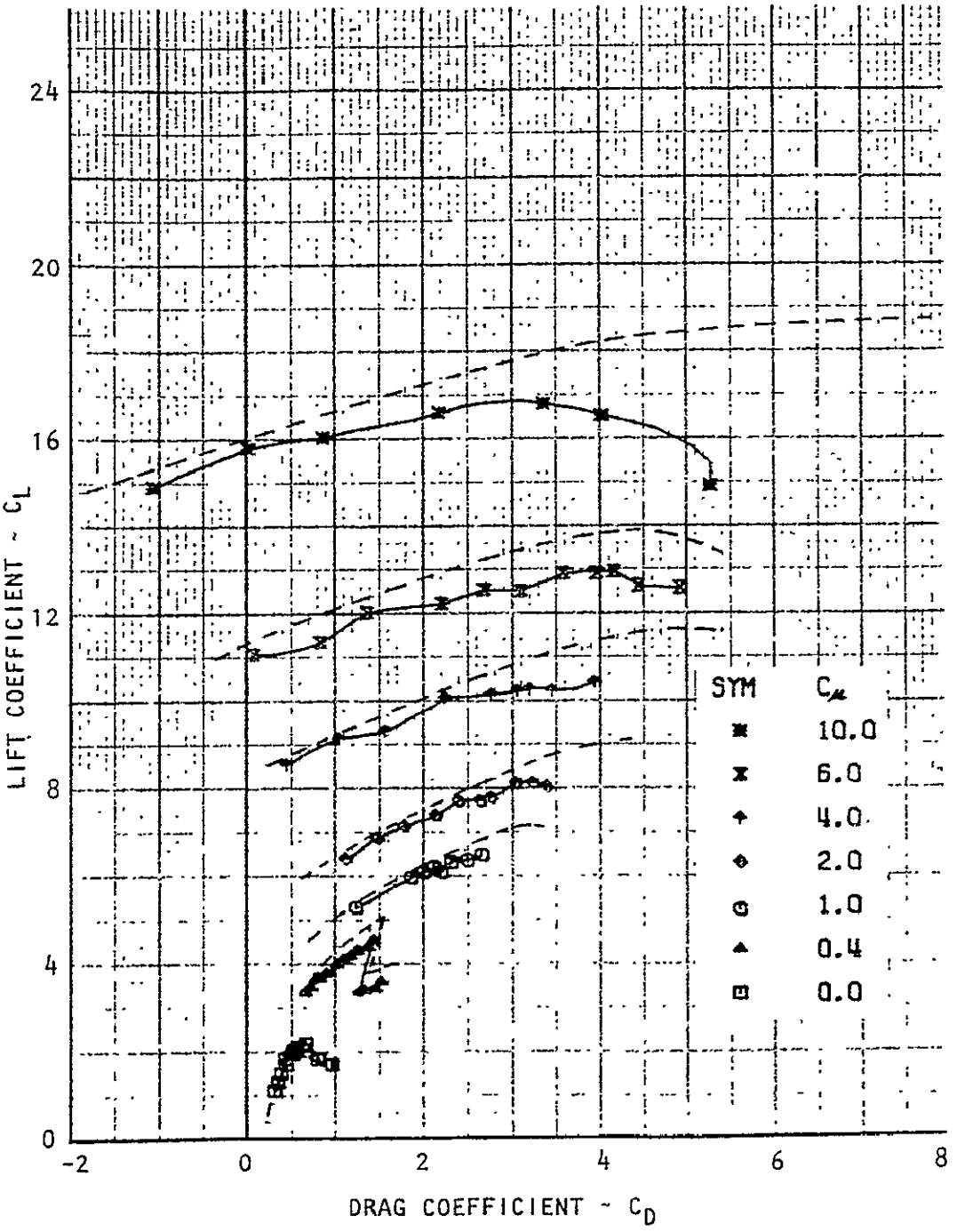

Figure 5.3(b). Basic Drag Data, Swept Wing With Slats

CONFIGURATION: SWEPT WING WITH SLATS, (SA-1)
MODEL ON TUNNEL CENTERLINE

– – – NASA/AAMRDL 7 x 10 FOOT WIND TUNNEL - NO CORRECTIONS
——— LOCKHEED 30 x 43 INCH WIND TUNNEL - CORRECTED FOR BLOCKAGE AND WALL EFFECTS

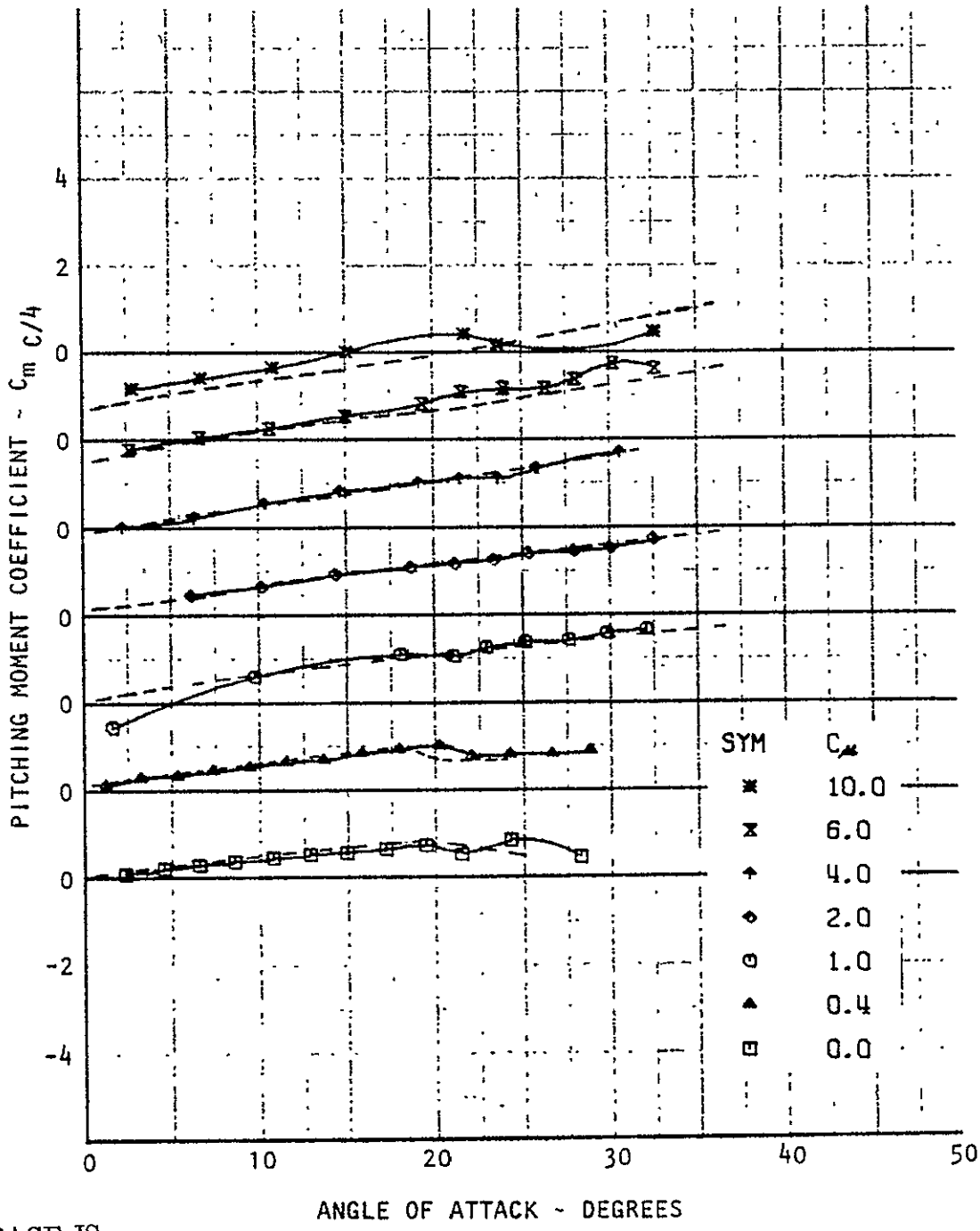

ORIGINAL PAGE IS
OF POOR QUALITY

Figure 5.3(c) Basic Pitching Moment Data, Swept Wing With Slats

CONFIGURATION: SWEPT WING WITH TIPS AND FULL SPAN SLATS (SB)
MODEL ON TUNNEL CENTERLINE

---- NASA/AAMRDL 7 x 10 FOOT WIND TUNNEL - NO CORRECTIONS
—— LOCKHEED 30 x 43 INCH WIND TUNNEL - CORRECTED FOR BLOCKAGE AND WALL EFFECTS

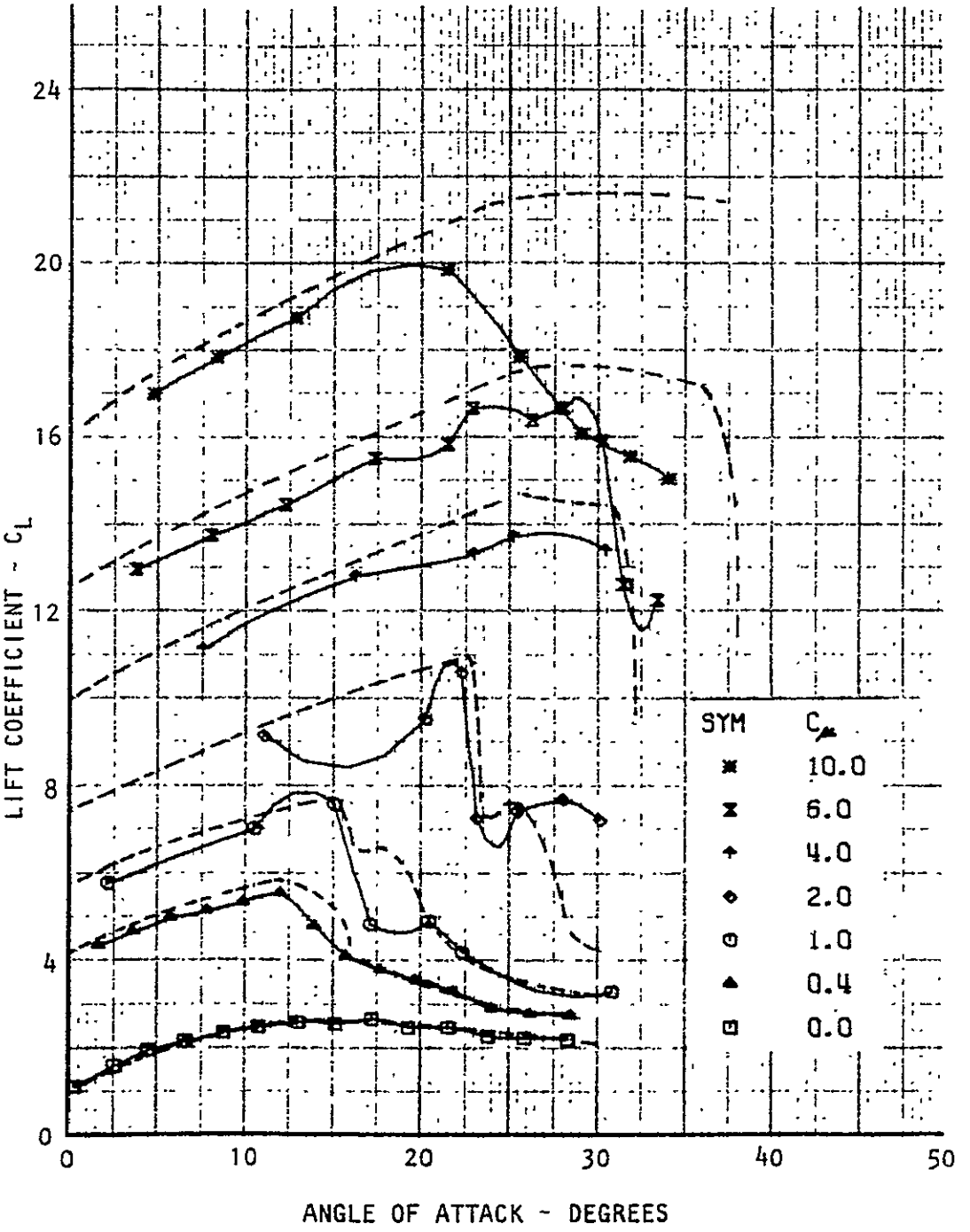

Figure 5.4(a) Basic Lift Data, Swept Wing With Tips and Full-Span Slats

CONFIGURATION: SWEPT WING WITH TIPS AND FULL SPAN SLATS (SB)
MODEL ON TUNNEL CENTERLINE

——— NASA/AAMRDL 7 x 10 FOOT WIND TUNNEL - NO CORRECTIONS
——— LOCKHEED 30 x 43 INCH WIND TUNNEL - CORRECTED FOR BLOCKAGE AND WALL EFFECTS

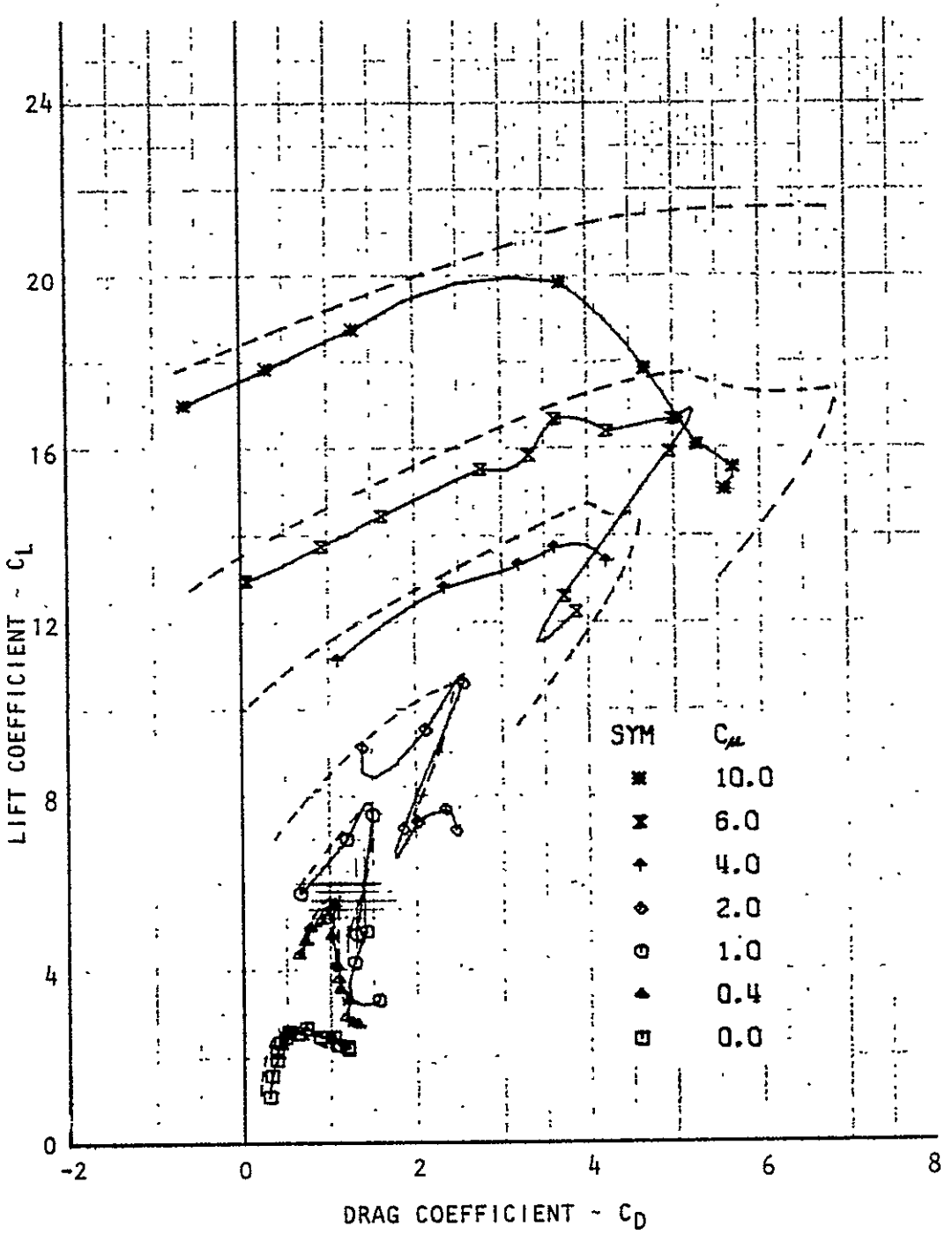

ORIGINAL PAGE IS
OF POOR QUALITY

Figure 5.4(b) Basic Drag Data, Swept Wing With Tips and Full-Span Slats

CONFIGURATION: SWEPT WING WITH TIPS AND FULL SPAN SLATS (SB)
MODEL ON TUNNEL CENTERLINE

--- NASA/AAMRDL 7 x 10 FOOT WIND TUNNEL - NO CORRECTIONS
—— LOCKHEED 30 x 43 INCH WIND TUNNEL - CORRECTED FOR BLOCKAGE AND WALL EFFECTS

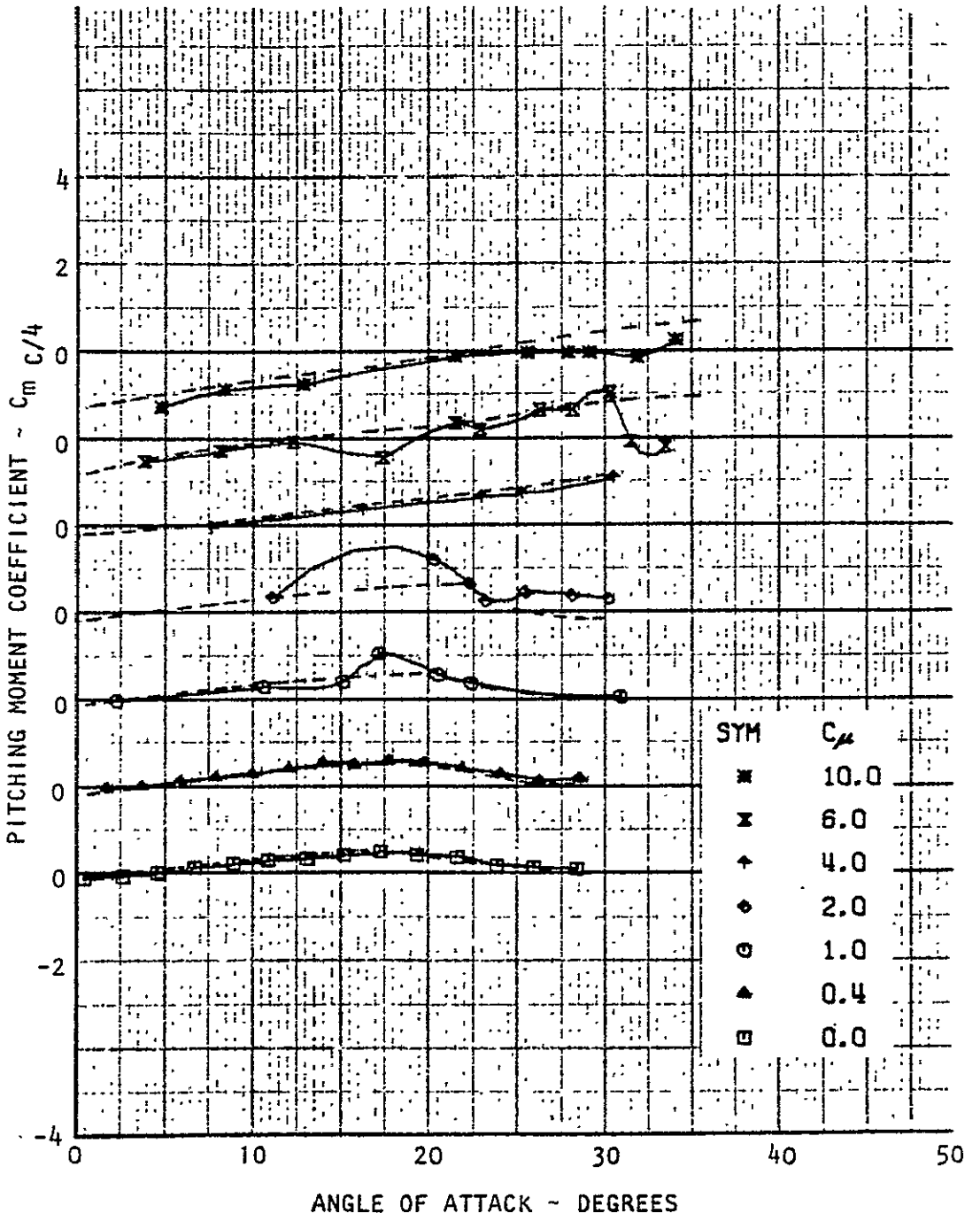

Figure 5.4(c) Basic Pitching Moment Data, Swept Wing With Lips and Full-Span Slats

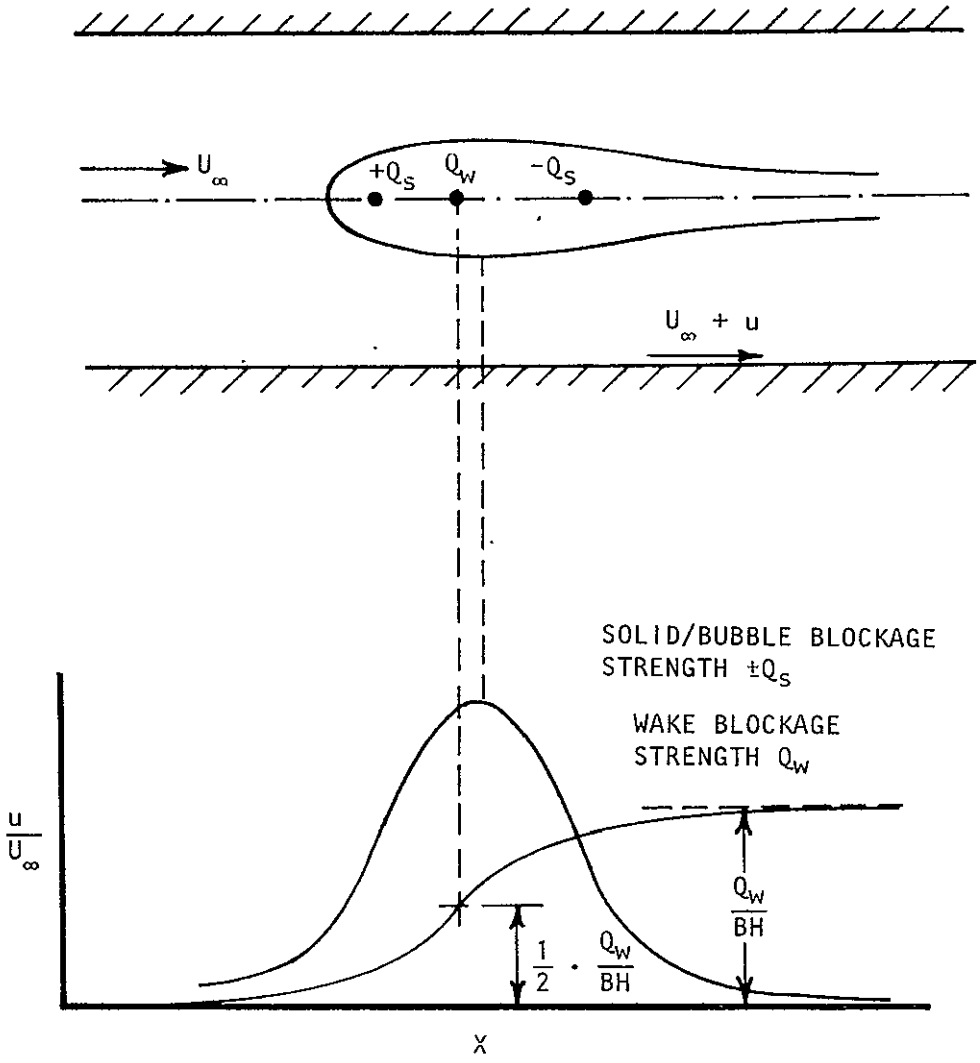

Figure 6.1 Effects at a Wind Tunnel Wall of Solid/Bubble and of Wake Blockage

ORIGINAL PAGE IS
OF POOR QUALITY

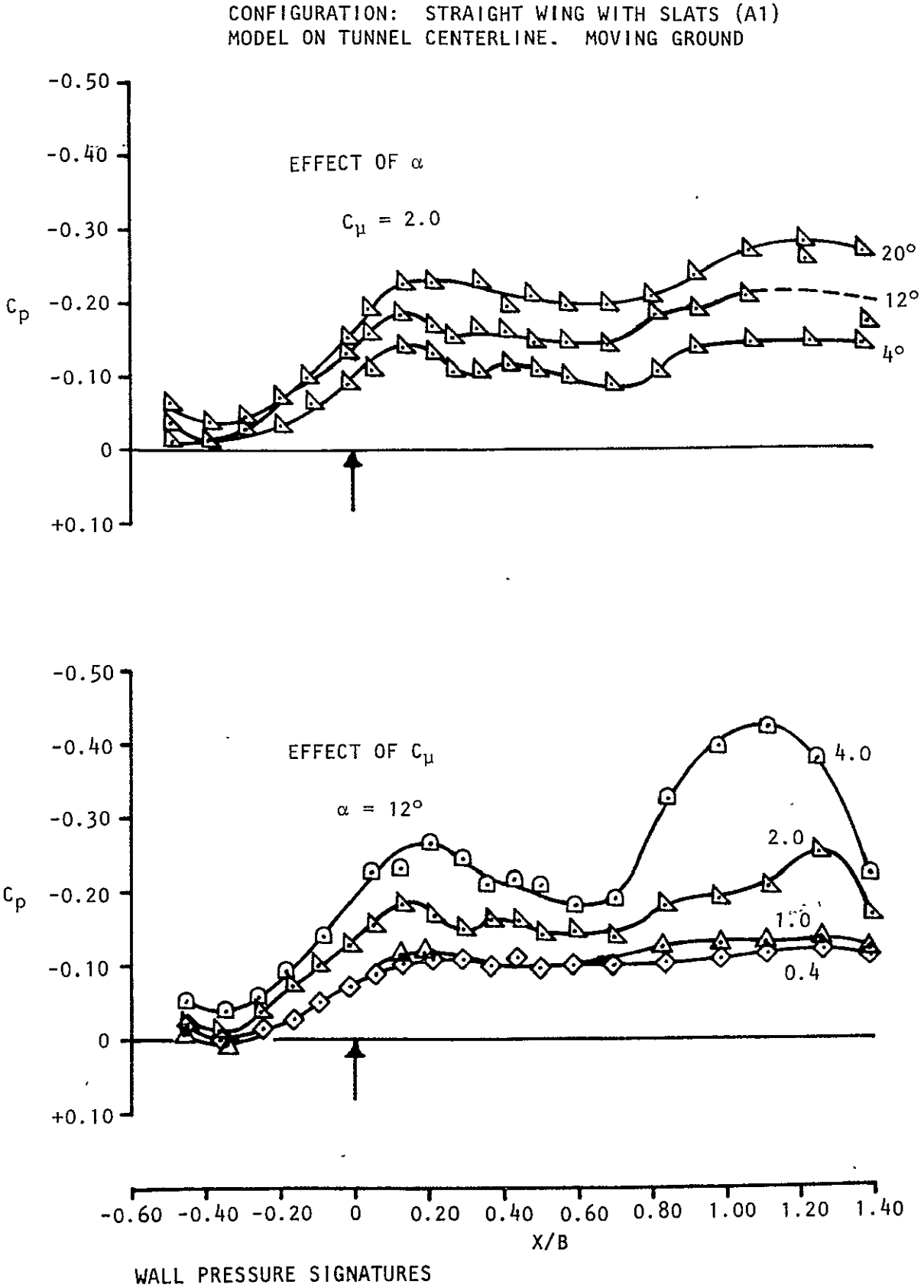

Figure 6.2 Effects of α and C_μ, $0 < C_L < 10$

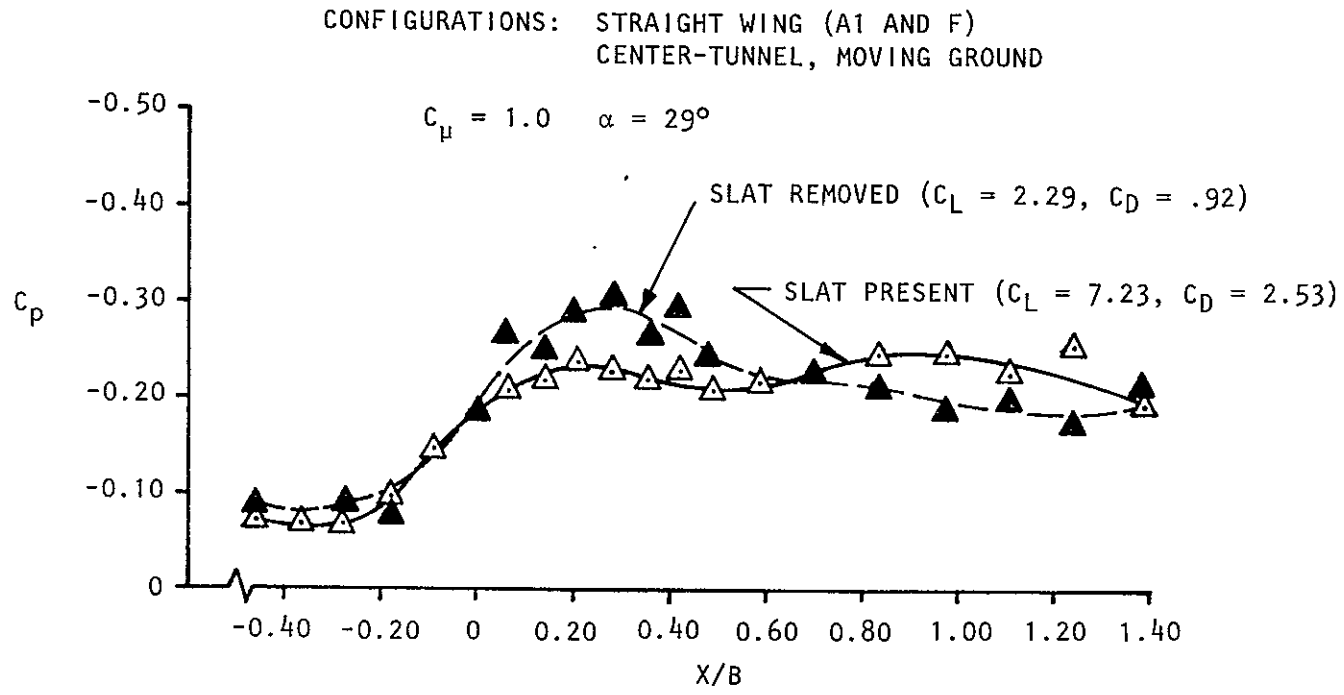

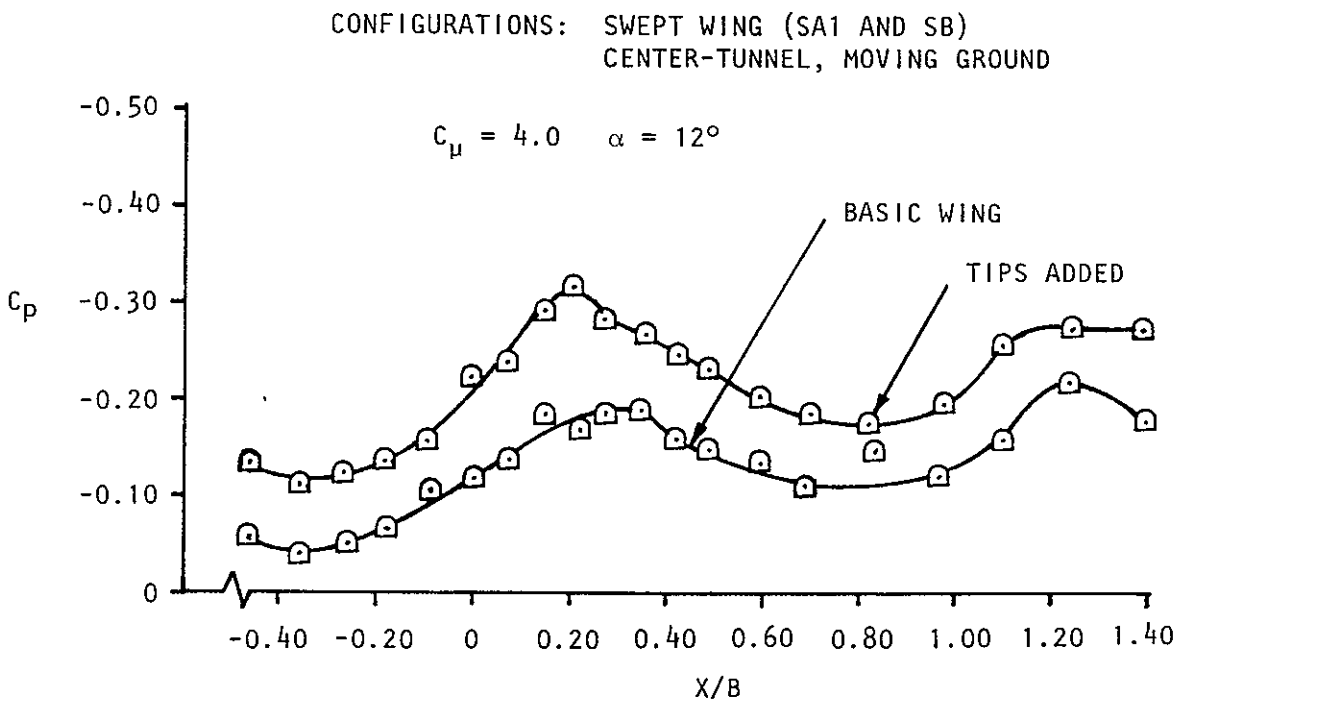

WALL PRESSURE SIGNATURES

Figure 6.3 Effects Of Wing Stall and of Adding Tips

ORIGINAL PAGE IS
OF POOR QUALITY

CONFIGURATIONS: STRAIGHT AND SWEPT WING WITH SLATS (A1 AND SA1)
MODEL ON TUNNEL CENTERLINE. MOVING GROUND.

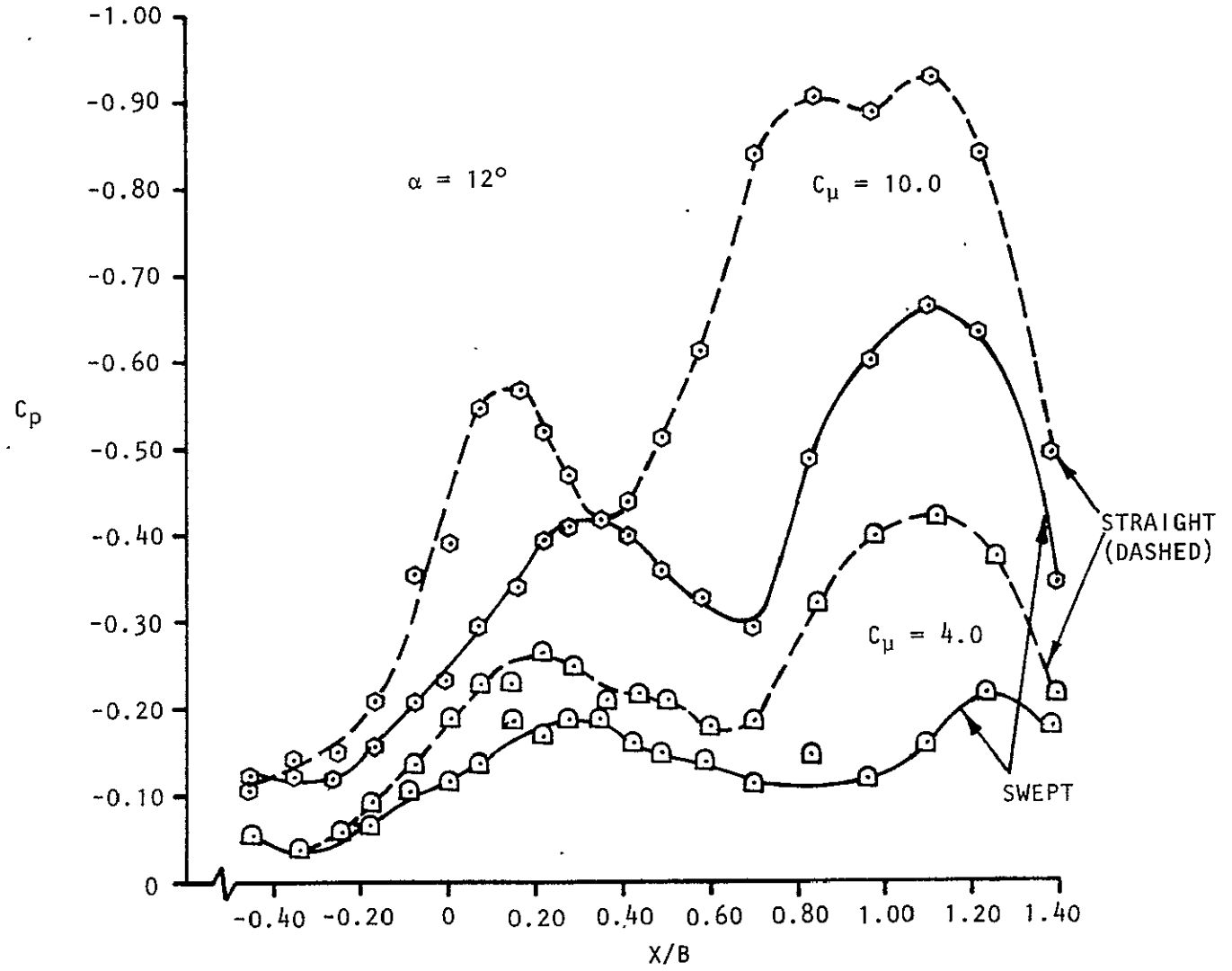

Figure 6.4 Wall Pressure Signatures for Basic Straight- and Swept-Wing Models

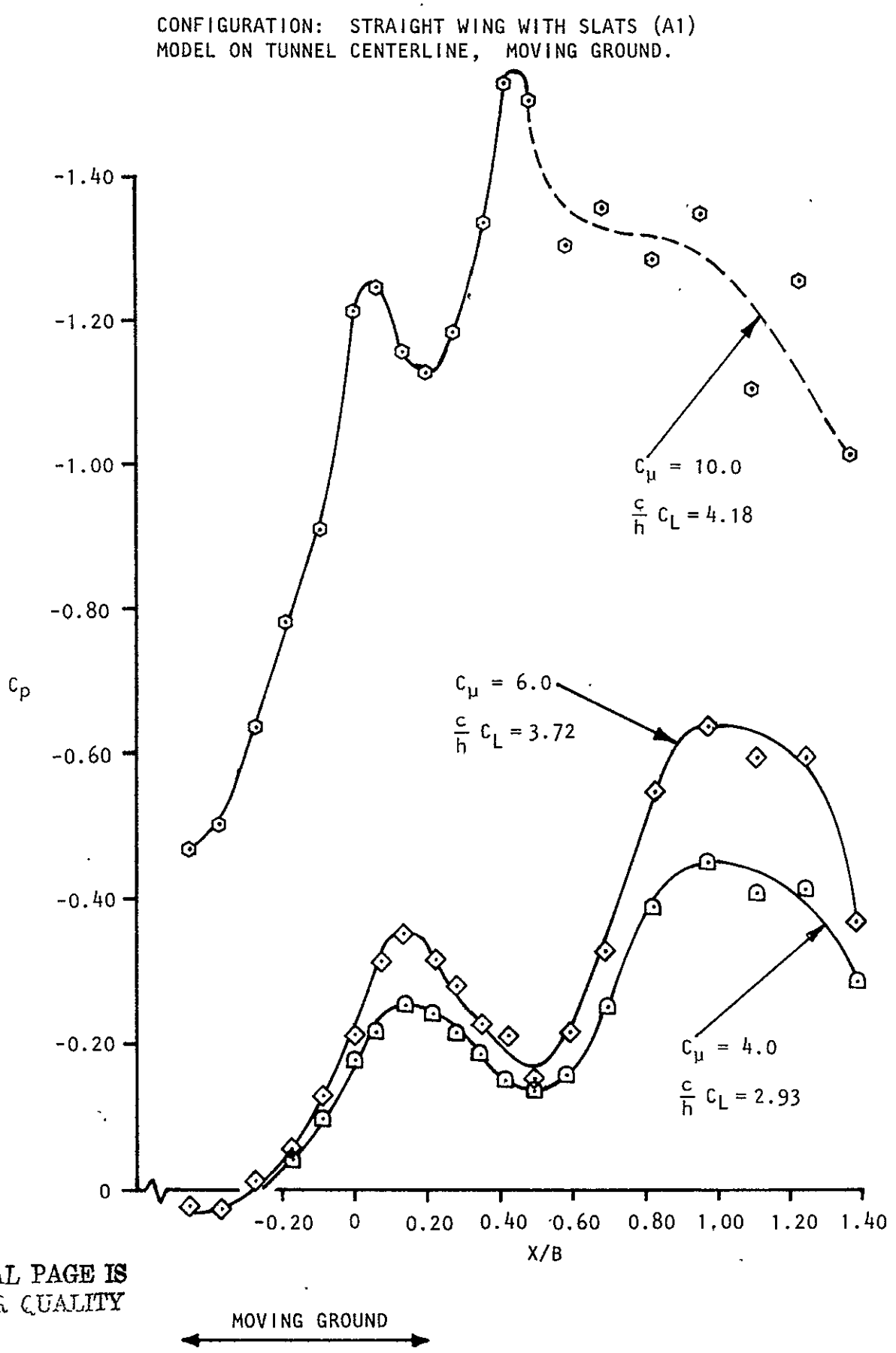

ORIGINAL PAGE IS
OF POOR QUALITY

Figure 6.5 Wall Pressure Signatures at High C_μ, α = 20°

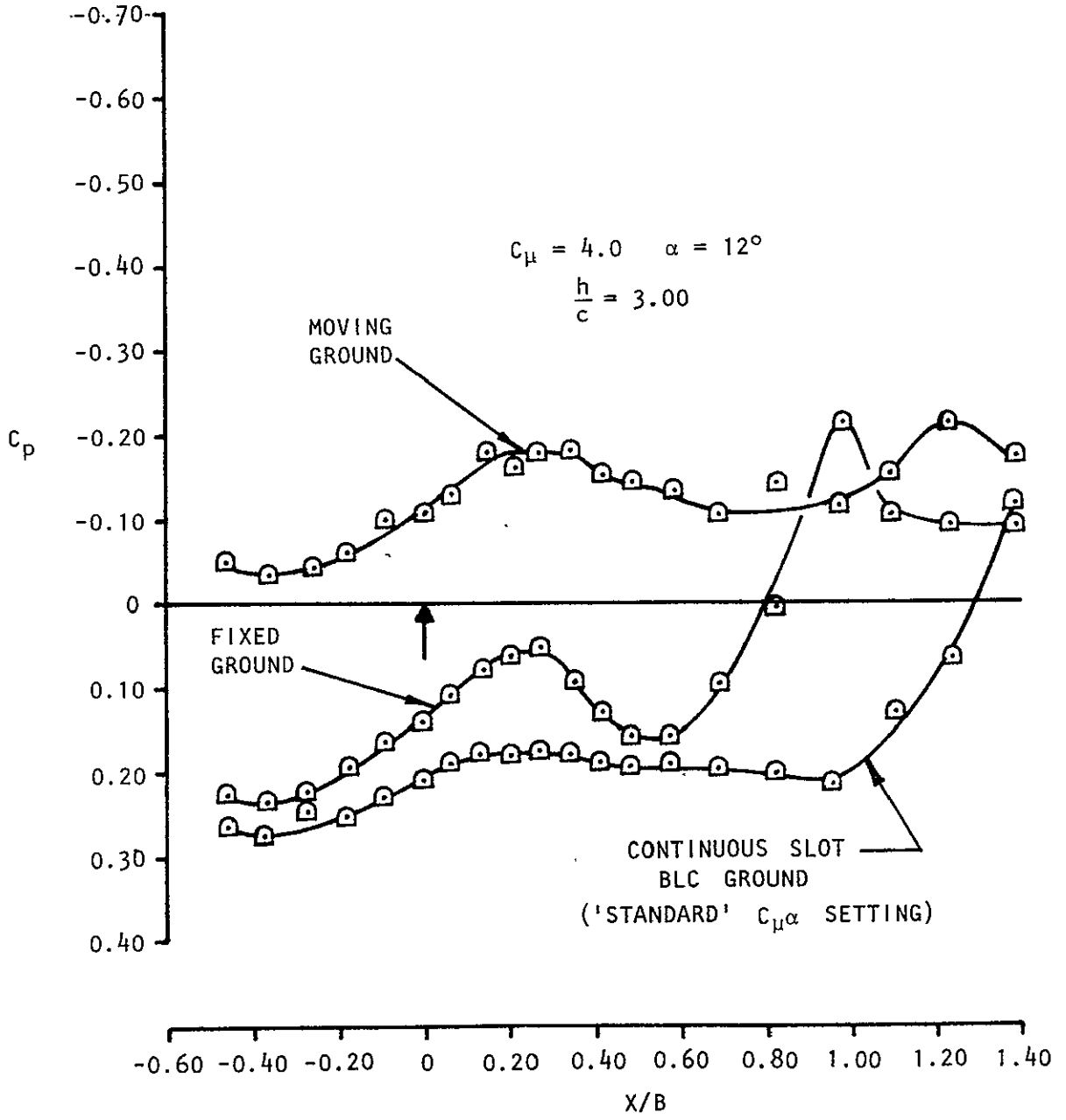

WALL PRESSURE SIGNATURES (SWEPT WING)

Figure 6.6 Effect of Ground Configuration

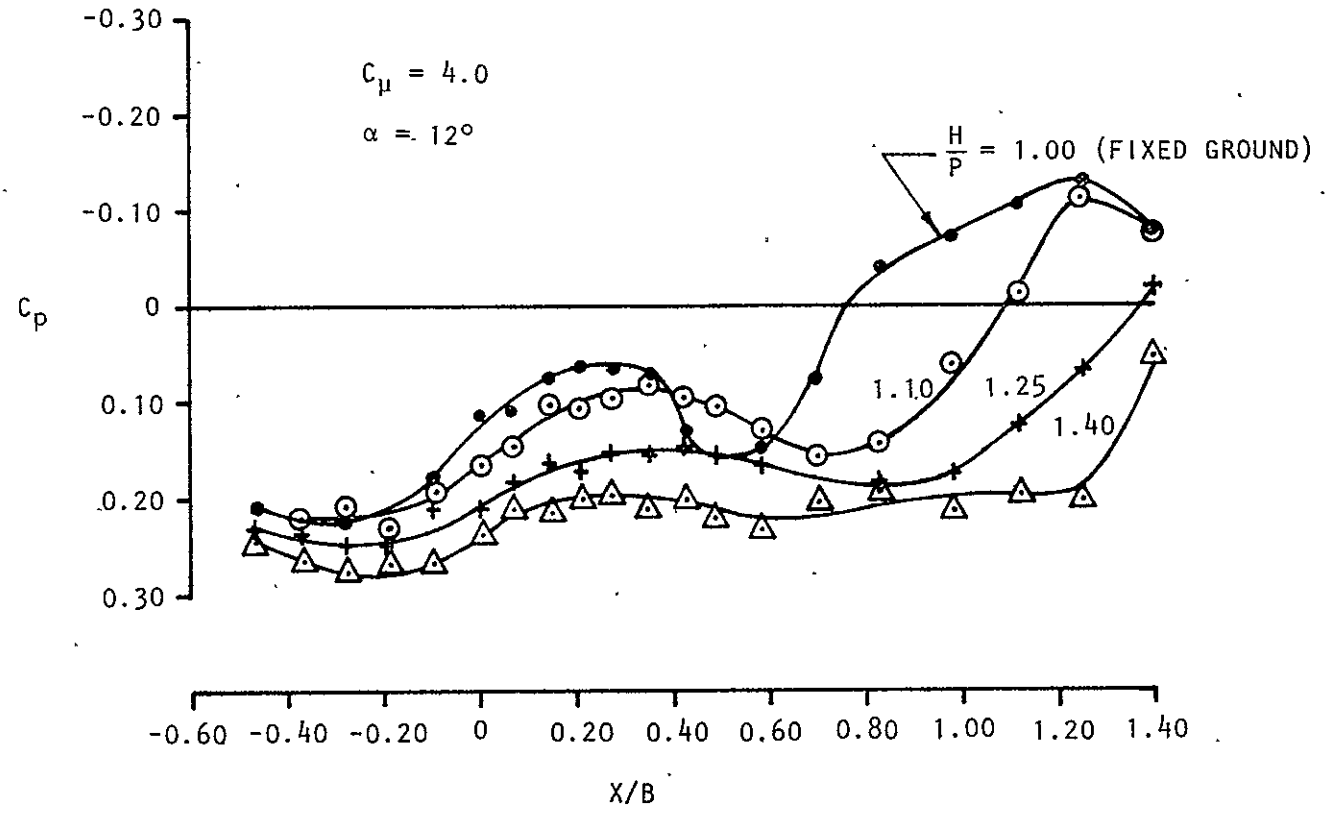

Figure 6.7 Effect of Ground-Blowing Pressure Ratio on Wall Pressure Signatures

ORIGINAL PAGE IS
OF POOR QUALITY

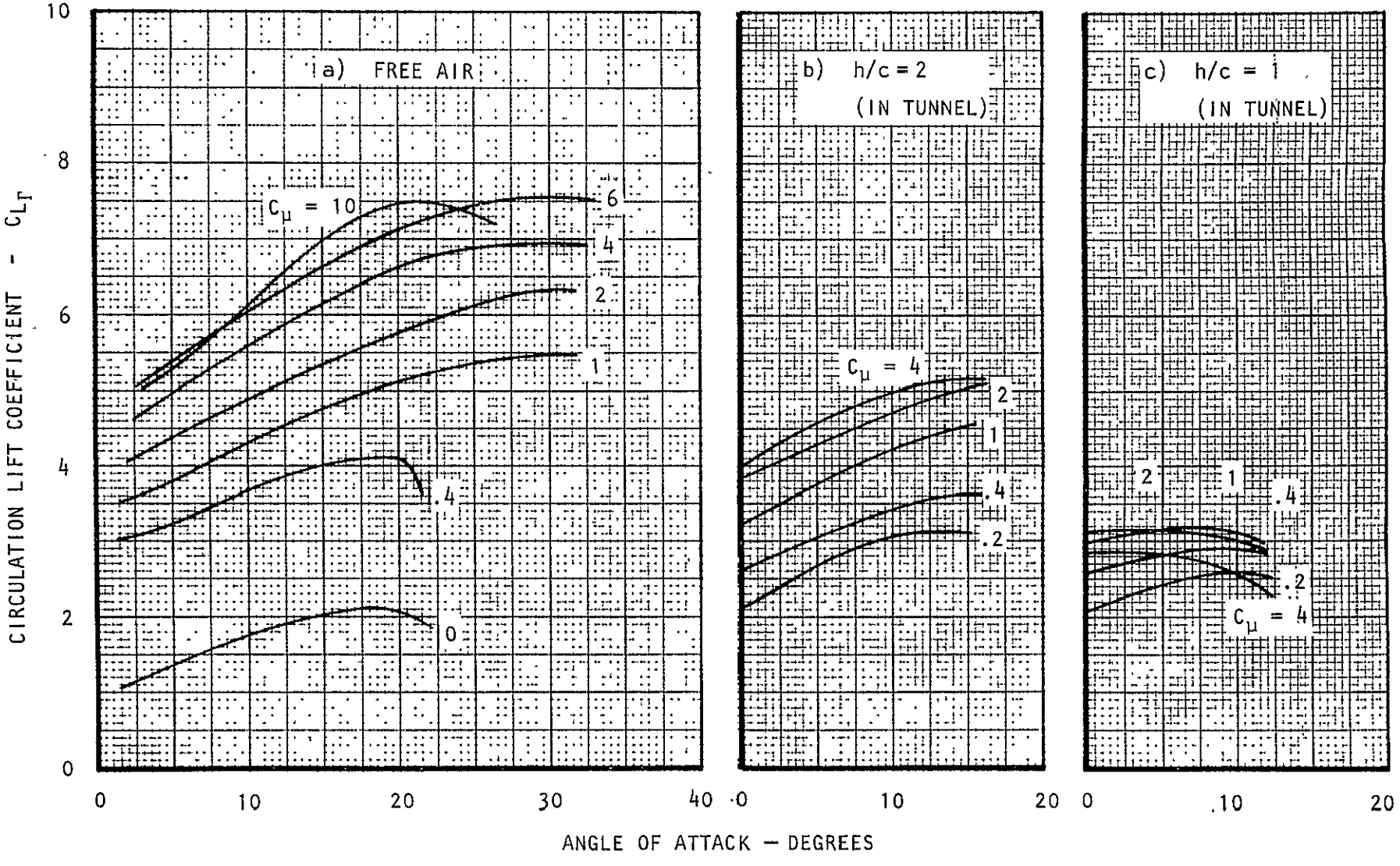

Figure 7.1 Limit Lift in Ground Effect (Basic Swept Configuration - Moving Ground)

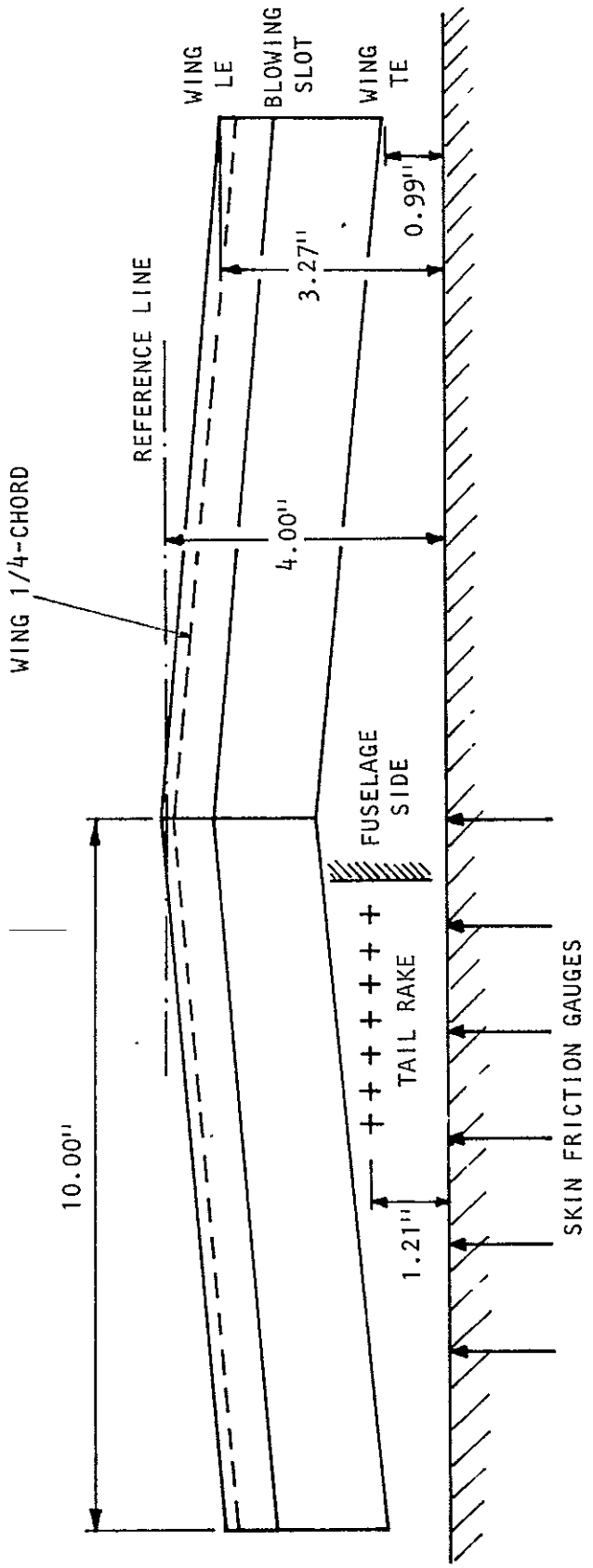

Figure 7.2 Aft View of Swept Wing at $\alpha = 12°$ and $h/c = 1.0$

ORIGINAL PAGE IS
OF POOR QUALITY

ORIGINAL PAGE IS
OF POOR QUALITY

C.2

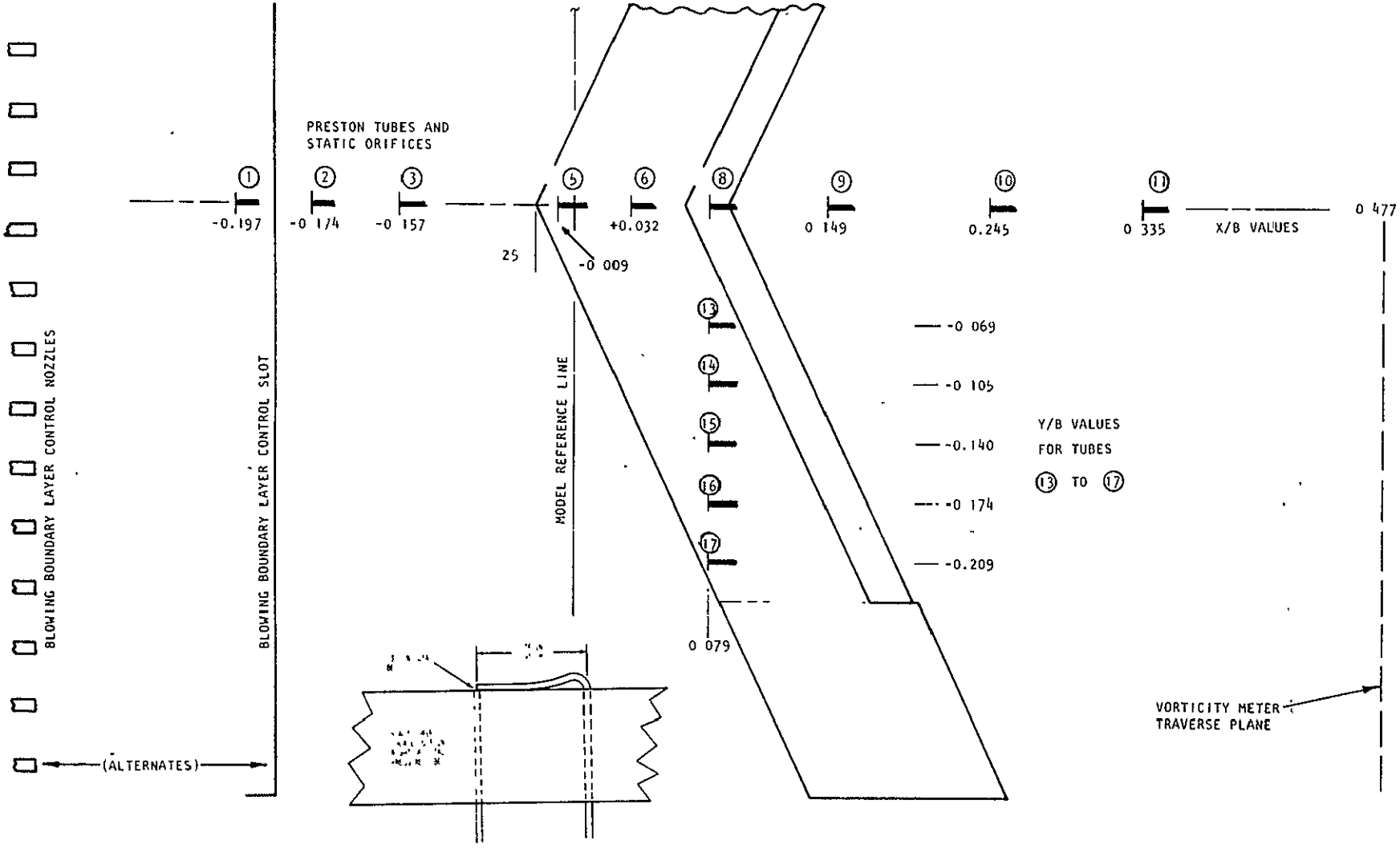

Figure 7.3 The BLC Ground: Blowing Positions and Instrumentation Details

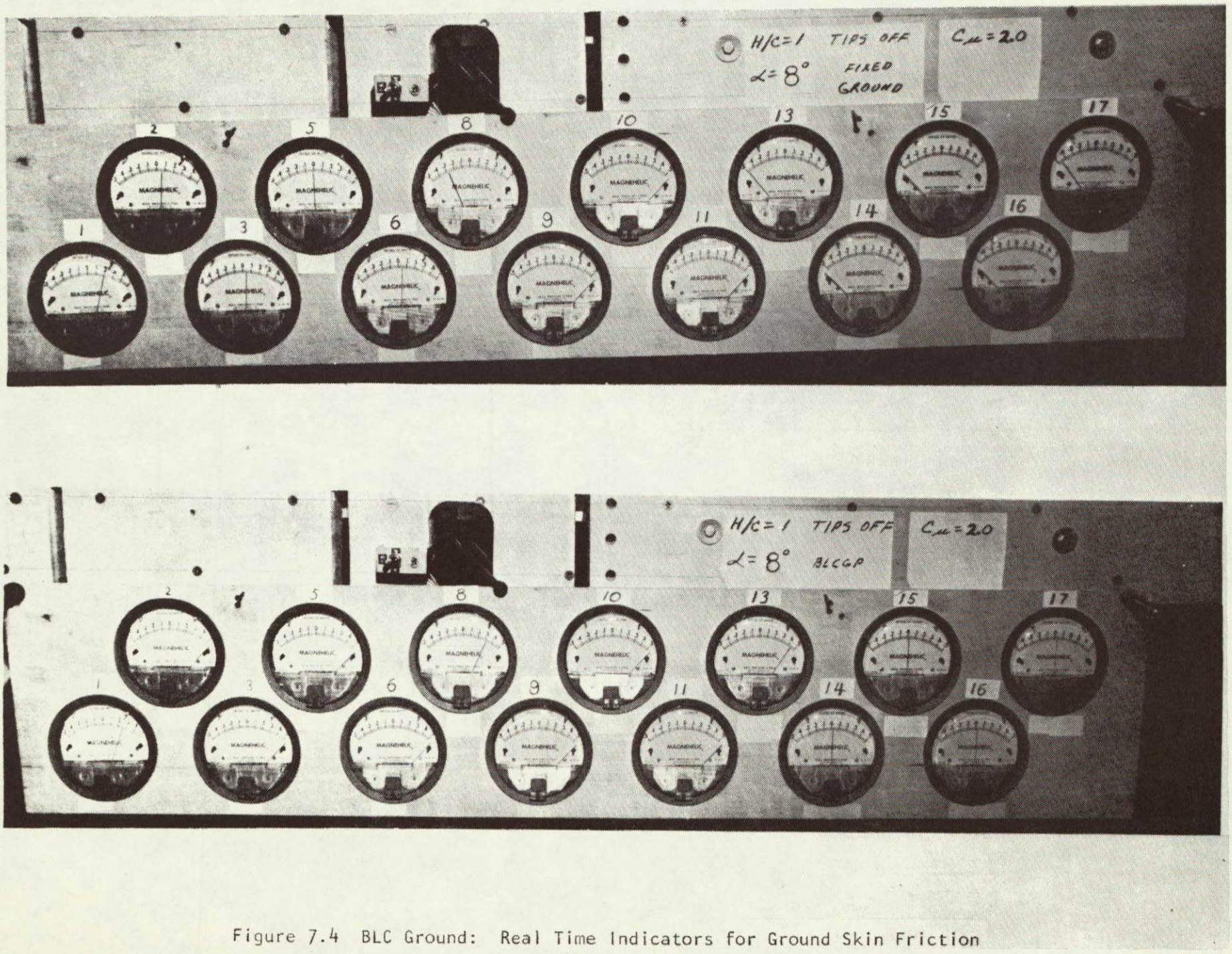

Figure 7.4 BLC Ground: Real Time Indicators for Ground Skin Friction

ORIGINAL PAGE IS
OF POOR QUALITY

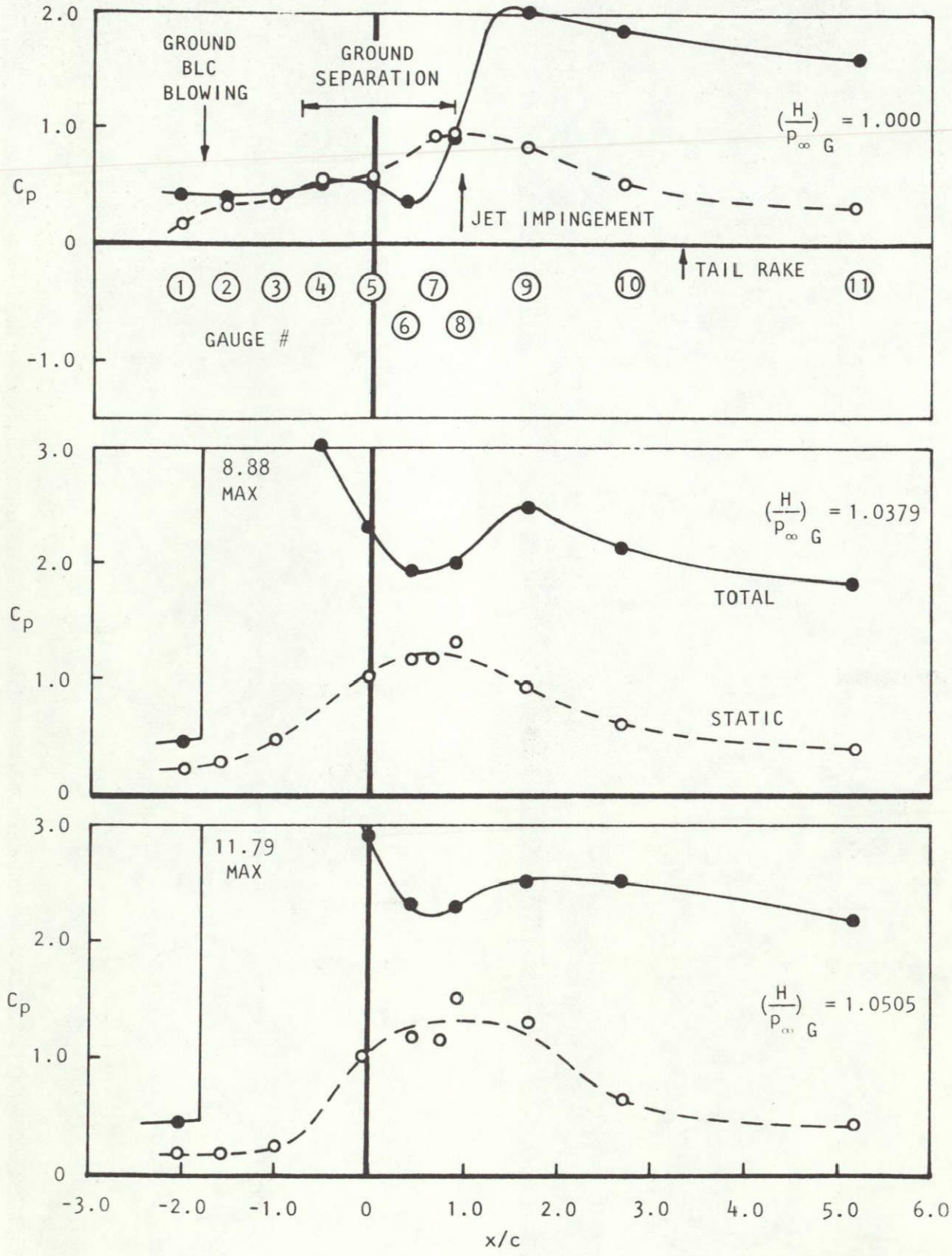

Figure 7.5 Typical Ground Pressures Below Model $\mathcal{L}$
($h/c = 1.0$, $C_\mu = 1.0$, $\alpha = 10^\circ$)

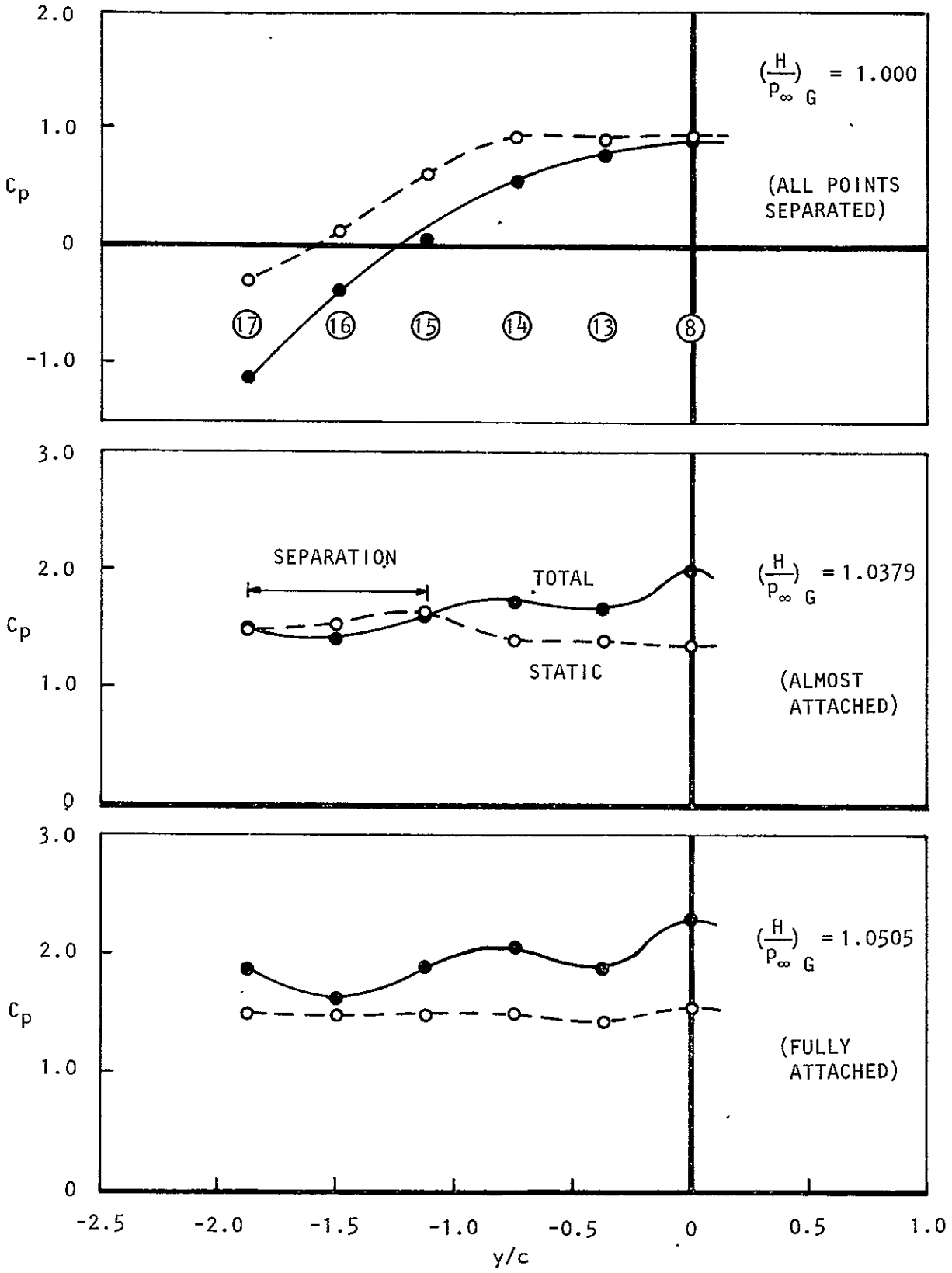

Figure 7.6 Typical Ground Pressures Along a Transverse Line Below the Model ($x/c = 0.85$) ($h/c = 1.0$, $C_\mu = 1.0$, $\alpha = 10$)

ORIGINAL PAGE IS
OF POOR QUALITY

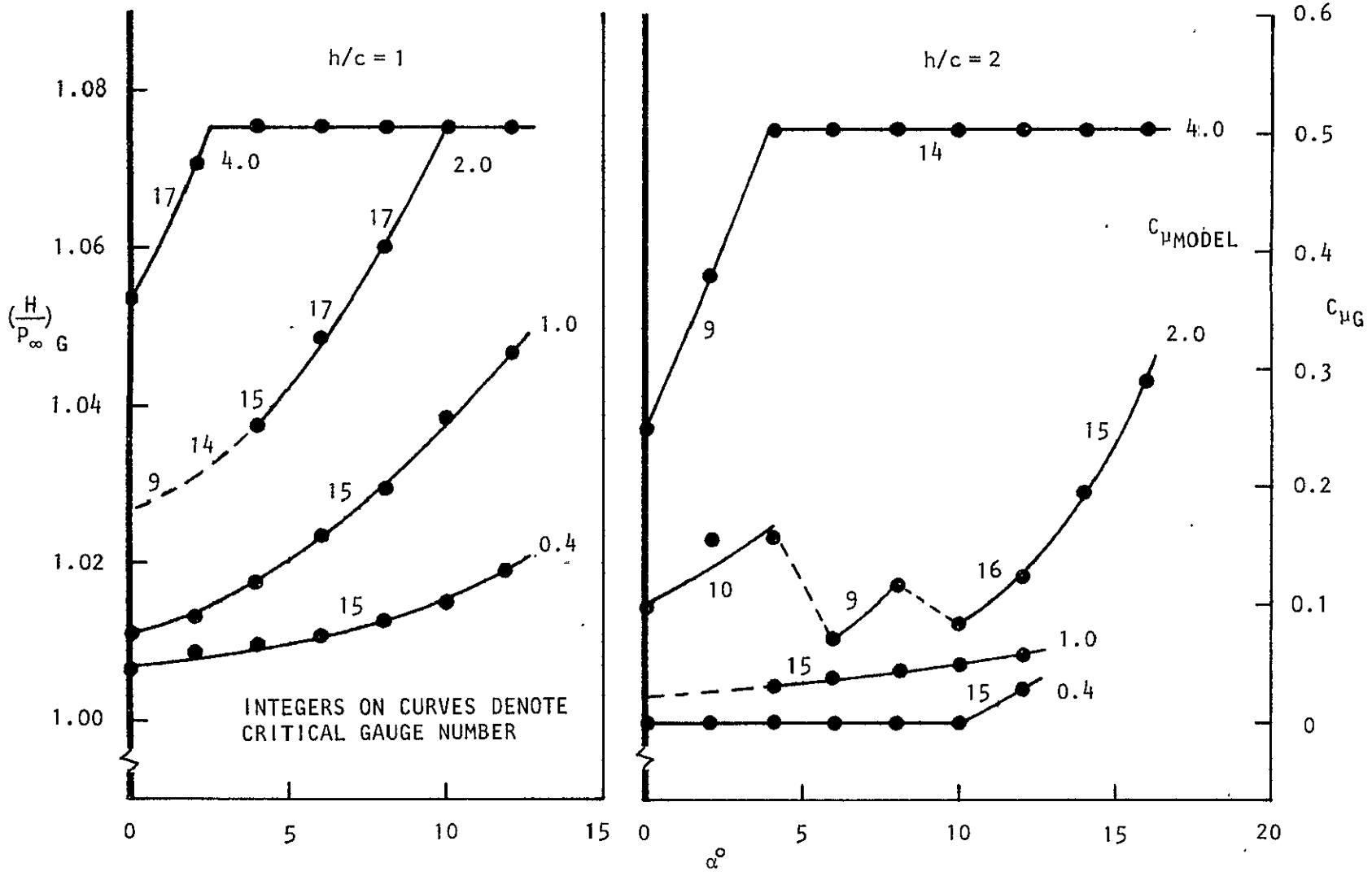

Figure 7.7 Settings for Continuous Slot Ground BLC (Basic Swept Wing)

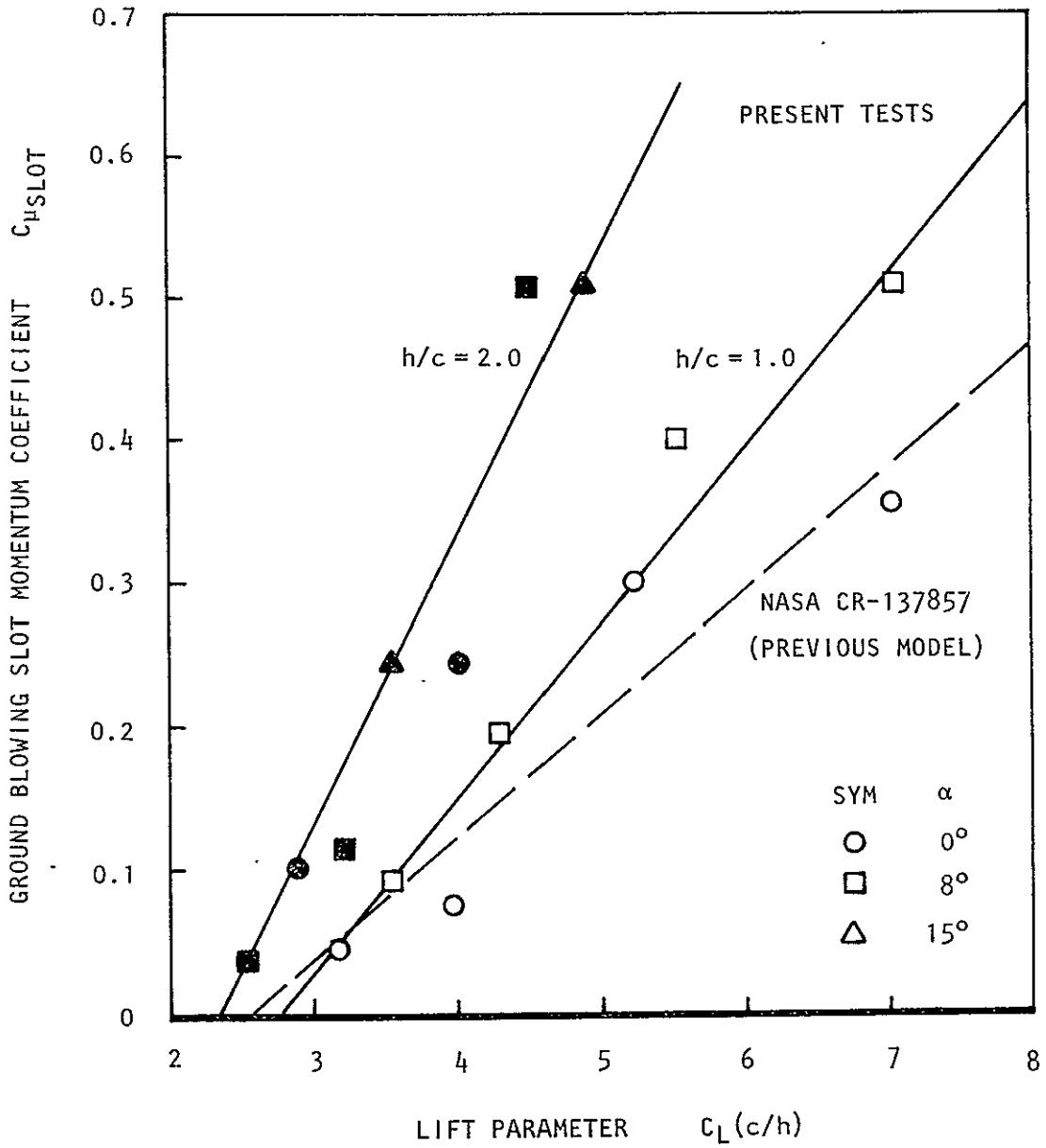

Figure 7.8 Present and Previous Ground Blowing BLC Requirements

ORIGINAL PAGE IS
OF POOR QUALITY

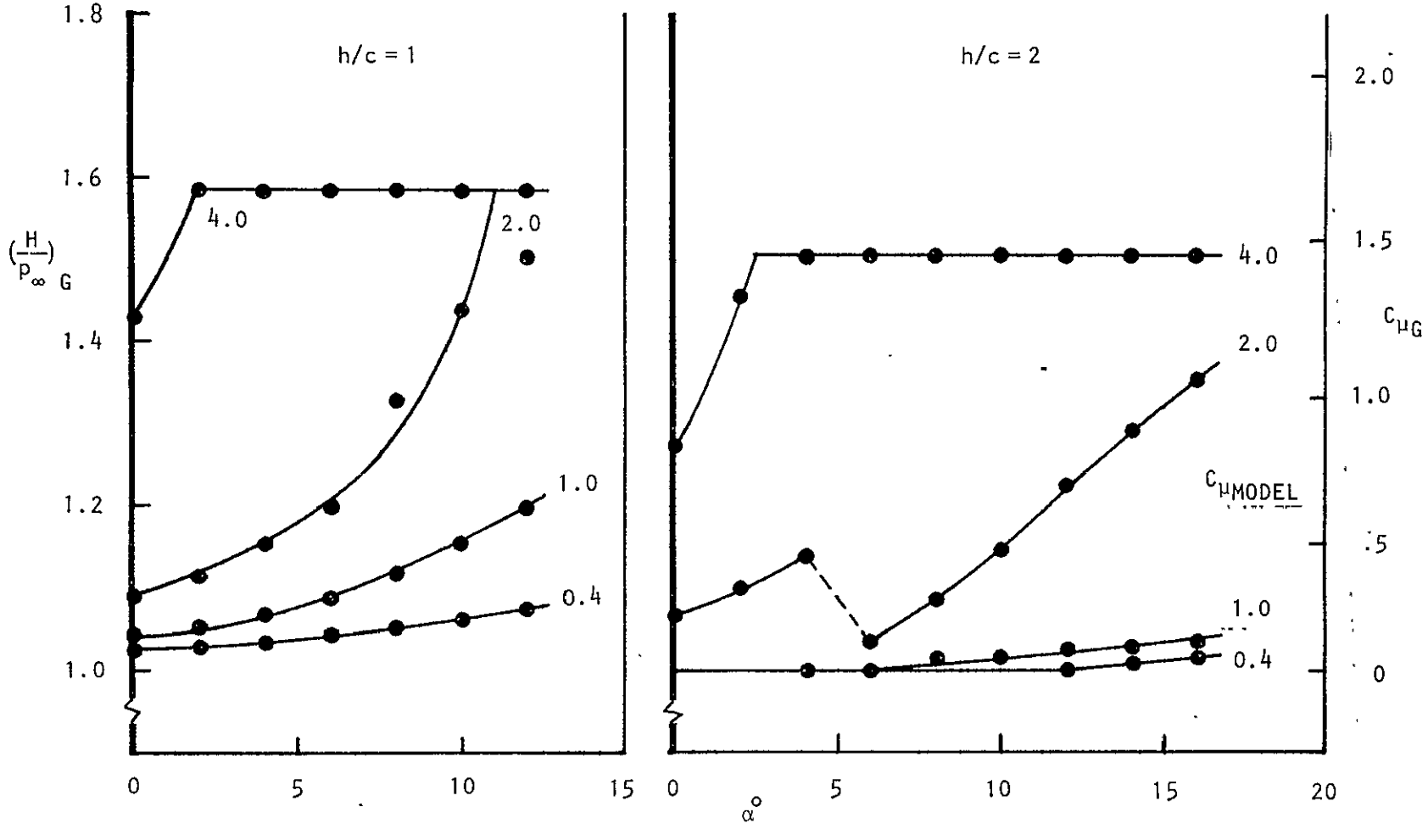

Figure 7.9 Settings for Multiple Nozzle Ground BLC (Basic Swept Wing)

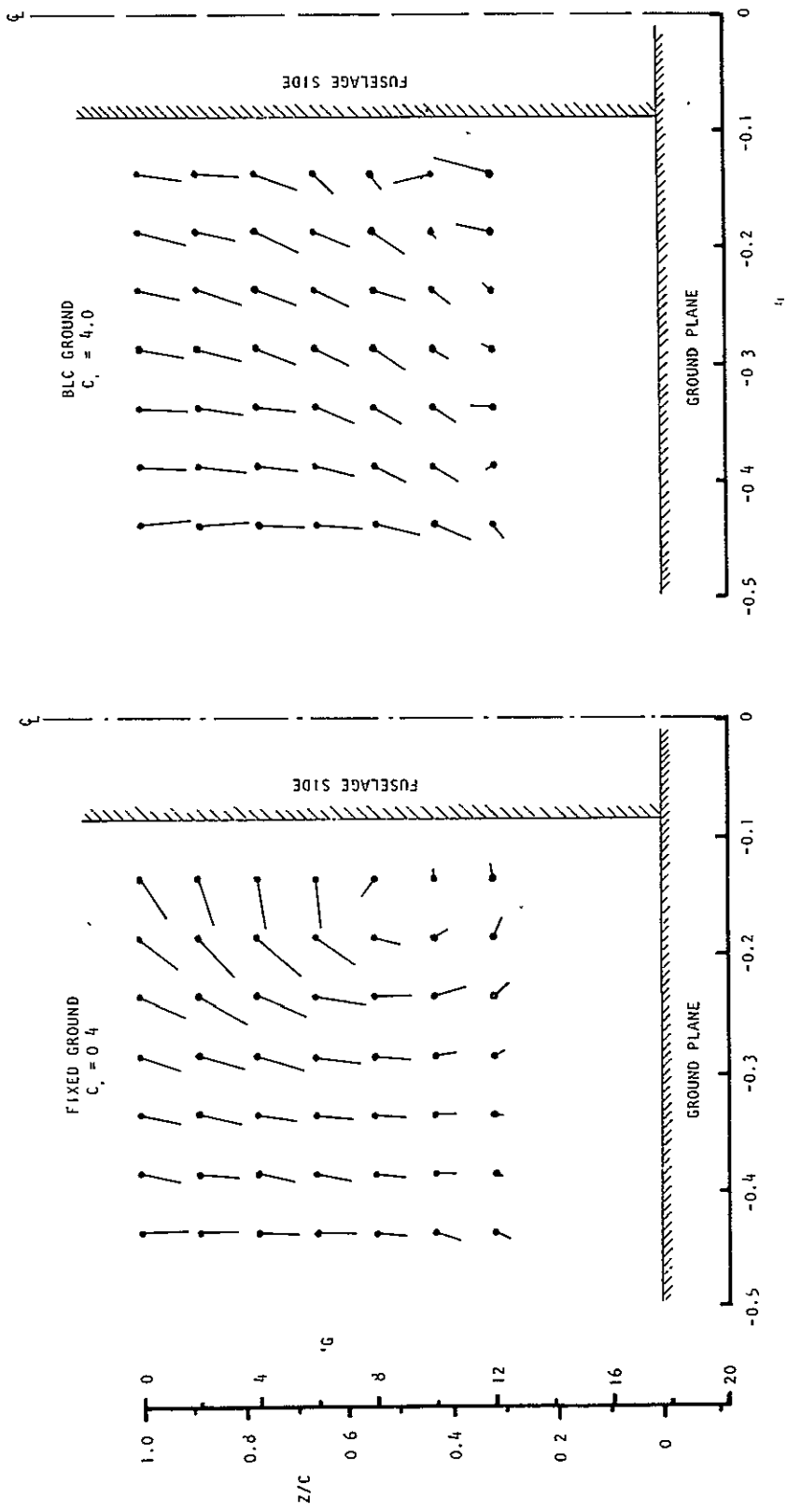

Figure 7.10 Cross Flow at the Tailplane Position (x/c = 3.28), h/c = 1.0

ORIGINAL PAGE IS
OF POOR QUALITY

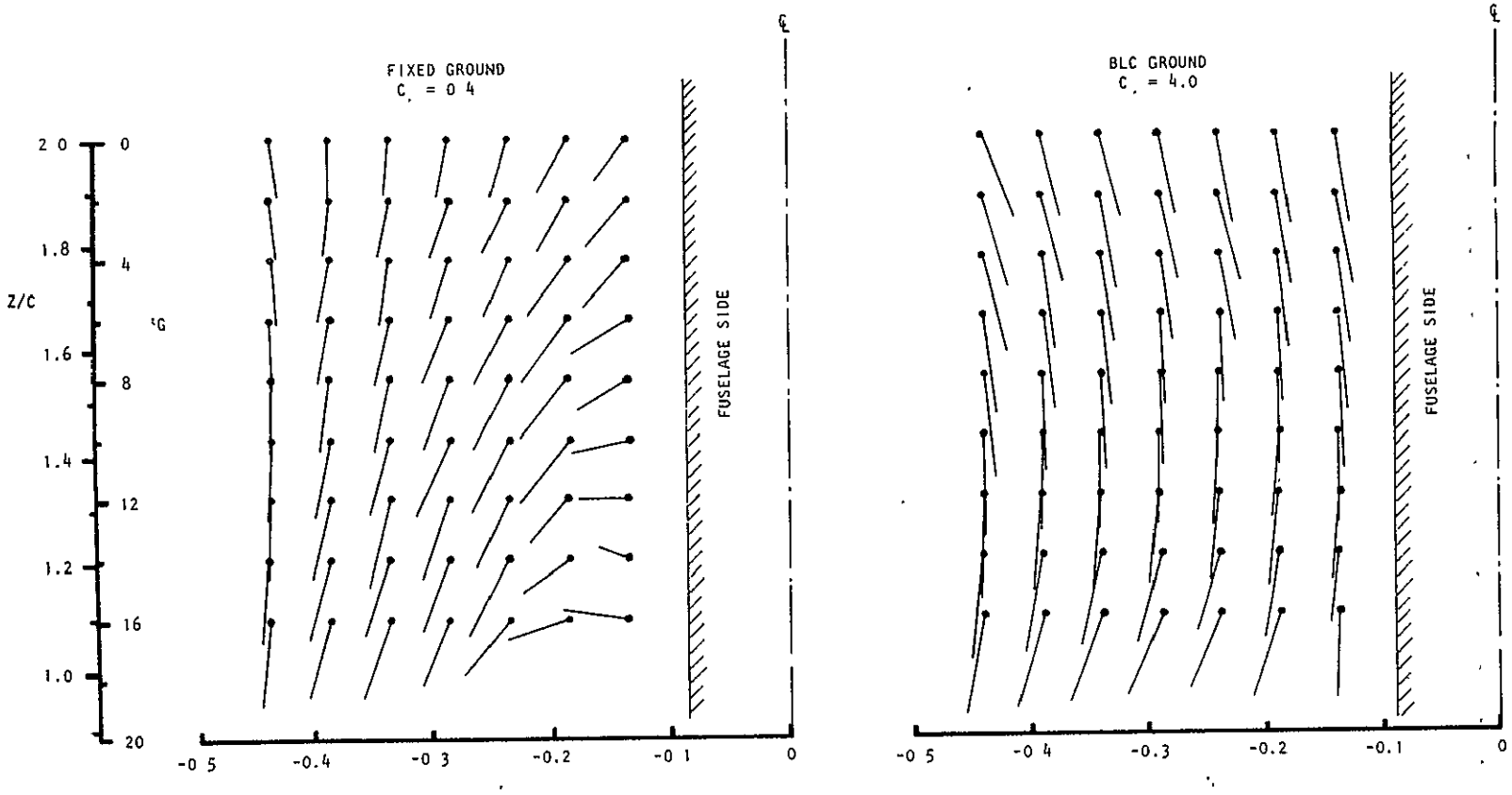

Figure 7.11 Cross Flow at the Tailplane Position (x/c = 3.28), h/c = 2.0

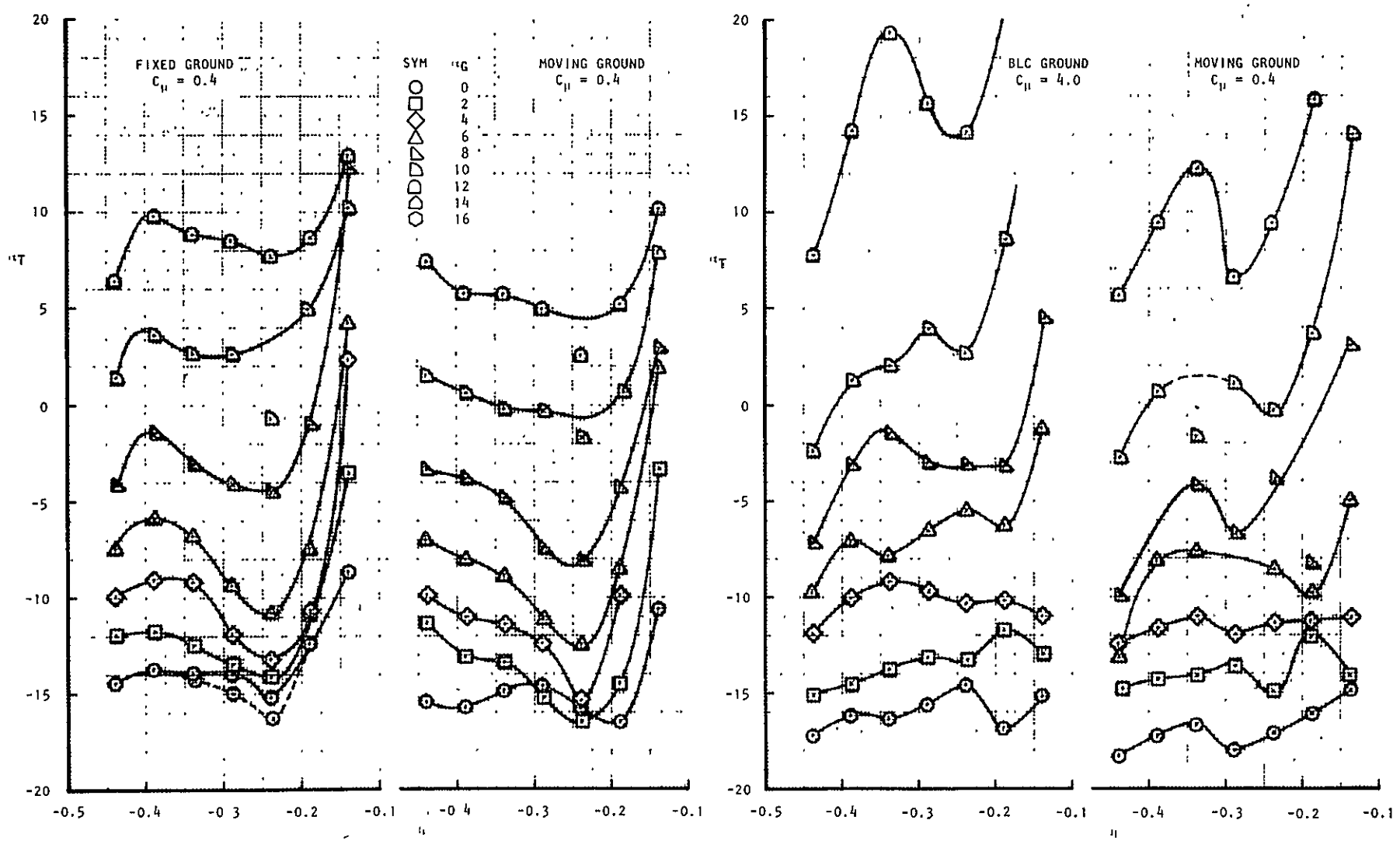

Figure 7.12 Pitch Angles at the Tailplane Position, h/c = 1.0

ORIGINAL PAGE IS
OF POOR QUALITY

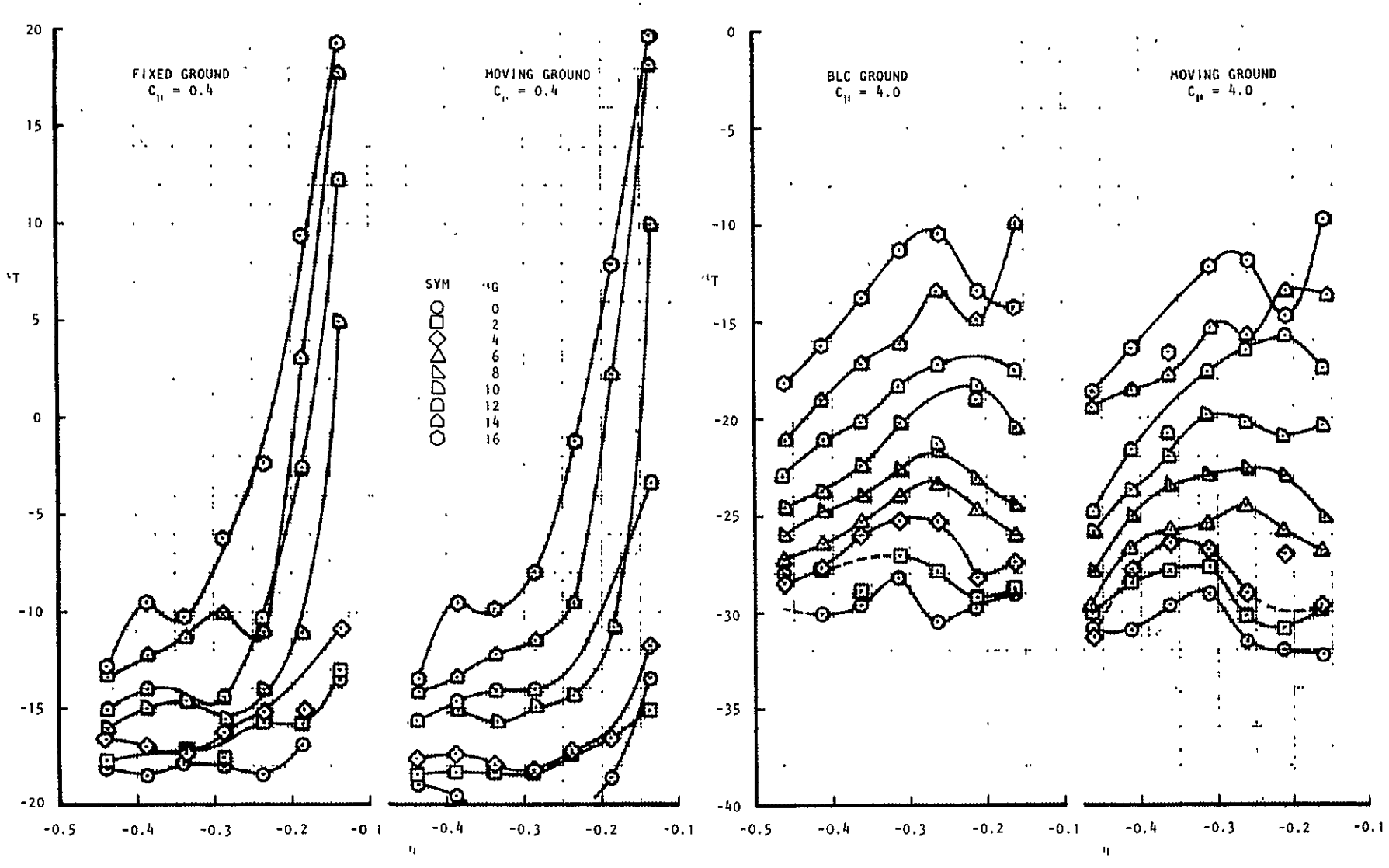

Figure 7.13 Pitch Angles at the Tailplane Position, h/c = 2.0

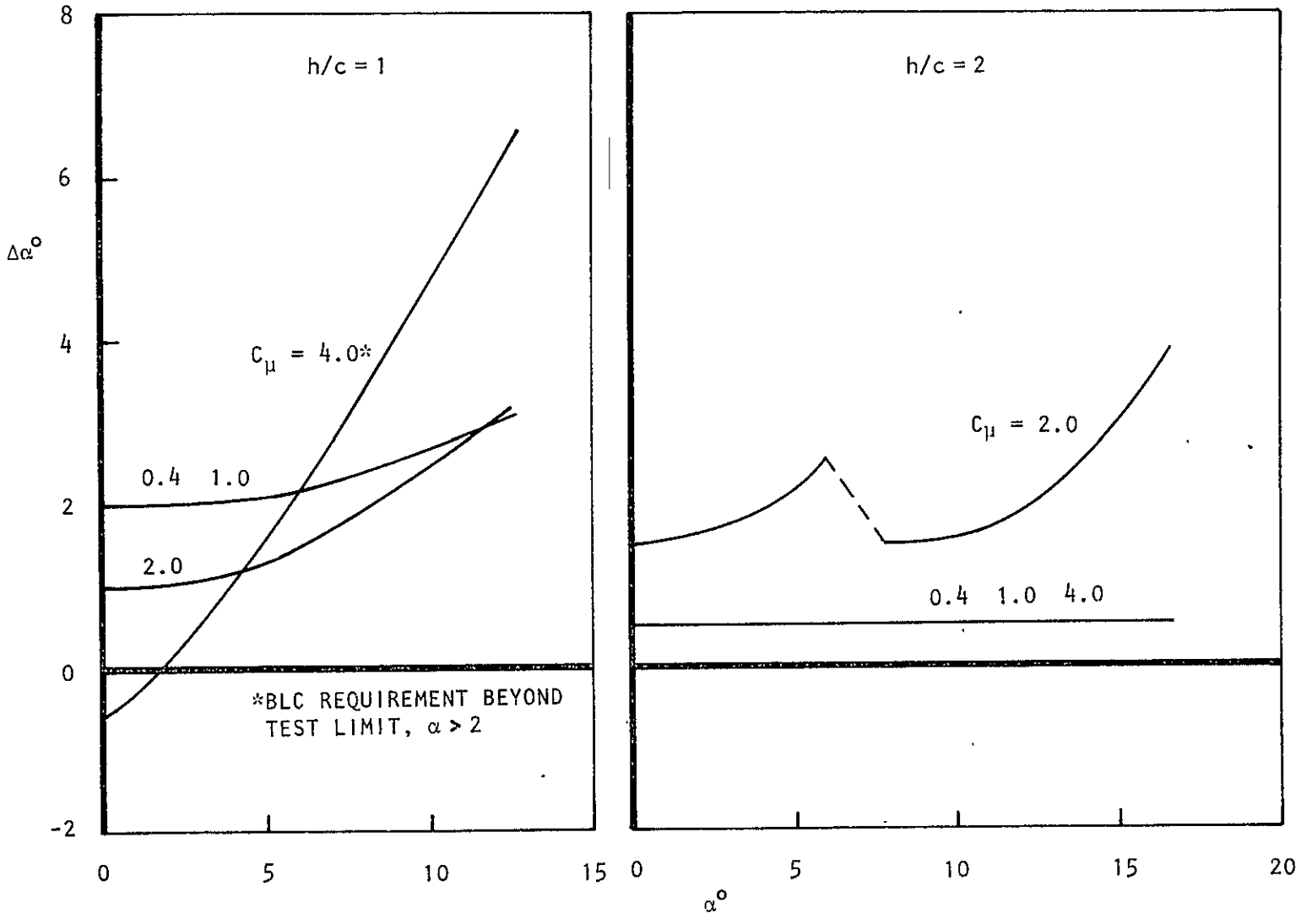

Figure 7.14 Tailplane Upwash Increment for Ground BLC

ORIGINAL PAGE IS
OF POOR QUALITY

GROUND BOUNDARY LAYER CONTROL VIA:			h/c = 1.0		h/c = 2.0	
			NO TIPS	WITH TIPS	NO TIPS	WITH TIPS
	CONTINUOUS SLOT	L	8.1	8.2	8.3	8.4
		D	8.5	8.6	8.7	8.8
		M	8.9	8.10	8.11	8.12
	MULTIPLE NOZZLES	L	8.13	8.14	8.15	8.16
		D	8.17	8.18	8.19	8.20
		M	8.21	8.22	8.23	8.24

Figure 8.0 Figure Index for Ground Effects Data

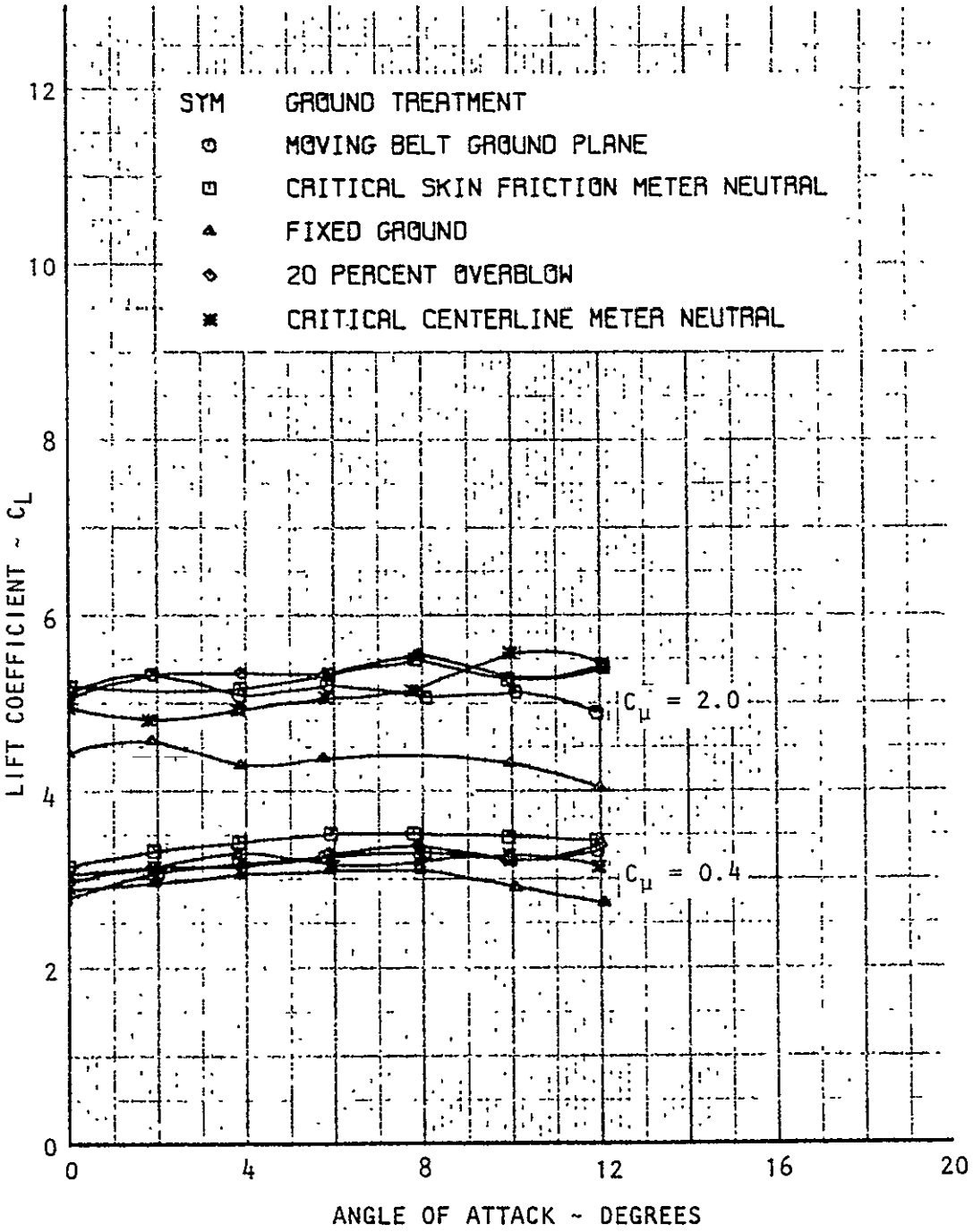

Figure 8.1(a) Lift Data in Ground Effect, h/c = 1, Basic Swept Wing (Ground BLC: Continuous Slot)

ORIGINAL PAGE IS
OF POOR QUALITY

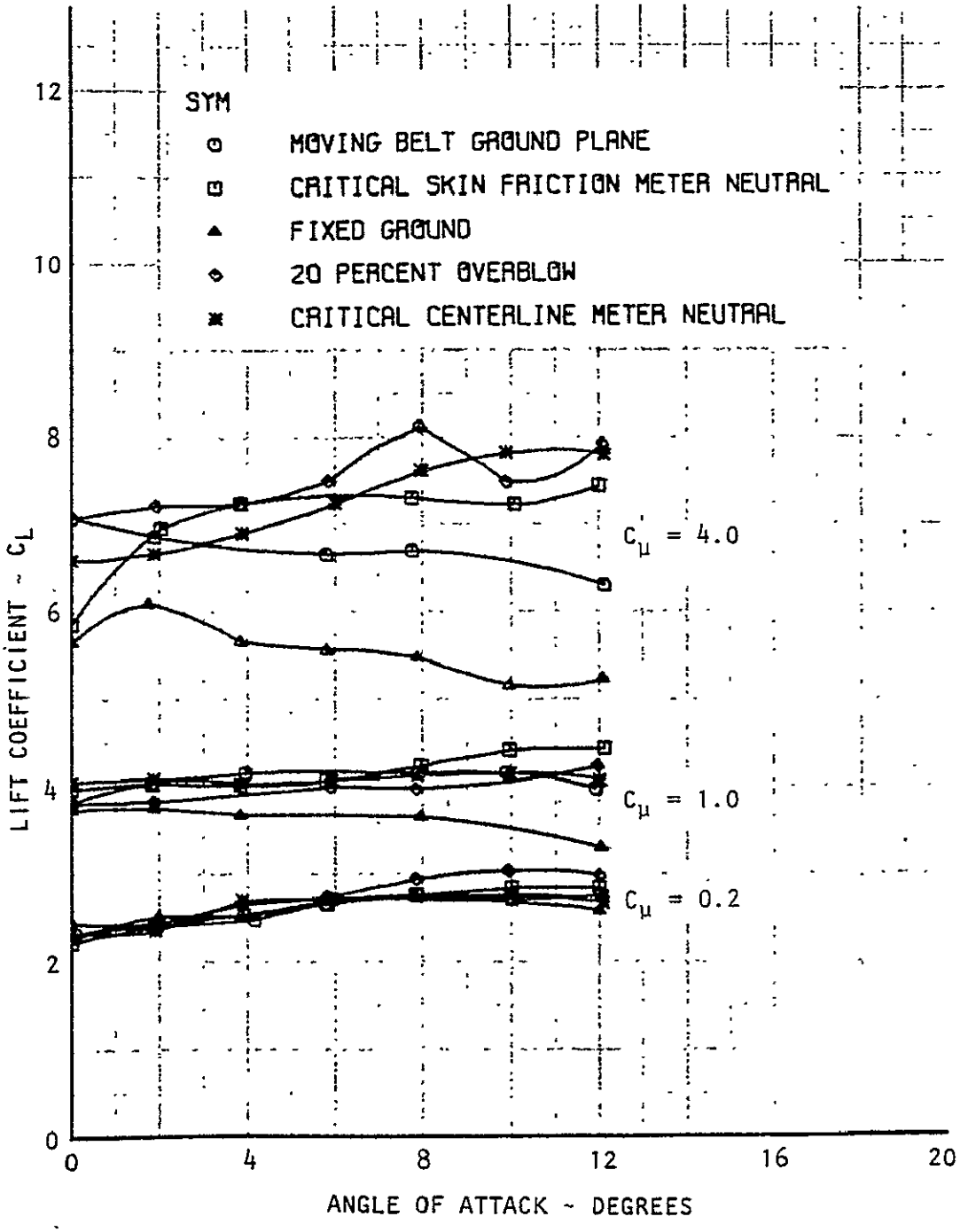

Figure 8.1(b) Lift Data in Ground Effect, h/c = 1, Basic Swept Wing (Ground BLC: Continuous Slot)

ORIGINAL PAGE IS
OF POOR QUALITY

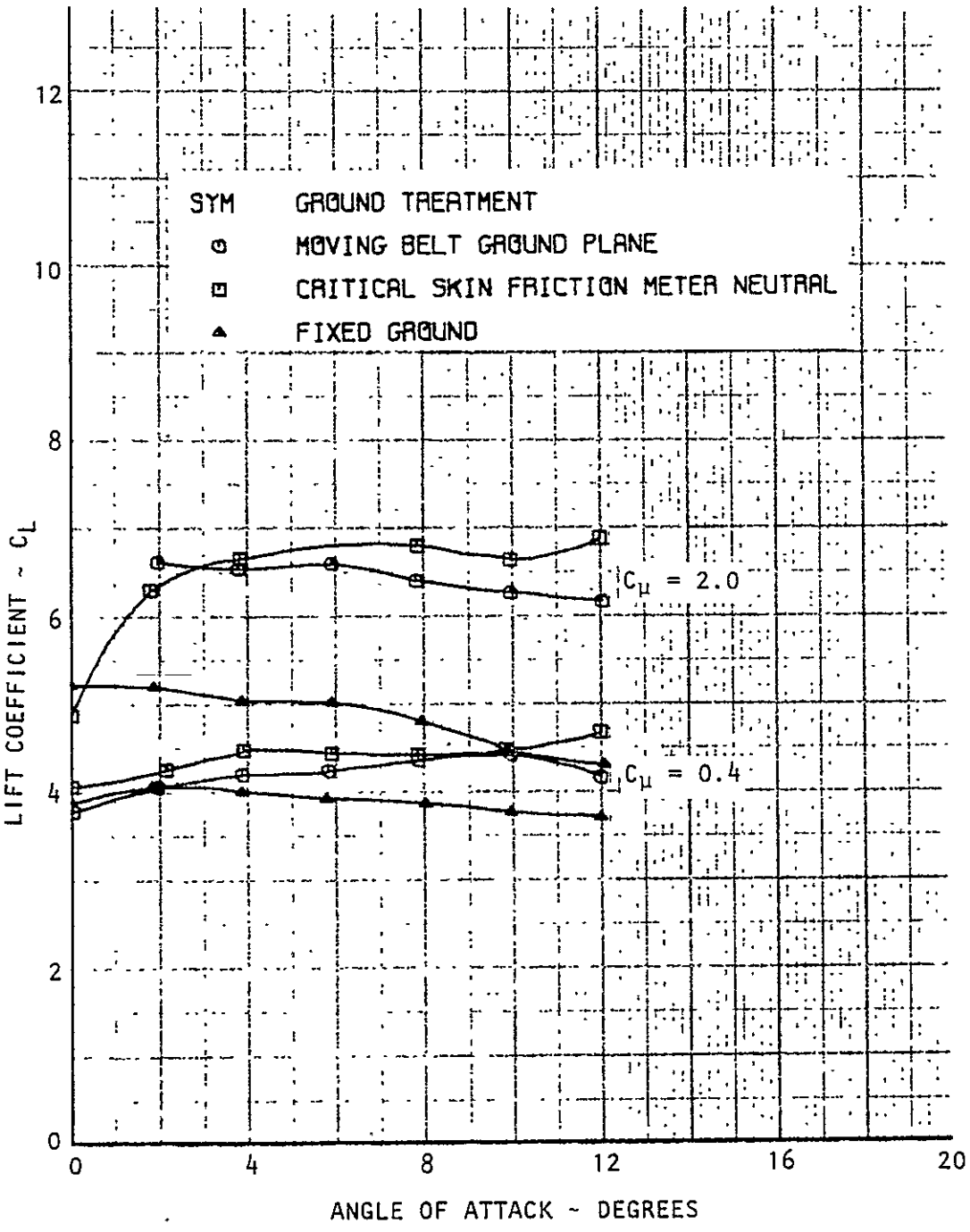

Figure 8.2(a) Lift Data in Ground Effect, h/c = 1, Swept Wing with Tips
(Ground BLC: Continuous Slot)

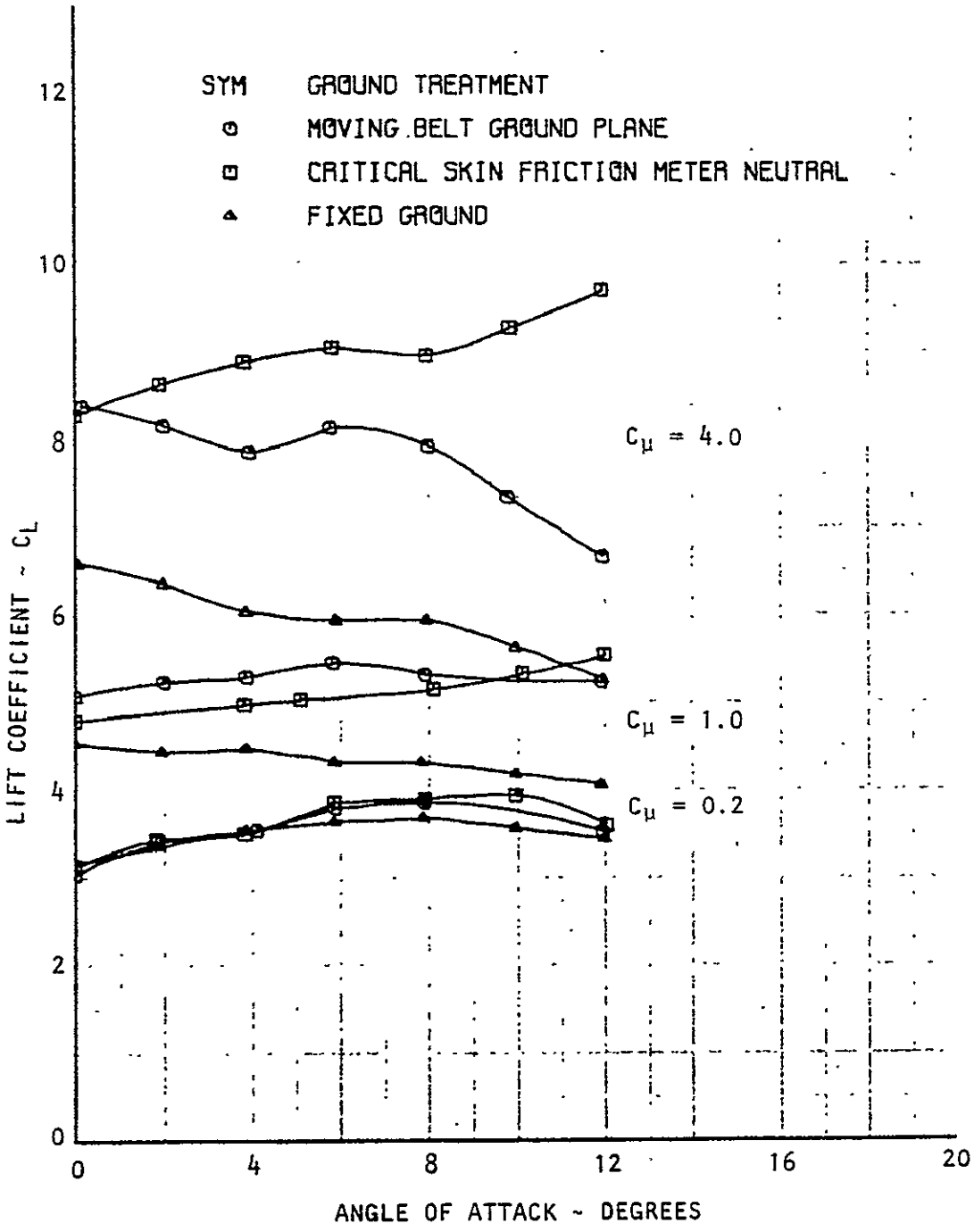

Figure 8.2(b) Lift Data in Ground Effect, h/c = 1, Swept Wing with Tips (Ground BLC: Continuous Slot)

ORIGINAL PAGE IS
OF POOR QUALITY

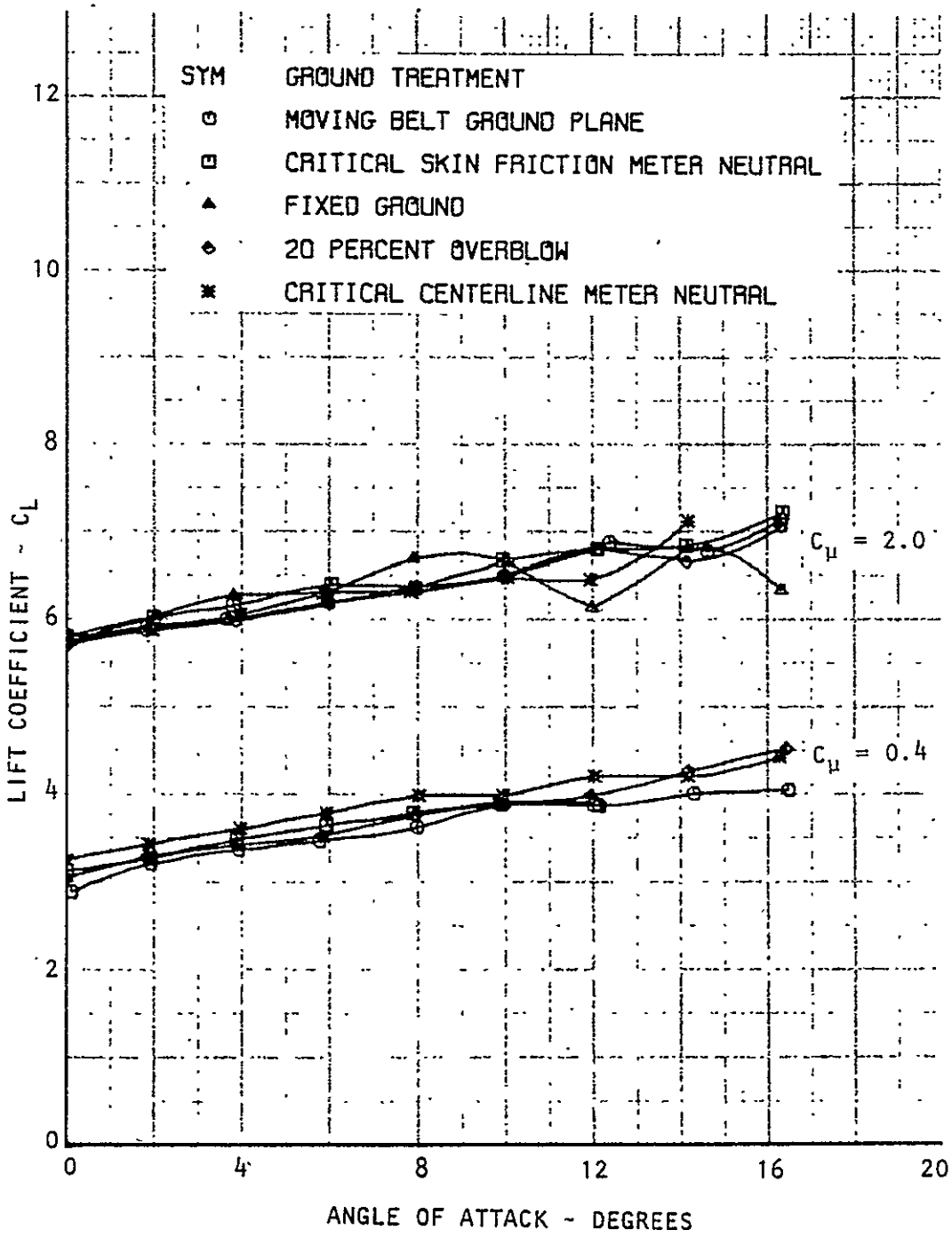

Figure 8.3(a) Lift Data in Ground Effect, h/c = 2, Basic Swept Wing (Ground BLC: Continuous Slot)

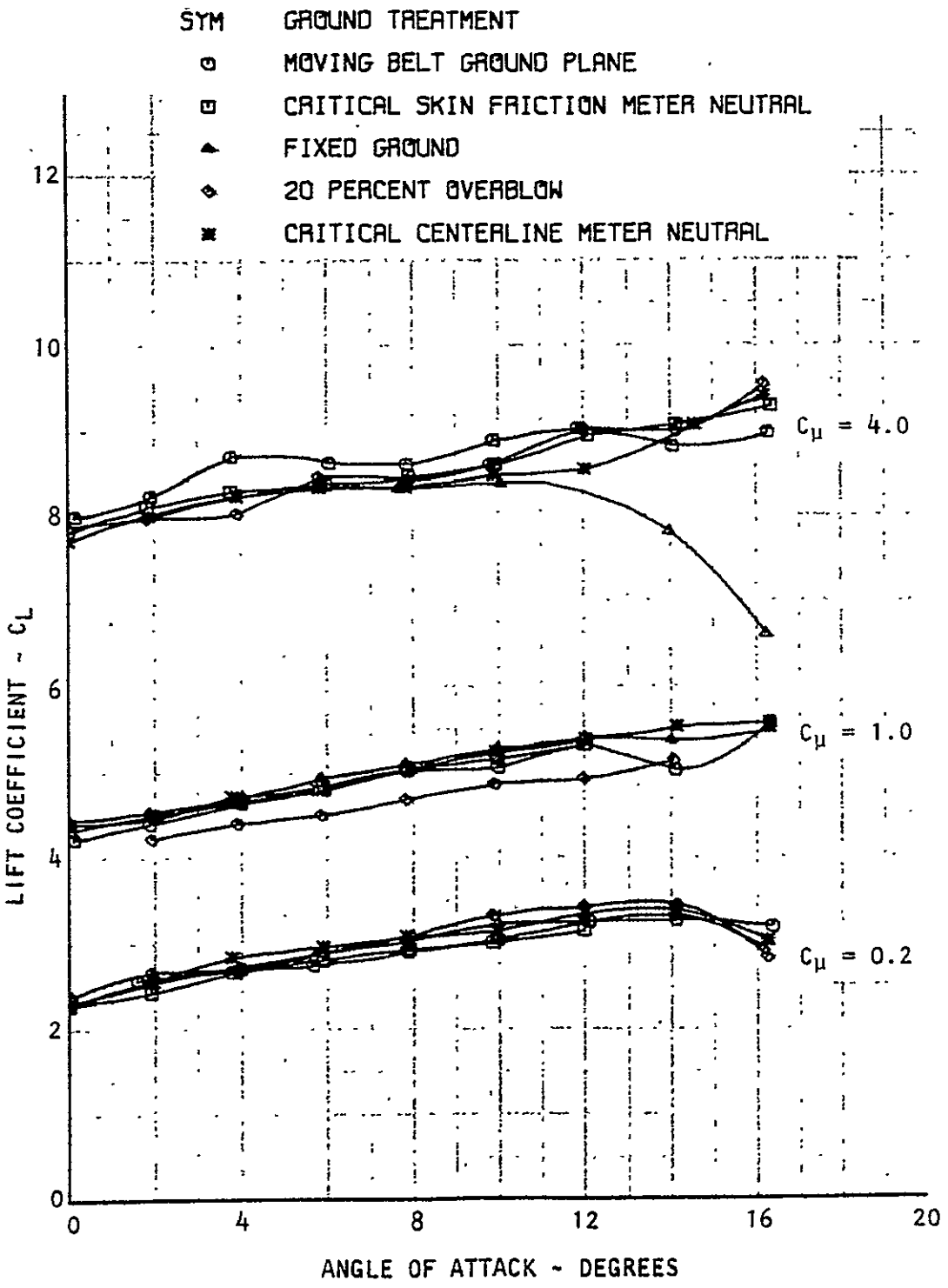

Figure 8.3(b) Lift Data in Ground Effect, h/c = 2, Basic Swept Wing (Ground BLC: Continuous Slot)

ORIGINAL PAGE IS
OF POOR QUALITY

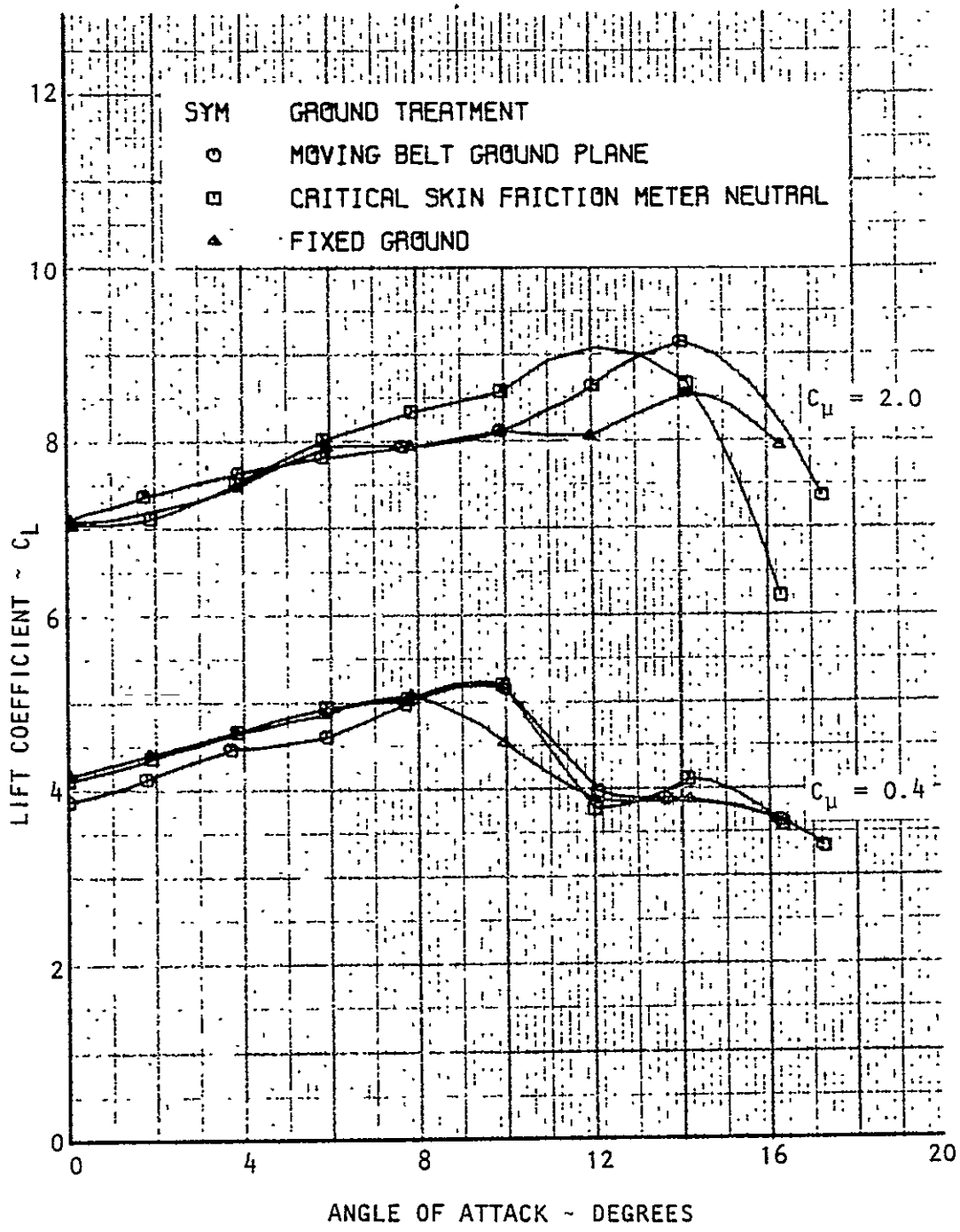

Figure 8.4(a) Lift Data in Ground Effect, h/c = 2, Swept Wing With Tips (Ground BLC: Continuous Slot)

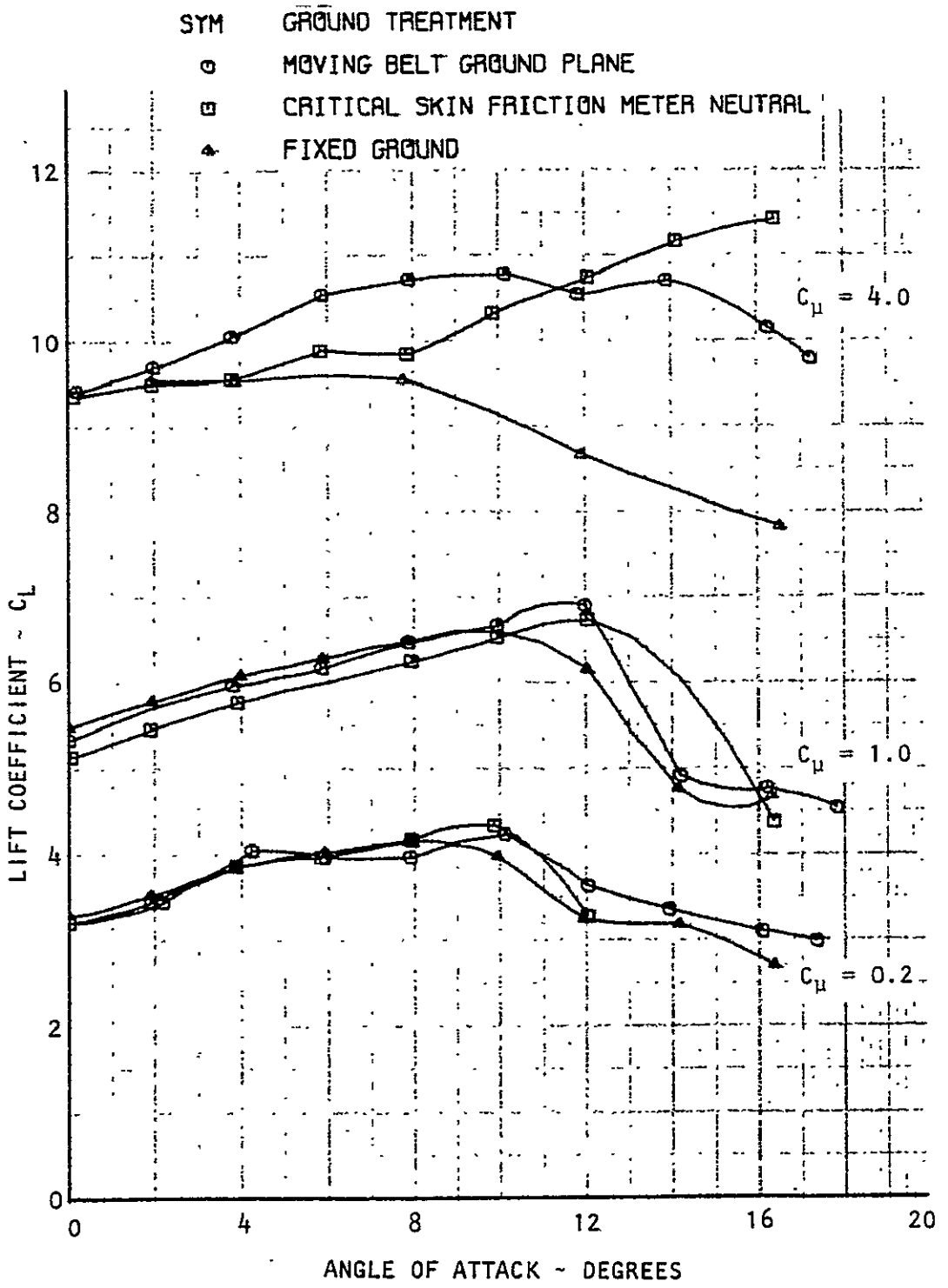

Figure 8.4(b) Lift Data in Ground Effect, h/c = 2, Swept Wing with Tips (Ground BLC: Continuous Slot)

ORIGINAL PAGE IS
OF POOR QUALITY

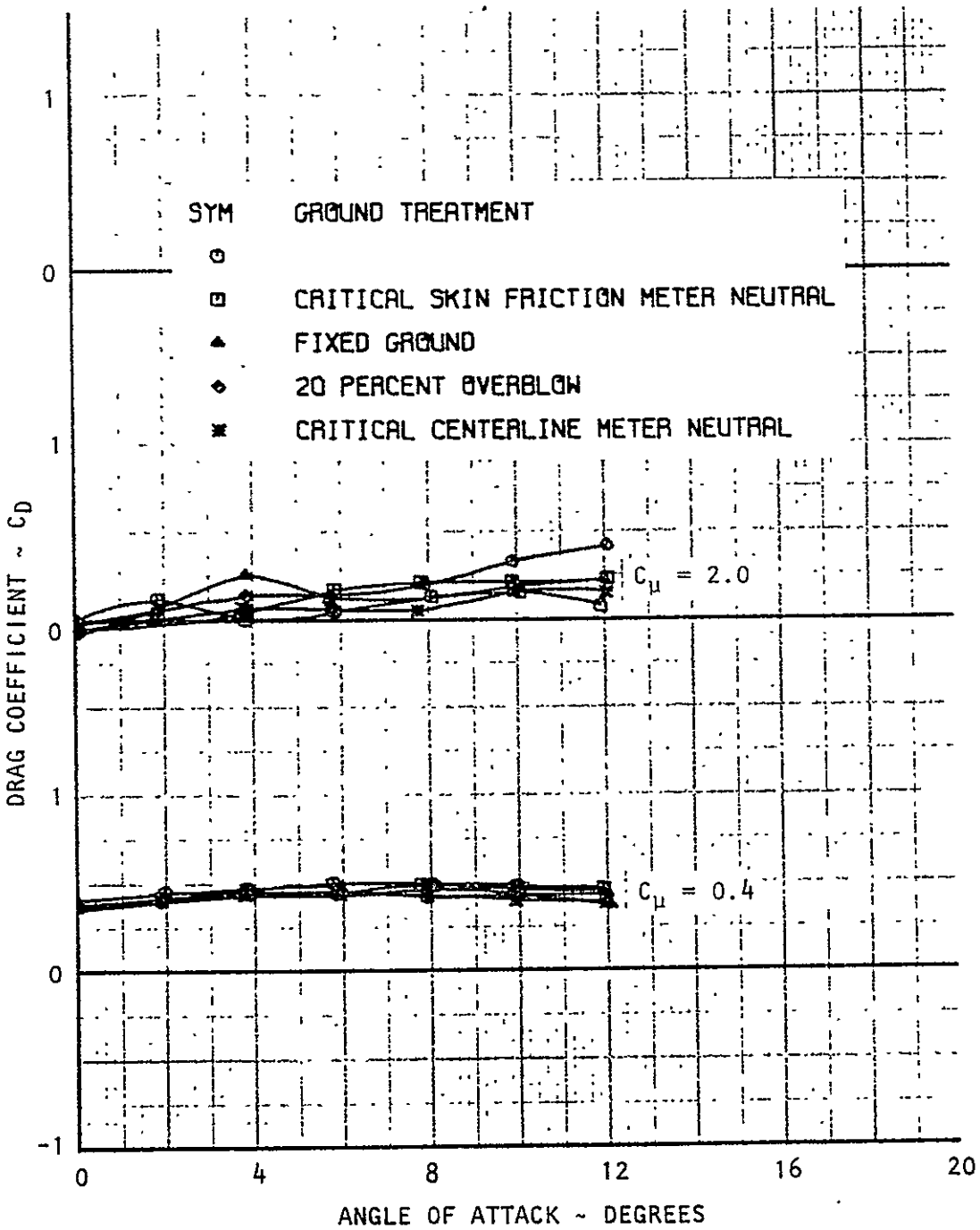

Figure 8.5(a) Drag Data in Ground Effect, h/c = 1, Basic Swept Wing (Ground BLC: Continuous Slot)

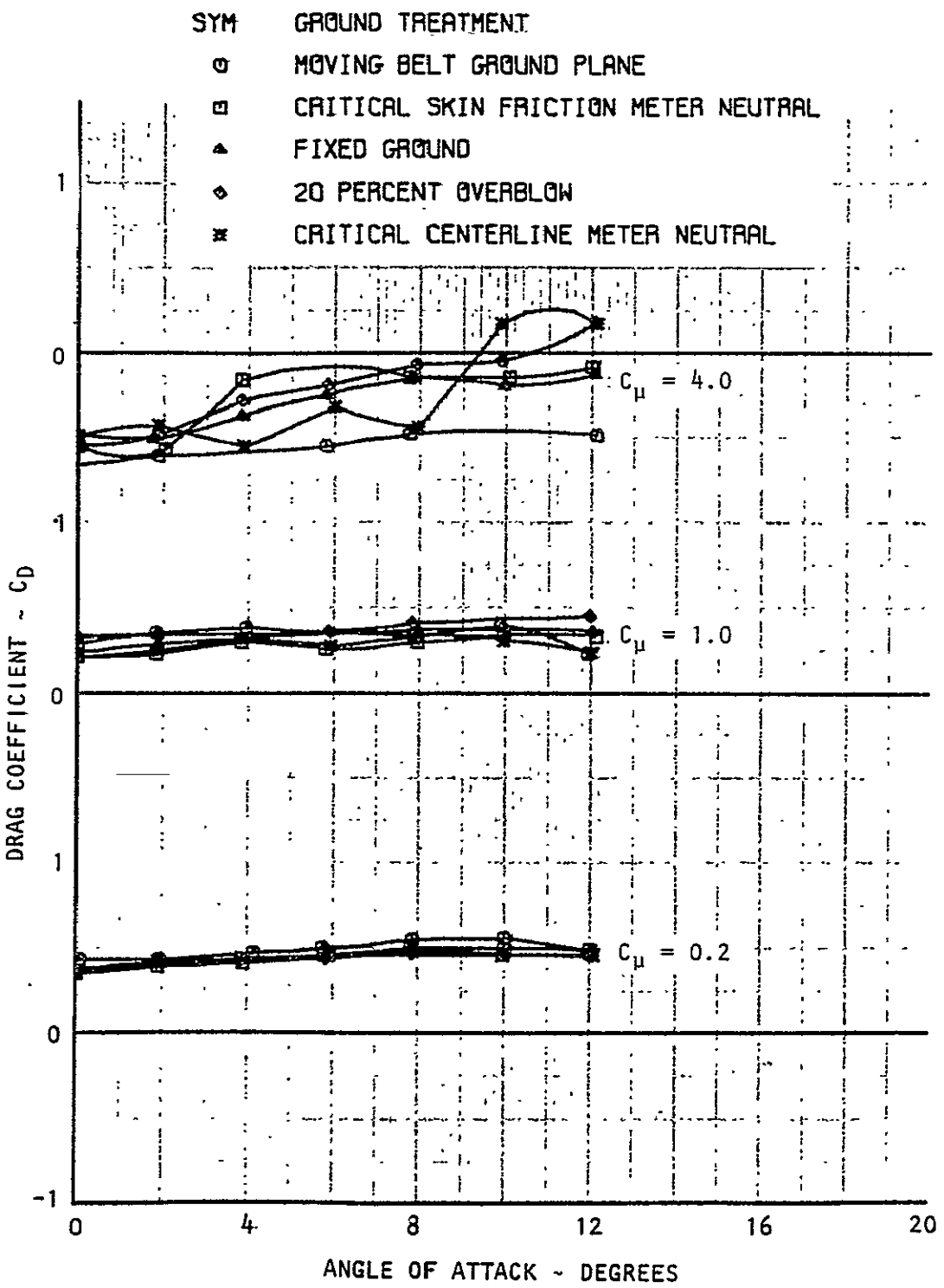

Figure 8.5(b) Drag Data in Ground Effect, h/c = 1, Basic Swept Wing (Ground BLC: Continuous Slot)

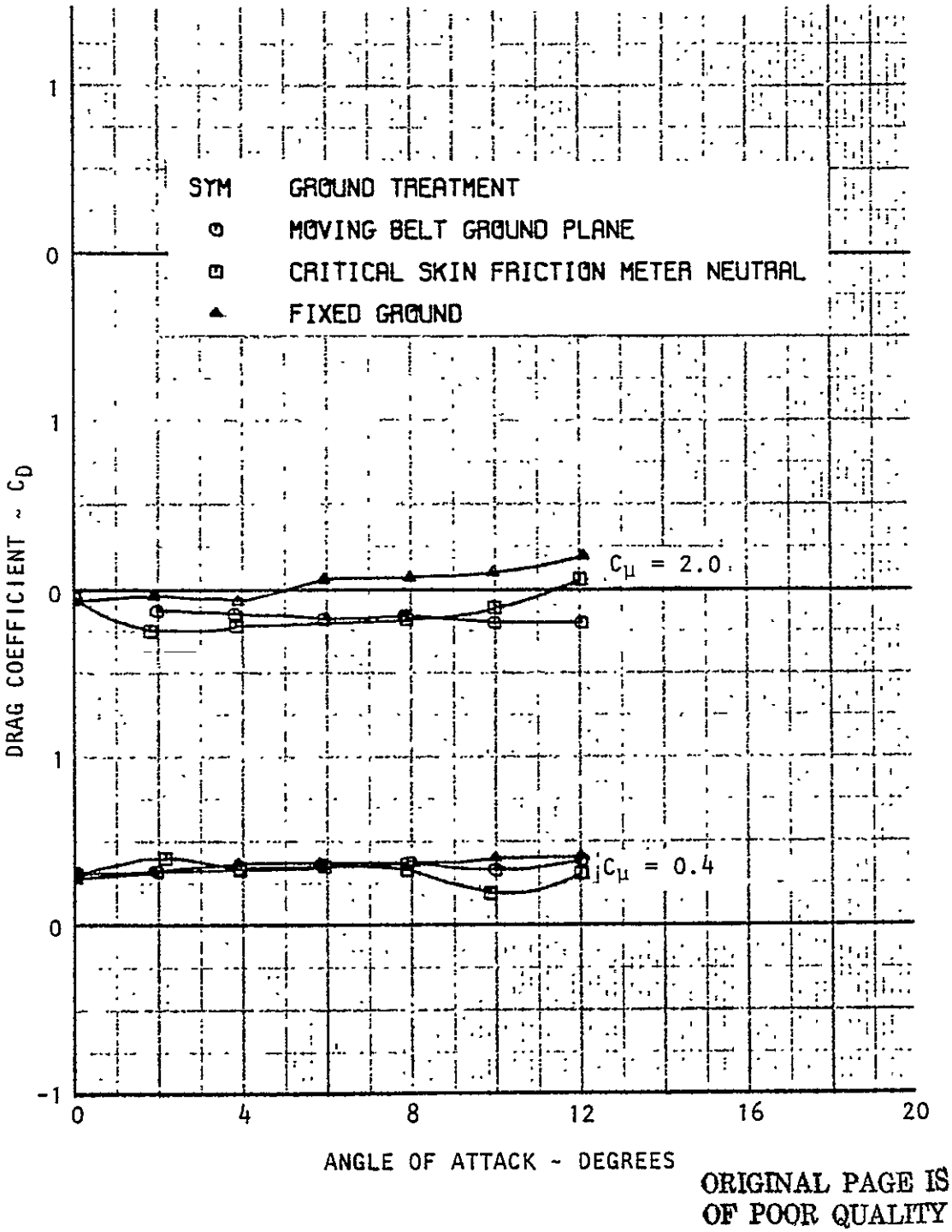

ORIGINAL PAGE IS
OF POOR QUALITY

Figure 8.6(a) Drag Data in Ground Effect, h/c = 1, Swept Wing With Tips (Ground BLC: Continuous Slot)

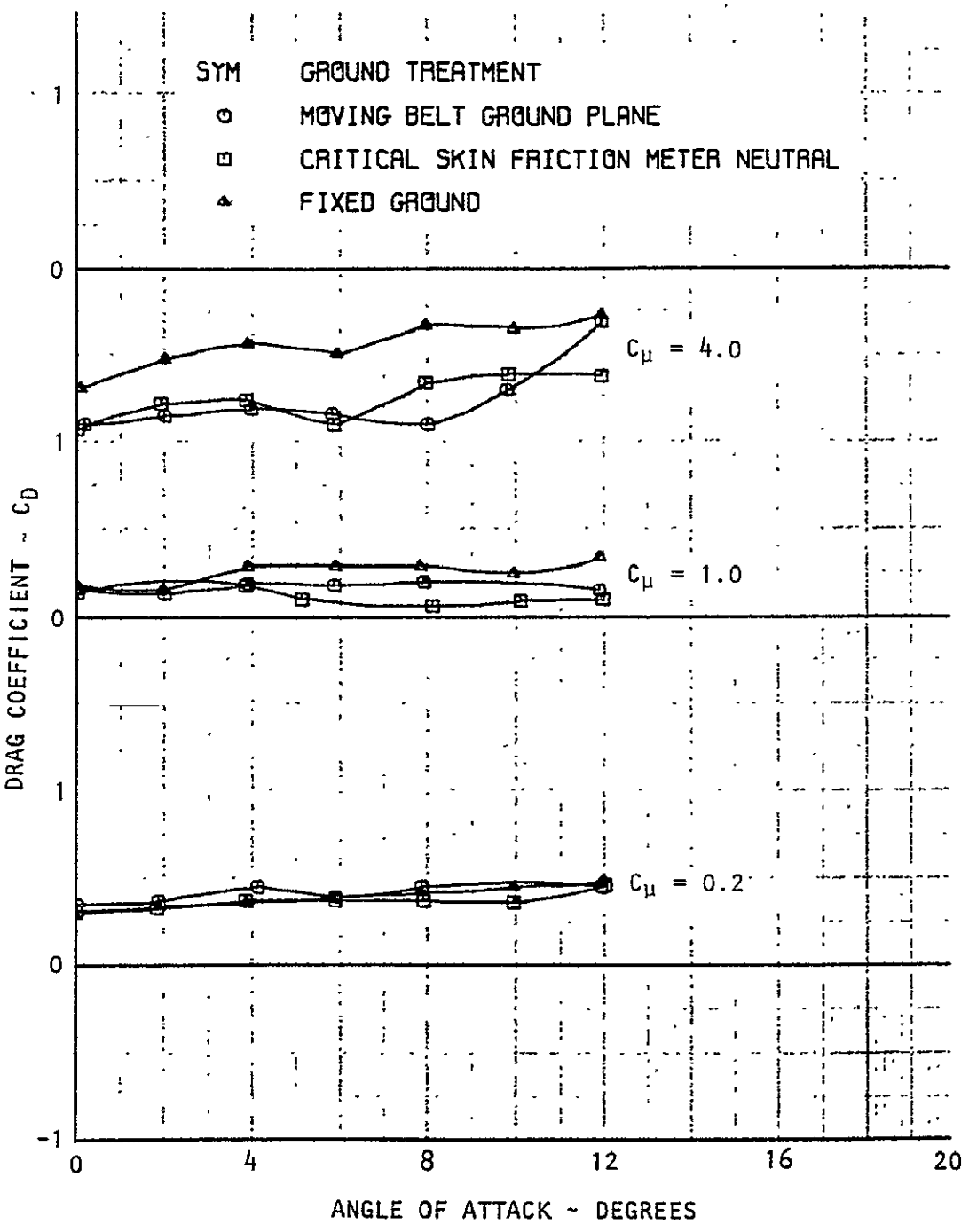

Figure 8.6(b) Drag Data in Ground Effect, h/c = 1, Swept Wing with Tips (Ground BLC: Continuous Slot)

ORIGINAL PAGE IS
OF POOR QUALITY

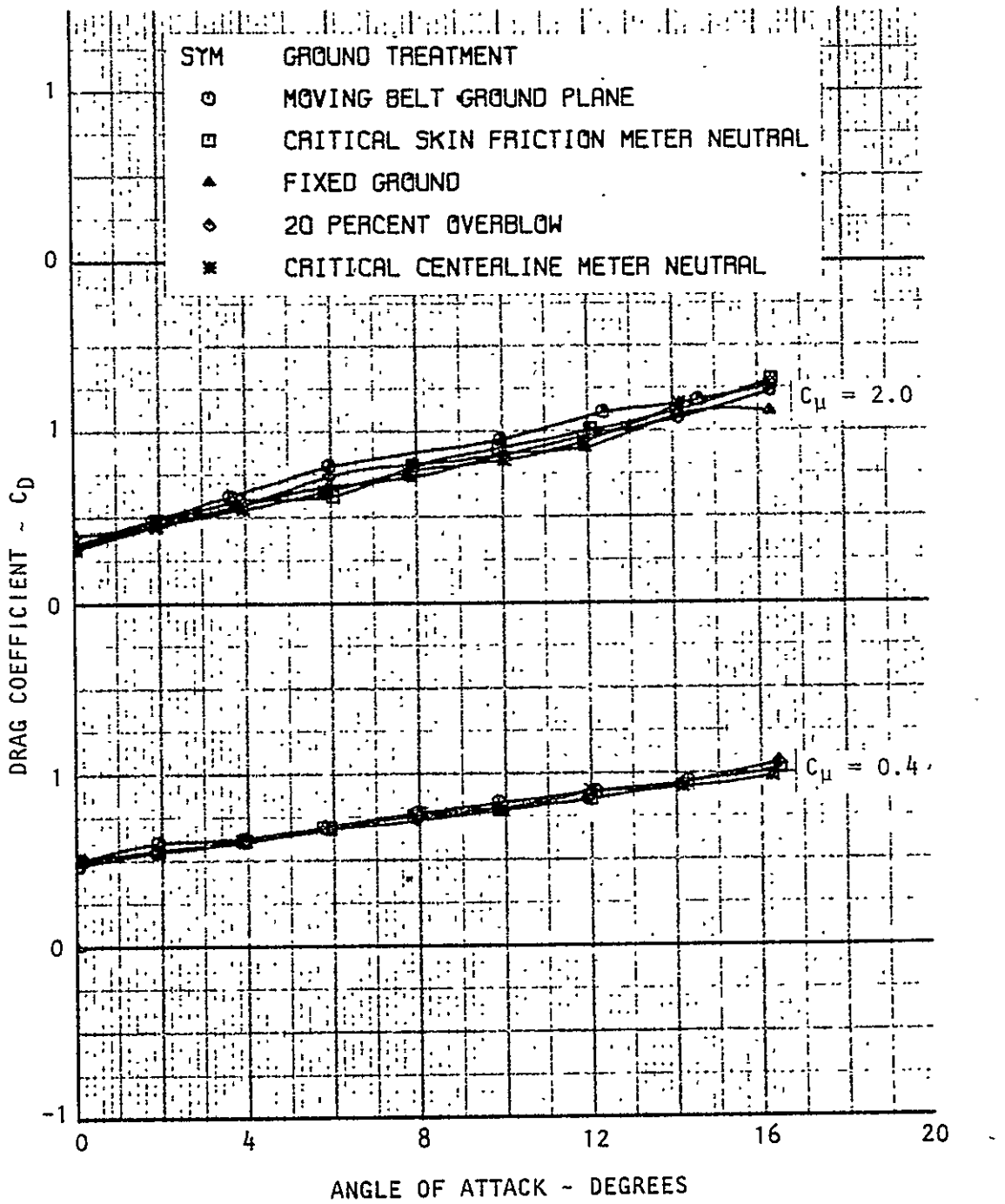

Figure 8.7(a) Drag Data in Ground Effect, h/c = 2, Basic Swept Wing (Ground BLC: Continuous Slot)

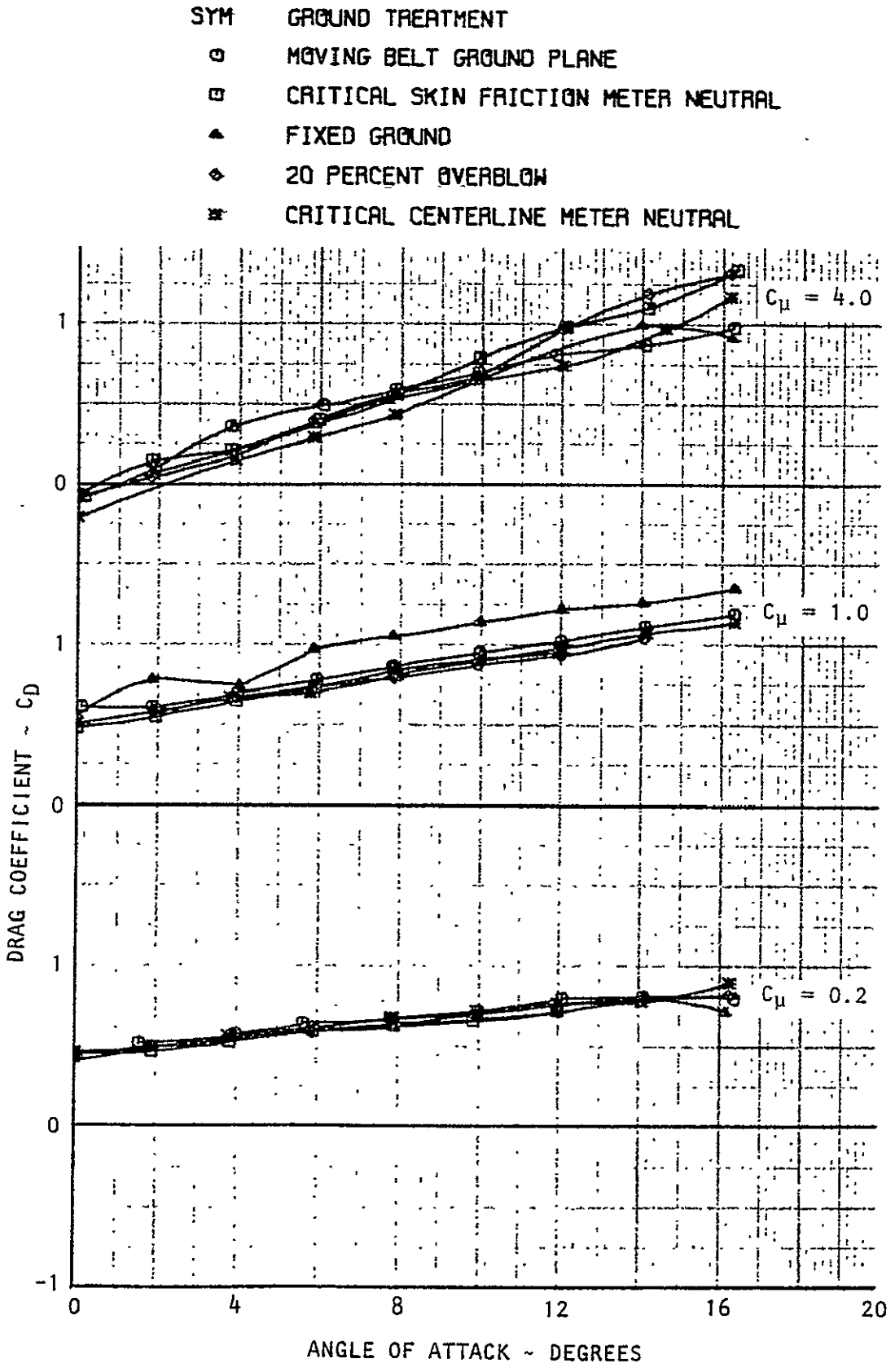

Figure 8.7(b) Drag Data in Ground Effect, h/c = 2, Basic Swept Wing (Ground BLC: Continuous Slot)

ORIGINAL PAGE IS
OF POOR QUALITY

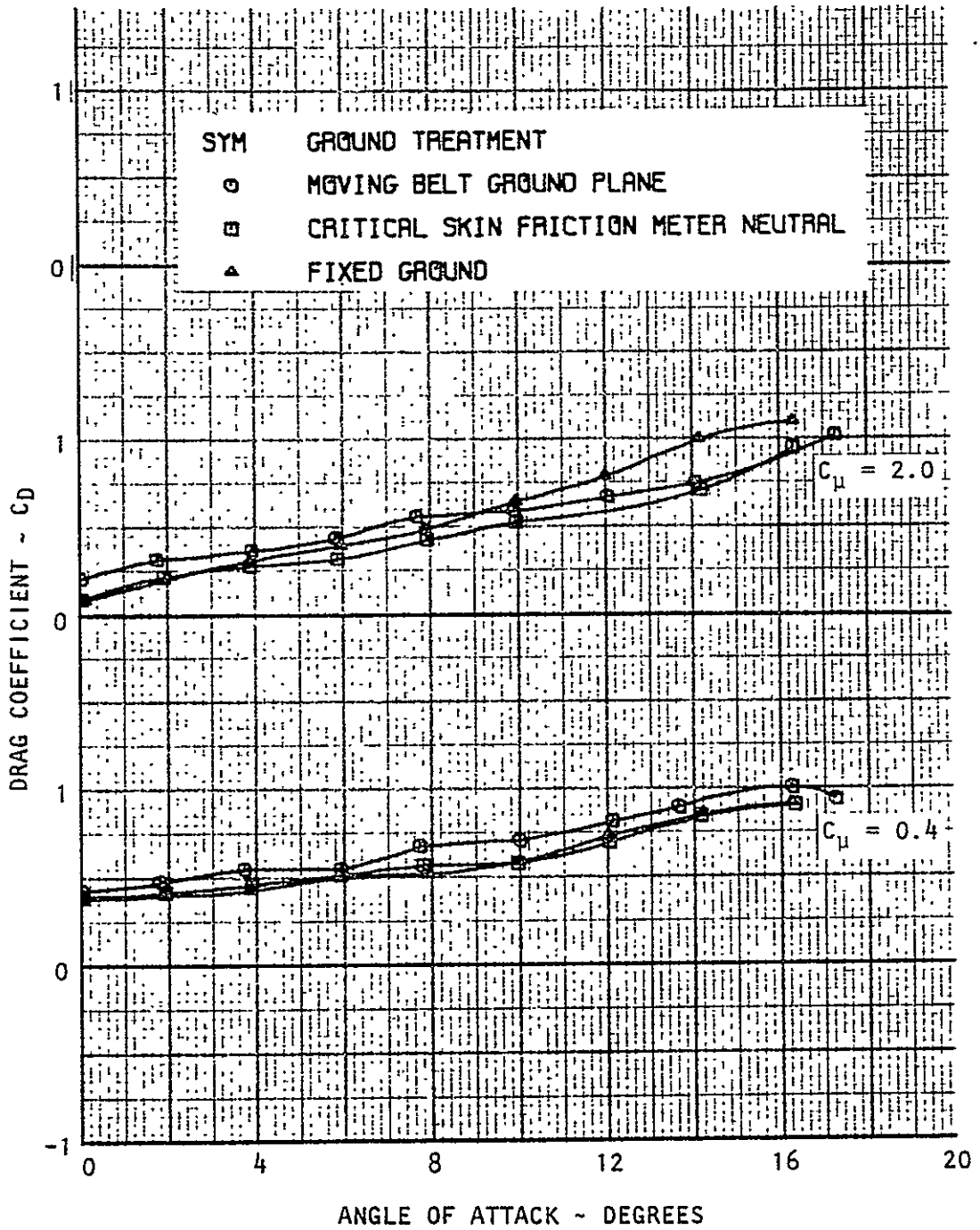

Figure 8.8(a) Drag Data in Ground Effect, h/c = 2, Swept Wing With Tips (Ground BLC: Continuous Slot)

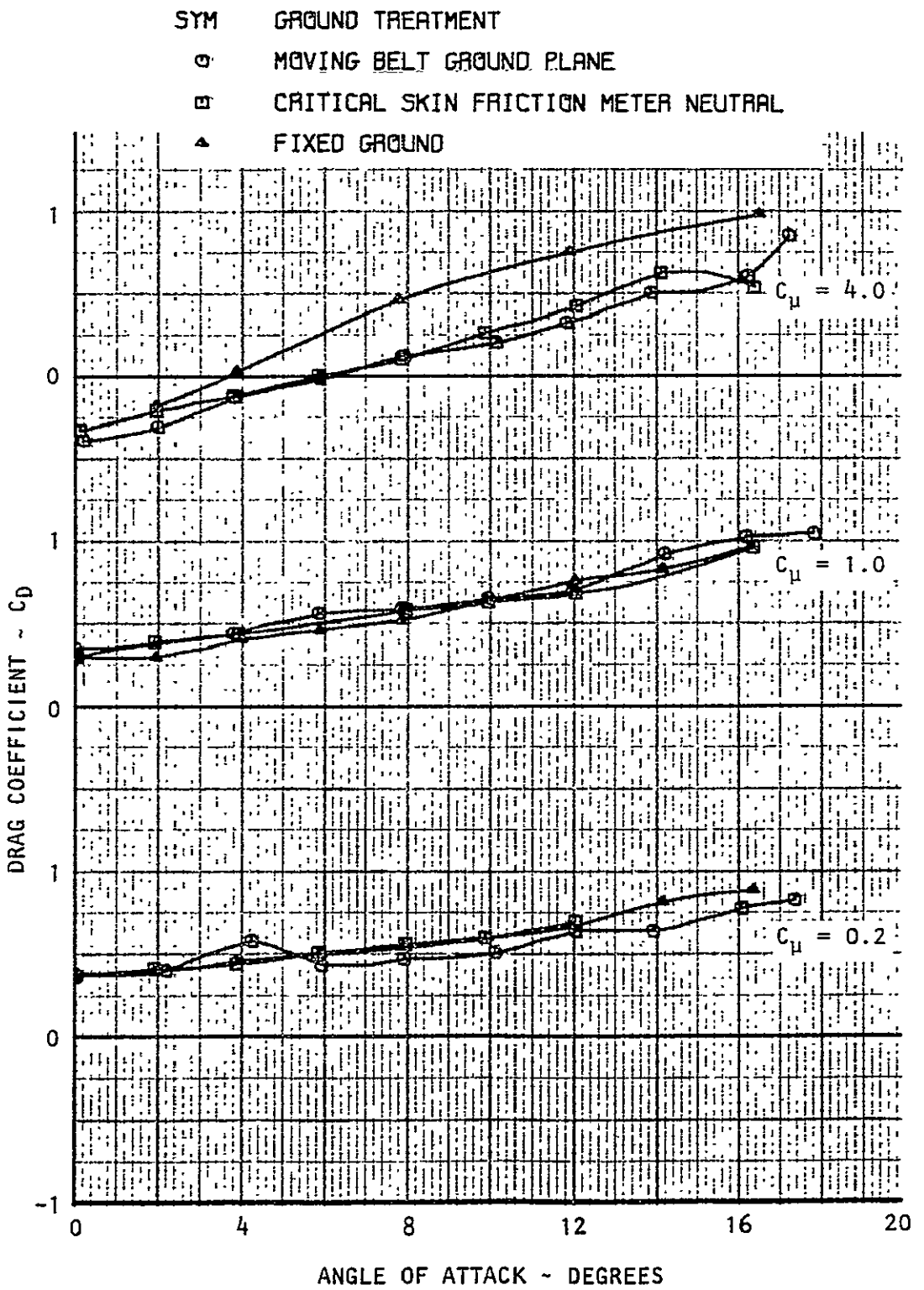

Figure 8.8(b) Drag Data in Ground Effect, h/c = 2, Swept Wing With Tips (Ground BLC: Continuous Slot)

ORIGINAL PAGE IS
OF POOR QUALITY

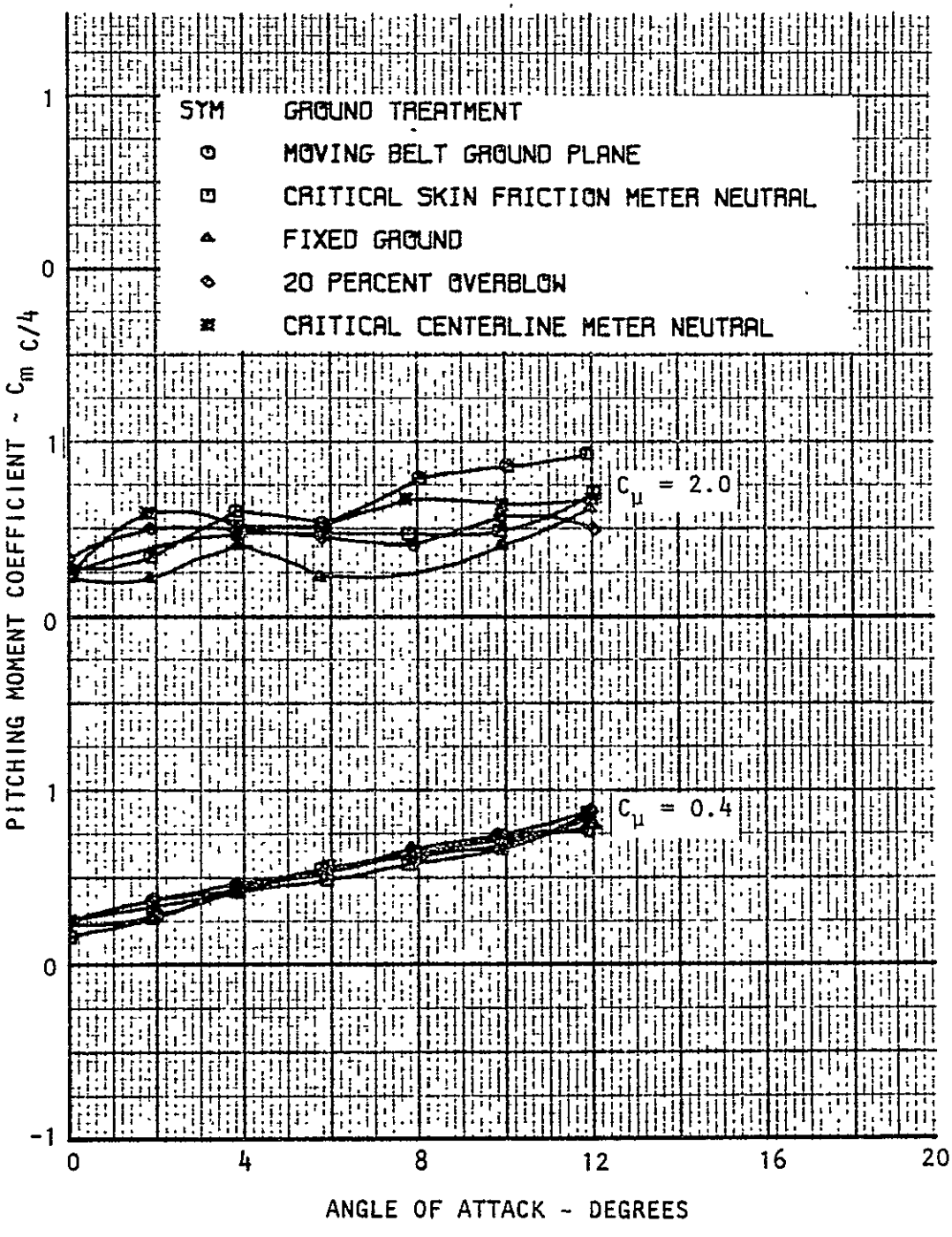

Figure 8.9(a) Pitching Moment Data in Ground Effect, h/c = 1, Basic Swept Wing (Ground BLC: Continuous Slot)

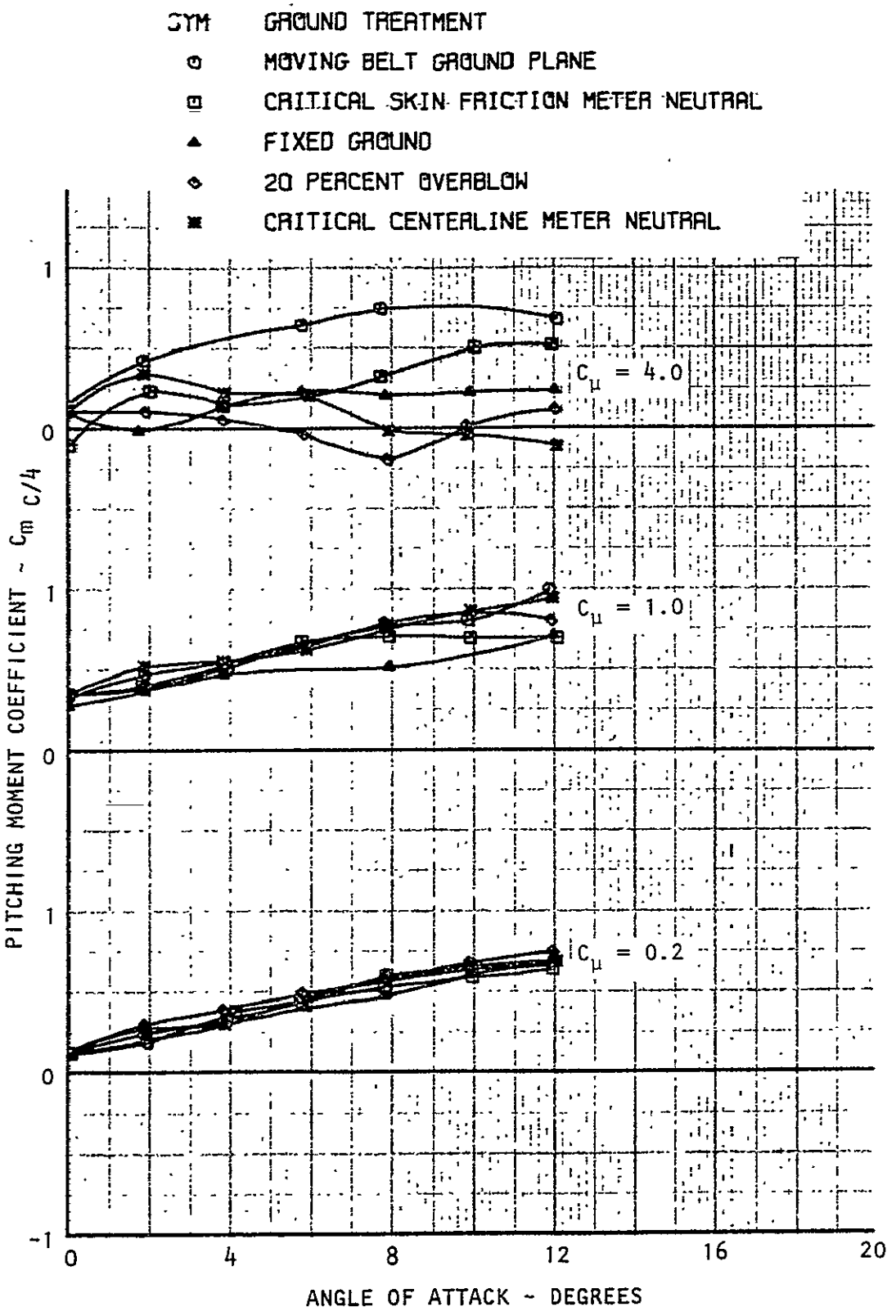

Figure 8.9(b) Pitching Moment Data in Ground Effect, h/c = 1, Basic Swept Wing (Ground BLC: Continuous Slot)

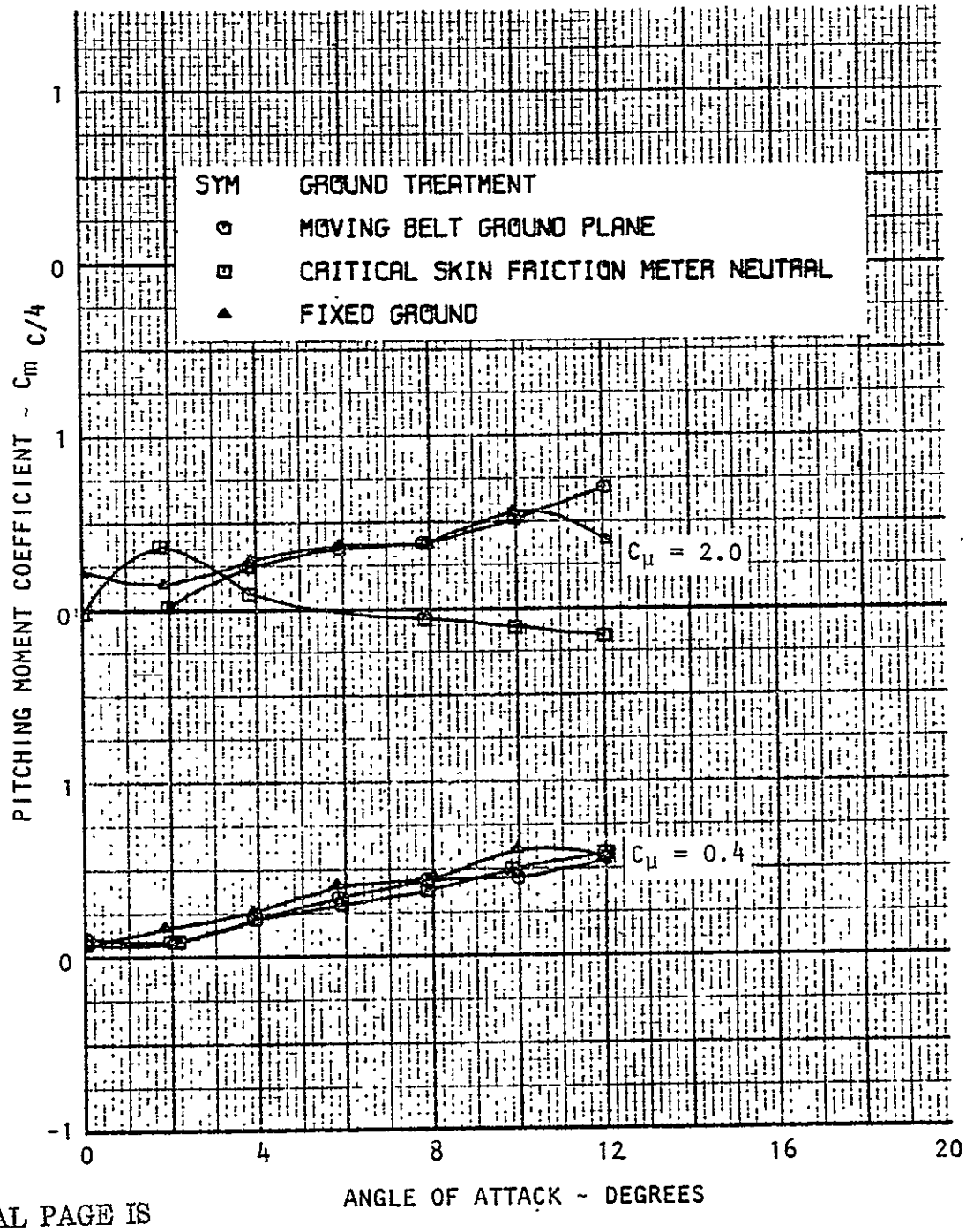

ORIGINAL PAGE IS
OF POOR QUALITY

Figure 8.10(a) Pitching Moment Data in Ground Effect, h/c = 1, Swept Wing With Tips (Ground BLC: Continuous Slot)

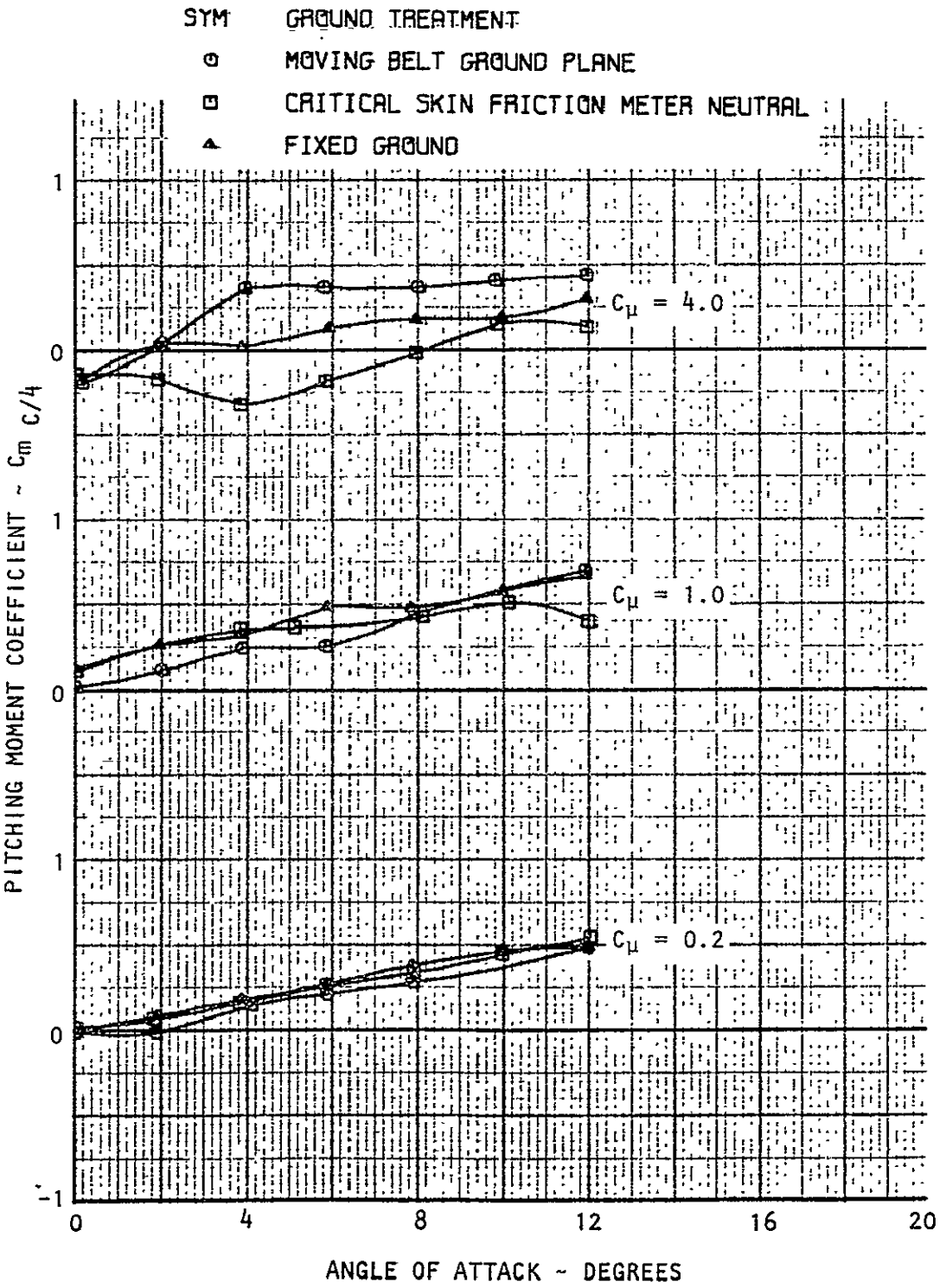

Figure 8.10(b) Pitching Moment Data in Ground Effect, h/c = 1, Swept Wing With Tips (Ground BLC: Continuous Slot)

ORIGINAL PAGE IS
OF POOR QUALITY

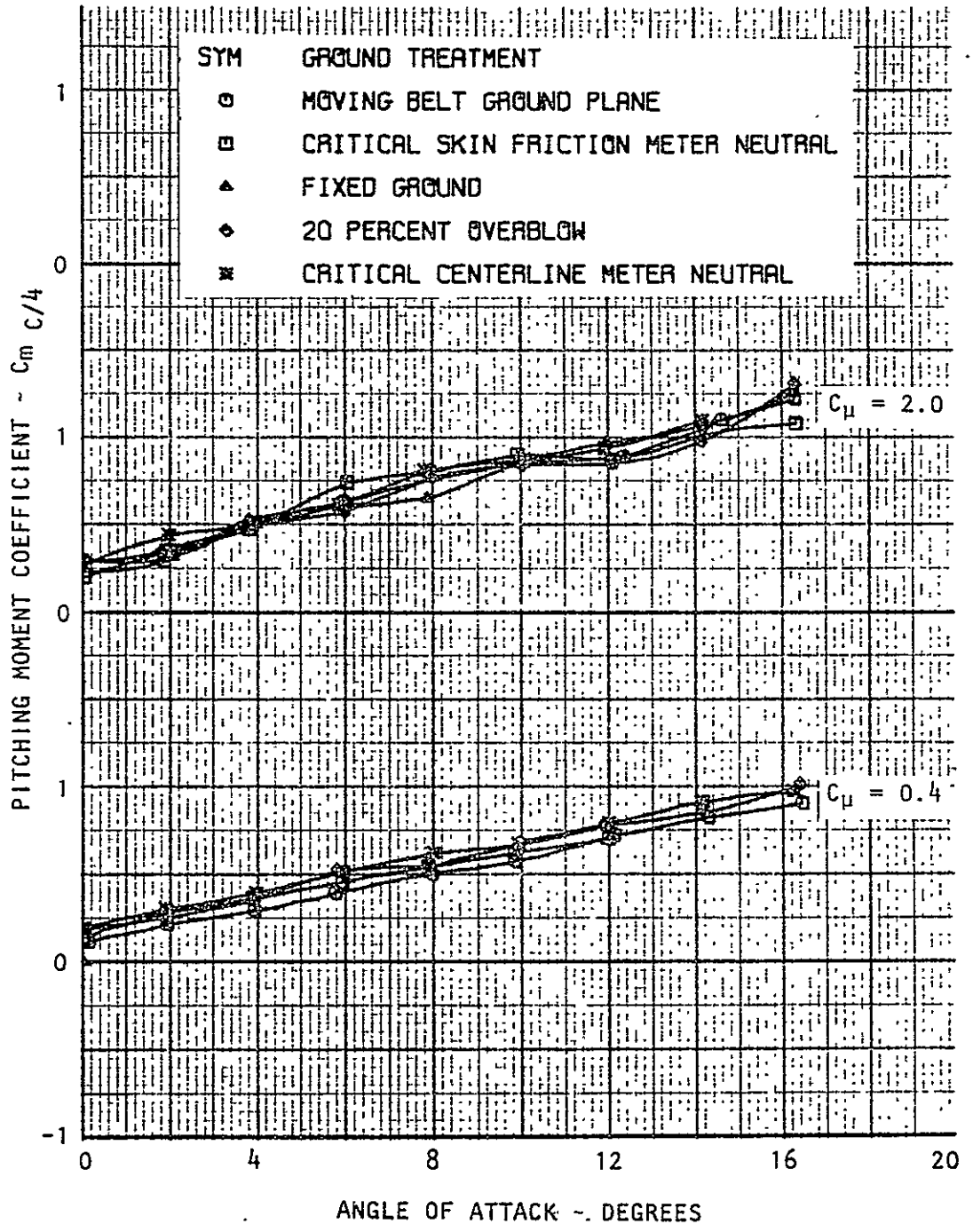

Figure 8.11(a) Pitching Moment Data in Ground Effect, h/c = 2, Basic Swept Wing (Ground BLC: Continuous Slot)

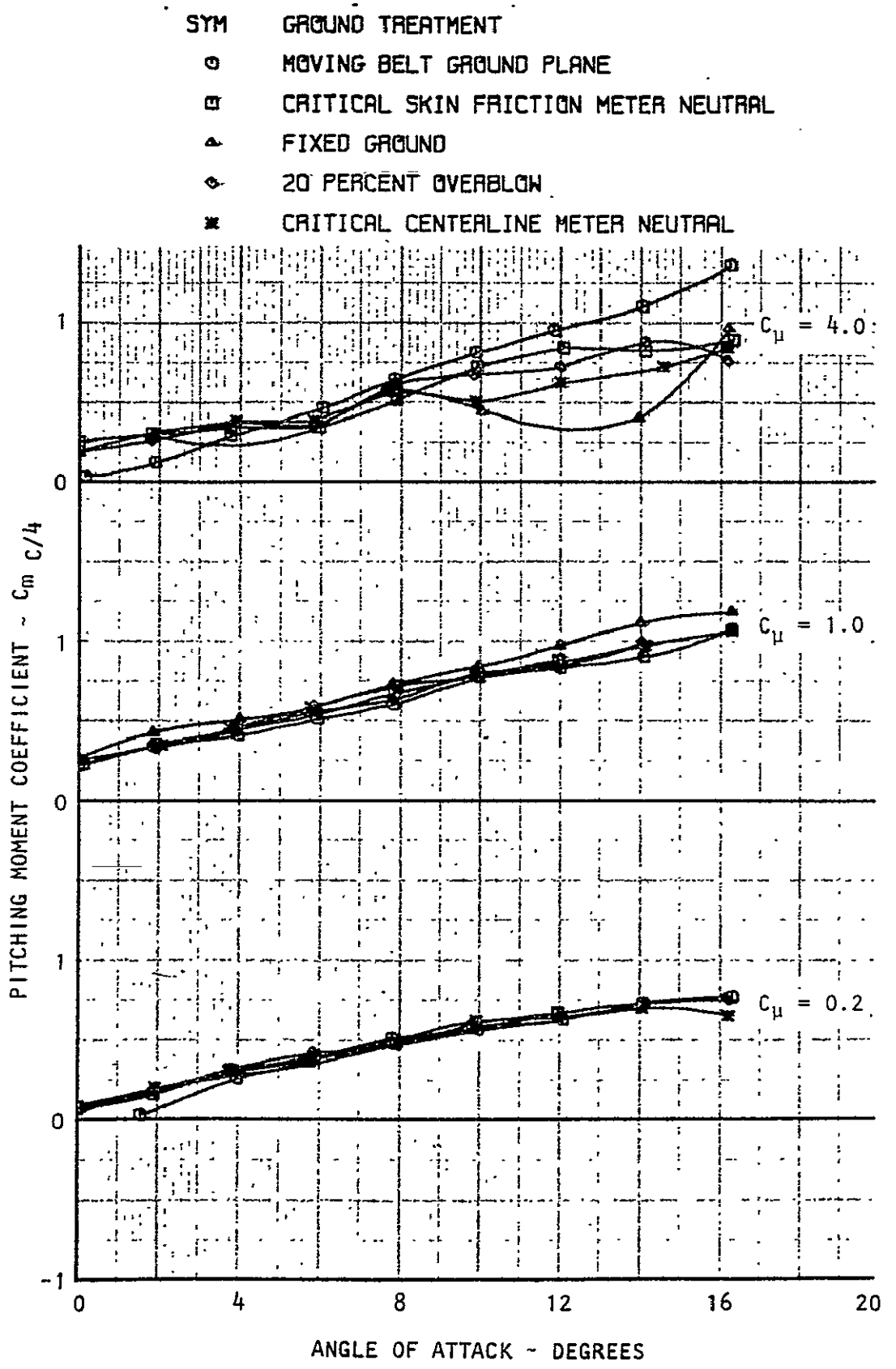

Figure 8.11(b) Pitching Moment Data in Ground Effect, h/c = 2, Basic Swept Wing (Ground BLC: Continuous Slot)

ORIGINAL PAGE IS
OF POOR QUALITY

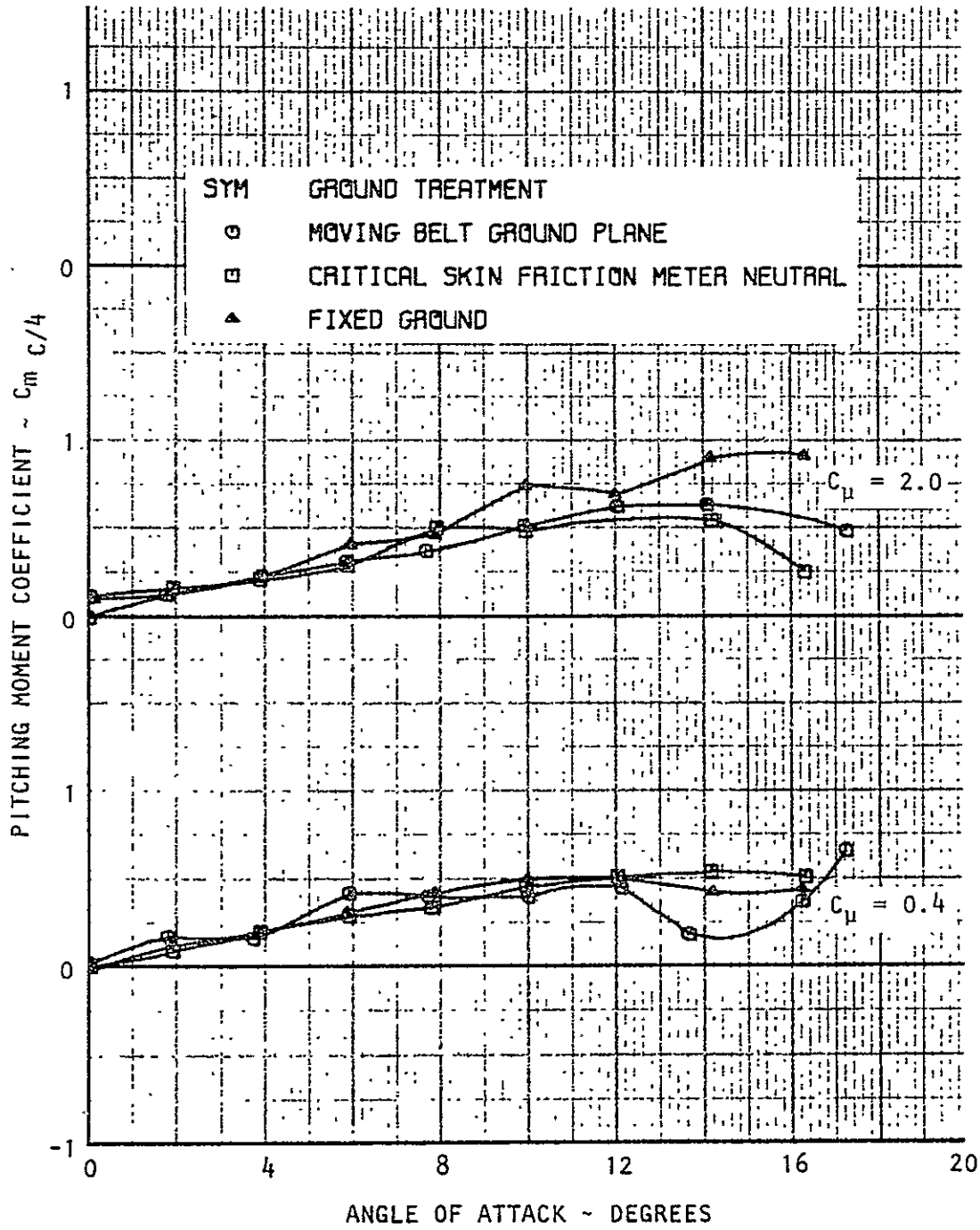

Figure 8.12(a) Pitching Moment Data in Ground Effect, h/c = 2, Basic Swept Wing With Tips (Ground BLC: Continuous Slot)

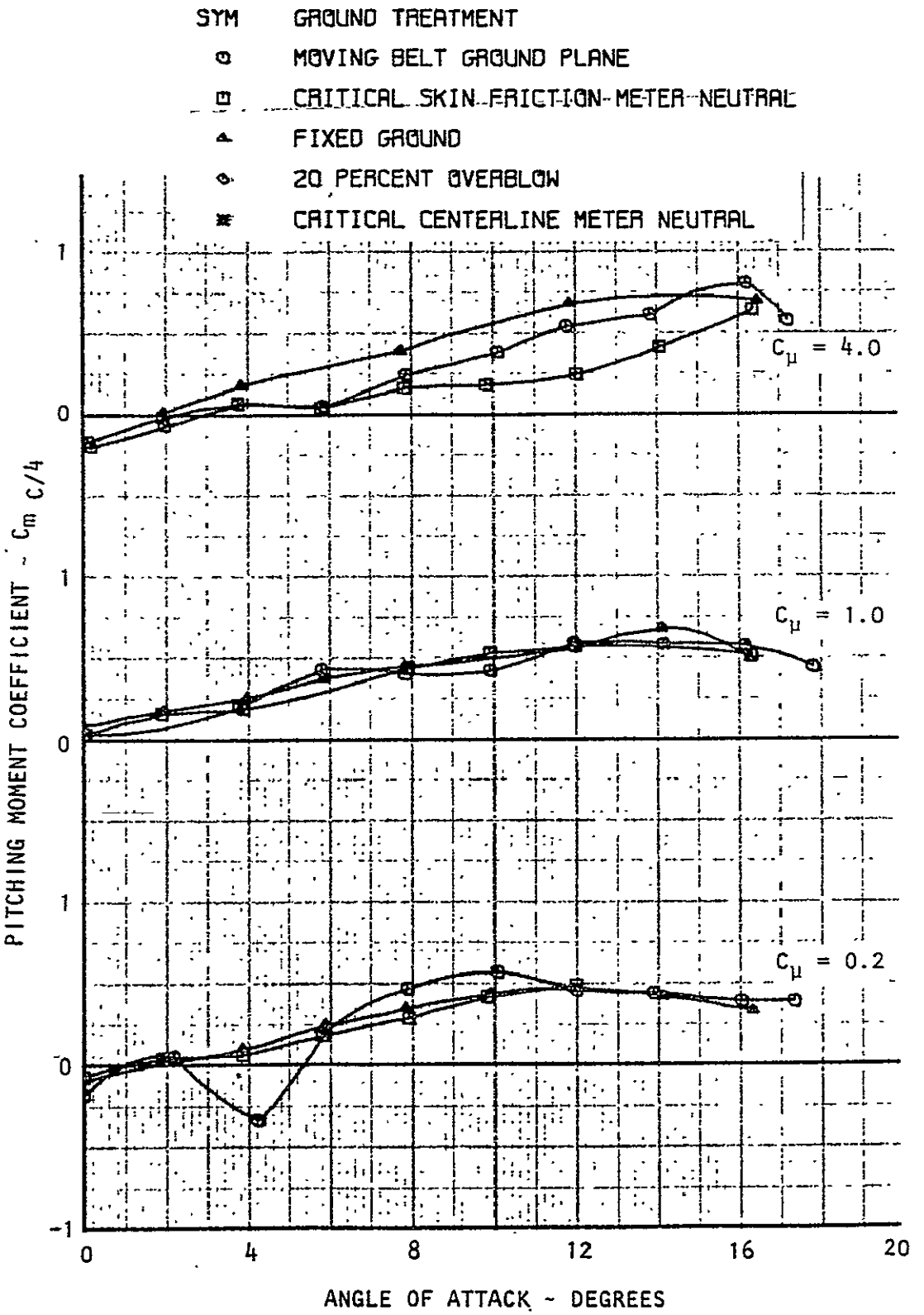

Figure 8.12(b) Pitching Moment Data in Ground Effect, h/c = 2, Basic Swept Wing With Tips (Ground BLC: Continuous Slot)

ORIGINAL PAGE IS
OF POOR QUALITY

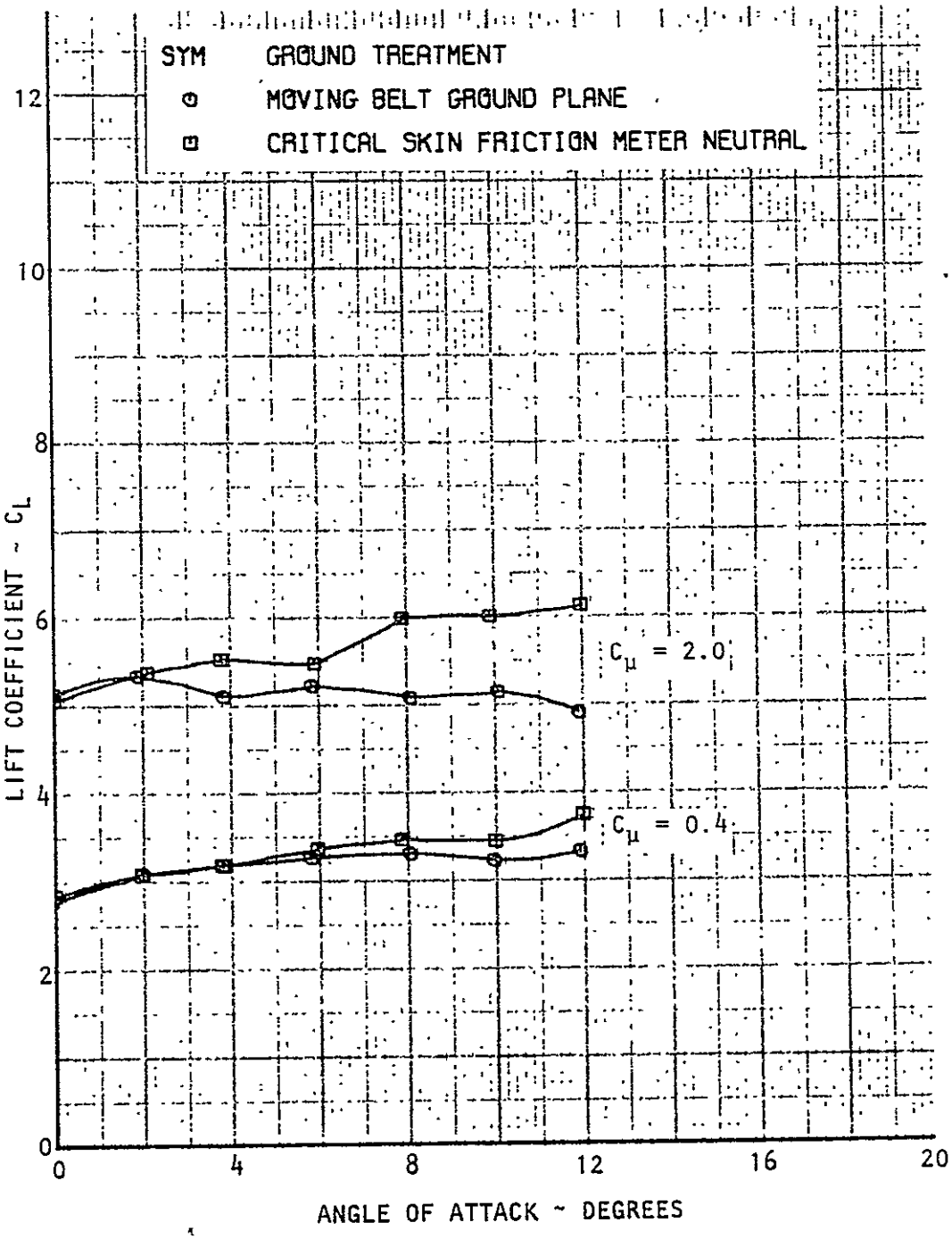

Figure 8.13(a) Lift Data in Ground Effect, h/c = 1, Basic Swept Wing (Ground BLC: Multiple Nozzles)

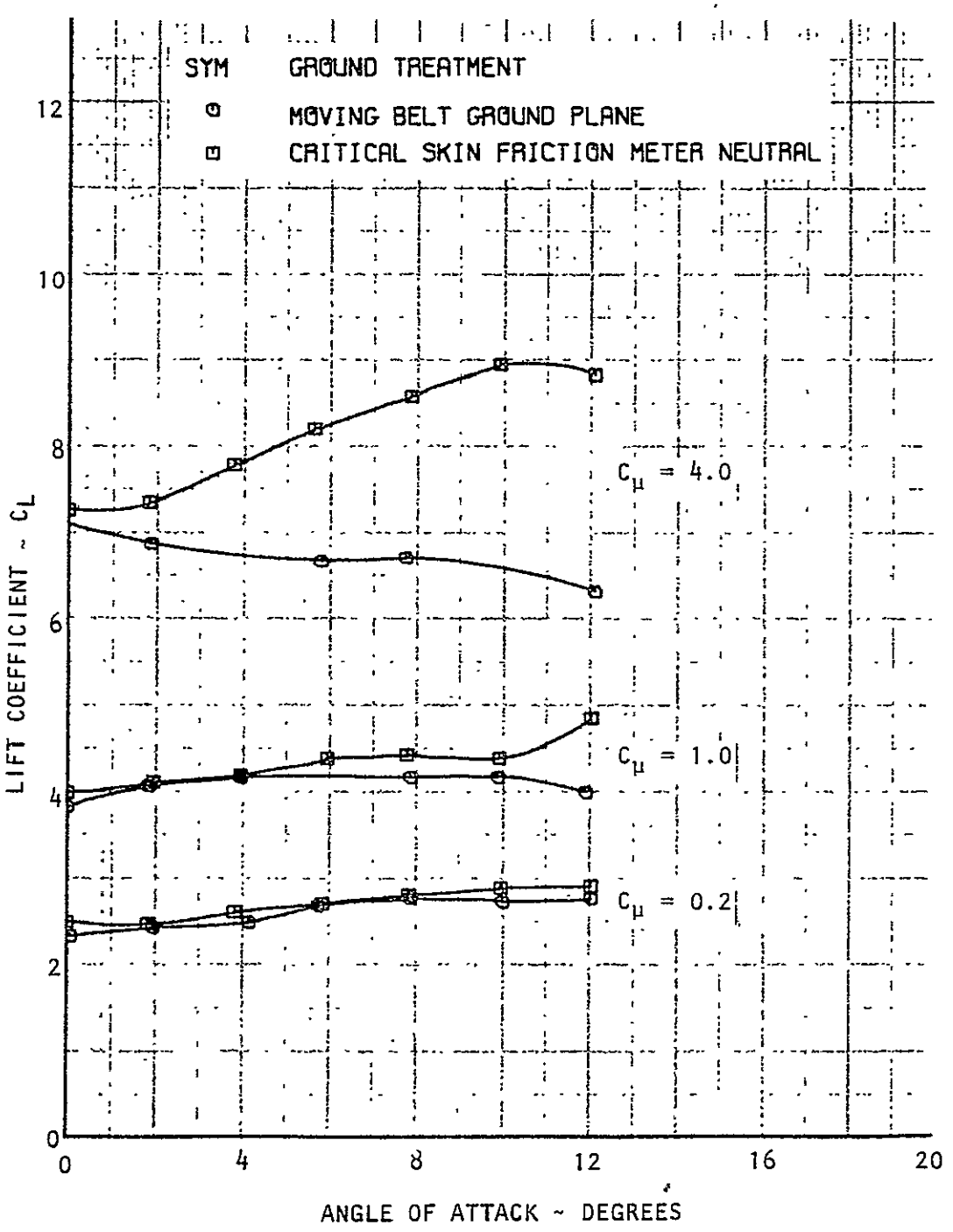

Figure 8.13(b) Lift Data in Ground Effect, h/c = 1, Basic Swept Wing (Ground BLC: Multiple Nozzles)

ORIGINAL PAGE IS
OF POOR QUALITY

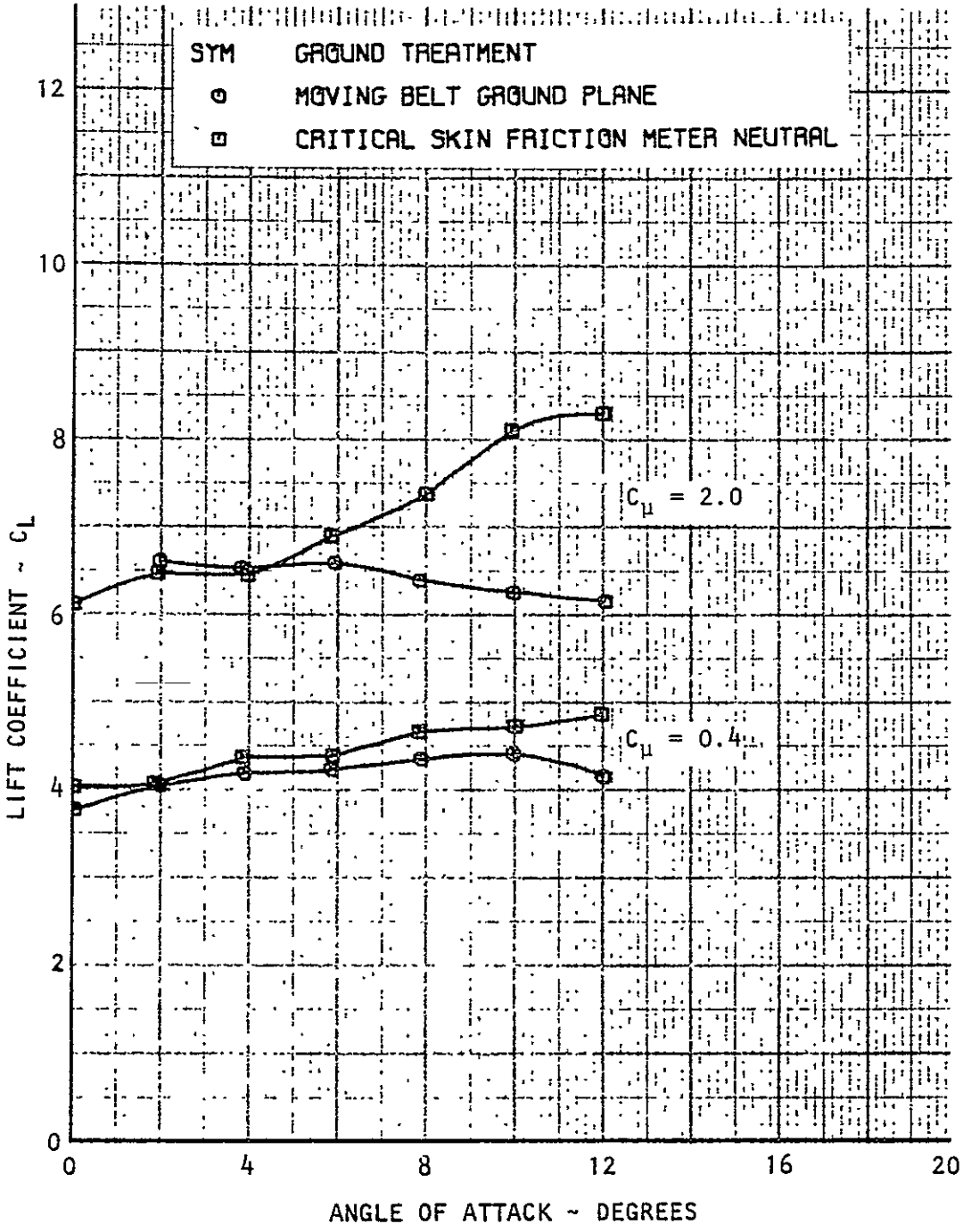

Figure 8.14(a) Lift Data in Ground Effect, h/c = 1, Swept Wing With Tips (Ground BLC: Multiple Nozzles)

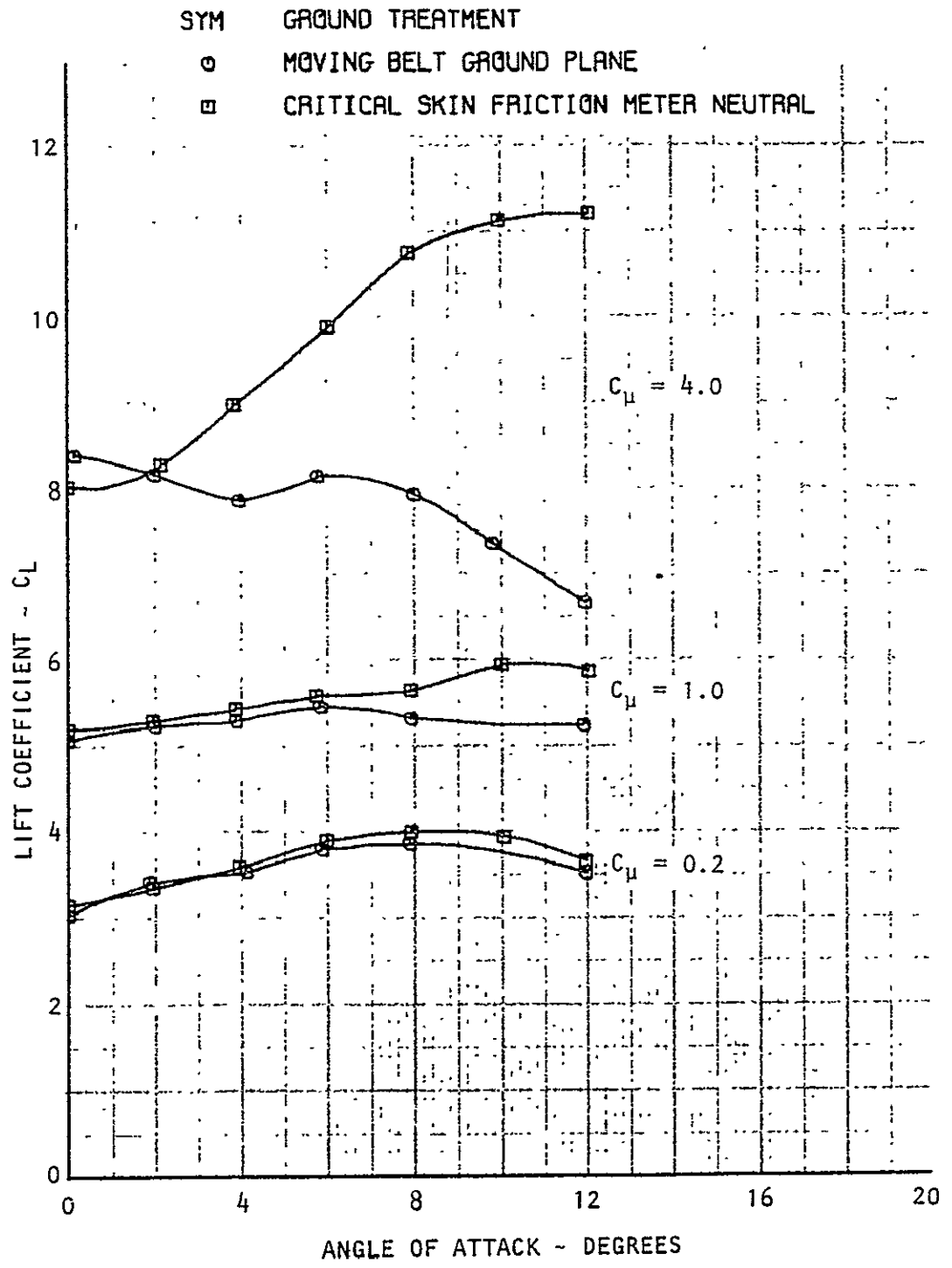

Figure 8.14(b) Lift Data in Ground Effect, h/c = 1, Swept Wing With Tips (Ground BLC: Multiple Nozzles)

ORIGINAL PAGE IS
OF POOR QUALITY

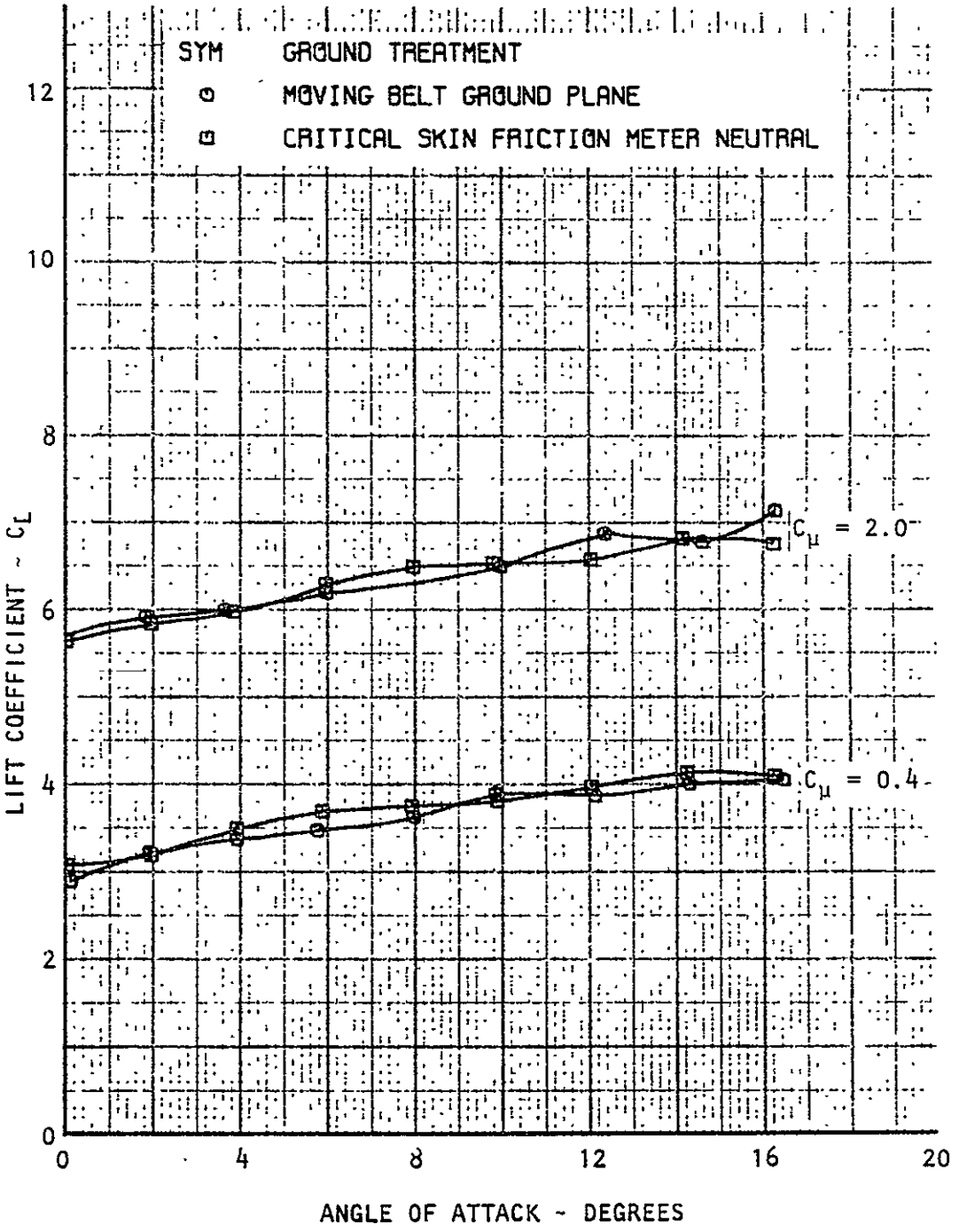

Figure 8.15(a) Lift Data in Ground Effect, h/c = 2, Basic Swept Wing (Ground BLC: Multiple Nozzles)

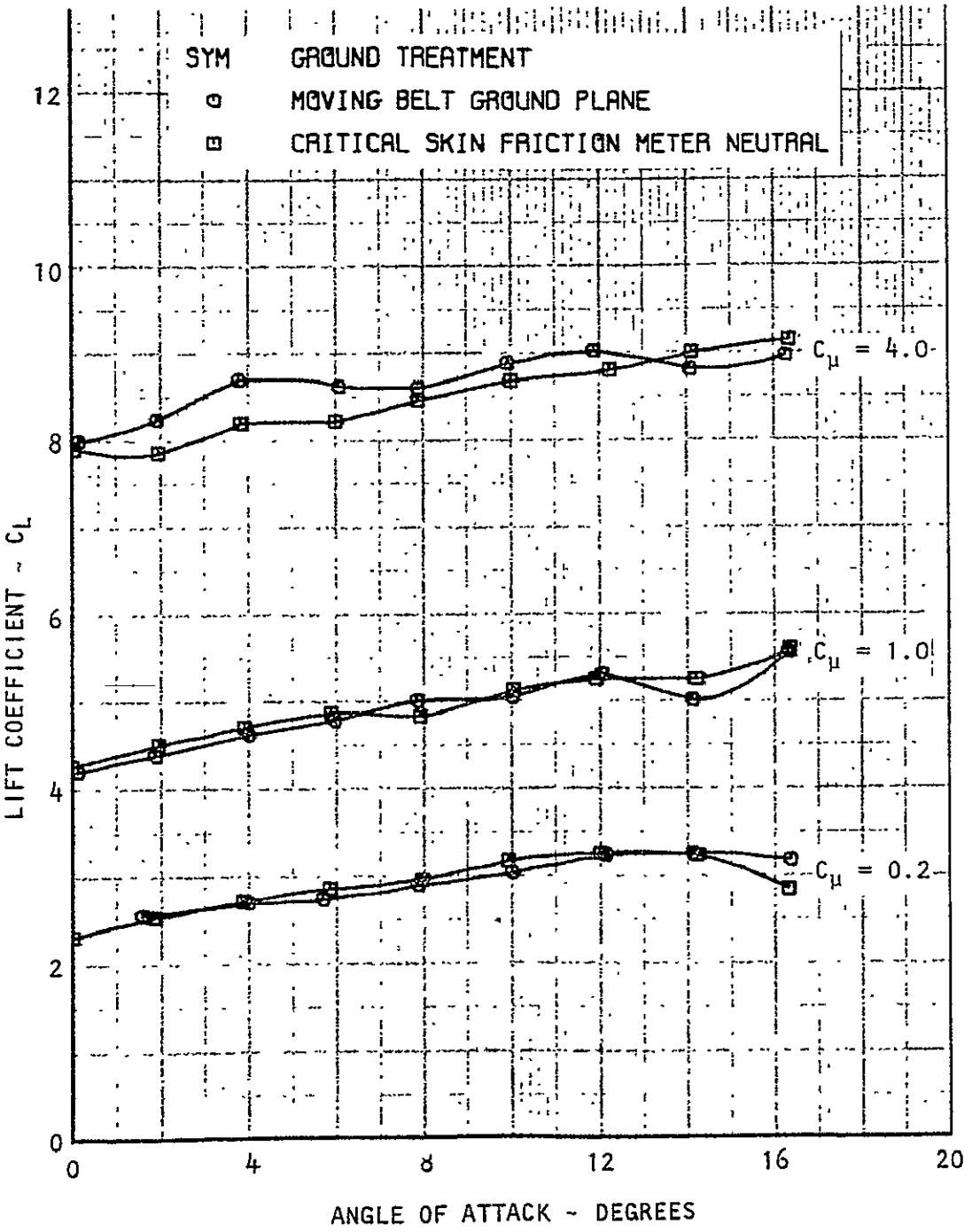

Figure 8.15(b) Lift Data in Ground Effect, h/c = 2, Basic Swept Wing (Ground BLC: Multiple Nozzles)

ORIGINAL PAGE IS
OF POOR QUALITY

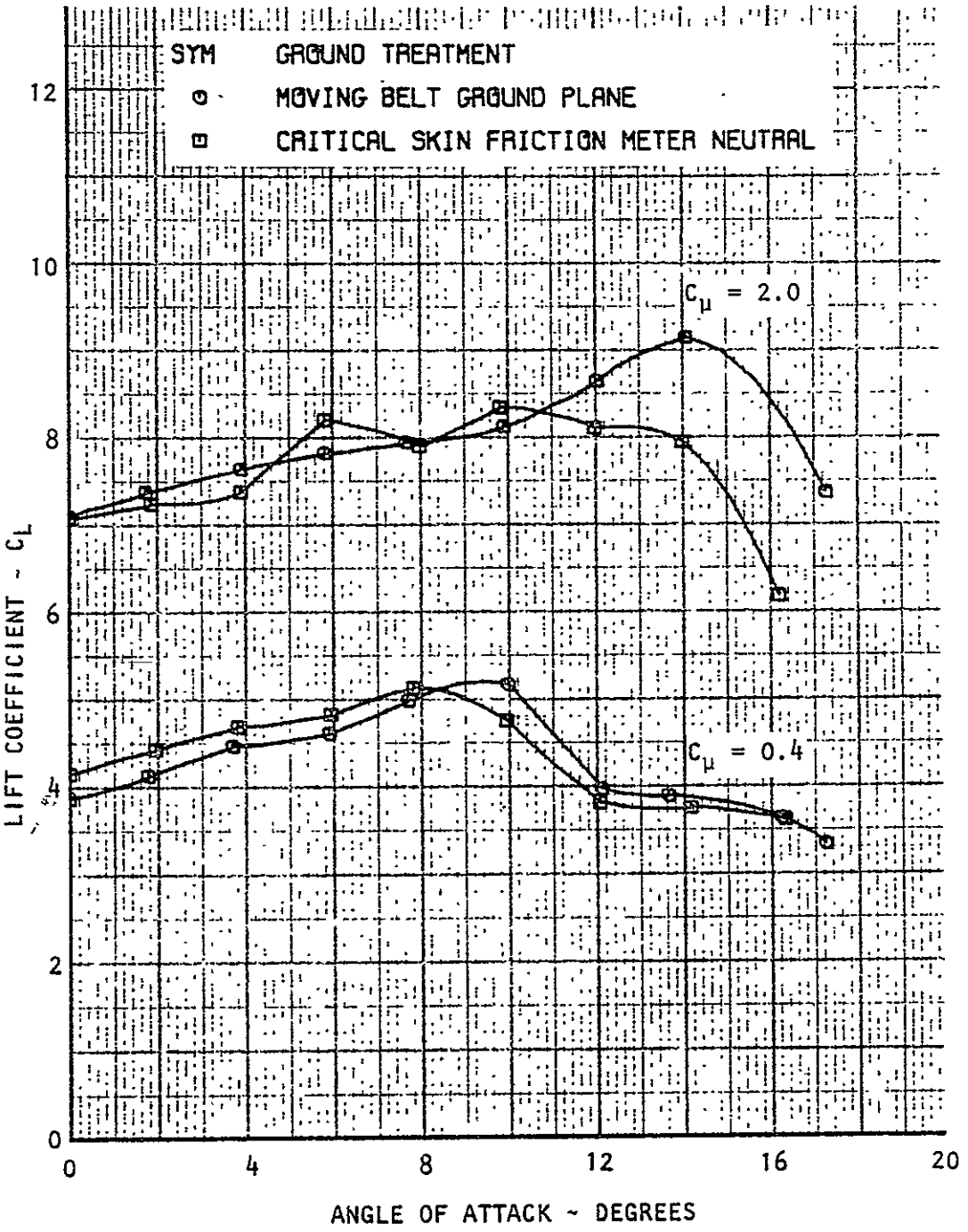

Figure 8.16(a) Lift Data in Ground Effect, h/c = 2, Swept Wing With Tips (Ground BLC: Multiple Nozzles)

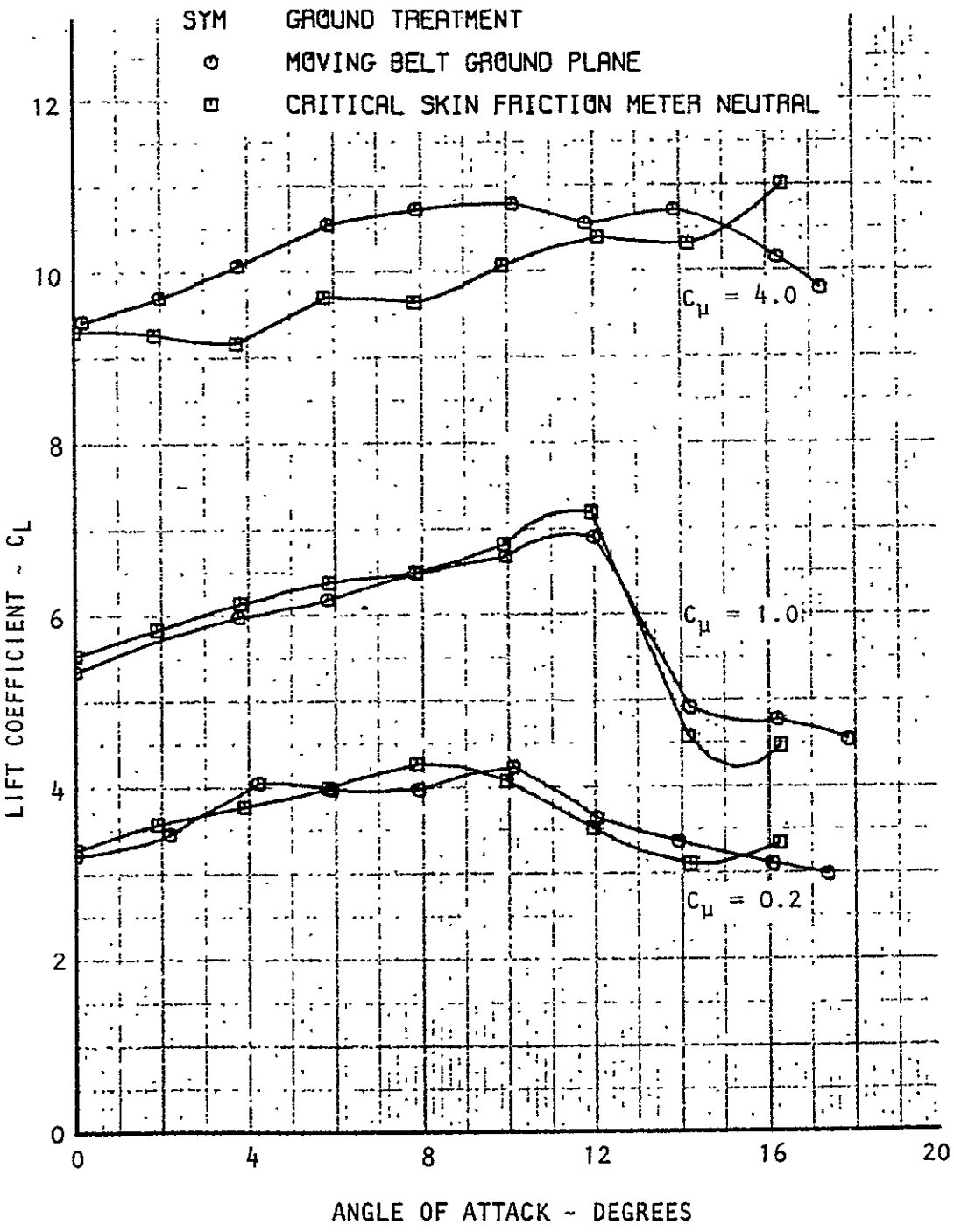

Figure 8.16(b) Lift Data in Ground Effect, h/c = 2, Swept Wing With Tips (Ground BLC: Multiple Nozzles)

ORIGINAL PAGE IS
OF POOR QUALITY

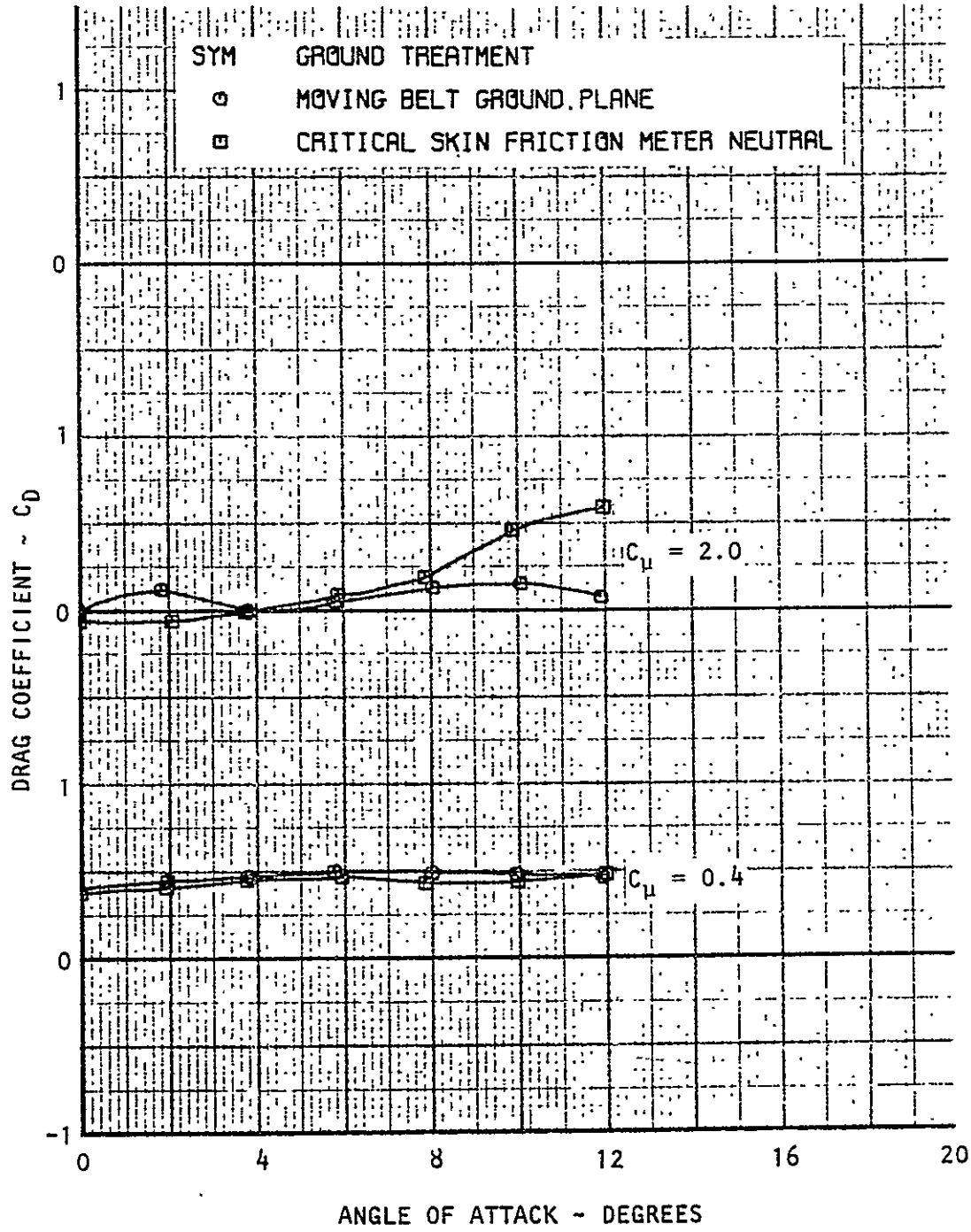

Figure 8.17(a) Drag Data in Ground Effect, h/c = 1, Basic Swept Wing (Ground BLC: Multiple Nozzles)

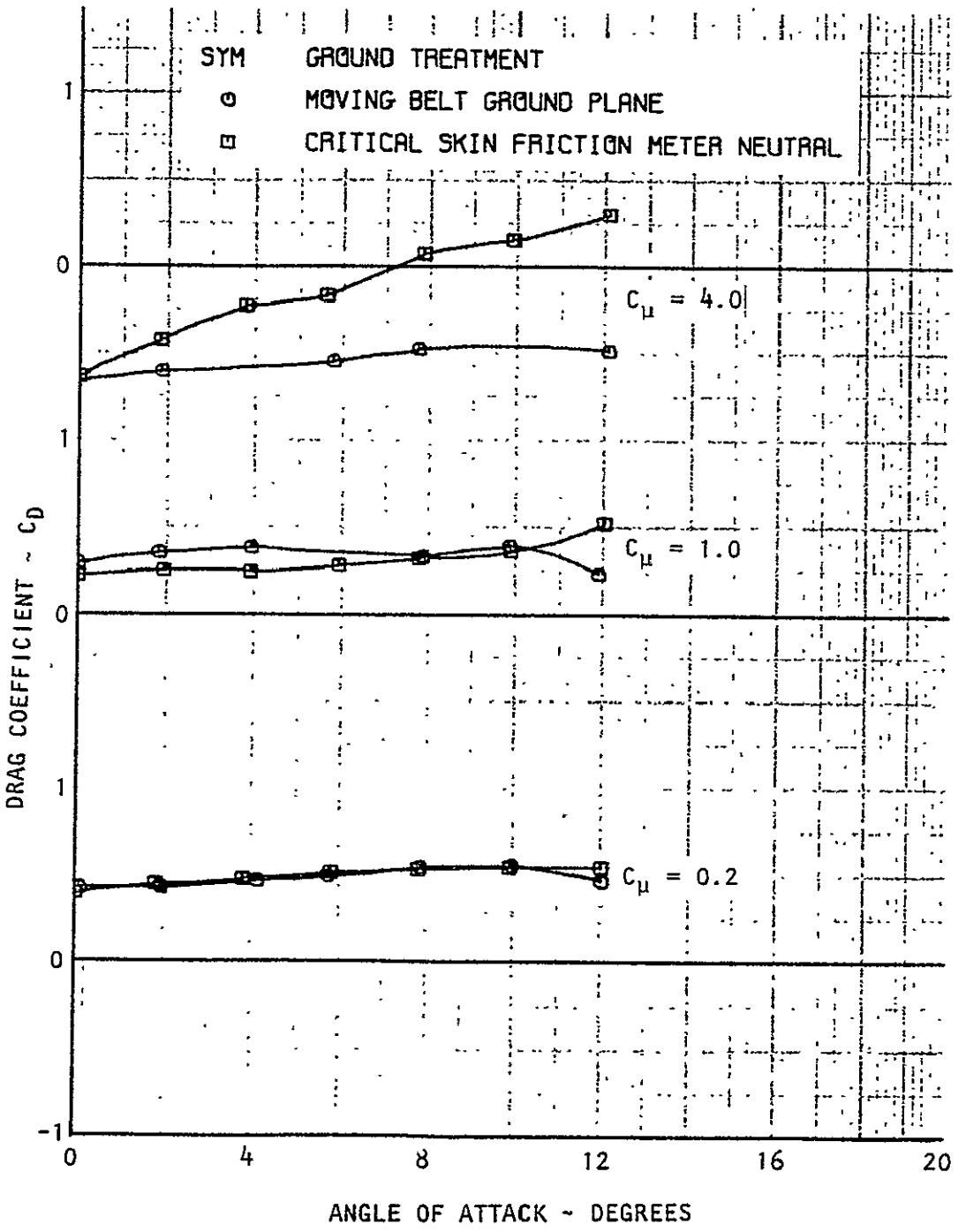

Figure 8.17(b) Drag Data in Ground Effect, h/c = 1, Basic Swept Wing (Ground BLC: Multiple Nozzles)

ORIGINAL PAGE IS
OF POOR QUALITY

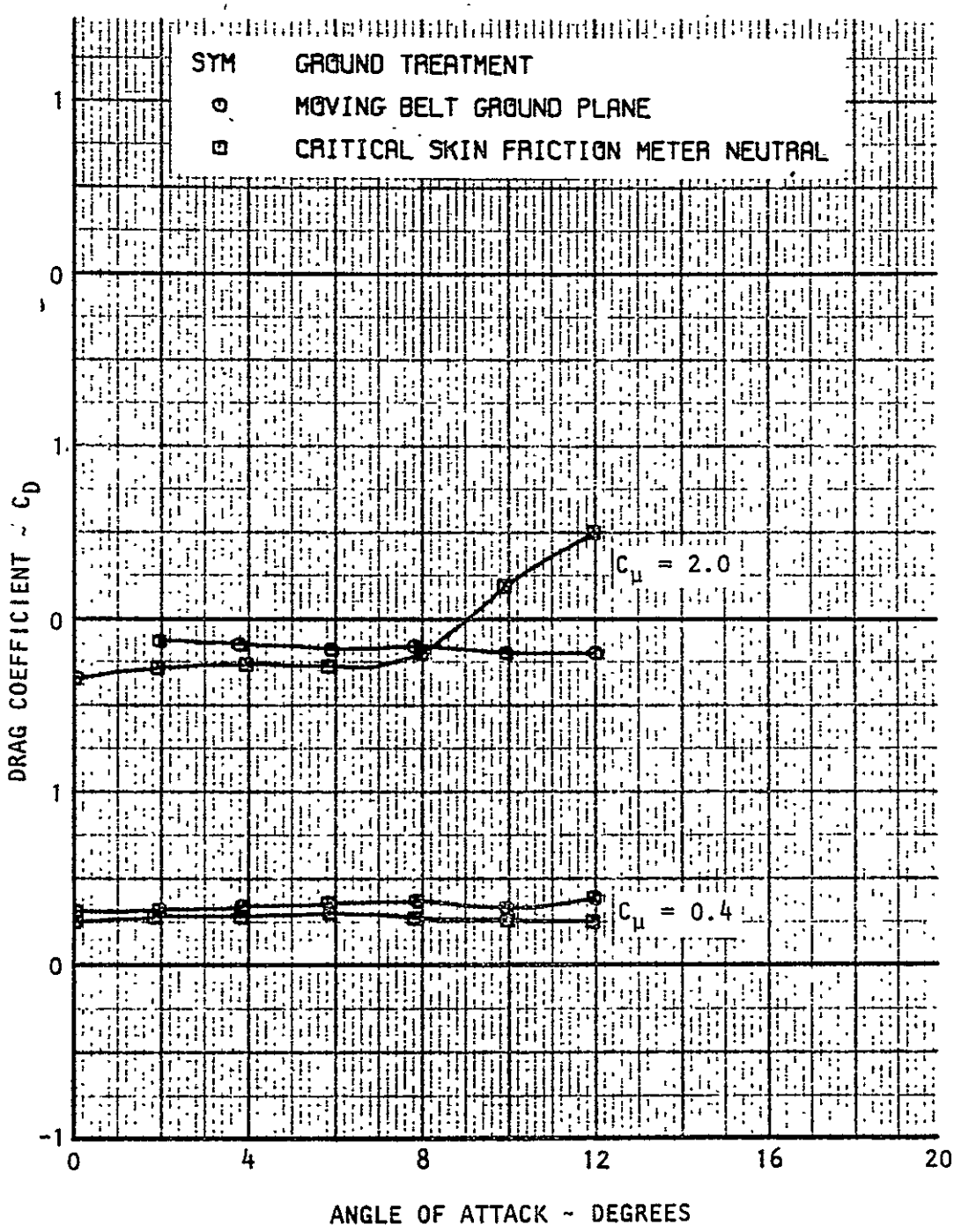

Figure 8.18(a) Drag Data in Ground Effect, h/c = 1, Swept Wing With Tips (Ground BLC: Multiple Nozzles)

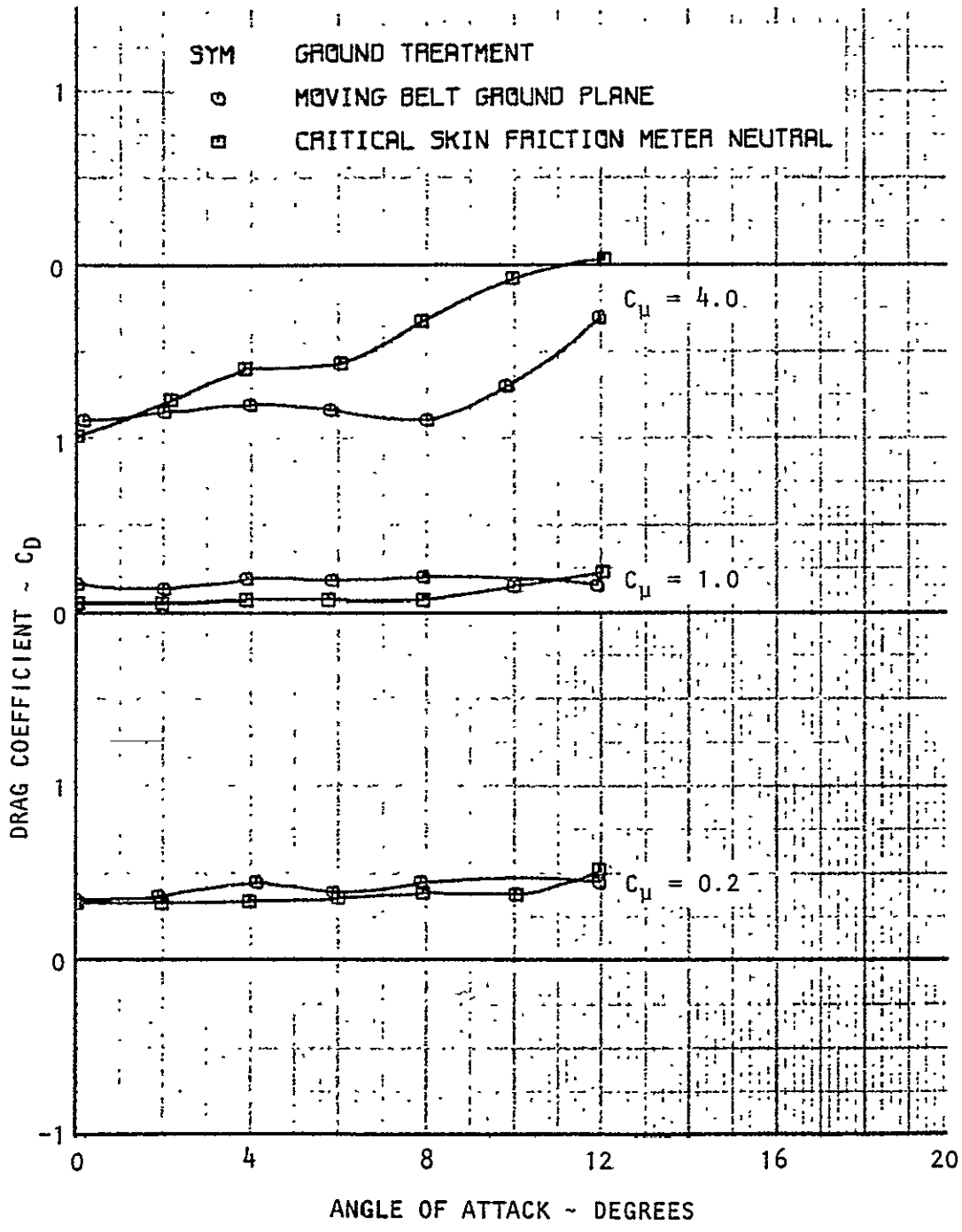

Figure 8.18(b) Drag Data in Ground Effect, h/c = 1, Swept Wing With Tips (Ground BLC: Multiple Nozzles)

ORIGINAL PAGE IS
OF POOR QUALITY

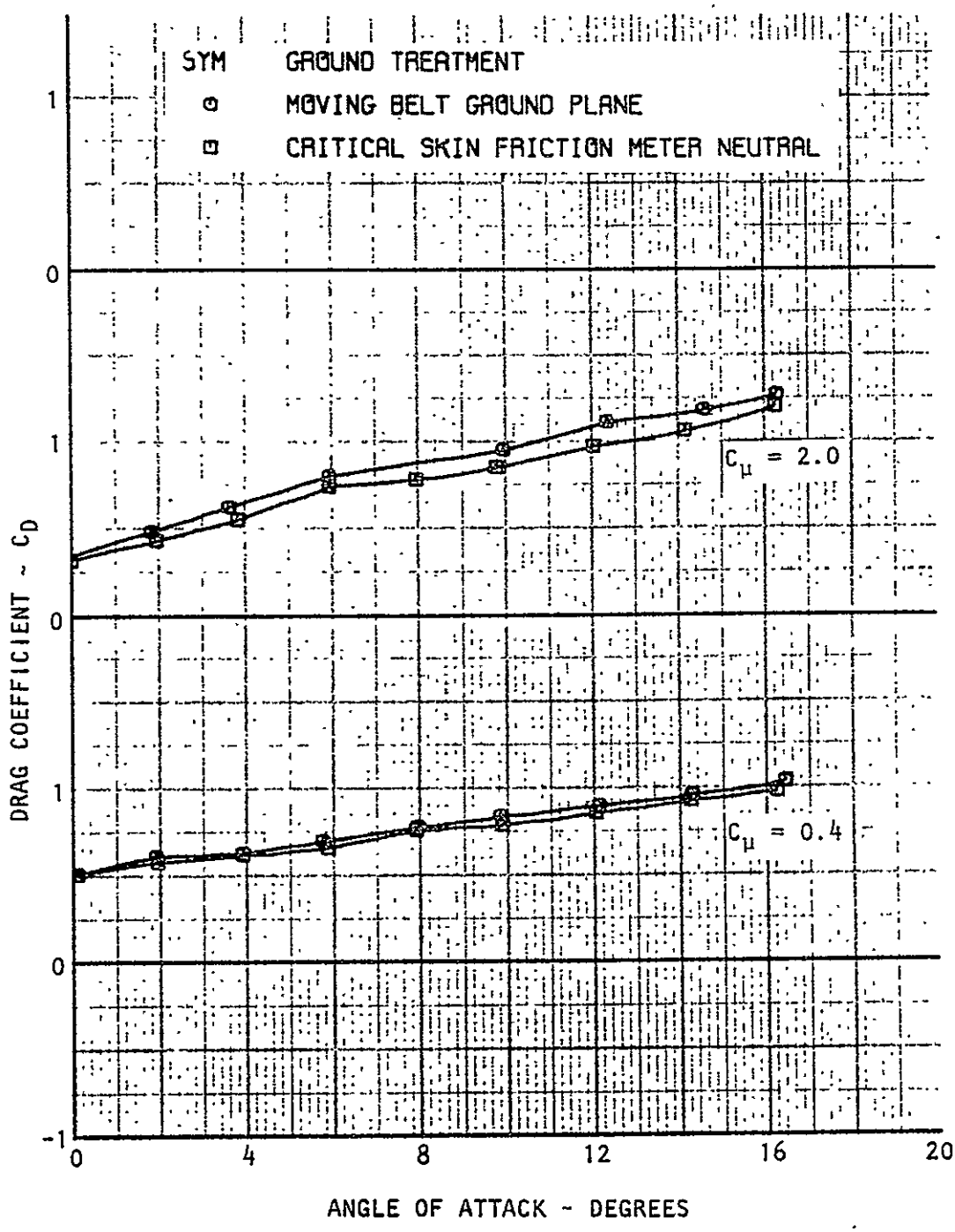

Figure 8.19(a) Drag Data in Ground Effect, h/c = 2, Basic Swept Wing (Ground BLC: Multiple Nozzles)

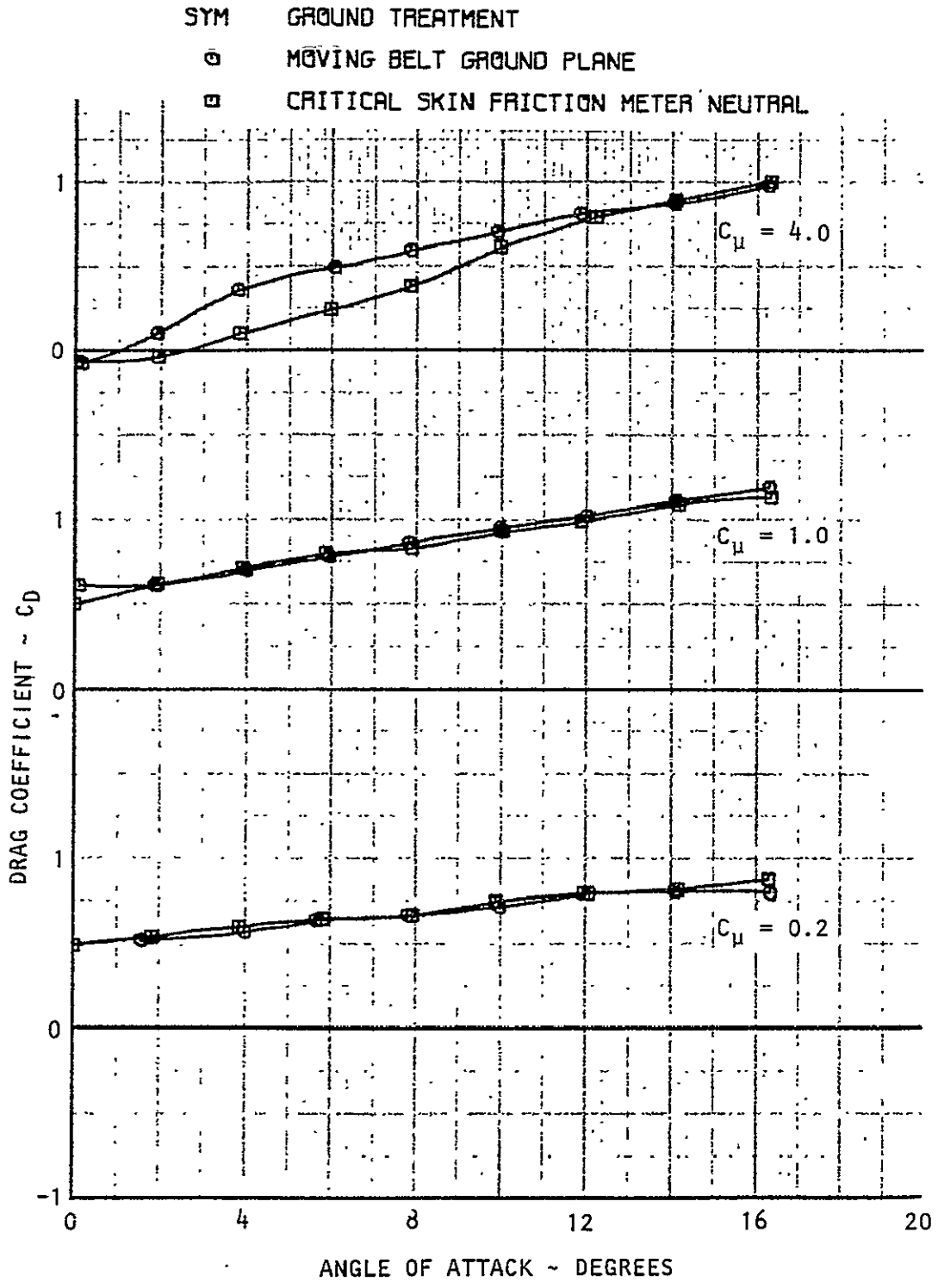

Figure 8.19(b) Drag Data in Ground Effect, h/c = 2, Basic Swept Wing (Ground BLC: Multiple Nozzles)

ORIGINAL PAGE IS
OF POOR QUALITY

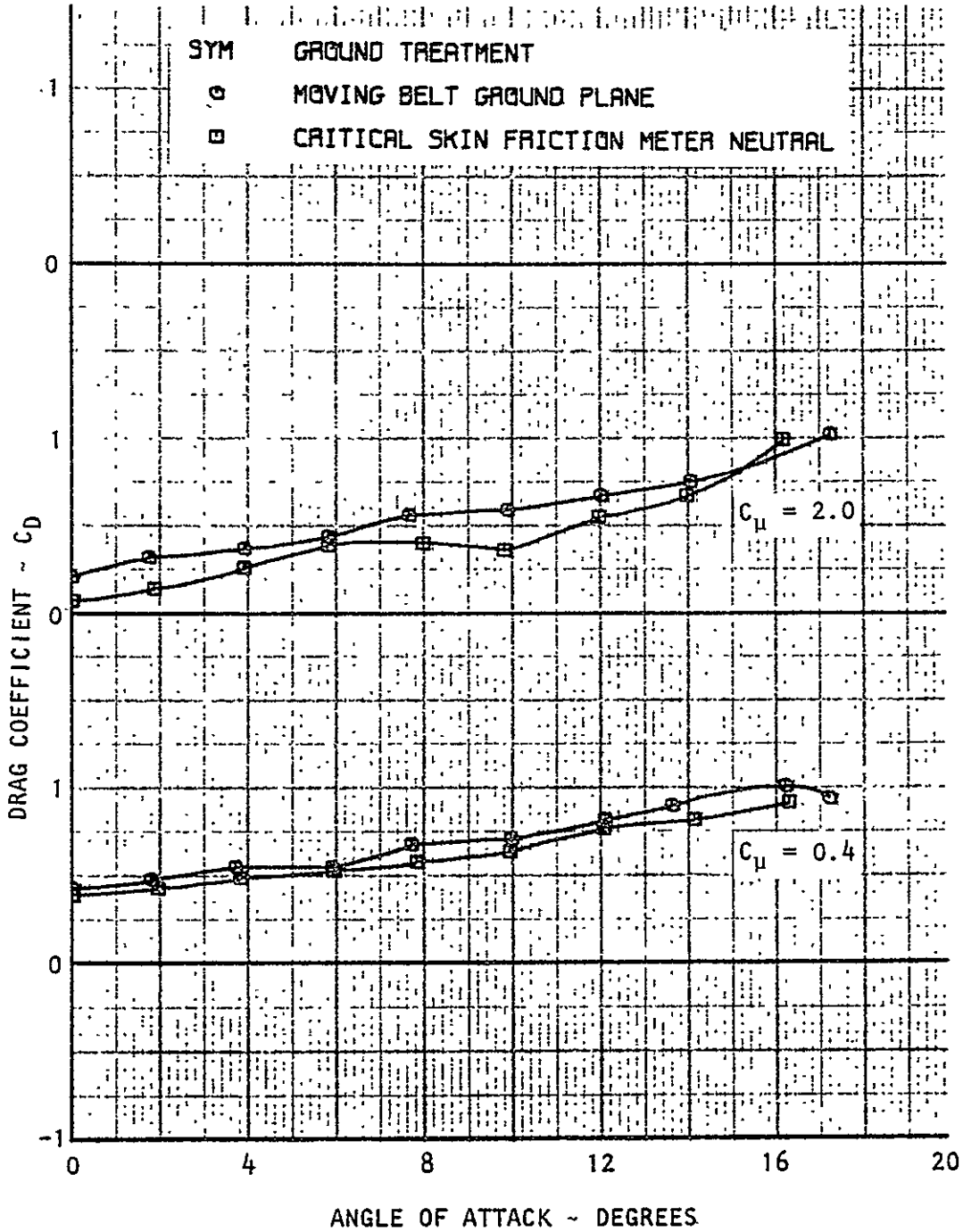

Figure 8.20(a) Drag Data in Ground Effect, h/c = 2, Swept Wing With Tips (Ground BLC: Multiple Nozzles)

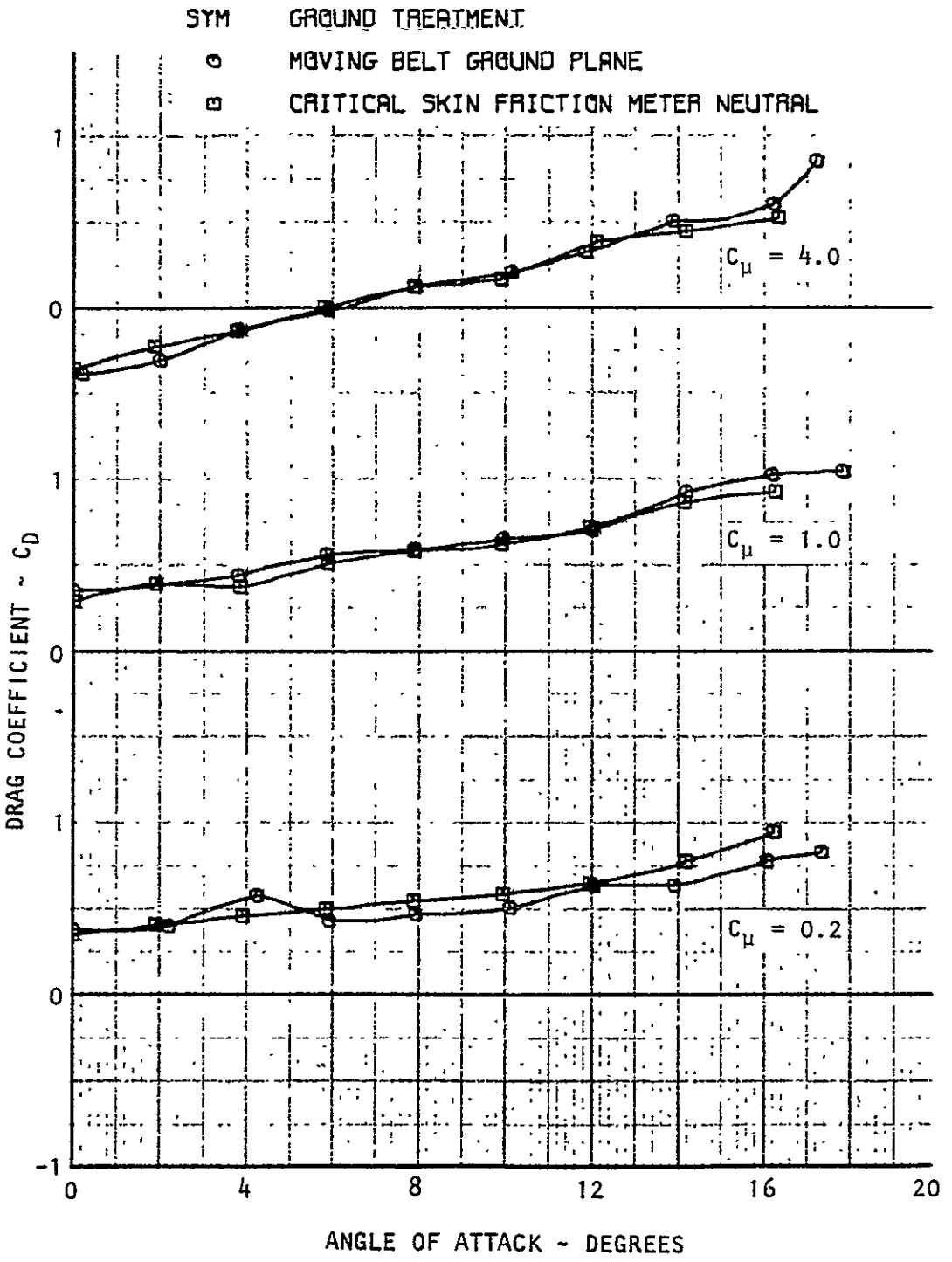

Figure 8.20(b) Drag Data in Ground Effect, h/c = 2, Swept Wing With Tips (Ground BLC: Multiple Nozzles)

ORIGINAL PAGE IS
OF POOR QUALITY

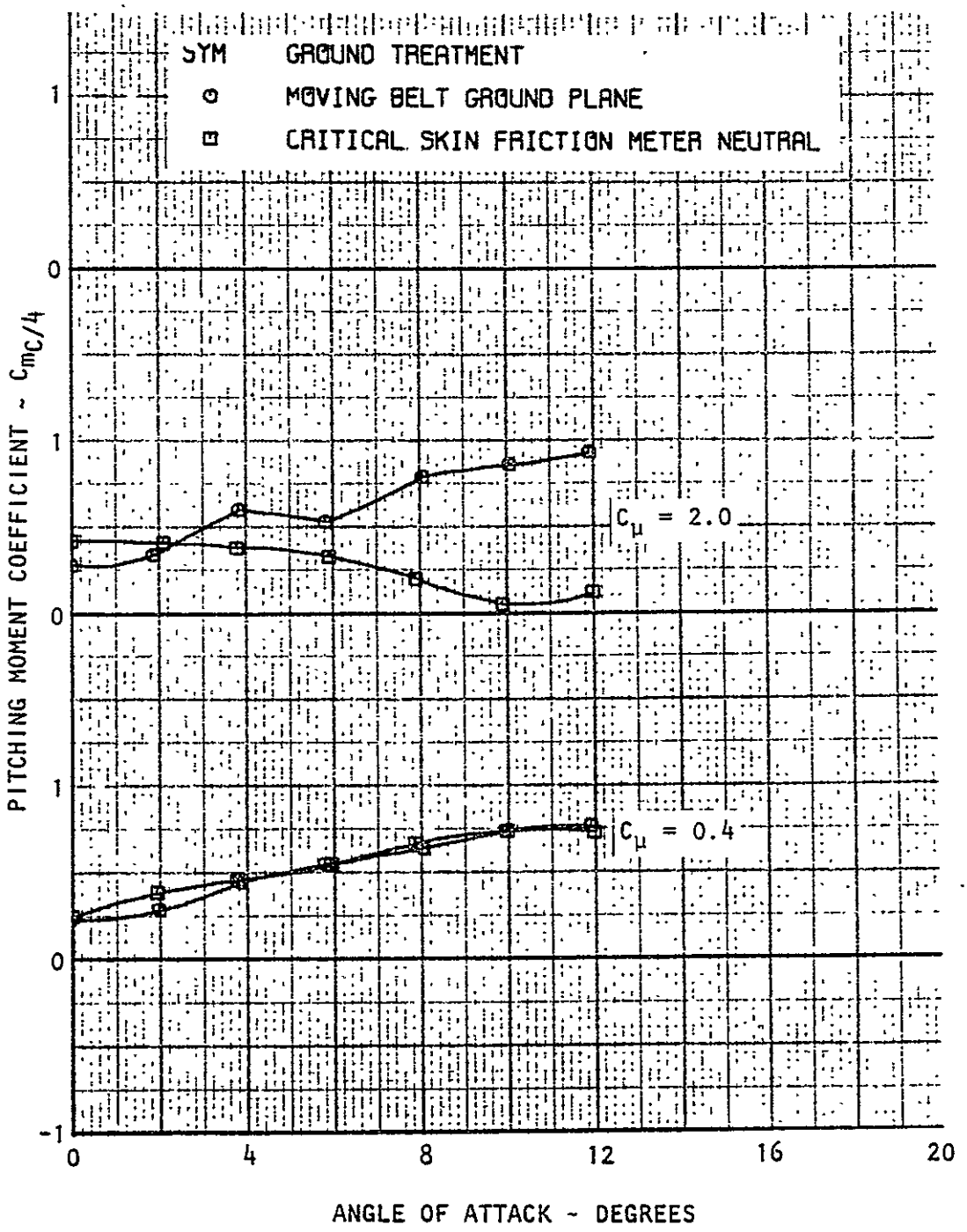

Figure 8.21(a) Pitching Moment Data in Ground Effect, h/c = 1, Basic Swept Wing (Ground BLC: Multiple Nozzles)

ORIGINAL PAGE IS
OF POOR QUALITY.

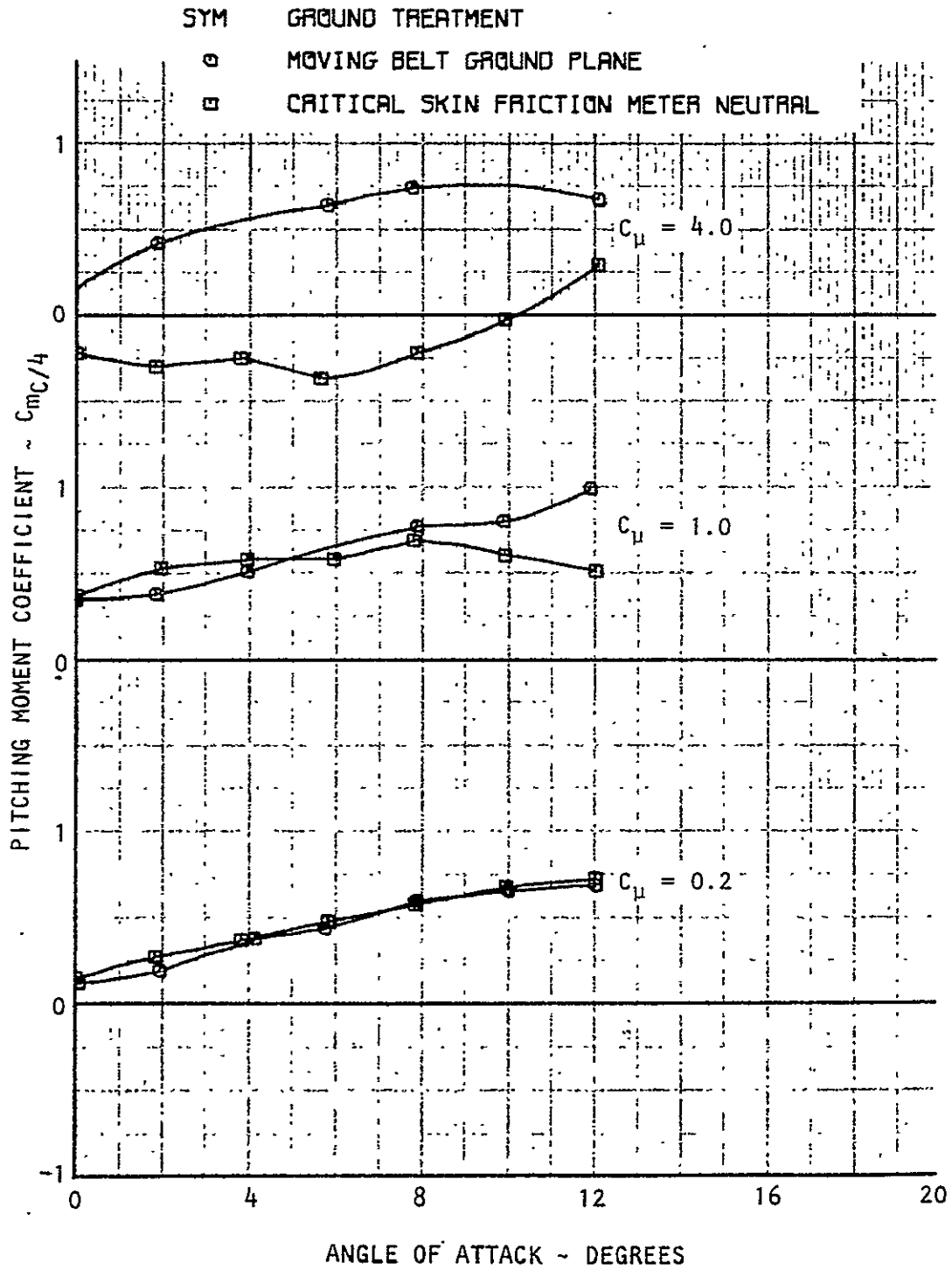

Figure 8.21(b) Pitching Moment Data in Ground Effect, h/c = 1, Basic Swept Wing (Ground BLC: Multiple Nozzles)

ORIGINAL PAGE IS
OF POOR QUALITY

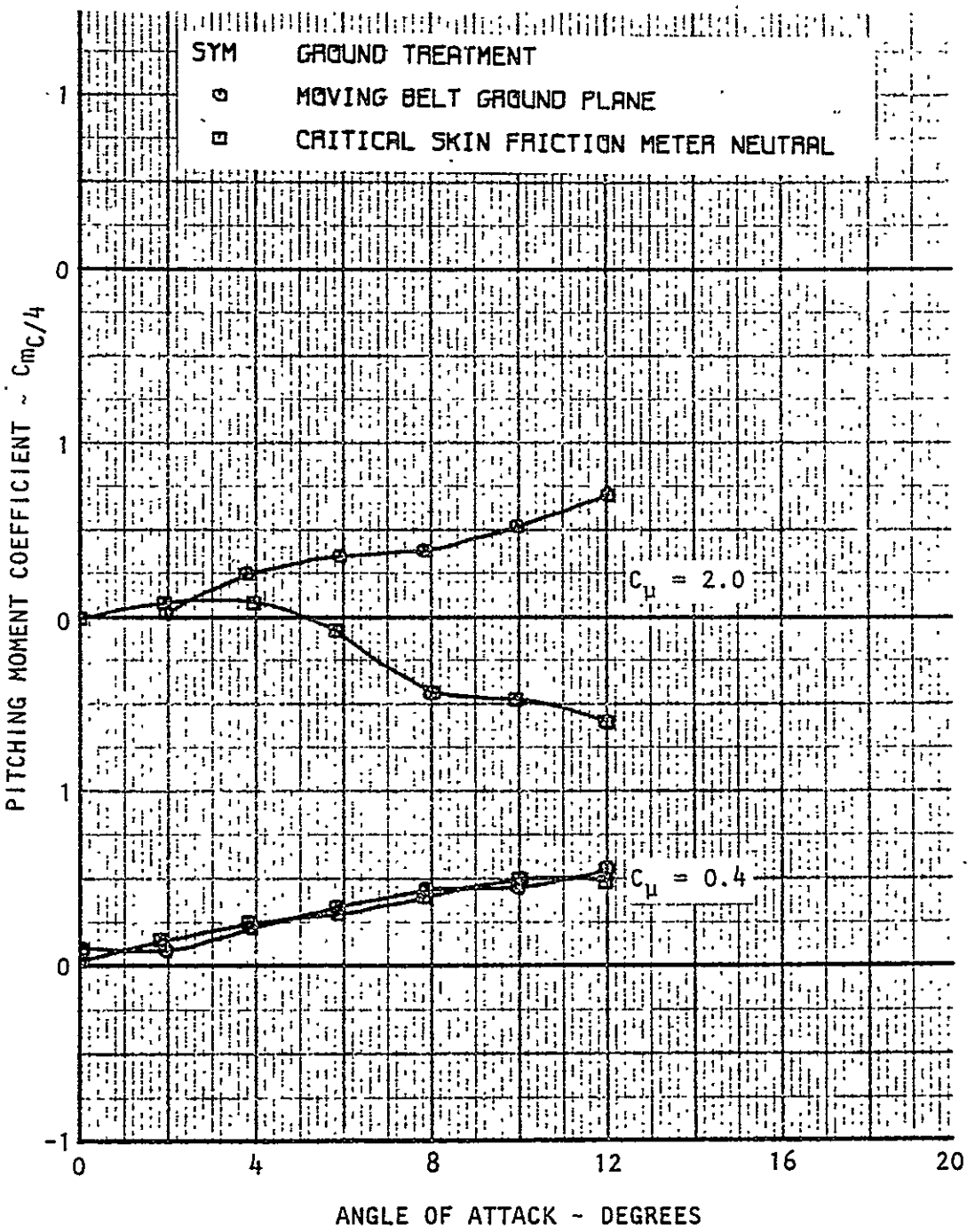

Figure 8.22(a) Pitching Moment Data in Ground Effect, h/c = 1, Swept Wing With Tips (Ground BLC: Multiple Nozzles)

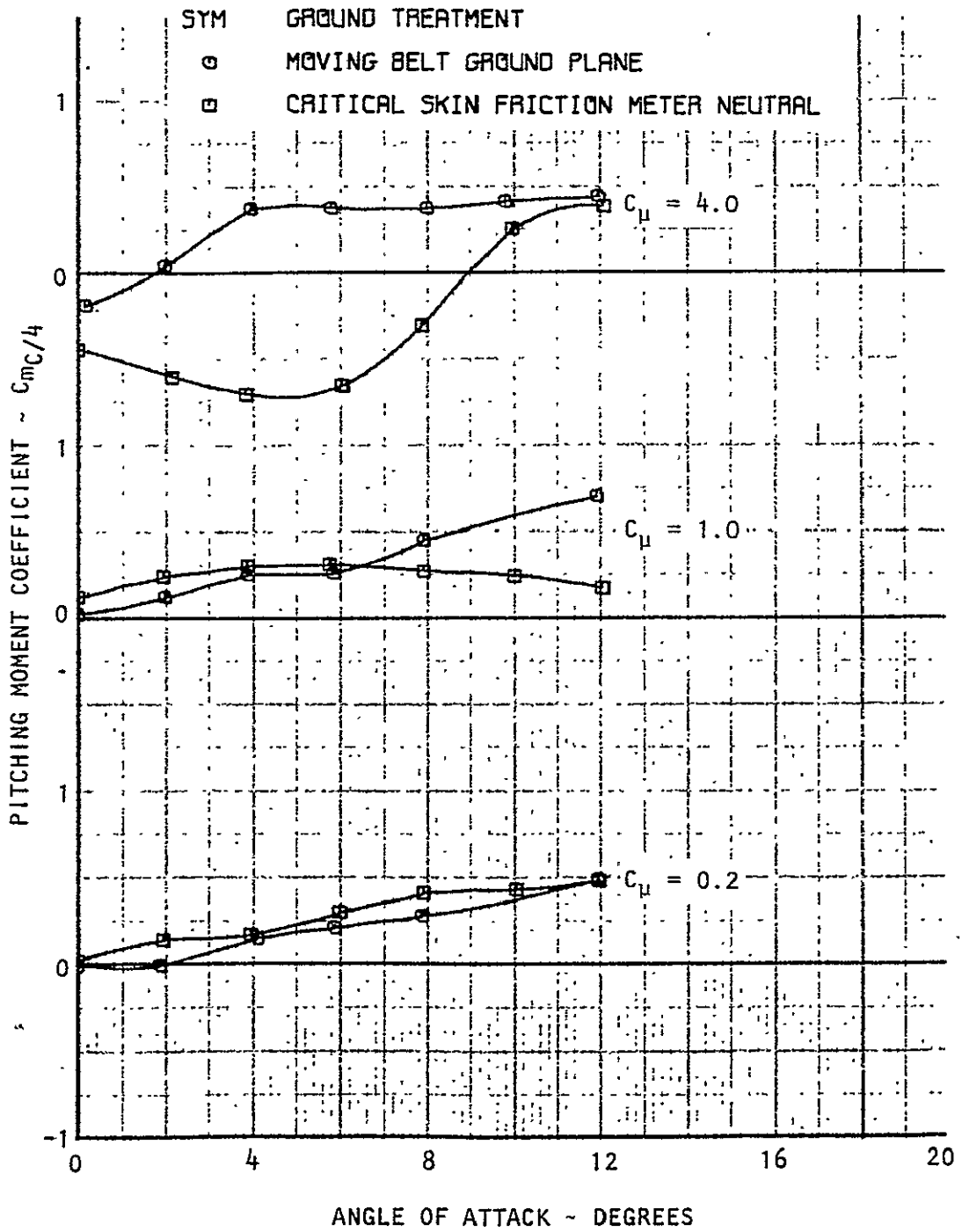

Figure 8.22(b) Pitching Moment Data in Ground Effect, h/c = 1, Swept Wing With Tips (Ground BLC: Multiple Nozzles)

ORIGINAL PAGE IS
OF POOR QUALITY

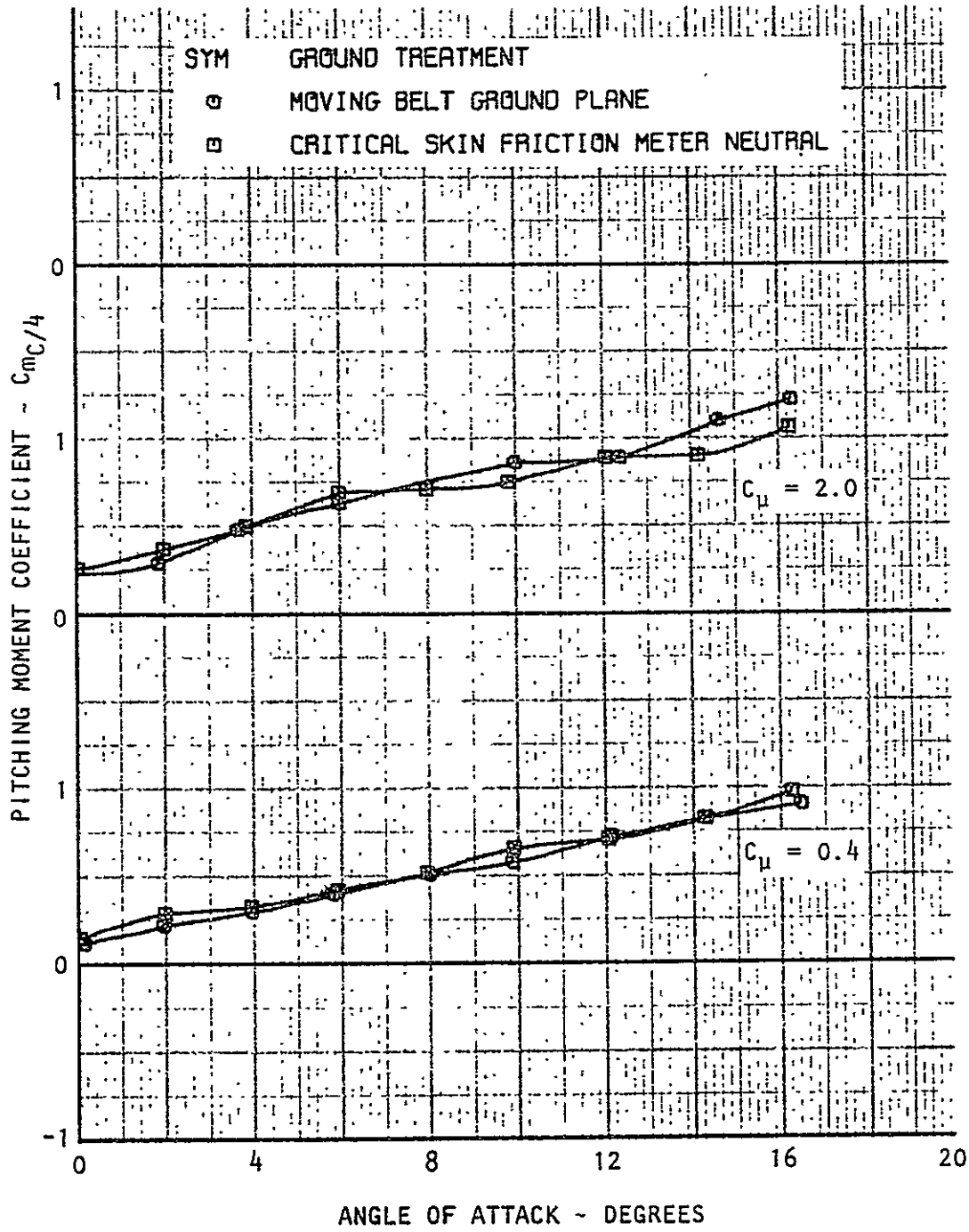

Figure 8.23(a) Pitching Moment Data in Ground Effect, h/c = 2, Basic Swept Wing (Ground BLC: Multiple Nozzles)

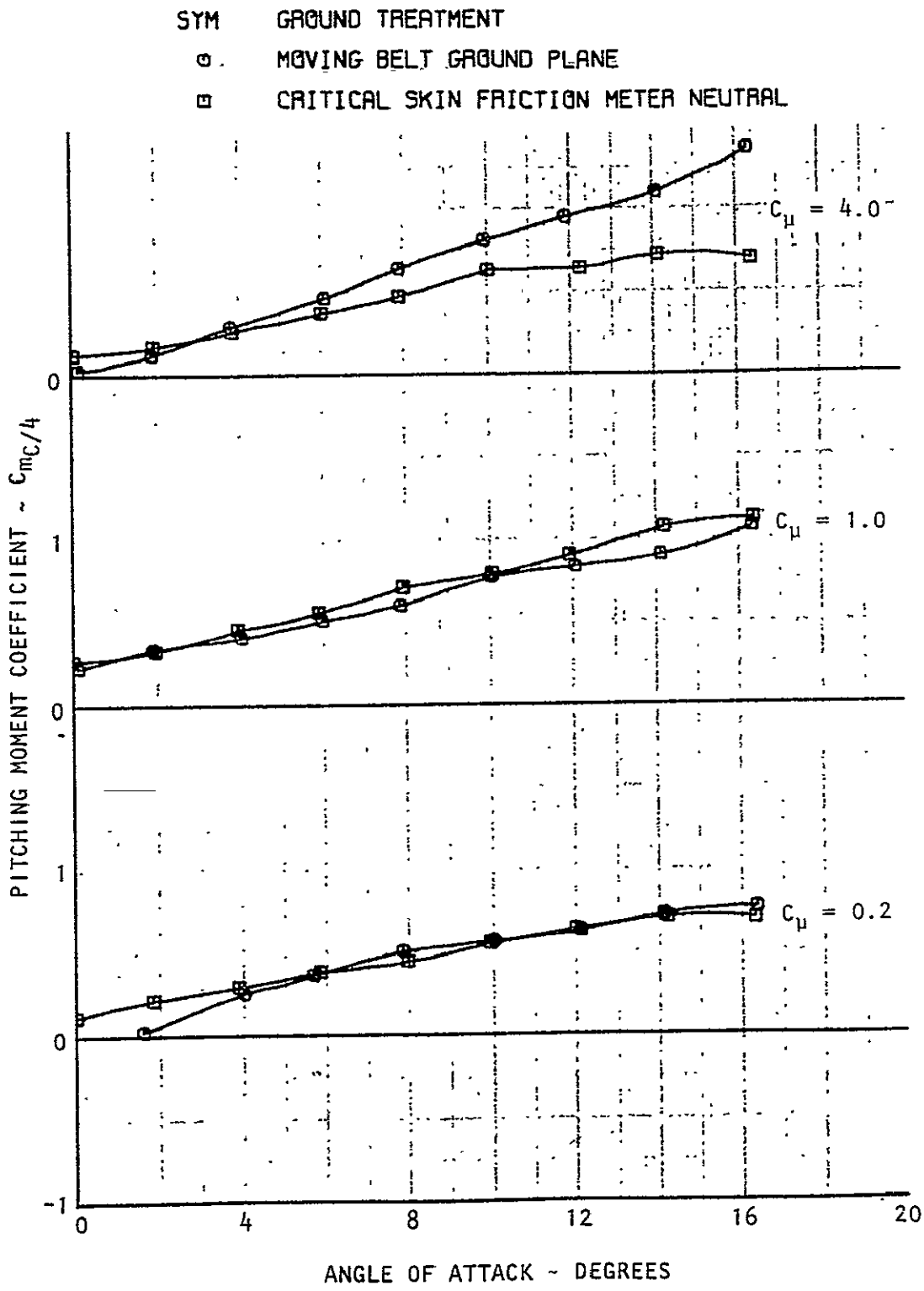

Figure 8.23(b) Pitching Moment Data in Ground Effect, h/c = 2, Basic Swept Wing (Ground BLC: Multiple Nozzles)

ORIGINAL PAGE IS
OF POOR QUALITY

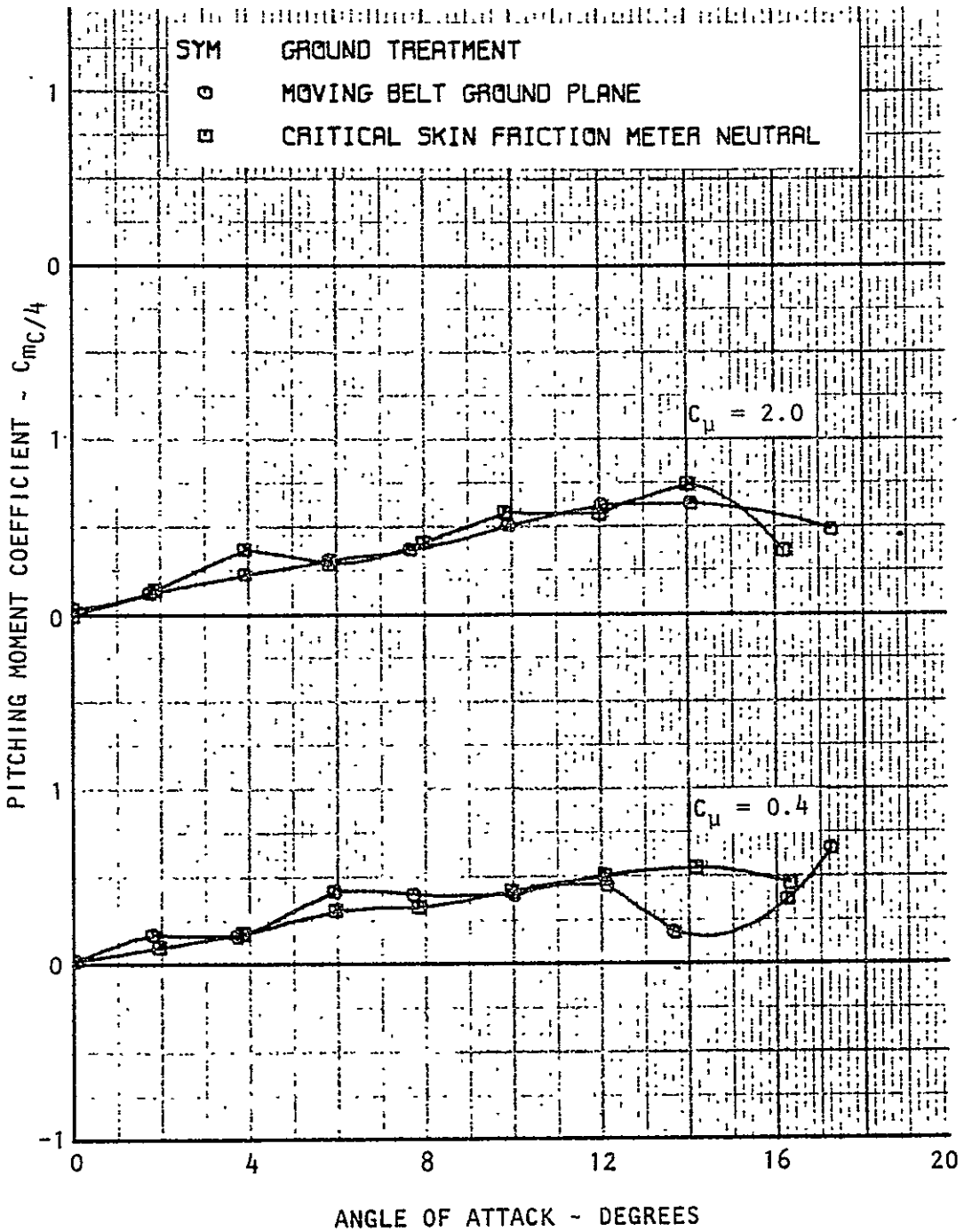

Figure 8.24(a) Pitching Moment Data in Ground Effect, h/c = 2, Swept Wing With Tips (Ground BLC: Multiple Nozzles)

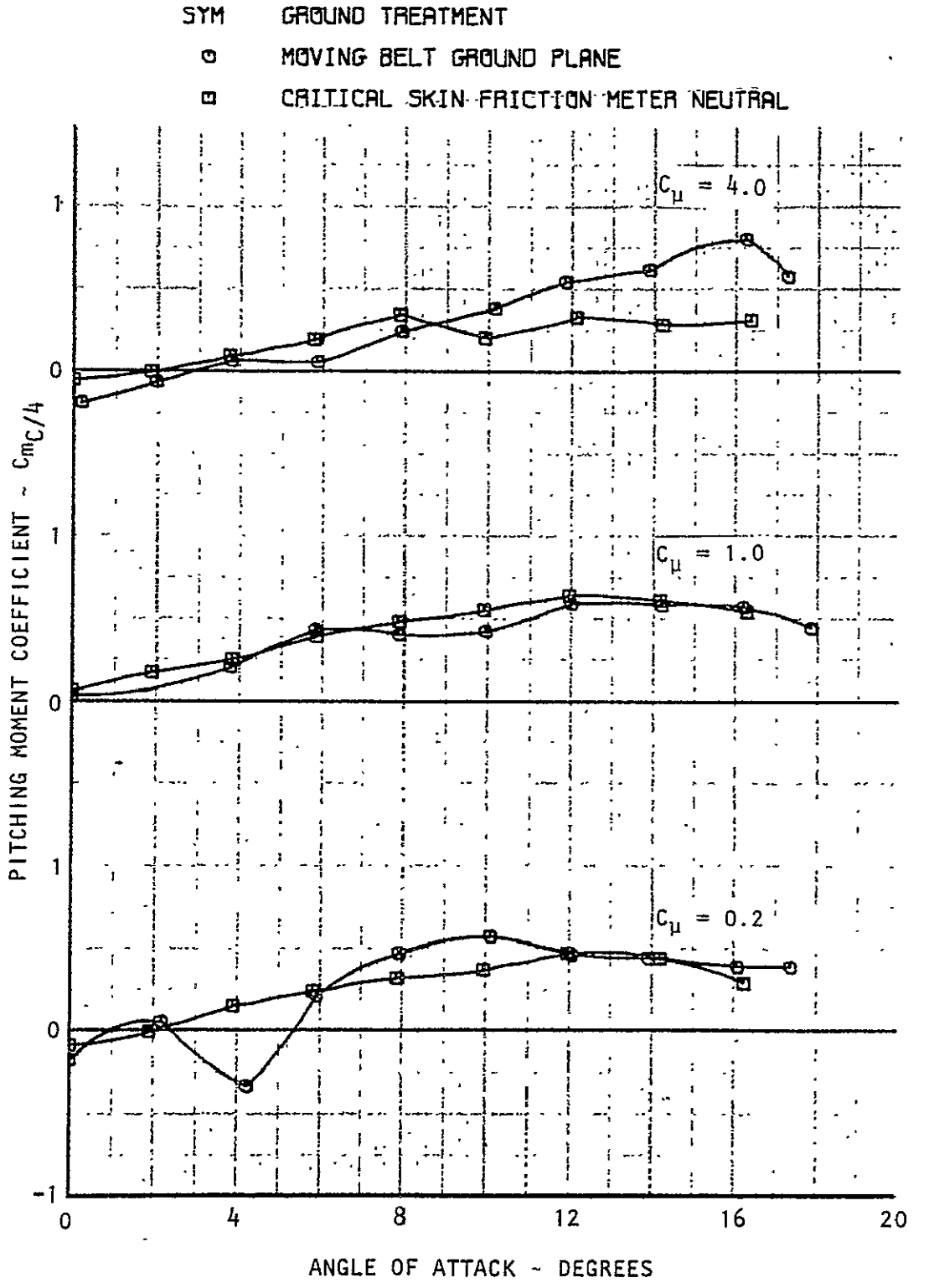

Figure 8.24(b) Pitching Moment Data in Ground Effect, h/c = 2, Swept Wing With Tips (Ground BLC: Multiple Nozzles)